ALMA MATER STUDIORUM - UNIVERSITÀ DI BOLOGNA

SCUOLA DI INGEGNERIA E ARCHITETTURA

DIPARTIMENTO DI INGEGNERIA CIVILE

International Master Course in Civil Engineering

TESI DI LAUREA

in
Geotechnical Engineering

NUMERICAL INVESTIGATION OF STIFFNESS EFFECTS ON LATERALLY LOADED MONOPILES

CANDIDATO

Elena Paolazzi

RELATORE:

Professore Guido Gottardi

CORRELATORICE

Varvara Zania

Anno Accademico 2012/13

Sessione II

Abstract – italiano

L'obiettivo della tesi è investigare la risposta del terreno a pali di fondazione soggetti a carico laterale attraverso metodi numerici. La ricerca è svolta sul comportamento delle tensioni ultime del terreno sia in caso di pali rigidi che flessibili. Viene utilizato un progemma di calcolo ad elementi finiti (Abquas) che simula il sistema palo-terreno con buona prrossimazione.

Attualmente esistono varie formule suggerite dall'Euro Codice e dal API (American Petroleum Institute) per calcolare la capacità portante di un palo, ma nessuna prende in considerazione la rigidezza e la forma del palo o il tipo di installazione con il quale il palo è stato infisso nel terreno.

Per investigare gli effetti della rigidezza del palo, tre tipi di palo di acciaio sono stati utilizzati (pali cavi e pieni). La ricerca è stata effettuata grazie all'utilizzo di tre modelli matematici che sono stati creati per stdiare il fenomeno(uno per ogni tipo di palo). Le caratteristiche del suolo sono state modificate variando i parametri del "elemento suolo" nei vari modelli. Una forza concentrata di 0.4 kN in direzione orizzontale è stata applicata in cima al palo ad una distanza di 15 diametri sul livello del suolo. Sono stati estratti i dati relativi allo spostamento orizzontale e alle tensioni del palo.

La ricerca, confrontata con esperimenti di laboratorio in centrifuga, ha portato a diverse conclusioni relative alle curve di rottura del sistema palo-terreno. In generale la rigidezza del palo non influenza l'inviluppo di rottura del sistema palo-terreno, mentre le curve pressione-spostamento orizzontale subiscono leggere variazioni. E' invece molto evidente, soprattutto dalle prove in centrifuga, l'effetto del tipo di installazione sulla capacità portante di un palo soggetto a carico laterale. Il tipo di istallazione infatti, modifica le caratteristiche del terreno e quindi anche la resistenza del suolo al carico laterale del palo viene modificata.

Abstract – English

Purpose:

The purpose of this study is to compare the lateral response of three types of steel piles installed under different conditions (standard gravity g and increase of gravity of 25g) in sandy soil. The effects of different installation procedure and different type of piles with different stiffness are investigated on the response of lateral load piles.

Procedure:

In the study, data are taken from Lab test in centrifuge[1] and numerical models in Abaqus during the lateral loading of three 0.4cm-diameter piles where the soil is clean fine sand.
In the present thesis the numerical models are described and the results are compared with the lab tests and the actual theory in order to understand the behaviour of lateral loaded monopiles. Three numerical models are created to study type of piles with different stiffness; flexile piles (hollow plugged piles and hollow unplugged piles) and rigid piles. Since some numerical problems occur in the installation phase, in the three models just the loading phase is performed changing several soil properties.
The results are analysed in order to study failure mechanism and the ultimate load of the pile. Therefore curves Lateral-load-deflection and Moment-rotation are plotted. Moreover the moment distribution along the pile depth and the soil resistance p as function of deflection y are analysed (p-y curves).

Results:

The comparison with lab test suggests that stiffness effects in lateral loaded piles do not modify the lateral load capacity but, since the failure mechanism depend on the type of piles , the p-y curves are slightly different for the three types of pile. On the other hand the lab tests shows that the installation effects, that alter the soil conditions, are significantly relevant on the lateral load behavior. Indeed the variation of soil properties in the numerical models induces a large variation of the pile resistance.

Table of contents

0.Introduction

0.1 Motivation

In this study, the lateral response of monopiles embedded in sand is investigated, since the actual methodology is not calibrated for design of large diameter stiff monopiles and does not account for stiffness and installation effects.

Nowadays new wind farms are being constructed in deeper and deeper waters and the type of foundations for such offshore wind turbines is the monopile. A monopile is a single large diameter tubular steel pile driven 5 to 6 times its diameter (4-6 meters) into the seabed. This structure is subject to the lateral loads from wind and waves, which determine a force with a significant eccentricity at the base of the pile[2].

In design method, the lateral load capacity is determined by considering two different failure mechanisms: (1) ultimate soil resistance and (2) acceptable lateral deflection of single piles. In rigid piles the failure is due to the shear failure of the soil against the pile (1° criterion); while in flexible piles the ultimate capacity can also be reached due to the excessive lateral deflection (2° criterion)[3]. The lateral load pile response can be evaluated assuming a linear elastic or non-linear elastic behaviour of the soil. In the first one the Winkler-soil-model(1867) is assumed, the soil along the pile is considered as a series of infinitely closely spaced independent and elastic springs with a constant stiffness at each depth. Assuming a nonlinear behaviour, the soil stiffness is not constant and there is a non-linear relationship between the soil resistance and its displacement (p-y curve). The large diameter stiff monopiles exhibits a nonlinear behaviour of the soil and consequently the ultimate soil resistance, the soil stiffness and the lateral load capacity depend on the p-y curves ,but the ones recommended by the American Petroleum Institute (API)do not consider the installation and stiffness effects.

0.2 Scope of the work

The scope of this work is to study installation and stiffness effect on the response of a lateral loaded monopiles in clean fine sand.
This thesis is focus on the stiffness effects investigated with numerical models and it is a comparison to the thesis entitled “Centrifuge testing for installation and stiffness effects on lateral load behaviour of monopiles”[1].
The lateral capacity and the soil stiffness at different depth of three-dimensional numerical models of rigid and flexible piles embedded in sandy soil are estimated. The the friction angle and interface friction properties of the pile are the parameters which vary in the F.E. Models.

1. Background - theory

The theory behind this study regards geotechnical knowledge and some overall information about Finite Element Modelling.
Geotechnical theory about the design of lateral loaded mopiles is cohesionless soil is presented in paragraph 1.1. Even if the numerical models do not consider the installation phase, it is presented a summary of the actual theory concerning both axial and lateral load needed to better compare FEM results to centrifuge test.

1.1 Design of piles

In this chapter two theoretical aspects regarding the pile behaviour are introduced: (1) the end bearing capacity which is to account during the installation phase and (2) the lateral response to compare with tests results. These are two different load carrying mechanisms and the corresponding resistance. This provides the resistance of the pile to axial and lateral loading respectively.

1.1.1 Axial Load Capacity

The ultimate load that can be applied to a given pile depends on the resistance that the pile can produce in terms of side friction (shaft resistance) and point bearing resistance.[2]

Therefore, the ultimate bearing capacity is computed by use of the following equation:

$$Q_t = Q_s + Q_b$$

Q_s: total skin-friction resistance

Q_b: total end bearing resistance

According to Meyerhof's theory (1951-1976), the end bearing capacity of the tip of the pile can be assumed to increase linearly to a critical depth and then remains constant. The end bearing capacity can be determined as follows:

$$Q_b = \sigma_v' N_q A_p$$

σ_v': the vertical effective stress at the pile tip

$$\sigma_v' = \gamma' z$$

N_q: bearing capacity factor, which depends on the friction angle φ of the soil as reported in Figure 1.1 or it can be calculated according to the Terzaghi's formula (1943):

$$N_q = e^{\pi tan\varphi} tan^2\left(45 + \frac{\varphi}{2}\right)$$

A_p : gross end area of the pile

The diagram reported in Figure 1.1 has been traced considering several loading tests taken from different sources. Meyerof (1953) used the length to diameter ratio L_c/d, whose value corresponds to the penetration depth for which the bearing capacity reaches the limit.

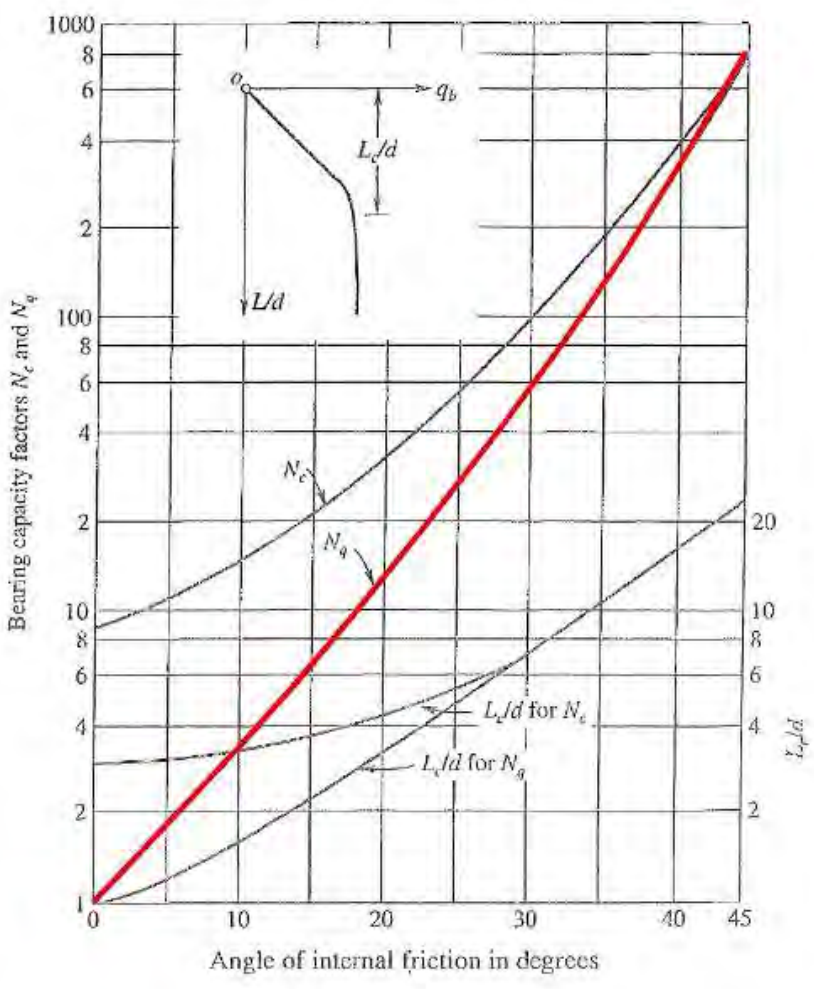

Figure 1.1: bearing capacity factor according to Meyerof's theory

And the shaft resistance can be obtained as:

$$Q_s = \int_L \tau_f A_s dz$$

where

τ_f: skin friction

A_s: side surface area of the pile

Since the origin of skin friction in granular soils is due to the frictional interaction between piles and granular material, the unit skin friction can be expressed as:

$$\tau_f = K\tan\delta\sigma'_{v0} \leq \tau_{f,max}$$

where

K: coefficient of lateral earth

$$K = \begin{cases} 0.8 \text{ for open} - \text{ended, unplugged piles} \\ 1 \text{ for closed} - \text{ended or plugged piles} \end{cases}$$

σ'_{v0}: effective overburden pressure at the point in question

δ: friction angle between the soil and the pile wall

1.1.2 Lateral Load Capacity

For proper functioning of structures subject to lateral load, two criteria must be satisfied: (1) a pile should be safe against ultimate failure (H_u); and (2) horizontal deflection (y) at working loads should be within the permissible limit. The ultimate lateral resistance and the working load deflection of single piles depend of the dimensions, the strengths, and the fixity conditions at the top on the deformation characteristics of the soil surrounding the loaded pile [3].The lateral response can be determined considering different assumptions of the soil and pile behavior.
Regarding the behavior of the pile, two failure mechanisms can be distinguished. For “rigid” piles the behavior is elastic and the yielding does not occur; while in “flexible” piles the plastic hinge formation has to account. In this study, the “rigid” pile behavior is only considered.

1.1.2.1 Lateral Load Capacity Based on Ultimate Load

From literature the common procedures to estimate the ultimate lateral resistance are the Brinch Hansen’s theory (1970) [2] and the Broms’ theory (1965)[4]. The latest is presented and discussed in this study. Broms assumed that the rigid pile developing negligible elastic deformation, whereas the considered failure mode is rigid body rotation. In addition, the active pressure at the back of the pile and friction soil-pile interaction are neglected. In cohesionless soils the assumed lateral earth pressure distribution at failure for a laterally loaded pile is shown in Figure 1.2.

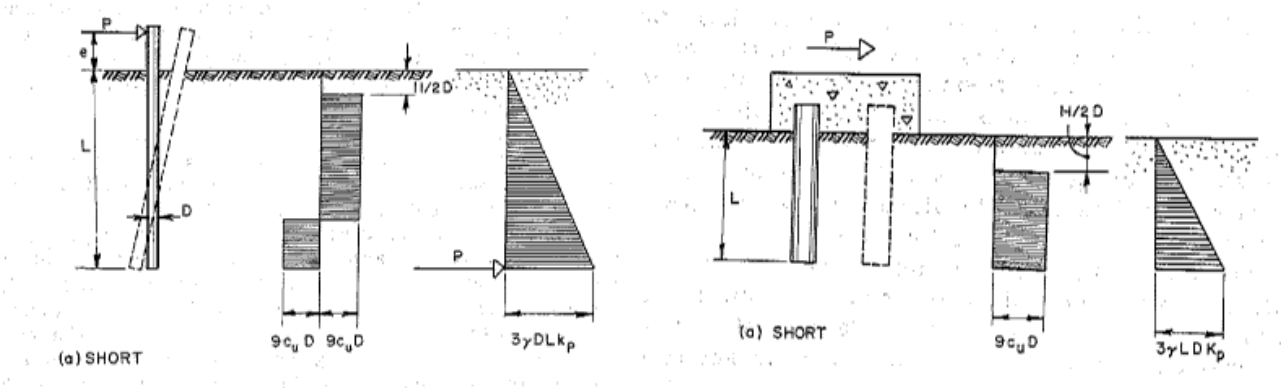

Figure 1.2: failure mode for short - free head pile (on the left) and short, restrained piles (on the left) [4].

The lateral earth pressure distributions shown in Figure 1.2, derive from the following considerations. At failure, it is possible to recognize that the soil disposed in front of the loaded pile moves upwards, whereas the soil in back of the pile moves into space created at the back of the laterally loaded pile. Around a depth of one pile diameter below the ground level the lateral earth pressure can be calculated by Terzarghi's theory, while below this depth it is observed the arching within the soil in proximity of the pile and this affects considerably the lateral earth pressures. For depths greater than one pile diameter, the passive lateral earth pressures, at failure, overcome the Rankine passive pressure, whereas the lateral earth pressure achieving on the back side significantly smaller than the active Rankine lateral earth pressure. Comparison with available test data have indicated that the lateral earth pressure at failure can be estimated as three times the passive Rankine earth pressure.

$$p_p = 3\sigma_v' K_p$$

where

σ_v': effective vertical overburden pressure

K_p: passive lateral earth pressure coefficient. which is a function of the friction angle φ $\rightarrow K_p = \frac{1+\sin\varphi}{1-\sin\varphi}$

As mentioned before, the maximum load calculated according to Broms' theory that can be applied on the pile depends on the type of failure mechanism ("rigid"/ "flexible" pile) and the fixity conditions at the top.

For this study the failure for rigid free head piles occurs when the pile rotates as a unit through the soil around a point located at the some depth below the ground surface [4]. The ultimate lateral resistance of the soil develops along the total length of the pile and it is given by the following formula:

$$H_u = \frac{0.5\gamma' D L^3 K_p}{e+L}$$

where

e: eccentricity

D: pile diameter

L: pile length

γ': effective unit weight

In addition, it is possible to estimate the maximum bending moment associated to H_u. The location of the maximum moment can be determined by the following equation:

$$f = 0.82\sqrt{\frac{H_u}{D\gamma' K_p}}$$

Thus, the maximum moment can be calculated as

$$M_{max} = H_u\left(e + \frac{2}{3}L\right)$$

When the maximum bending moment M_{max} value, due to the ultimate load H_u is larger than the yielding moment M_y for the pile material, then obviously the pile behaves as a "flexible" pile and the actual ultimate lateral load H_u can be computed by setting $M_{max} = M_y$.

1.1.2.2 Lateral Load Capacity Based on Deflection

The true stress-strain response of the soil can be described as elasto-plastic. Analytical theories account only for the elastic response of the soil, while numerical methods need to be employed in order to consider the full elasto-plastic (nonlinear) soil response. Two commonly adopted methods to determine the lateral deflection are discussed in the ensuing sections.

- ***Elastic soil response***

The theory of the beam in an elastic foundation is given by Hetenyi (1946) and the following assumptions are considered:

- linear soil response
- pile is straight with uniform cross section
- longitudinal plane of symmetry
- pile material is homogeneous and isotropic
- elastic pile response
- Young modulus is the same for loading and unloading
- deflections due to shearing are small
- transverse deflections are small

In order to derive the equation of deflection, the equilibrium of moments for an infinitely small unloaded element, bounded by two horizontals a distance dx apart (see Figure 1.3), is presented in the following formula.

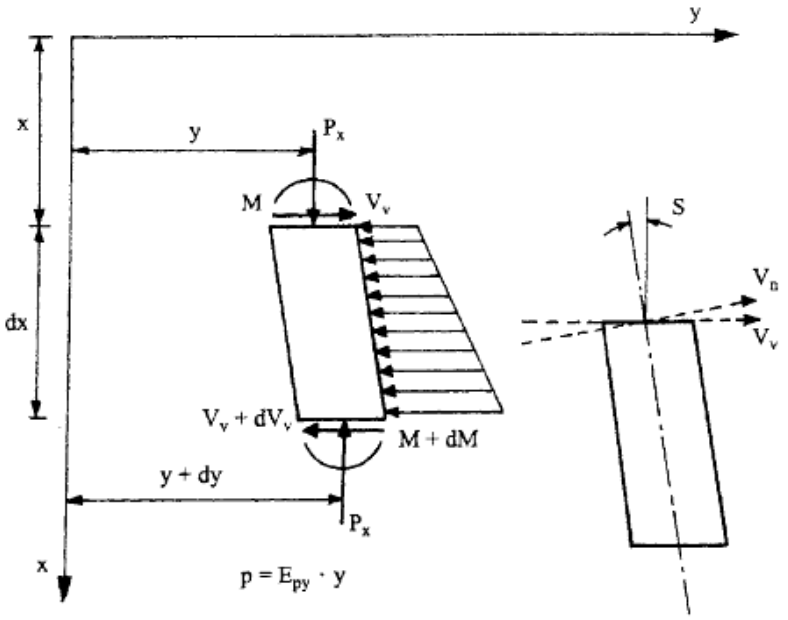

Figure 1.3: element from a beam column (after Hetenyi, 1946) [5]

$$(M + dM) - M + P_x dy - V_v dz = 0$$

Simplifying, the expression below is obtained:

$$\frac{dM}{dz} + P_x \frac{dy}{dz} - V_v = 0$$

Differentiating the previous expression with respect to x, the following equation is obtained:

$$\frac{d^2M}{dz^2} + P_x \frac{d^2y}{dz^2} - \frac{dV_v}{dz} = 0$$

The following identities are noted:

$$\frac{d^2M}{dz^2} = E_p I_p \frac{d^4y}{dz^4}; \quad \frac{dV_v}{dz} = p$$

where

E_p: elastic modulus of the pile

I_p: moment of inertia of the pile

p: the unit soil reaction

And at working loads the lateral deflection can be estimated by assuming that the unit soil reaction p increases linearly with increasing lateral deflection y as defined as:

$$p = k_h y$$

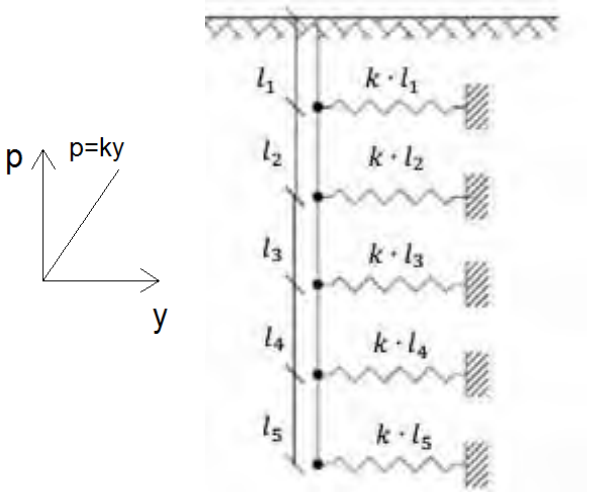

Figure 1.4: sketch of the model

The governing differential equation for the pile's deflection is the following:

$$E_p I_p \frac{d^4y}{d^4z} + P_x \frac{d^2y}{dz^2} - k_h y = 0$$

where

y: pile deflection

z: depth along the pile

k_h: is the coefficient of horizontal subgrade reaction, that depends of the deformation properties of the soil and on the dimension and stiffness of the pile.
In cohesionless soil, the lateral deflection of the pile can be computed considering that the coefficient of lateral subgrade reaction increasing linearly with depth and it is constant with the deflection:

$$k_h = \frac{n_h z}{D}$$

where

z: depth along the pile

n_h: coefficient which depends on the relative density of the soil

D: diameter of the loaded area

A simpler form of the differential equation if the assumptions are made that no axial load is applied, that the bending stiffness $E_p\ I_p$ is constant with depth. Thus, a reduced expression of the differential equation is:

$$E_p I_p \frac{d^4 y}{d^4 z} + 4\beta^4 y = 0$$

in which

$$\beta = 4\frac{k_h}{E_p I_p}$$

The solution may be directly written as

$$y = e^{\beta x}(C_1 \cos(\beta z) + C_2 \sin(\beta z)) + e^{-\beta x}(C_3 \cos(\beta z) - C_4 \sin(\beta z))$$

The coefficients of the integration are calculated according to the boundary conditions.

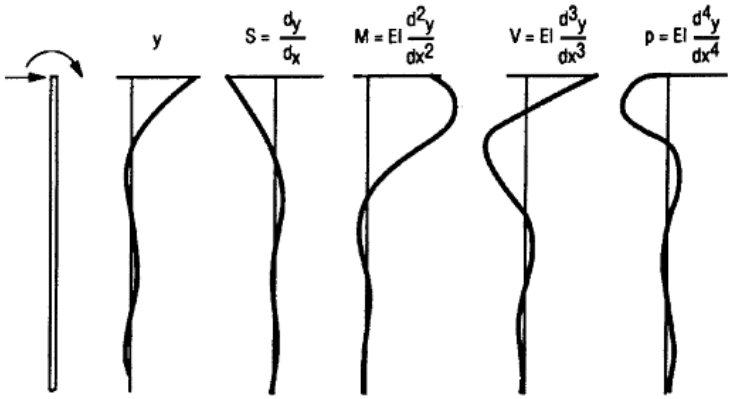

Figure 1.5: deflection, rotation, bending moment, shear and soil reaction obtained from a complete solution [4]

- ***Nonlinear soil response***

The key to determining the behavior of a pile under lateral loading is the ability to develop a family of curves (p-y curves) that give soil reaction as a function of the lateral deflection of a pile [3]. The nonlinear differential equation is the same of the one abovementioned, but the assumption of linear soil response is not account as expressed in the following formula:

$$E_p I_p \frac{d^4 y}{d^4 z} + P_x \frac{d^2 y}{dz^2} - k_h(y) y = 0$$

where

E_p: elastic modulus of the pile

I_p: moment of inertia of the pile

z: depth along the pile

y: deflection

$k_h(y)$: subgrade reaction, which varies nonlinearly with deflection y

The third member of the equation is the lateral earth pressure p and it can be calculated with $p - y$ curves approach. Once obtained the $p - y$ curves, the pile deflection, pile rotation, bending moment, shear and soil reaction for any load applied to the pile can be obtained solving the differential equations.

The p-y approach has been widely used to design piles subjected to lateral static or dynamic loading [4]. Based on the p-y approach the lateral soil-structure interaction can be modeled using empirically derived nonlinear uncoupled springs, so-called p-y curves, as boundary conditions in structural analysis.

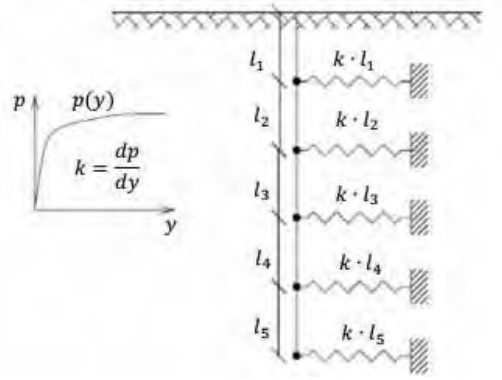

Figure 1.6: illustration of p-y method [5]

The stiffness of this springs, so the shape of the p-y curves depend on many variables as depth and soil properties. The American Petroleum Institute (API) developed a set of formulas to estimate the p-y curves for different type of soil. In the following paragraph it is shown the procedure for sandy soil.

p-y curves from code provisions API

The p-y curves adopted by the API are based on the method developed by O'Neil and Murchison (1983) [6] and it is referred to as the extended hyperbolic model. The expression for p-y curves in sand is given as following:

—

where

A: empirical adjustment factor

: initial modulus of subgrade reaction

z: depth along the pile

: ultimate bearing capacity

p: resistance of the soil

y: displacement of the pile in the considered level.

The empirical adjustment factor A depending on the depth z and the pile diameter D is determined from equation (1.22):

—

The initial modulus of subgrade reaction is usually determined from Figure 1.7

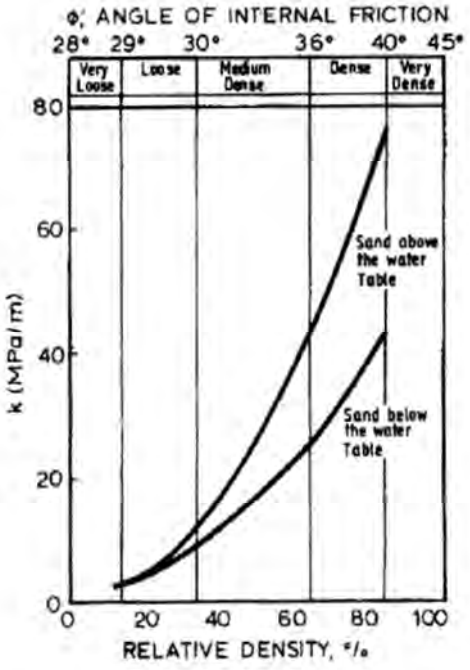

Figure 1.7: variation of k with φ' [8].

The method is based on the concept of ultimate soil resistance, p_u. The formulation of p_u given in the present API originates from the research report by O'Neill and Murchison who reviewed an article by Reese from 1962. In the formulation, two types of soil resistance are assumed to exist. Near the ground surface and in moderate depths a passive wedge develops to resist the lateral movement of the pile, and in greater depths the soil moves horizontally around the pile. The two formulas are referred to wedge failure mechanism and flow failure mechanism.

$$p_u = \min \begin{cases} (C_1 z + C_2 D)\gamma' z \\ C_3 D \gamma' z \end{cases}$$

where

C_1, C_2: coefficients determined from considerations on wedge failure

C_3: coefficient determined from considerations on flow failure

D: diameter of the pile

γ': effective weight of the soil

z: depth of the point considered

C_1, C_2, C_3 can be determined from Figure 1.8 to simplify the calculation of the p-y curves or from the analytical formulas according to the type of failure, reported in the next paragraphs.

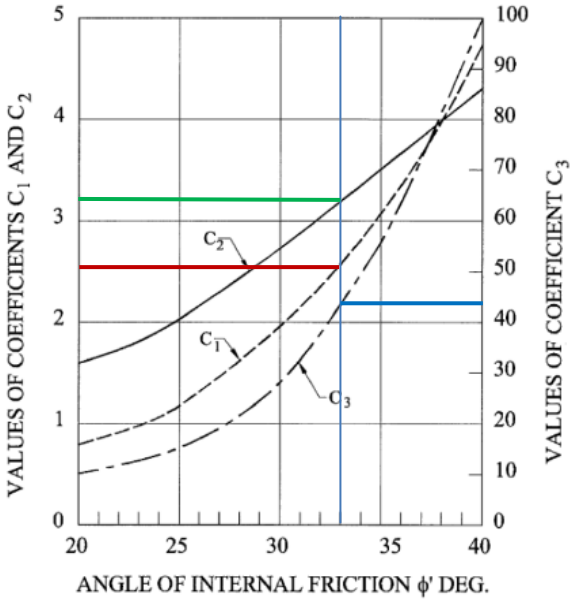

Figure 1.8: values of coefficients C1,C2,C3 according to φ'[1]

- **wedge failure**

For moderate depth and close to the ground surface a failure wedge is supposed to occur when the maximum capacity of the soil is achieved, and the ultimate resistance of the soil is then computed from this wedge. The assumed failure wedge is shown in Figure 1.9.

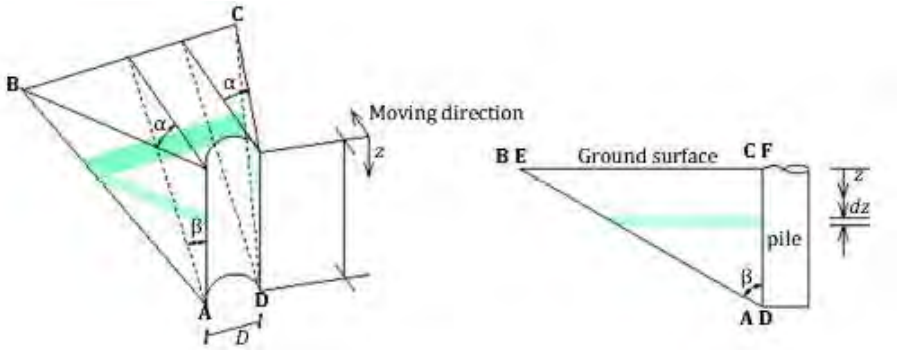

Figure 1.9: assumed failure wedge [5].The differential area is marked in green.

In wedge failure a mass of sand shaped as a wedge is pushed in front of the pile hence the planes ABC, DEF and ABED are failure planes and the Mohr-Coulomb failure criterion is used [5].

$$C_1 = \frac{K_0 \tan\varphi \sin\beta}{\tan(\beta-\varphi)\cos\alpha} + \frac{\tan^2\beta \tan\alpha}{\tan(\beta-\varphi)} + K_0 \tan\beta(\tan\varphi\sin\beta - \tan\alpha)$$

$$C_2 = \frac{\tan\beta}{\tan(\beta-\varphi)} - \tan^2(45° - \alpha)$$

- **flow failure**

For some depth below the surface, the soil moves horizontally around the pile instead of moving upwards following the wedge mechanism. This type of failure is referred to as flow failure, see Figure 1.10.

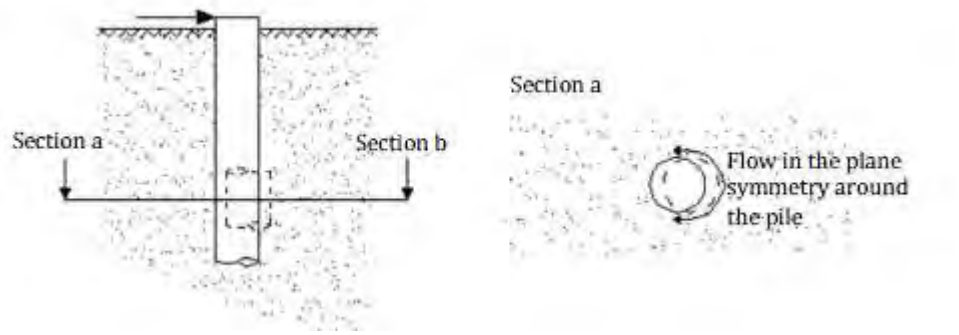

Figure 1.10: flow failure [5]

In this case C_3 is computed as

$$C_3 = 0.4 tan\varphi tan^4\beta + tan^2(45° - \alpha) tan^8\beta$$

The nonlinear method considered is the lateral force deflection (p-y) approach. It accounts that the soil stiffness parameter k_h (subgrade reaction) is not constant and there is a non-linear relationship between the soil resistance and its displacement (equal to the pile deflection). The nonlinear differential equations considering deformed configurations are given by the following formula:

$$E_p I_p \frac{\mathrm{d}^4\mathrm{y}}{\mathrm{d}^4\mathrm{z}} + \mathrm{pD} = 0$$

They are solved applying the finite difference numerical technique. For each set of applied boundary loads, an iterative solution is needed which satisfies the static equilibrium and achieves compatibility between force and deflection in every element. Since the analysis is based on an iterative procedure, it is necessary to use a computer program to achieve a sufficient number of iteration and have a reliable solution .

In this study **D-PILE GROUP** software has been used, setting from the beginning Cap method option which models a nonlinear behavior of the soil.

D-PILE GROUP

D-PILE GROUP (formerly known as MPile) enables the analysis of the three-dimensional behavior of single piles and pile groups. D-PILE GROUP describes the relation between pile and surrounding soil by the use of lateral and axial vertical soil springs along the piles. The program provides several calculation models, which mainly are *Poulus model*, where linear soil behavior is considered and *Cap model*, in which the nonlinear soil response is examined. In this case of study the model adopted is *Cap model*, for which D-PILE GROUP determines the nonlinear relation between the force and displacement on basis of a design rule which can be selected by the user (e.g. API or NEN Dutch standard) [7]. Cap model is based on p-y curve, but it does not account pile-soil-pile interaction.

This program uses the finite element method to study the pile behavior and the stiffness matrix analysis method for the soil behavior. First, the pile is discretized into a number of one-dimensional (beam) elements. From structural analysis, the stiffness relation can be written for a free pile element. The solution of the n equations corresponding to the pile discretization gives the deflection of the pile at each depth. If the pile is assumed to be a beam on an elastic foundation, then the modulus of lateral subgrade reaction k_h at any depth can be related to the lateral pile deflection at that depth. Hence the spring stiffness can be expressed as the modulus of lateral subgrade reaction k_h [3]. If the soil behavior is considered nonlinear then the computer code begins with an arbitrary set of values for k_h and solves for a set of deflections along the length of the pile. The p-y curves are employed and new values of k_h are obtained and a new set of y-values is computed. The new values of y are

compared with the previous set and the solution continues until convergence occurs where all values of y for the present computation are within a given tolerance of the values of y in the just previous solution. The tolerance is set at a very small value of deflection to ensure an accurate solution of the difference equations [2].

The program interface requires standard soil parameters for each layer, which are distinguished between soil type (sand and clay) and load type (drained, undrained and cyclic).

1.2 Finite Element Modelling

Numerical methods have been used form the 90's to solve complex problems and investigate phiscal phenomena. In this paragraph the basic of the Finite Element Method is explained and then a brief overview of the past numerical models regarding Lateral loaded piles is presented. [8]

1.2.1 Basics and history of the Finite Element Method

Finite element models are based on the Principle of Virtual Displacement and in this chapter is shown the derivation of the general formulation FEM from the PVD.

A three dimensional body that models the structure to analyse is defined in a global coordinated system XYZ. (See Figure 1.11)

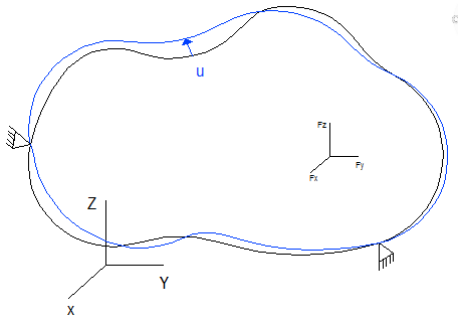

Figure1.11: sketch 3D body

It is subjected to a set of forces and is properly constrained with different type of supports. The set of forces is made by: body forces per unit volume f^B(including also dynamic forces) , distributed surface forces f^S(as water pressure) and concentrated surface forces F^I at point i ; all the forces have components in the three directions of the global coordinate system.

The unknown of the problem are global displacements U, strains ε and stresses σ of the structure, all function of a global reference system XYZ.

The principle of virtual displacements states that, given a virtual displacement that satisfied the Boundary conditions imposed by the constrains, the external work computed by the set of forces is equal to the internal work of the body.

$$\int_v \varepsilon^T \sigma dV = \int_V U^T f^B dV + \int_S U^{ST} f^s dS + \sum U^i F^i$$

In finite element analysis, the structure is idealized as an assemblage of element and the displacements of structure will be express in terms of the displacements of the elements in order to invoke the Principle of Virtual Displacement.

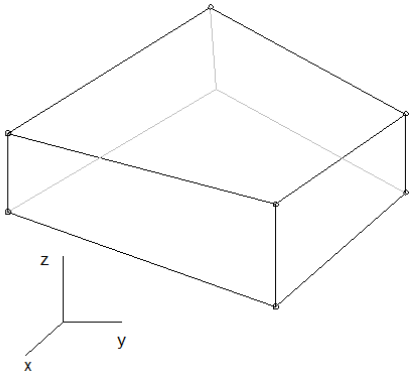

Figure1.12: example of Brick element

To be more general Brick element (8 nodes) are chosen in this explanation (Figure 1.12). If displacement of each Brick element is a function of the nodal point displacement expressed in terms of local coordinate system (xyz), then also the displacement of the structure is a function of the nodal point displacement.

Now to pass from the local coordinate system to the global one, the major assumption of the finite element discretization is considered. For every element m:

$$u^m = H^m \widehat{U}$$

The displacement of element m in the local coordinate system (u^m) is equal to the displacement interpolation matrix, function of the local system,(H^m) times all the nodal point displacements that occur in the finite element discretization ($\widehat{U}$).

From the finite element assumption the strain and the stresses in element m can be derived:

$$\varepsilon^m = B^m \widehat{U} \text{Compatibility condition}$$

$$\sigma^m = C^m \varepsilon^m + \sigma_o^m \text{Stress} - \text{strain low}$$

where: B^m: strain interpolation matrix (derived differentiating the rows of matrix H^m)

C^m: stress strain matrix (dependent on the material)

σ_o^m: initial stress

Beside the Compatibility condition and the stress-strain law, the last condition to be fulfilled in the Finite Element analysis is the equilibrium. The Equilibrium condition is embodied in principle of virtual work.
Since the Principle of Virtual Displacement is applied at the finite element discretization and the differential equations of the equilibrium are solved numerically , the equilibrium conditions at element level is satisfied in an approximate way. But if the finite element discretization is appropriate(means convergence is satisfied), encasing the number of elements, the approximate solution converges to the real one.
The first step is to rewrite the principle of virtual displacement as sum of integration over the elements and then the assumption of finite element discretization, the compatibility condition and the stain law are substituted. It means that the principle of virtual displacement is rewritten in terms of nodal point displacement and interpolation matrixes and it satisfied the boundary conditions.[9]
The solution of the problem is found solving the system of matrixes based on the principal for virtual displacements n times, every time reaching a more accurate solution. The iterative procedure and the dimension of the matrixes require the use of computer programs as Abaqus.

1.2.1Numerical modelling of laterally loaded piles

Three dimensional finite element modelling can be used to predict the lateral pile response. The more relevant studies dealing with this computational approach are analysed in this paragraph. First of all a finite element model should[10]:

- Replicate as precisely as possible the response of the upper soil, i.e. upward bulging in front of the pile and gap backward.
- Account non linear stress-strain soil behaviour.

The earliest studies, conducted by Dan A. Brown and Chine-FengShiein the 90's [11, 12], analyzed the response of a flexible pile, and demonstrating the impact of the before mentioned assumptions on a accurate 3D FE model.
The analysis conducted in the first study [11] includes gap formation and plastic deformation of the soil around the pile. A solid pile with modify stiffness is used to model an equivalent hollow pile. Von Mises and Drucker-Prager soil models are considered and frictional interface elements provide for slippage at the interface and gap formation. Results of this study indicate deformation patterns and development of areas of plastic deformation around the pile , moreover p-y curves are produced from the reduction of bending moment data.
In the second study [12] a similar model (Figure 1.13) was used to investigate several factors on p-y curves

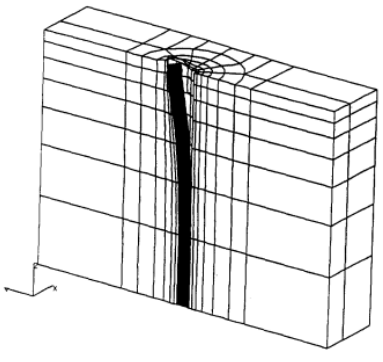

Figure 1.13: View of the 3D mesh with pile dipalced laterally [10]

derived from the model. The importance of appropriate simulation of contact between the pile and the soil was highlighted by examining the effect of different interface properties along the pile on computed p –y curves .
Few years after, King G. J. W. and Laman M. start to adopt FE modeling to calibrate and predict centrifuge tests [13]. In this study 3D finite element analysis are carried out using different linear and non linear programs and also using a linear axi-symetric program. Linear three dimensional programs seems fit more to the centrifuge tests.

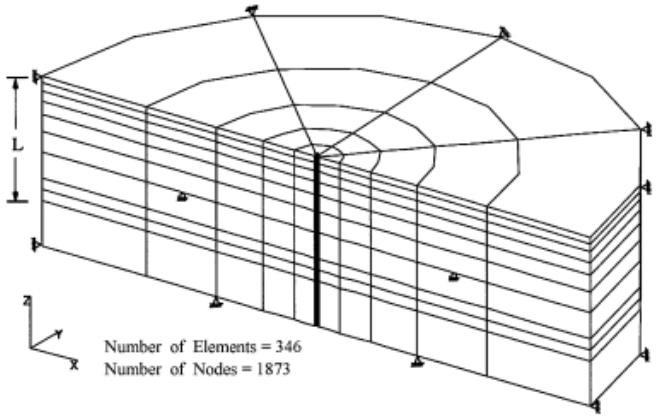

Figure 1.14:3D FE mesh used to analyse a pile subjected to lateral load [13]

The 3D FE Model developed by Chia-Cheng Fan and James H. Long [14], accounts for elastic-plastic sand behavior,slippage along the pile but not debonding, hence gap formulation was not modeled. The piles are modeled as linear elastic materials and the mesh used to analyze a pile subjected to lateral load is shown in Figure 1.14 . The computed load displacement curves fit well with the on site measured data, validating thus the accuracy of the modeling procedure. The effect of the pile stiffness on the p-y curves was not found significant, while the ultimate soil resistance was found to be strongly related to the coefficient of horizontal earthpressure and the soil dilatancy. The comparison between the ultimate soil resistance calculated numerically and the corresponding estimated applying of analytical procedures [2, 3,4], demonstrates that Hansen's method provides reasonable results.

The recent study of V. Zania and O. Hededal [16] the lateral capacity of three dimensional numerical models of 2m diameter rigid piles embedded in cohesionless soil is estimated using the software Abaqus. Both pile and soil are discretized with3D 20 nodes continuum elements, the dimension and the mesh of the Finite Element model are shown in Figure 1.15. The potential variability of the friction properties along the perimeter of the pile is considered changing the interface friction angle. This study shows that the interface properties affect the ultimate soil resistance and the stiffness of the soil pile response, while the effect of the pile stiffness (EI) in the lateral capacity of the pile and in the p-y curves results negligible for rigid piles.

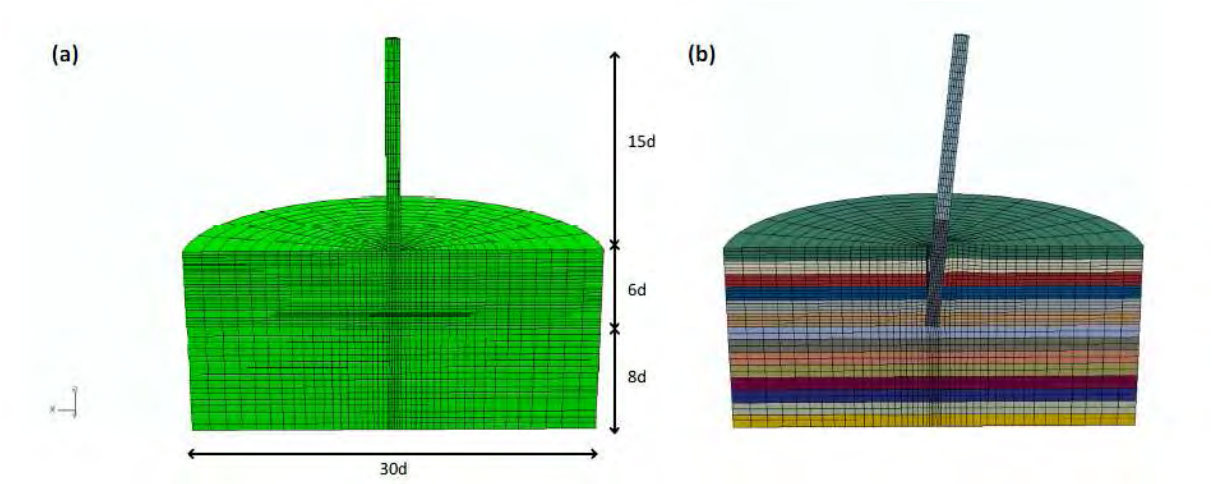

Figure 1.15: Finite element model developed and typical defomation pattern [16]

After the short review the following drawbacks regarding the lateral response of monopiles have been observed:

• ultimate soil resistance usually neglects the contribution of side shear resistance

• the p – y curves for cohesionless soils have been calibrated to the response of flexible piles modeled as rigid piles with equivalent stiffness, hence their validity for rigid and flexible piles is questionable

• 3D FE models of rigid piles have been studied reentry [16] and the procedure adopted is used in this thesis as guide line.

The current study aims at investigating the lateral response of rigid and flexible monopiles in cohesionless soil subject to load with high eccentricity. Hence advanced 3D FE models were developed and the soil nonlinearity, the pile type, and the geometric nonlinearity induced by sliding along the soil – pile interface and gap formation are taken into account. The effects of pile stiffness and soil properties are analyzed.

The generated failure mechanism resembles closely to the one reported in the literature. The lateral bearing capacity in the different type of piles is analyzed and compared with Broms' theory. The calculated pressure distribution, ultimate soil resistance and the generated p – y curves are matched to the corresponding proposed in the literature for rigid piles embedded in cohesionless soil (API curves).

1 Methodology

Since the objective of this thesis is to simulate the lab tests computed in the centrifuge using Finite Element Modelling, the first step is analysing the setup of the experiments to recreate it in the software Abaqus as close as possible.
In the experiments there are two phases: installation of the pile and application of lateral load. An effective procedure to model the installation phase in the numerical model for the flexible piles has been studied using a simplified problem; but the solution found was not applicable. Due to numerical problems the solution for the problem was giving not reliable solution in terms of contact pressure as it is shown in appendix 3. For this reason it have been chose to model just the second phase of the experiments.

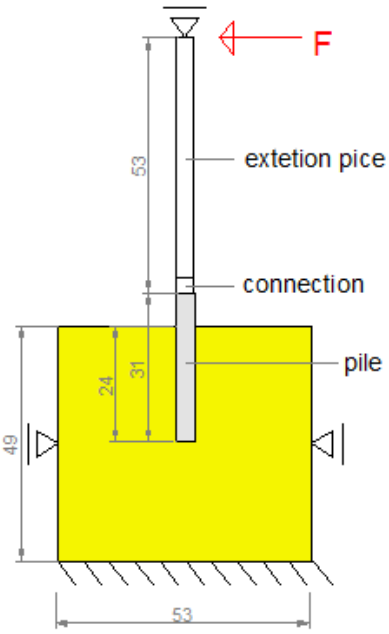

In order to investigate the lateral response of piles due to horizontal applied load with large eccentricity, 3D finite element models are developed. The selected pile diameter is 4 cm, the same of the lab tests which corresponds to a prototype diameter of 1m, reassembly the foundation of offshore platforms and wind turbines. The static schemeand the dimensionsof the soil-pile system that have been modelled in according to the lab conditions are represented in Figure 2.1.The embedment depth of the pile is 6 diameters (24cm) and the eccentricity of the lateral force is equal to 15 times the diameter. The dimension of the soil are the same of the barrel that contains the sand during the experiments

Figure1.1: Sketch 2D of the problem, measures in centimeters

1.2 Finite element modelling

Three 3D finite element models have been developed, one for each type of pile.
Hereafter all the features of the model for the rigid pile are explained in details; the models for the flexible piles are slightly different and the variations are reported below.

1.2.1 Laterally loaded rigid pile

In this paragraph the model of the rigid pile is described in terms of geometry, mesh discretization, material properties, load steps, boundary conditions, contact formulation.
The symmetry of the problem allows to take into account just half of the cylindrical pile and the corresponding surrounding soil.

Material Properties

In the model there are two materials the sand of the soil and the steel of the pile.
The properties of the steel are listed in Table 2.1; however two materials for the pile with different young modulus are created to simulate different cross-sections as it is explained in the next paragraph.
The soil material is medium-dense sand whose properties are in according to the lab test [1] and to the recent study on the effect of interface behaviour on laterally loaded rigid piles with FEM [16].
Since the unit weight of the sand sample in the 6 tests was respectively:16.37,17.03,16.32,15.93,16.7,16.39 kN/m^3[1], an average value of density has been chosen equal to 1.7 tn/m^3.
The strength of the soil is assumed to be constant along the pile depth and a Mohr-Culomb failure envelope characterized by angle of friction (φ) equal to 33° and a cohesion (c) equal to 6 kPa are selected in according to the results of the triaxial test performed on the lab sand [17].The graph in Figure 2.2 is used to estimate Young Modulus and the dilation angle, but note that it is referred to another cohesion coefficient, thus the values cannot be taken directly from the graph.

		Soil	Pile
Density	**ρ [tn/m^3]**	1.7	7.8
Elasticbehaviour			
Young Modulus	**E [kPa]**	60 000	209 000 000
Poisson ratio		0.3	0.3
MohrCulombPlasticity			
Friction Angle	**ϕ**	33°	
Dailation Angle	**ψ**	8°	
Cohesion	**c [kPa]**	6	

Table 2.1: Materials Properties

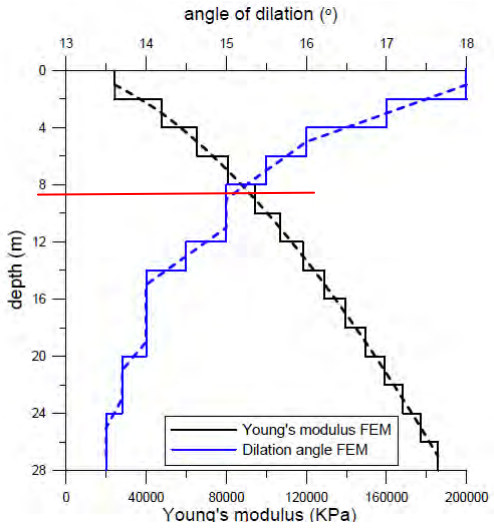

Figure 2.2: Variation of Young Modulus and dilation angle respect to depth [16] for φ= 33° and c = 3.5 kPa

Geometry

The model is made of 2 parts: pile and soil both created with solid elements in the rigid pile.

The part "pile" includes the rigid pile itself, the connection and extension piece. For the rigid pile the connection is identical to the extension piece. To simplify the calculation, just one part has been created for all these elements but a partition subdivides into section with different stiffness (see figure 2.2). The real geometry of the elements is shown in figures 2.3 and 2.4, in Abaqus it is used just the solid pile geometry and an equivalent Young Modulus is set for the extension piece in order to have the same stiffness of the real one.

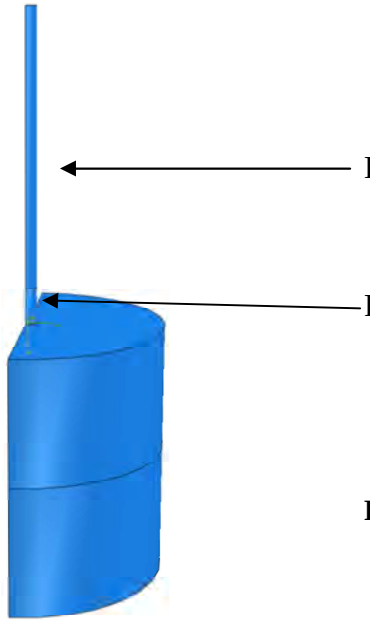

Figure 2.2: Geometry of the rigid pile model

Section 1: solidpile (0-31 cm)

- Moment of inertia $I = \frac{\pi D^4}{64} = 1.26 \cdot 10^{-7} m^4$
- Young Modulus E=209 000000kPa

Figure 2.3: real geometry of solid pile

Section 2: extension piece (0.31-0.84 cm)

- Moment of inertia $I = \frac{\pi D^4}{64} = 1.26 \cdot 10^{-7} m^4$ (calculated by Abaqus)
- Real moment of inertia $I_r = \frac{\pi (De^4 - Di^4)}{64} = 3.21 \cdot 10^{-8} m^4$
- Equivalent young Modulus $E_{eq} = \frac{E \cdot I_r}{I} = 53\ 48\ 200\ kPa$

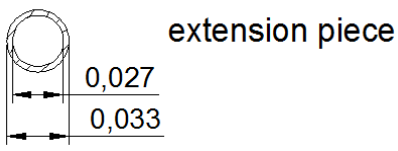

Figure 2.3: real geometry of extension piece

The equivalent Young Modulus in section 2 is adopted to obtain the real stiffness with an inaccurate geometry (of a full extension piece instead of a hollow smaller element).

Since the installation phase is not modelled, the shape of the soil is already adapted to the pile structure (Figure 2.4). To have this shape in Abaqus, half cylinder of soil has been created and then it have been cut by the pile with the command “cut geometry” in the module Assembly. Than the partitions show is figure 2.4 are done otherwise it is not possible to mesh the soil.

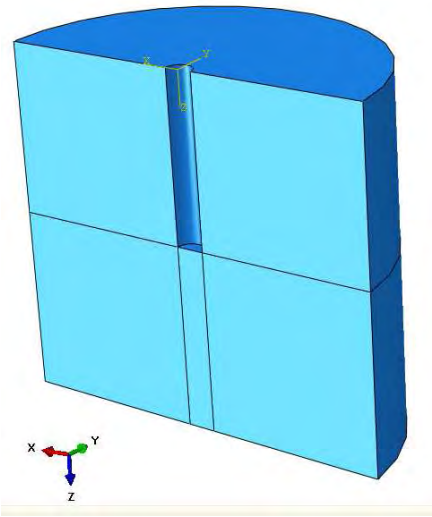

Figure 2.4:geometry of the part “soil”

Mesh discretization

Both pile and soil are discretized using 3D 20 nodes continuum elements (C3D20).It is set to have 12 elements along the pile circumference, this pair number helps in the calculation of the section moment along the depth of the pile (see appendix I). The element size of the soil close to the pile is approximately 0.003x0.003x0.009m (x,y,z) and it increase gradually to the borders (Figure 2.5). The element size of pile is the same in the 31 cm close to the soil (rigid pile part) and the height of the elements is double in the rest (connection and extension piece).

A more refine mesh adjacent to the interface soil-pile help to calculate precisely the contact algorithm and the solution of the mathematical equations that find the equilibrium of the problem; hence to calculate as accurately as possible the distribution of the normal and shear stresses along the perimeter. On the other hand the number of elements of the system pile-soil cannot be too high otherwise the time to solve the problem become too long, for this reason the element size is increased far from the interface pile-soil. [18]

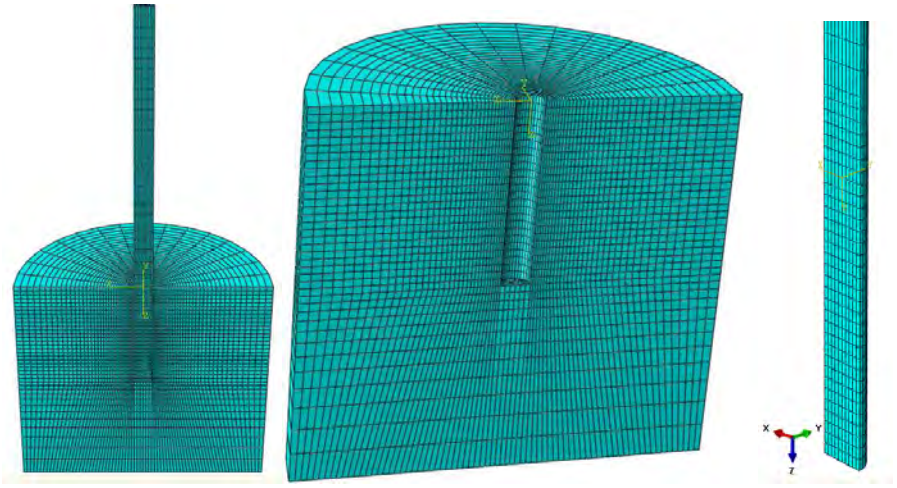

Figure 2.5: mesh discretization of the finite element model of the rigid pile

Load Step

It is chosen to adopt Abaqus Standard that applies Hiber-Hughes-Taylor operators in the computation instead of Abaqus Explicit because, even if is slower , it allows more functions and it better represent the contact formulation.[18]

The problem is divided into 6 steps in order to facilitate the solution of the mathematical equations.

- Step 0 (initial step): the geostatic stress, the boundary conditions and the contact formulation are created.
- Step 1(geostatic equilibrium): the gravity 1g is applied at the soil (load 1) and this step permit Abaqus to check for the equilibrium between the geostatic stress and applied loads plusboundary conditions
- Step 1b(intermediate step): before the incense for gravity to accelerate the computation
- Step 1c (increase of gravity): the gravity on the soil (load 1) is increased to 25g and another force of 25g is applied on the pile (load 2)
- Step 2: application of half lateral force at the top of the pile (load 3)
- Step3: increase of the lateral load to the required value

Boundary conditions

The boundaries are placed along the border of the element soil to block the movement and simulate the barrel of the lab test. Since solid elements do not have rotational degree of freedom, rotation is prevent blocking displacement in all the nodes of the surface that is required to be fix.[1]

Moreover a hinge is placed at the top of the extension piece since in the lab the load cell is attached to the frame but is free to rotate in the force direction.

1.Encastre at base of the soil element

2. hinge at the lateral face of the soil element

3. hinge at top of the pile, it must be applied on two pints in the line perpendicular to the lateral force (Figure 2.6) otherwise the pile gets stuck at the top.

4. symmetry of half cylindrical pile and soil

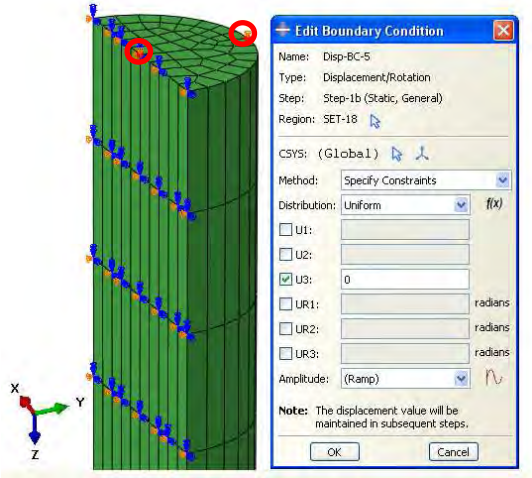

Figure 2.6: hinge at the top pile

Static Loads

The geostatic stress and three extra loads are applied in the system at different steps as it is explained later on.

The geostatic stress in the soil is an elevation-dependent initial stresses. When a geostatic stress state is prescribed for a particular element set, the stress in the vertical direction (assumed to be the *z*-direction in three-dimensional models) is assumed to vary piecewise linearly with this vertical coordinate and the displacement remains zero [18] (see Figure 2.7).

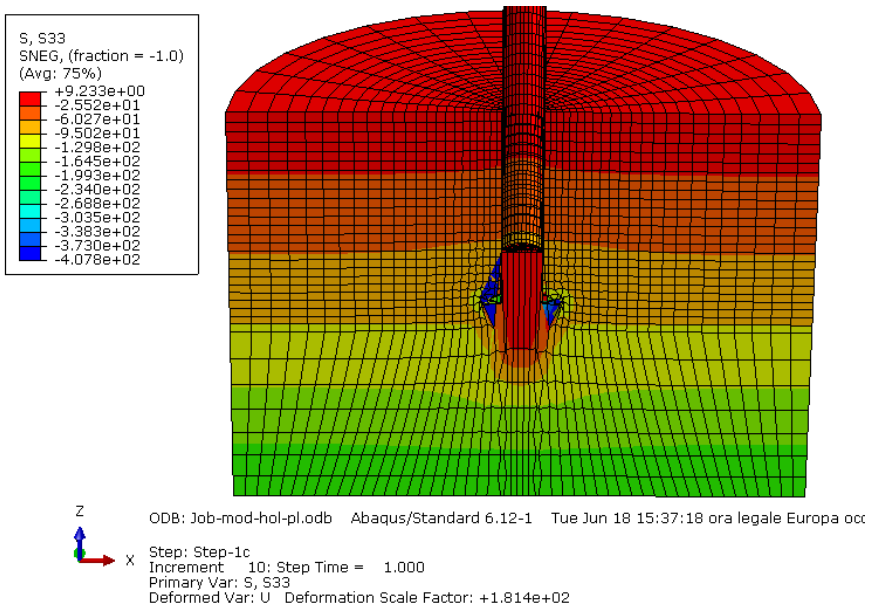

Figure 2.7: stress in the vertical direction S33 in the soil part

For the vertical stress component, two pairs of stress and elevation values are given to define the stress throughout the element set. For material points lying between the two elevations given, Abaqus will use linear interpolation to determine the initial stress; for points lying outside the two elevations given, Abaqus will use linear extrapolation. In addition, horizontal (lateral in x and y direction) stress components are given by entering one or two "coefficients of lateral stress," which define the lateral direct stress components as the vertical stress at the point multiplied by the value of the coefficient. The values of the stresses are calculated with the following formulas and the input of the program are shown in Table 2.2.

Predinedfield		
σ_v1	0	kPa
z1	0	m
σ_v2	-3.05	kPa
z2	0.49	m
Ko	0.428	

Table 2.2: parameters for the predifinied field

Vertical stress: $\sigma_v = \gamma \cdot z = \rho \cdot g \cdot z$

Horizontal stress: $\sigma_h = K_o \sigma_v$

where K_o: coefficient of vertical stress→ $K_o = \frac{\nu}{1-\nu} = \frac{0.3}{1-0.3} = 0.428$

The other loads in the FE Model are the gravity and the lateral force.

Load 1 is the gravity load applied on the soil. It is set in the first steps equal to g=9.81m/s^2 in order to equilibrate the geostatic stress and have zero deformations; than it increase to 25g=245.25m/s^2.

Load 2 is the gravity applied at the pile equal to 25g in the second steps of the calculation.

The gravity is set 25g during the lateral load application to simulate the lab test where the gravity is increased with a centrifuge to study the behavior of prototype pile of 1m diameter.

Load 3 is the lateral force at the top of the extension piece. It is a point load applied on the highest right node of the pile (extension piece). At first the intensity is 0.45kN and in the next step it increase to 0.9kN, this procedure is done in order to ensure the achievement of solution.

Contact Formulation

A contact formulation is assigned along the perimeter of the pile , in order to model the soil-pile interaction.
The contact algorithm to establish between soil and pile is very important because if it is not appropriate, it can create problems to the solution of the model.
Between the lateral face of the pile and the soil it is chosen a contact pair algorithm instead of a general contact. Both of them are based on surface definition, contact interaction, surface properties and mechanical properties. Even if the general contact has a simplified definition, the contact pair is selected because is more specific for this problem.

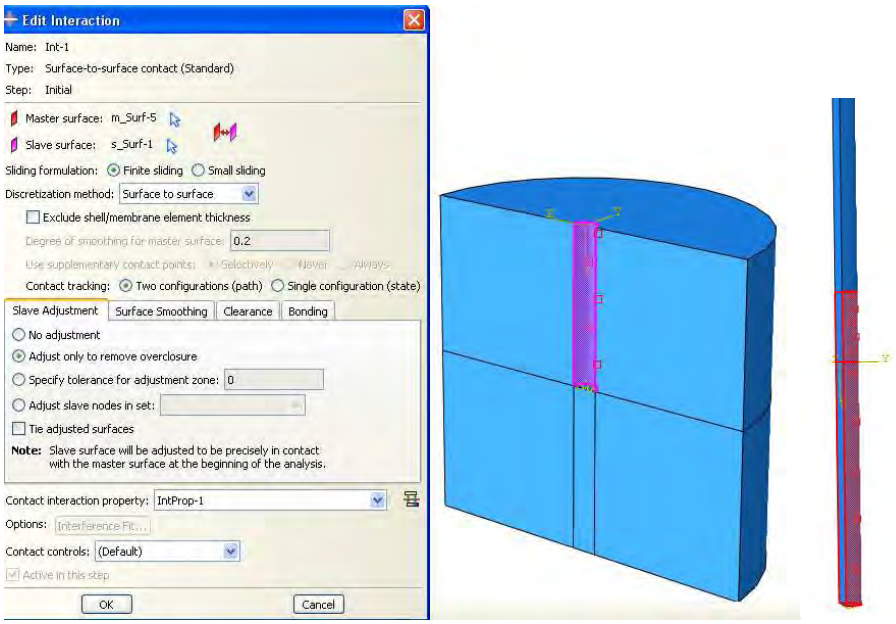

Figure 2.8: surface involved in the Contact formulation

The two surface for the interaction are highlighted in Figure 2.8, the master surface(red) is the pile one and the slave surface (purple) is the soil one. The type of interaction is surface-to surface with finite sliding formulation and the slave surface is adjusted to remove overclosure. The shear behaviour is assumed to follow the Coulomb friction law. Therefore in Abaqus, it sets, in the interaction property , a Tangential Behaviour with penalty friction formulation whose friction coefficient is equal to:

$$tg\delta = tg\left(\frac{2}{3}\varphi\right) = 0.4329$$

The normal behaviour is considered rigid-plastic permitting thus zero tensional stresses and zero elastic deformation normal to the surface. So it is included a Normal Behaviour with hard contact that allows separation after the contact of the nodes.
Between the base of the pile and the soil a tie constrain is established. The master surface is always the pile because is more rigid.

In order to study soil and interface properties, the simulation have been run three times.
The first one with properties listed before that are assumed as the reference one.
Then the interface soil friction coefficient have been increased from $tg\left(\frac{2}{3}\varphi\right)$ =0.44329 to $tg(\varphi)$ =0.649. The interface friction angle depends on the shape and the characteristic of the elements in contact, usually for concrete walls foundation in ground it is used $\frac{2}{3}\varphi$ and when the interface is between element of the same material it is used φ. It means that an interface soil friction coefficient equal to $tg(\varphi)$ is an extreme values that shows how this parameter effect the results.
The model has been run with an angle of fiction φ equal to 36° instead of 33°.

1.2.2 Laterally loaded flexible pile

The model for flexible piles is very similar to the one for the rigid pile. The main difference is that the piles are made of shell elements and the other differences regard the geometry and mesh discretization.
There are two different flexible piles: the hollow unplugged pile and the hollow plugged pile.

Geometry

The flexible piles are hollow piles with a thickness of 15mm (0.0015m) and the same length of the rigid pile.

They are made in Abaqus of three sections with different stiffness but same geometry. The real geometries are shown in Figures 2.9 and 2.10

Section 1: pile (0-31 cm)

- Moment of inertia $I = \frac{\pi\,(D_e{}^4 - D_i{}^4)}{64} = 1.78 \cdot 10^{-8} m^4$
- Young Modulus E=209 000 000 kPa

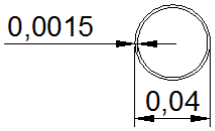

hollow pile

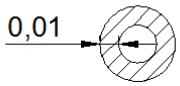

connection

Section 2: connection (31-34cm)

- Real moment of inertia $I_r = \frac{\pi\,(De^4 - Di^4)}{64} = 8.59 \cdot 10^{-8} m^4$
- Equivalent young Modulus $E_{eq} = \frac{E \cdot I_r}{I}$=220080000kPa

Figure 2.9: real geometry of pile and connection .

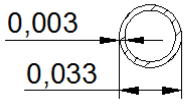

extension piece

Section 3: extension piece (0.34-0.84 cm)

- Real moment of inertia $I_r = \frac{\pi\,(De^4 - Di^4)}{64} = 3.37 \cdot 10^{-8} m^4$
- Equivalent young Modulus $E_{eq} = \frac{E \cdot I_r}{I}$ =131962000kPa

Figure 2.9: real geometry of extension piece

The unplugged pile has the soil also inside the pile because from the experiments it is known that the soil flows into the pile without the formation of soil plug.(Figure 2.10 a)
The plugged pile is a cylindrical shell element tied with a circular steel plate created using shell elements. In the plugged pile the soil cannot flow inside since there is a plug at the bottom. The connection between cylinder and plate is made by a tie constrain. (Figure 2.10b)

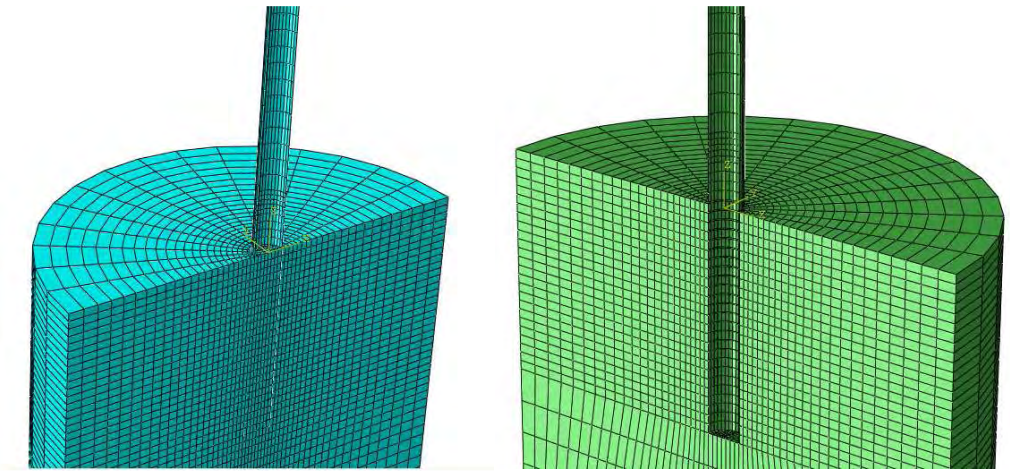

Figure 2.10: Finite Element Models of (a) unplugged and (b) plugged hollow piles

Since thin shell elements deform significantly in the surrounding of the load applied, the lateral force cannot be applied directly in one node of the pile. A Reference Point in the middle of the pile is created and it is connected with the pile trough a rigid body(Figure 2.11). This connection transmits equally the lateral force to the upper nodes of the pile and avoid a concentrated deformation of the pile in the application point of the force.

Figure 2.11: Application point of the lateral load

Mesh discretization

The flexible piles are discretised with 8 nodes shell elements with reduced integration (S8R). The mesh is made applying the same criteria of the rigid pile, starting from 12 elements for each circumference of the pile.
Also the models of the flexible piles are run adopting the reference soil properties and the increasing angle of friction and interface shear strength, in the same way it has been performed for the rigid pile.

2 Results of numerical investigation

In this chapter the results of the three numerical model are presented. Each model has been run applying the reference soil and then changing some soil parameters.
The parameters of the reference soil are shown in Table 2.1 of paragraph 2.1 and in particular the angle of friction is ϕ=33° and the interface shear strength δ=2/3ϕ. During the second run of each model the interface shear strength is increased to δ=ϕ while the angle of friction remains constant. In the last run the friction angle is increased to ϕ=36° while the interface shear strength remains δ=2/3ϕ. It has been chosen to change just one parameter per time in order to better understand the effects of this variation.

The graphs presented in this chapter are the following:

- Lateral Force – horizontal displacement at the top of the pile. The lateral force is applied at 15D= 57 cm from the sand surface and it increases with time until the maximum force is reached. The horizontal displacement is at 3 cm from the sand surface, this level has been defined because in the lab tests at the same position there is a displacement transducer. This type of graph shows when the ultimate Force is reach and how the young modulus changes increasing the force.
- Bending Moment –rotation at the top of the pile. The bending moment is obtained multiplying the Lateral Force by the eccentricity (0.57m). The rotation is obtained with the following formula:
- $r = \frac{y(3cm) - y(5cm)}{2cm}$ [rad]
- The point where the rotation is obtained is at 4 cm from the sand surface, a little bit below the top of the pile because at the same position is calculated the rotation from the lab tests.
- N.B. From the software Abaqus the output are in the nodes of the mesh (shown is chapter 2), hence the values of the deflection are not exactly at the required positions but in the closest node of the mesh. This approximation does not affect the reliability of the results.
- Moment distribution along the pile. The moment along the pile is obtained in according to the type of pile as it is explained in benchmark 1 and 2 . The moment distribution is plotted at different values of the lateral force.
- Plastic strain of the soil. It is an output of the softwer and it shows where the soil reach the yielding and how much it exceeds the deformation at the yielding. Figures of the soil are plotted at different values of the lateral force for the three type of pile in the reference soil.
- P-y curves.The deflection along the pile (y) is taken from nodes of the left side. The pressure is obtained by the second derivative of the moment distribution at each time instant. A polynomial interpolation of 6 degree has been fitted to each moment distribution corresponding a value of force. The 6th order equations of moments were

derived in 4 order equations and substituting the coordinate of pile depth, the pressure is established.

$$M(z) = c_1 z^6 + c_2 z^5 + c_3 z^4 + c_4 z^3 + c_5 z^2 + c_6 z + c_7$$

$$p(z) = \frac{\delta^2 M}{\delta z^2} = c_1 z^4 + c_2 z^3 + c_3 z^2 + c_4 z + c_5$$

From the p-y curves at different depth, the stiffenss kx and the ultimate soil strength are observed and compared with each other and with the API ones.

2.2 Laterally loaded flexible pile (unplugged)

The analytical methods explained in paragraph 1.1 establish a pressure distribution along the pile, by which all the other parameters depend. The assumption of the pressure distribution is based on the failure pattern within the soil. Hence, it is examined the failure mechanism after the analysis of the model for the unplugged pile under horizontal static load (see Figure 3.1). Figure 3.1 presents the minimum principal plastic strain that surrounds the pile within the soil when 0.45kN are applied at the top of the pile. Note that the force applied moves half of the system pile-soil, therefore to obtain the same effects to the whole system a double force is necessary.

The rainbow colours show the failure mechanism. A gap accrues at the back of the pile (left side), while at the left side the soil is sliding upwards along the soil-pile interface as the pile rotates and deflects. The deflection typical of flexible piles is more evident in Figure 3.1(b). The soil on back side of the pile in reality cannot form a vertical free standing edge because the sand should fill the gap at least until a certain depth. This approximation of the mathematical model is assumed to have a negligible impact on the results for monotonic load [15].

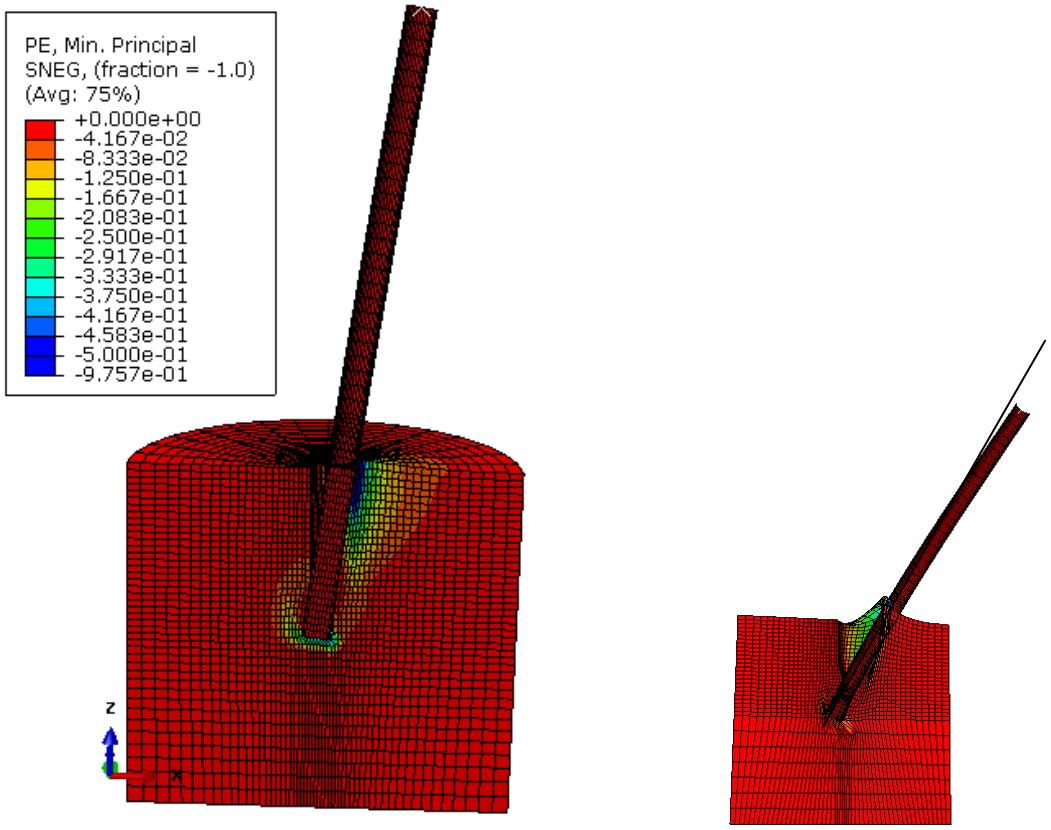

Figure 3.1: Plastic strain contours and failure pattern for hollow unplugged pile (a) real scale, (b) 1:4 scale

- Lateral force-horizontal displacement and Moment- rotation at the top of the pile

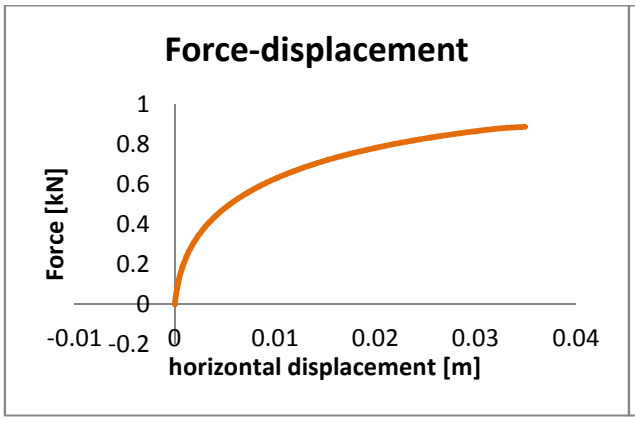

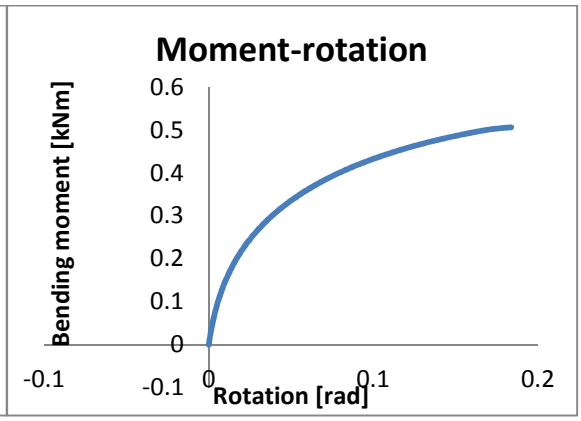

Figure 3.2: Force displacement curve in unplugged pile

Figure 3.3: Moment rotation curve in unplugged pile

The lateral force have an elastic behaviour just until 0.2kN, then the soil start to have plastic deformations. The maximum force is 0.89kN with a deflection 0.035 m. The ultimate force is not reached since the software killed the simulation when the soil is too distorted to compute the results, but it can be estimate not far from 0.9kN.

- Moment distribution along the pile (sand level 0.24m)

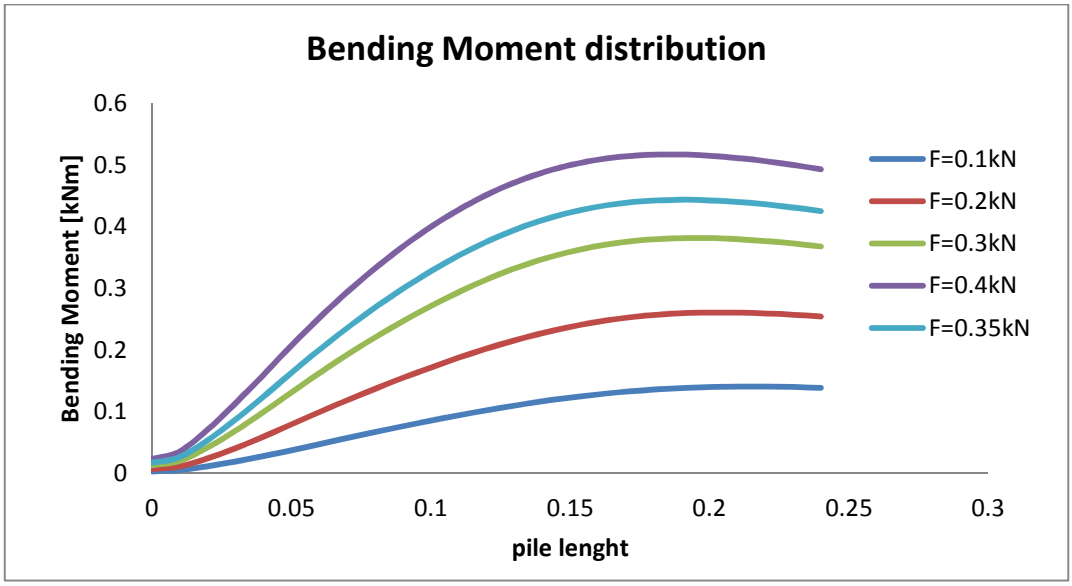

Figure 3.4: Bending moment distribution in unplugged pile

Bending moment is zero at the bottom of the pile (inside the sand) and it increase near the sand surface. For low forces the maximum value is at the sand surface, while after 0.3kN it moves gradually at ca. 6cm above the sand surface. It increase proportionally as the lateral force increase until approximately 0.5kNm, that is the same value obtained in the graph Moment rotation (Figure 3.3).For low values of forces (0.1kN,0.2kN) the soil does not reached the ultimate resistance since the force-displacement curve (figure3.2) is almost linear, and so the moment distribution follows the expected curve as if a linear elastic behaviour occurs [4].

- Plastic strain (PE min)

F=0.1kN

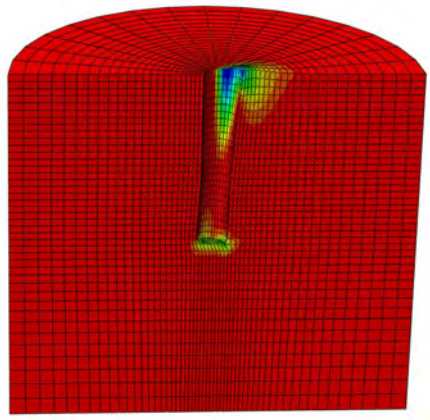

F=0.2kN

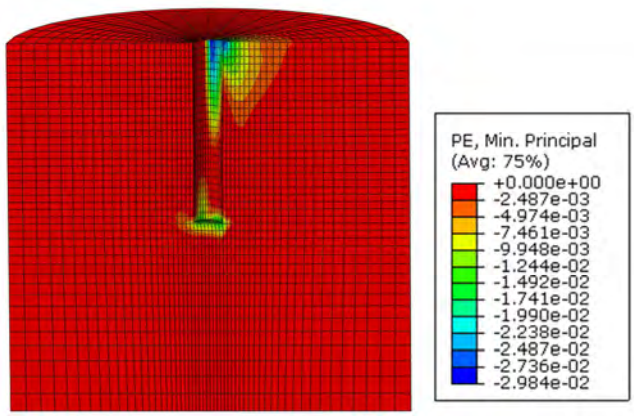

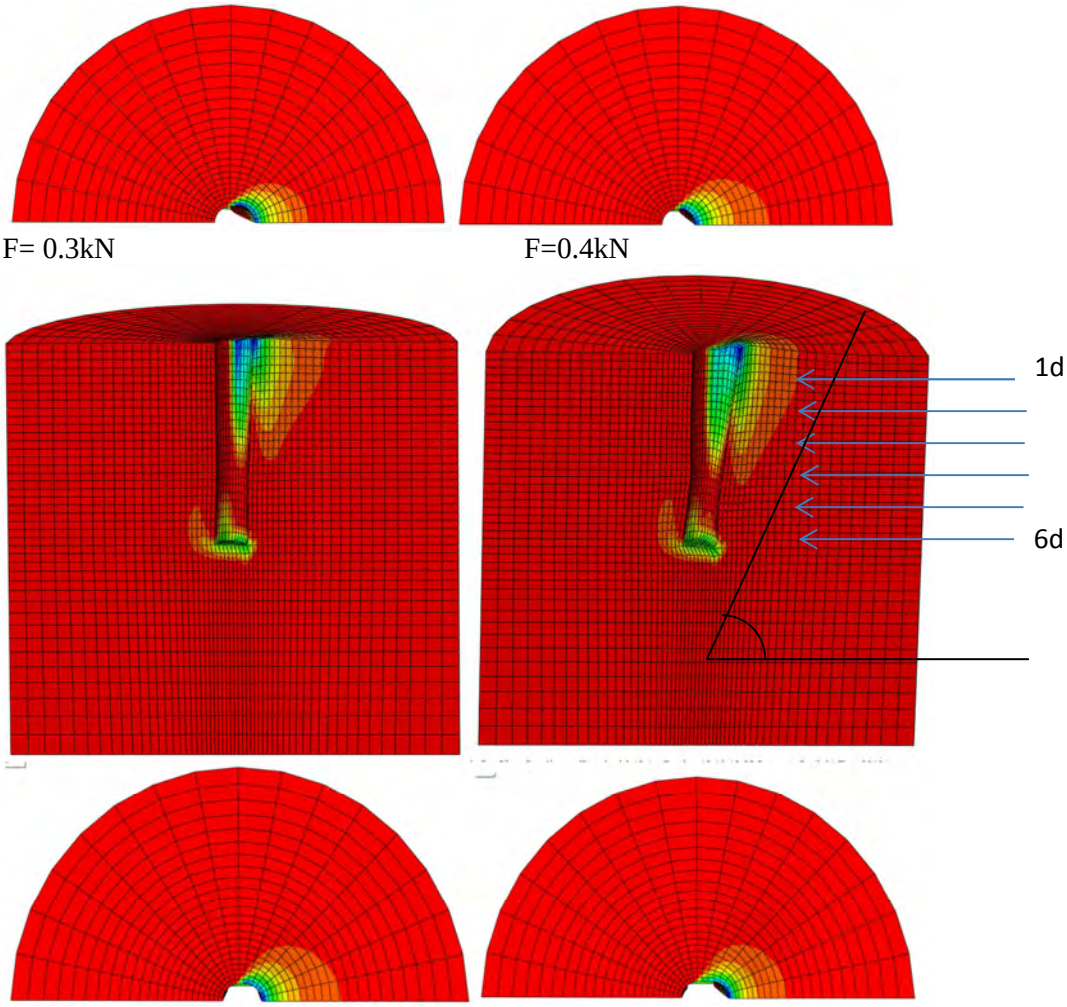

Figure 3.5: Plastic strain contours with increasing force in unplugged pile

The minimum principal plastic strain shows the failure pattern within the soil and the failure mechanisms. The wedge and flow failure for the soil are evident in this sketches and the p-y curves presented below are based on this mechanisms. Moreover from the figures it is evident at which soil level the failure is reached, that corresponds to the ultimate pressure in the p-y curves. For example at 0.4kN the failure is largely achieved at the depth of 1d and 2d while at 3d depth the pressure is near the ultimate value. Finally it is observed that the inclination of the failure wedge to the horizontal is approximately 60°, comparable with the theory 45°+φ/2.

- P-y curves at different depths

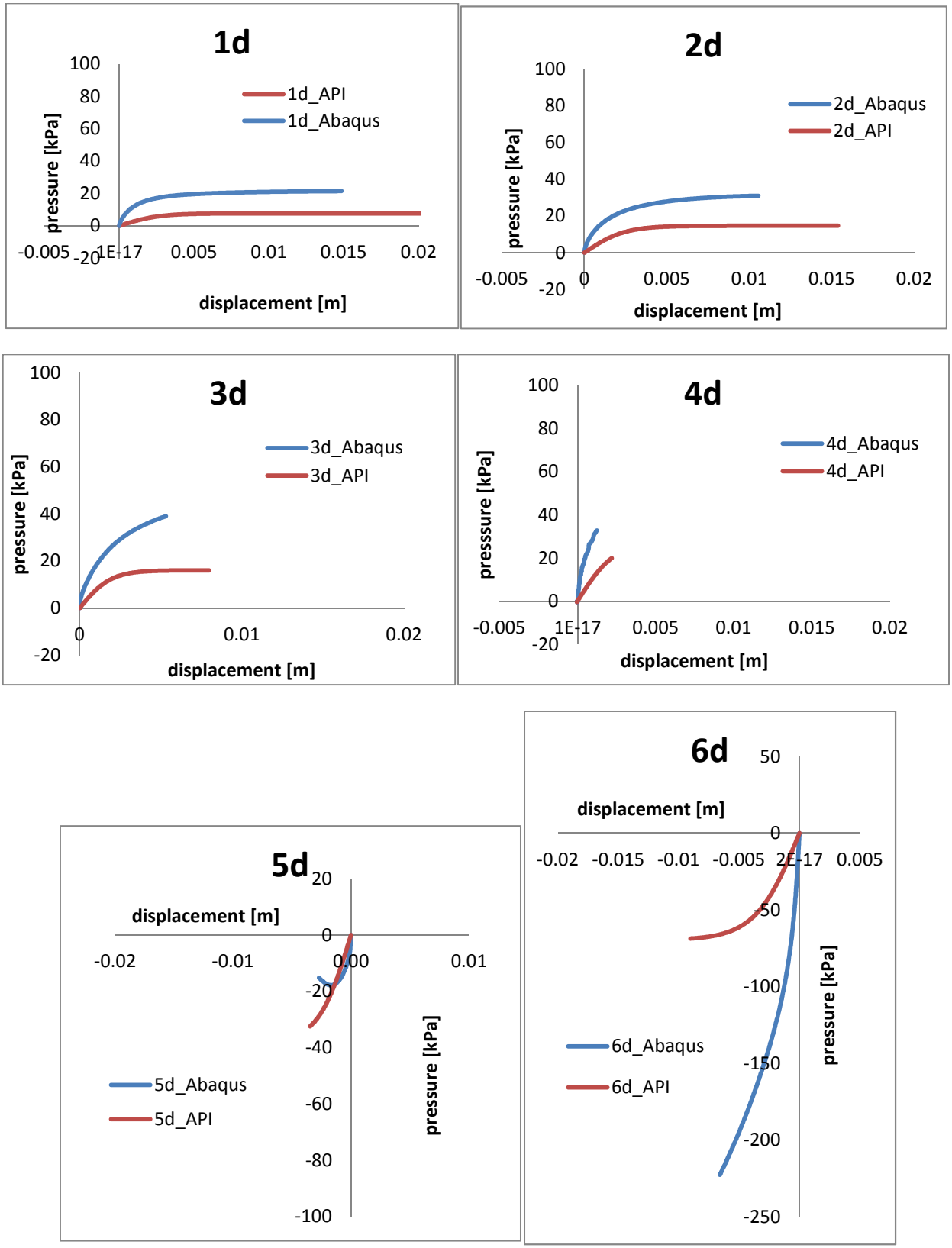

Figure 3.6: Comparison of p-y curves of unplugged pile with API [6] provision

The p-y curves obtained from the 3D numerical analysis (blue lines) exhibits a stiffness kx (initial inclination of the curve) that increases with depth of the pile. The ultimate soil resistance also rise up with the depth of the pile until 4d = 0.16m under the ground level and then it reaches negative values. Around 4d – 5d there should be the rotation point of the pile and it might cause the change of sign.

Increase of interface shear strength

The increment of interface shear strength does not change the failure mechanism of the system soil-pile but affects the lateral load capacity of the pile and the ultimate soil strength of the soil as figures 3.7 to 3.10 show.

- Lateral force-horizontal displacement curve and Moment- rotation curve at the top of the pile .

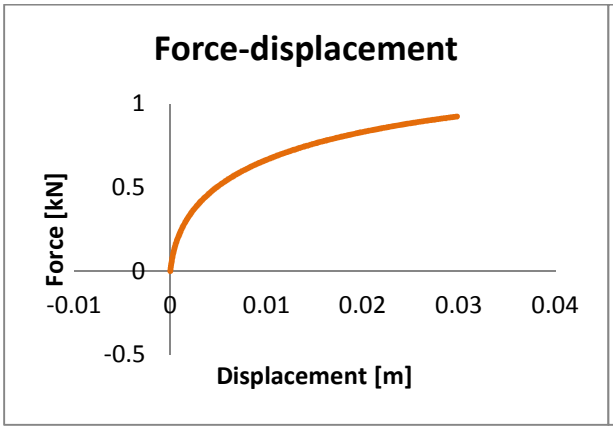

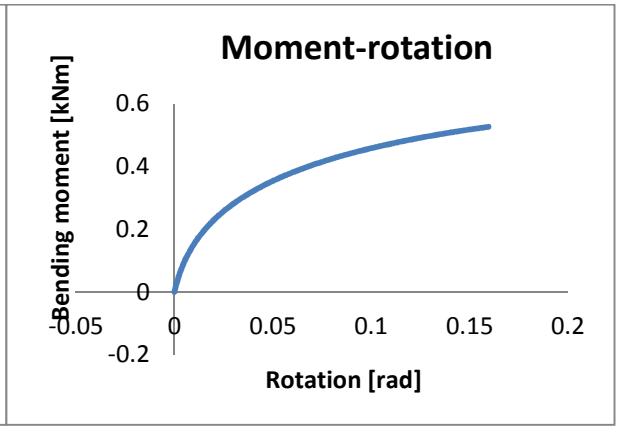

Figure 3.7: Force displacement curve in unplugged pile **Figure 3.8:**Moment rotation curve in unplugged pile

The ultimate force is not reached as in the reference soil but the same values of force produces a smaller displacement. The maximum force is 0.92kN corresponding to a deflection of 0.029m near the sand surface. The maximum moment 0.52kNm with a rotation of 0.16 rad (9.14°) is in the same position.

- Moment distribution along the pile (sand level 0.24m)

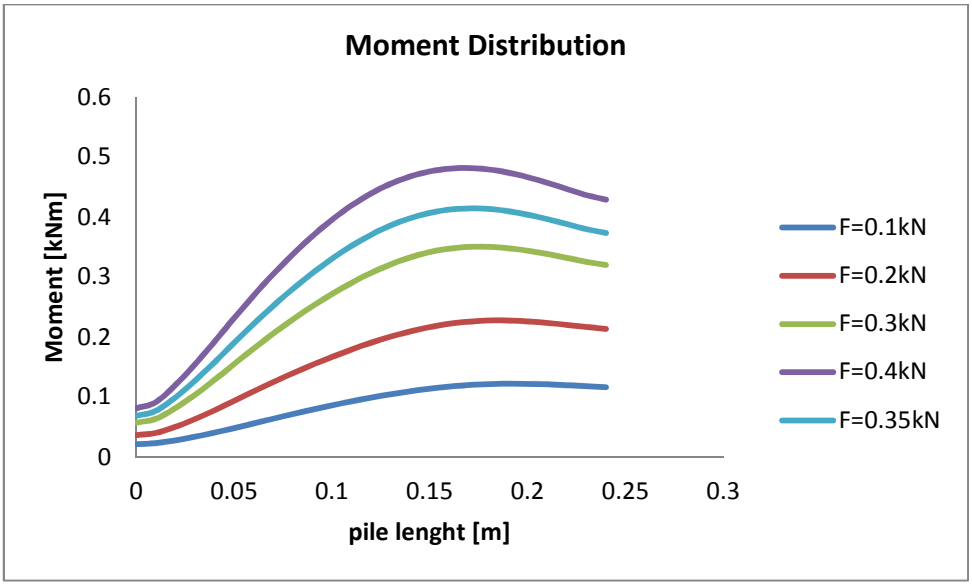

Figure 3.9: Bending moment distribution in unplugged pile

As in the reference soil, for low values of force the bending moment distribution is the one for elastic soil behaviour and the maximum moment is at the sand surface. Than for higher values of the lateral force the distribution varies and the maximum value moves gradually near the middle of the pile.

- P-y curves at different depth

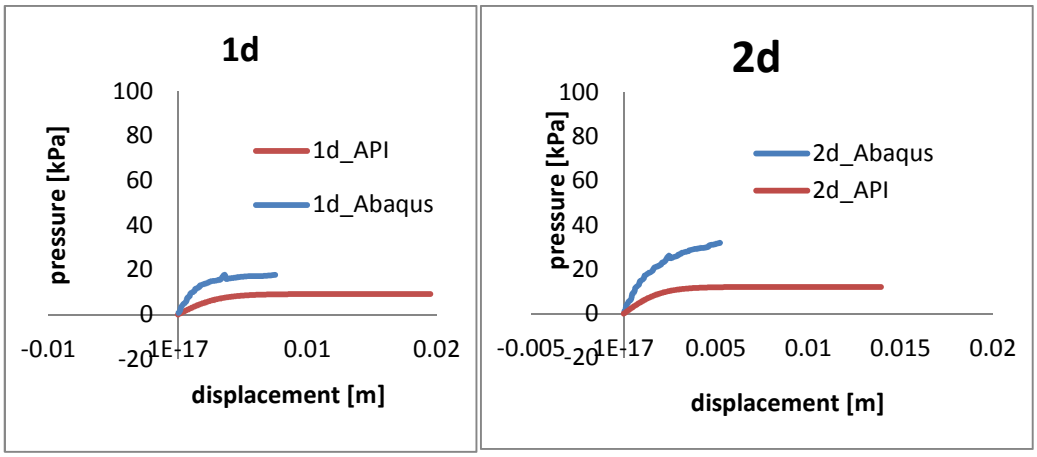

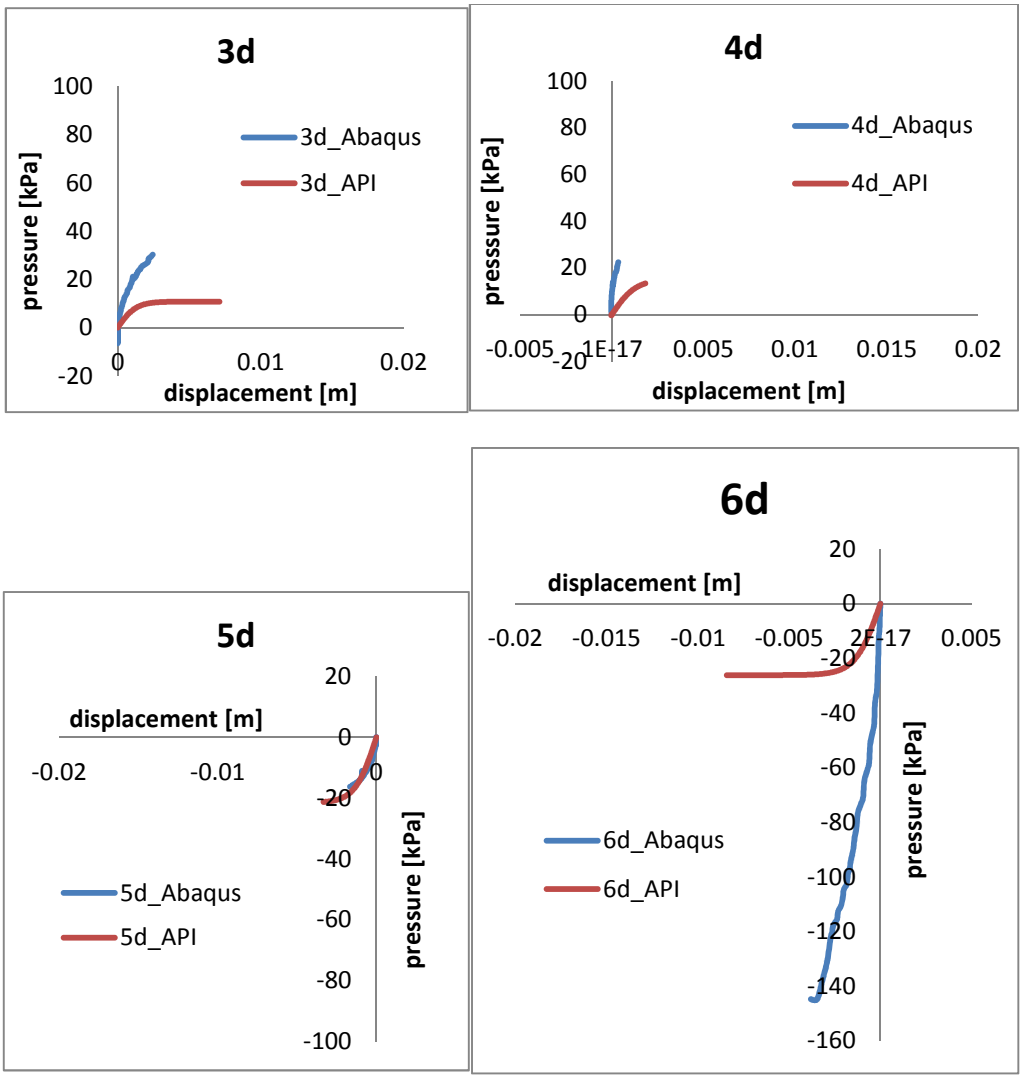

Figure 3.10: Comparison of p-y curves of unplugged pile with API [6] provision

The stiffness of the p-y curves obtained from the 3D numerical model (blue lines) increase as pile depth increase. The ultimate soil resistance is reached just at shallow depth (1d and 2d) but the pattern can be deduced from the graph; hence the value of ultimate soil resistance may increase with depth until 3d then it decreases and reach negative values.

Summarizing, the variation of interface shear strength does not change the pattern of the physical variables analysed, but the numerical values obtained are slightly different form the reference soil. In the next chapter a detailed comparison which underlines the variation of the lateral capacity and p-y curves is shown.

Increase of shear strength soil

The increment of shear strength of the soil does not change the failure mechanism of the system soil-pile but affect the values of lateral load capacity of the pile and the ultimate soil strength of the soil as figures 3.11 to 3.14 show.

- Lateral force-horizontal displacement curve and Moment- rotation curve at the top of the pile

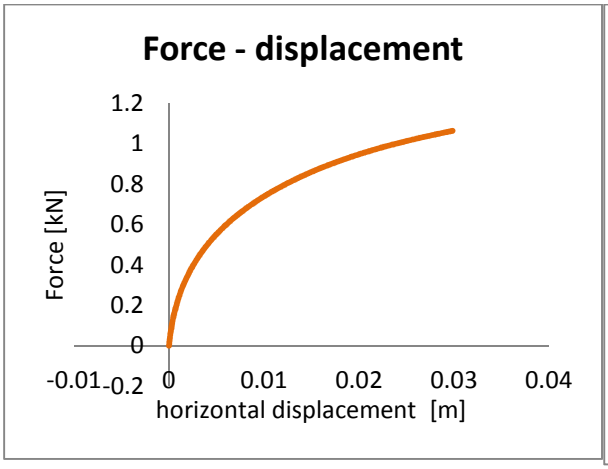

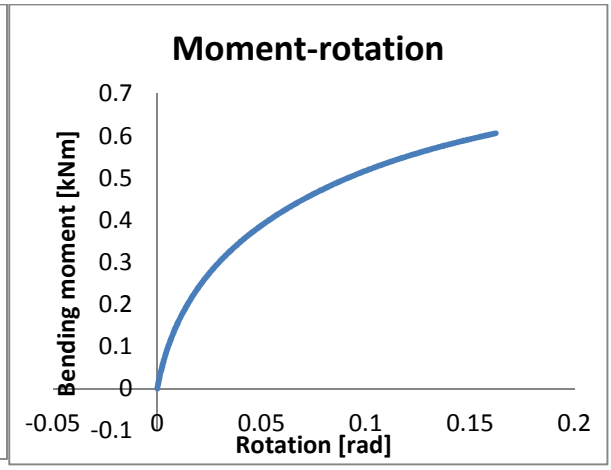

Figure 3.11: Force displacement curve in unplugged pile **Figure 3.12:**Moment rotation curvein unplugged pile

The lateral capacity is not reached but the value of the maximum force is 1.06kN with a deflection of 0.03m.The maximum moment is 0.60 kNm with a rotation of 0.16 rad (9.3°). The value of the maximum moment at 4 cm above the sand surface is comparable to the moment at the sand surface at 0.4 kN observed in figure 3.13.

- Bending Moment distribution along the pile (0.24m sand level)

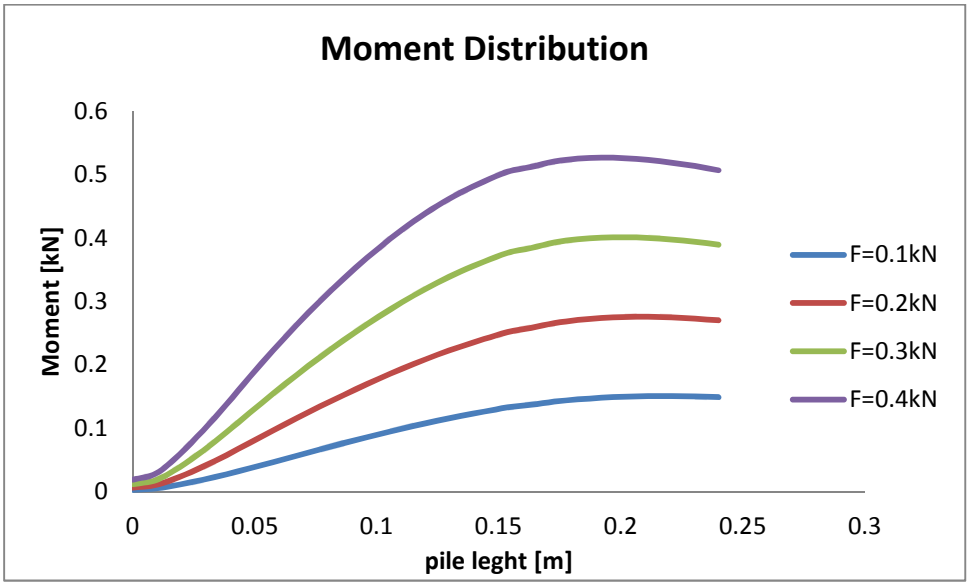

Figure 3.13: Bending moment distribution in unplugged pile

- P-y curves

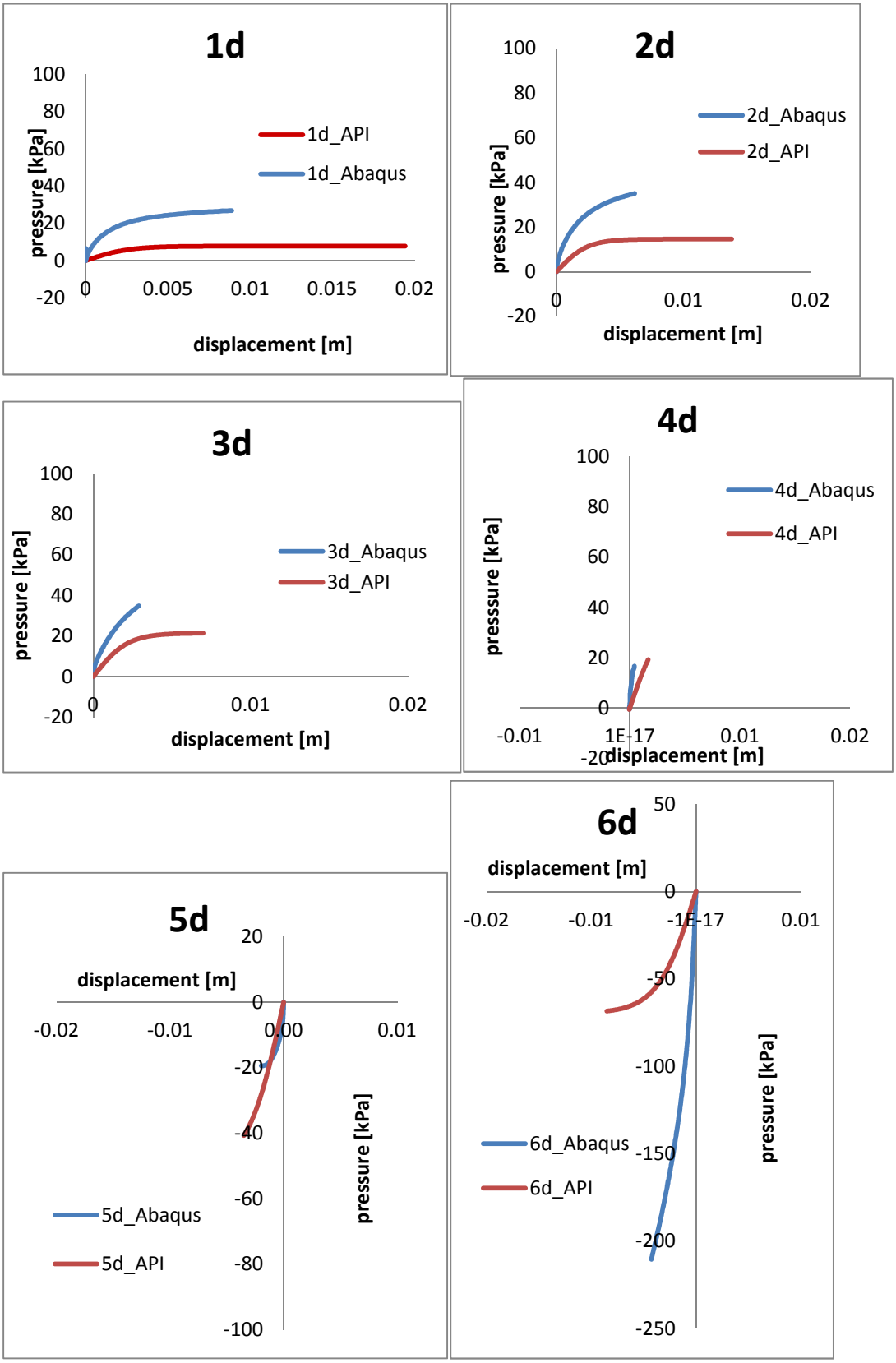

Figure 3.14: Comparison of p-y curves of unplugged pile with API [6] provision

Also the variation of soil shear strength does not change the pattern of the graphs analysed, but the numerical values obtained are slightly different from the reference soil. In the next chapter a detailed comparison which underlines the variation of the lateral capacity and p-y curves is shown.

2.3 Laterally loaded flexible pile (plugged)

It is expected a soil behaviour of the plugged flexible pile very similar to the rigid pile because the soil around the pile have the same shape and same properties. On the other hand the deformed configuration and the failure mechanism are expected to be very similar to the ones of the unplugged because both of the piles are flexible.

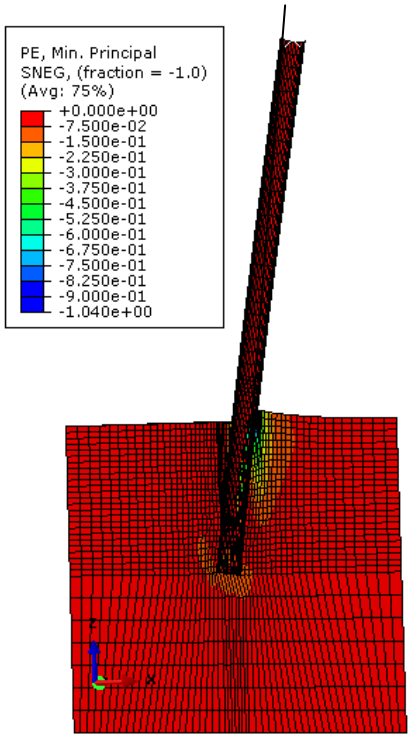

Figure 3.15: Plastic strain contours and failure pattern for hollow plugged pile

Figure 3.15 shows that there is not a rigid body failure since there is a small deformation of the pile very similar to the one of the hollow unplugged pile. The discrepancy from the rigid body failure is highlighted by the black line.

- Lateral force-horizontal displacement curve and Moment- rotation curve at the top of the pile

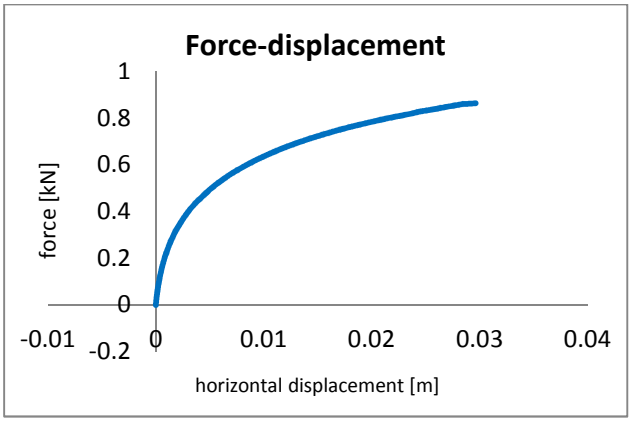

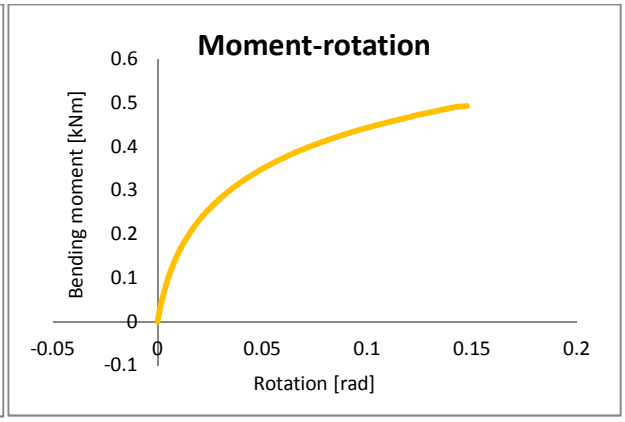

Figure 3.16: Force displacement curve in plugged pile **Figure 3.17:**Moment rotation curvein plugged pile

The maximum force is 0.86kN with a deflection of 0.029m and a maximum moment of 0.5kNm with a rotation of 0.15 radiant. The ultimate load is not reached in the hollow piles because of numerical problems of the shell elements in the software used .

- Bending Moment distribution along the pile (0.24m sand level)

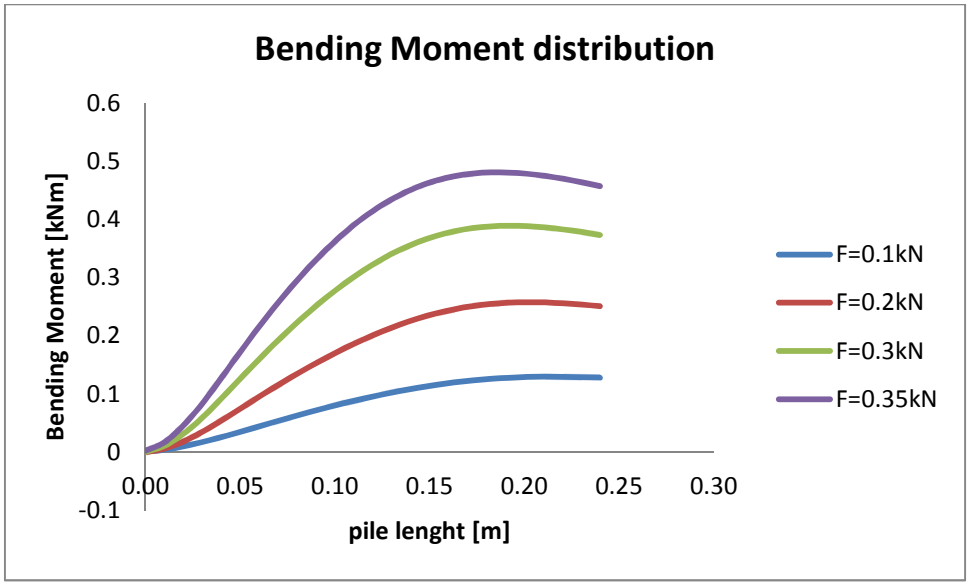

Figure 3.18: Bending moment distribution in plugged pile

The bending moment distribution at low value of forces is the one expected for linear elastic soil response. At higher values of lateral force the maximum value of the moment is located below the sand surface and the magnitude is comparable with the maximum bending moment in the moment-rotation curve(figure 3.17). The difference is due to the different positions and force magnitude analysed.

- Plastic strain

F = 0.1 kN

F=0.2 kN

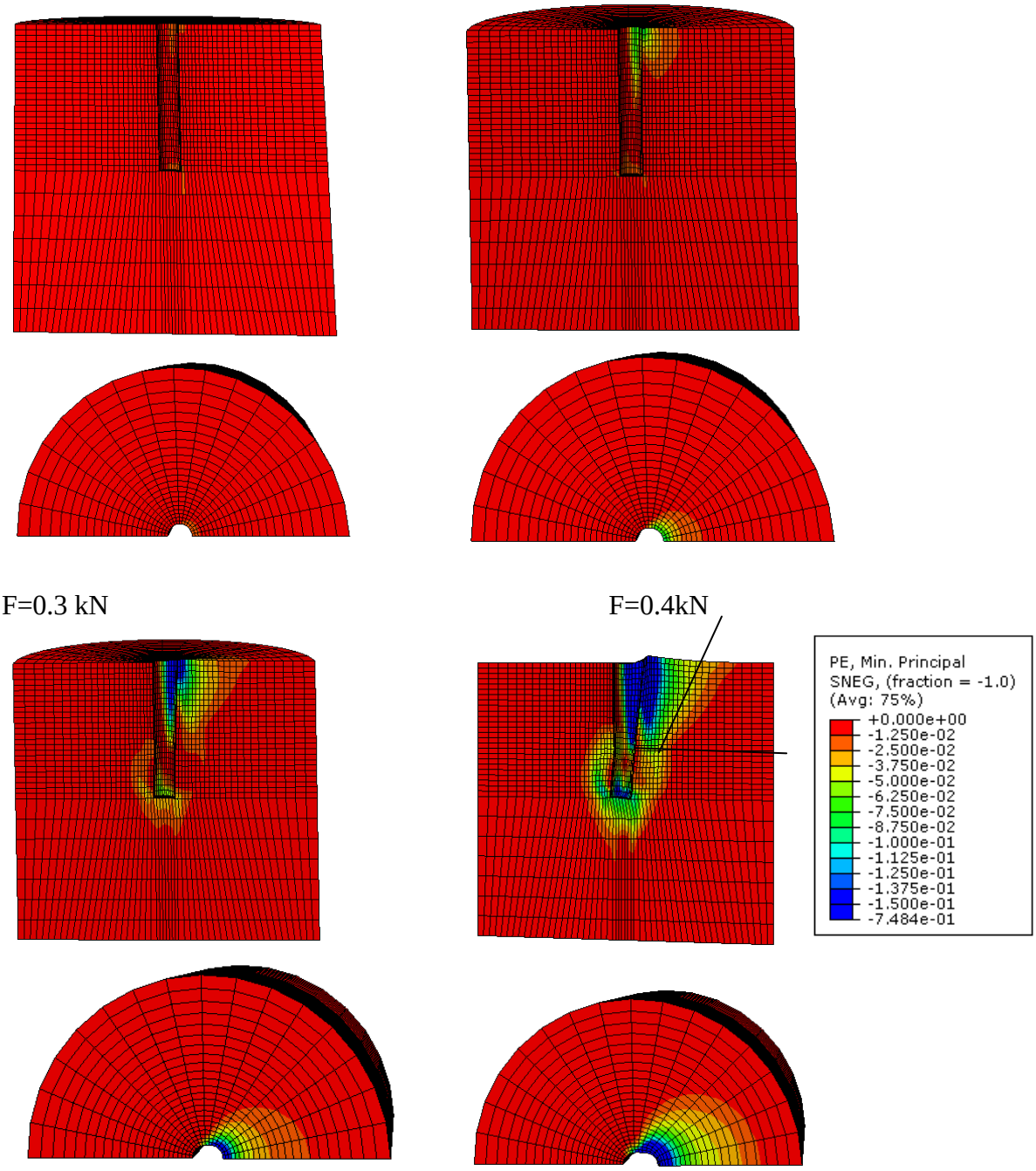

Figure 3.19: Plastic strain contours with increasing force in plugged pile

Also in the plugged pile the a failure wedge is developed until a depth of approximately 4d, and the inclination respect to the horizontal is almost 60°. The p-y curves presented below confirm the qualitative considerations noted from figure 3.19.

- P-y curves at different depth

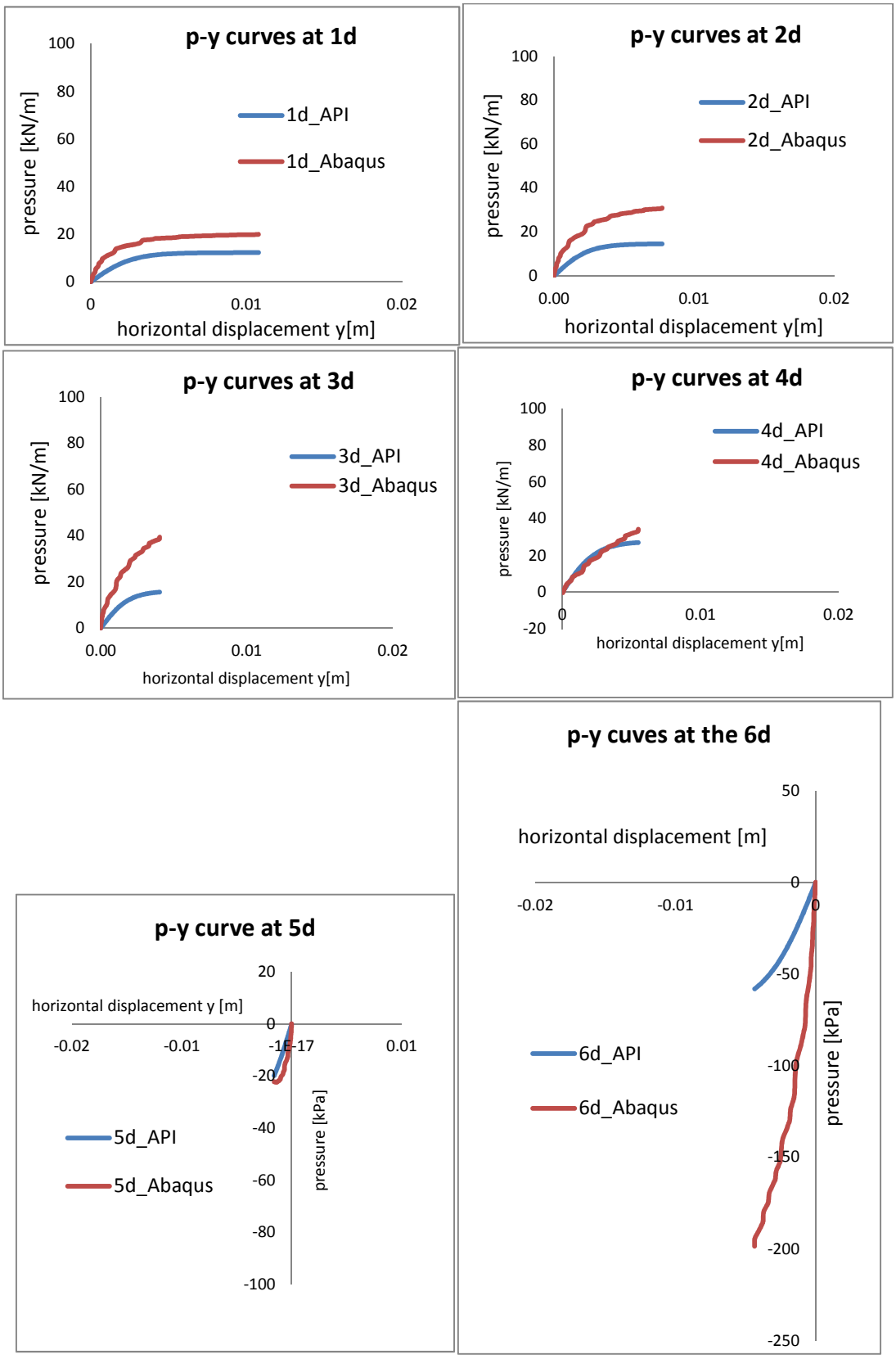

Figure 3.20: Comparison of p-y curves of plugged pile with API [6] provision

The p-y curves reached the ultimate shear strength just at the depth of 1d, 2d,3d, it means that the soil reach the plastic strain at this depth and so the height of the failure wedge corresponds approximately at 3d-4d.

Increase of interface shear strength

Since the plugged pile behaviour is very similar to the unplugged one, also in this case the increment of interface shear strength does not produce variation in the in the patterns of lateral forces, bending moments and pressure of the system pile-soil.

- Lateral force-horizontal displacement curve and Moment- rotation curve at the top of the pile

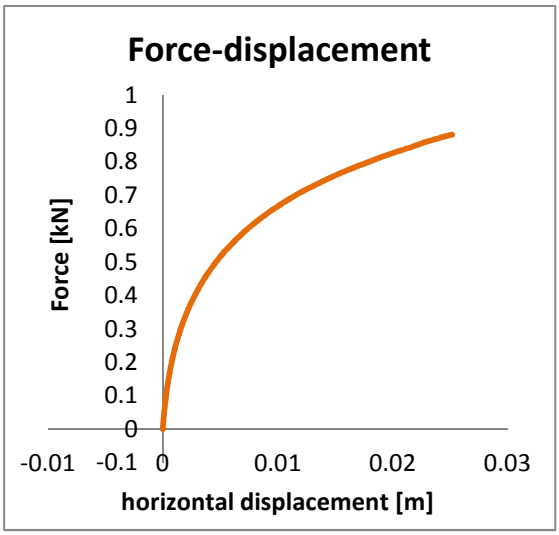

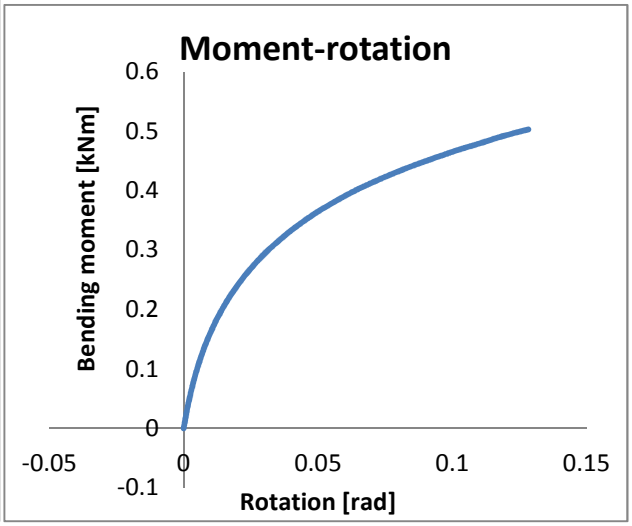

Figure 3.21: Force displacement curve in plugged pile **Figure 3.22:**Moment rotation curve in plugged pile

The lateral load capacity of the pile is not reached . The maximum force is 0.88 kN considering a deflection of 0.025m and the maximum moment is 0.53 kNm with a rotation of 0.148 radians

- Bending Moment distribution

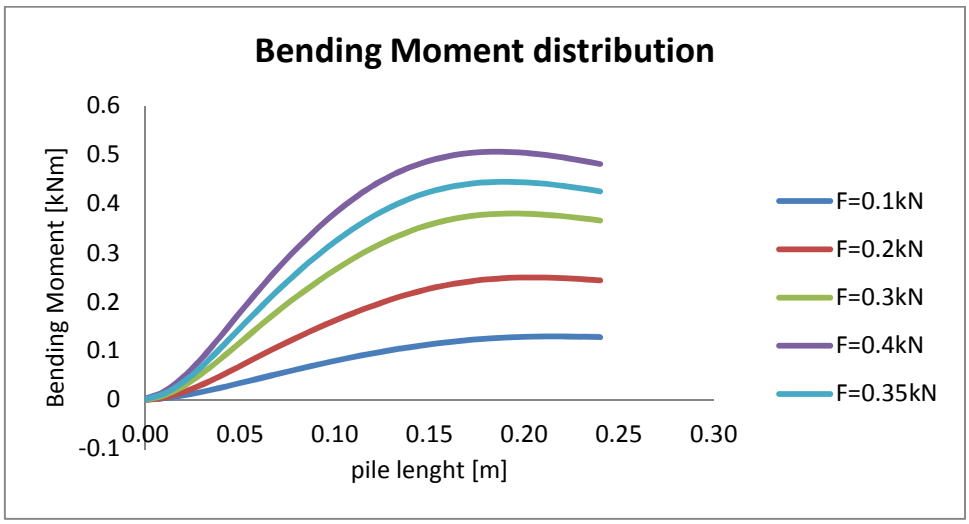

Figure 3.23: Bending moment distribution in plugged pile

- P-y curves

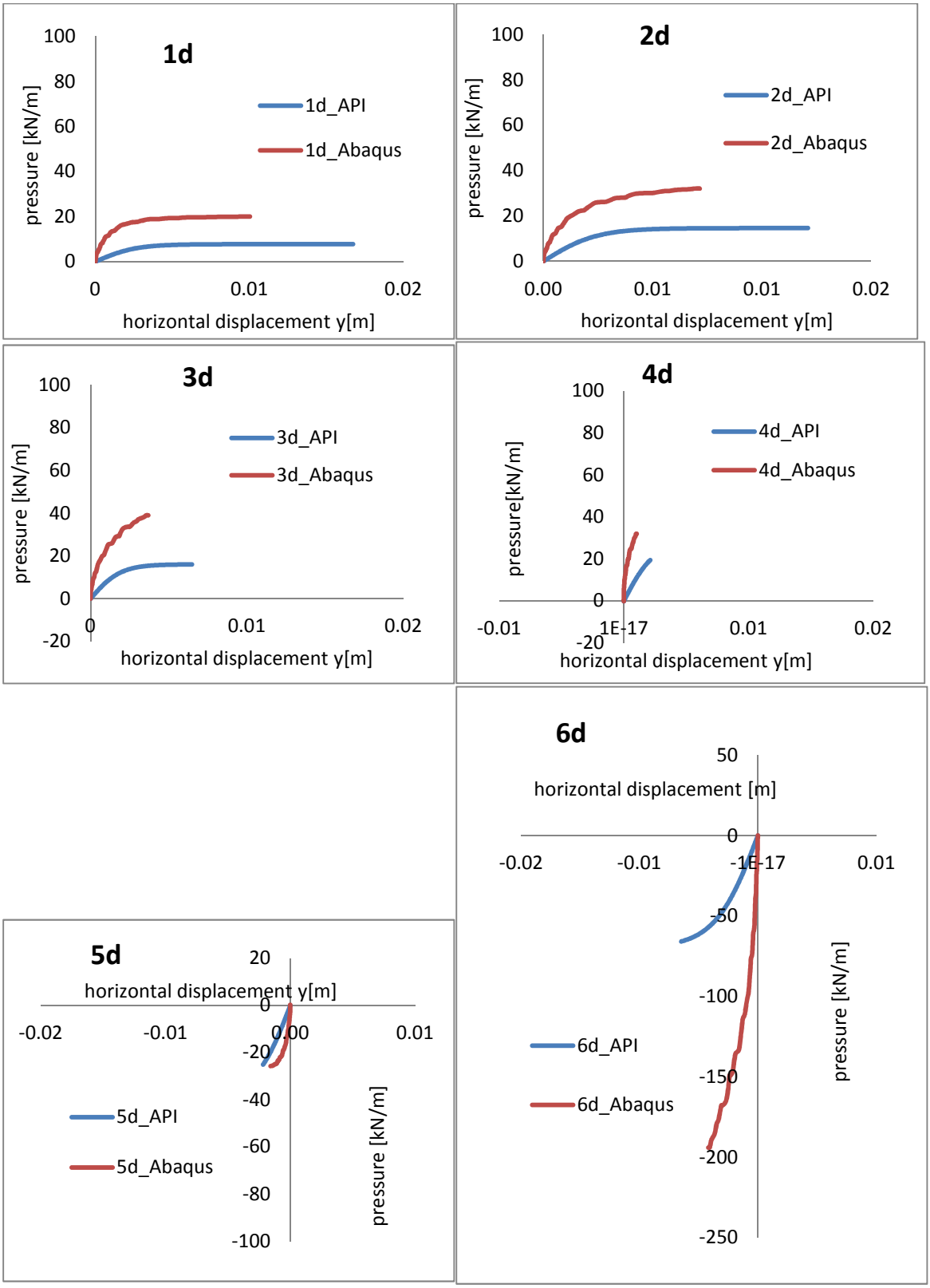

Figure 3.24: Comparison of p-y curves of plugged pile with API [6] provision

The pattern of the stiffness of the p-y curves and the ultimate soil resistance along the depth is always the same. The ultimate soil resistance is reached just for shallow depth.

The difference produced by the increased of interface shear strength can be seen in chapter 4 where the numerical values are compared.

Increase of shear strength soil

In figures 3.25 to 3.28 the effects of the increase of shear strength are presented.

- Lateral force-horizontal displacement curve and Moment- rotation curve at the top of the pile

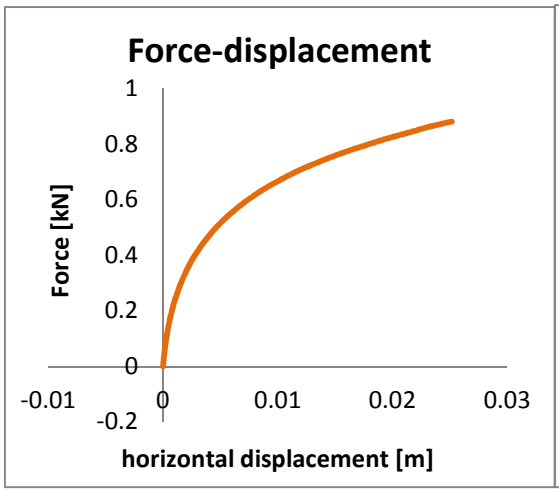

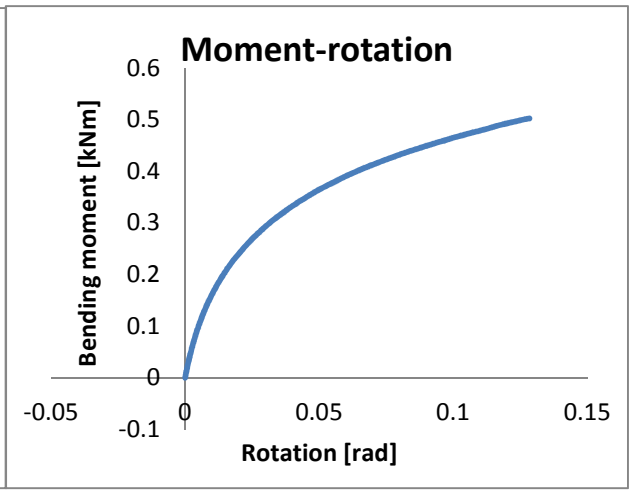

Figure 3.25: Force displacement curve in plugged pile **Figure 3.26:**Moment rotation curvein plugged pile

The maximum force is 0.88kN with a deflection 0.025m. The maximum moment is 0.503kNm at 0.123 radiants (7.3°).

- Moment distribution along the pile (sand level 0.24m)

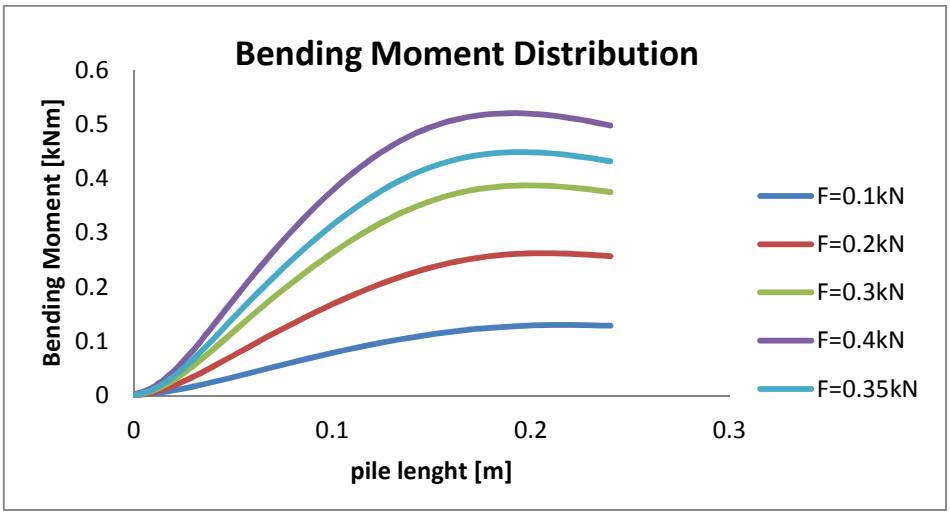

Figure 3.27: Bending moment distribution in plugged pile

- P-y curves at different depth

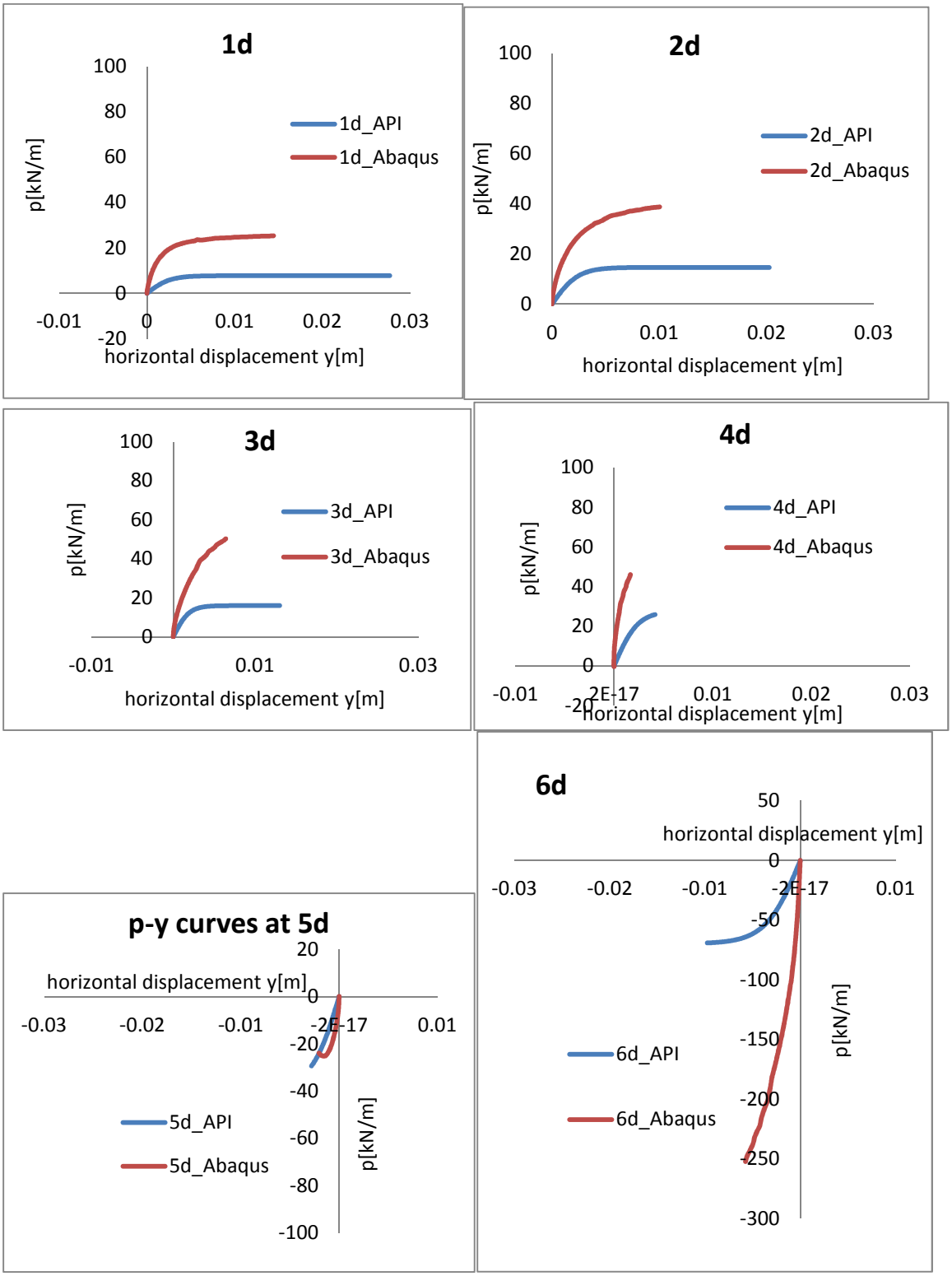

Figure 3.28: Comparison of p-y curves of plugged pile with API [6] provision

The characteristics of the graph are the same of the previous ones, hence in order to understand the differences graphs with comparison of the three soil types are shown in chapter 4.

2.4 Laterally loaded rigid pile

In the rigid pile mathematical problems during the solution of the model does not occur, so that the software can compute the results until the failure of the soil.

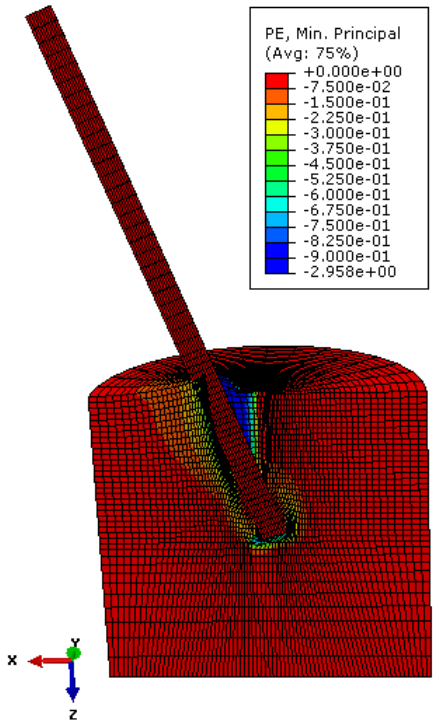

Figure 3.29: Plastic strain contours and failure pattern rigid pile

The displacement of the pile is bigger than the one of the flexible piles because in this case the pile reach the ultimate load.

The rigid body rotation, the bulging of soil at the side of the pile as well as the gap at the back side of the pile observed in Figure 3.29, are the main aspects of the failure mode of a rigid lateral loaded pile .

- Lateral force-horizontal displacement curve and Moment- rotation at the top of the pile curve

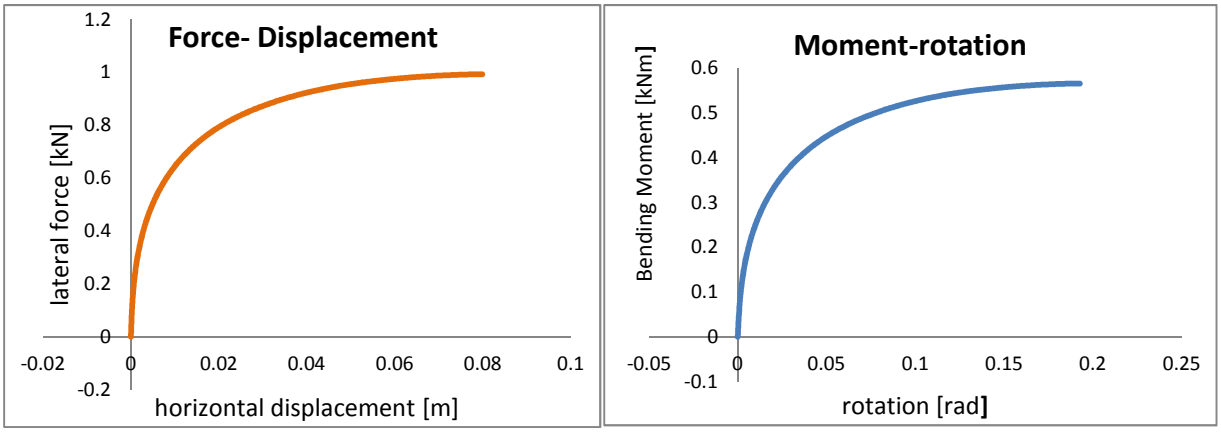

Figure 3.30: Force displacement curve in rigid pile **Figure 3.31:**Moment rotation curve in rigid pile

The maximum force correspond to the ultimate force and is equal to 0.99kN with a deflection of 7.8cm. The ultimate moment is 0.56kNm with a rotation of 0.19 rad (11°).
The pile reaches the lateral capacity , it can be seen in figure 3.30 because the force displacement curve became horizontal.

- Moment distribution along the pile (sand level 0.24m)

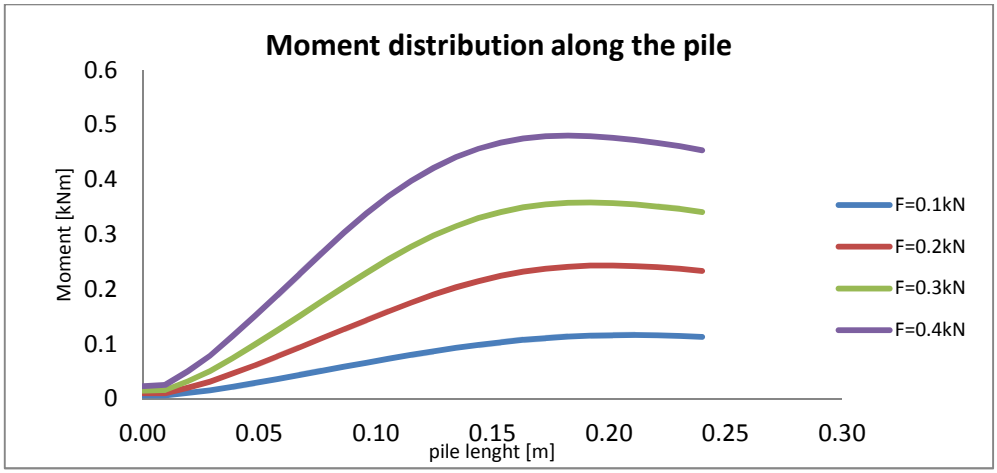

Figure 3.32: Bending moment distribution in rigid pile

Even if the failure mechanism of the rigid pile is different from the flexible ones, the pattern of moment distribution along the rigid pile is very similar to the one of the flexible piles. The bottom of the pile is not subject to bending moment. The position of the maximum moment is at the sand surface for low forces and it gradually moves as the force increases.

- Plastic strain

F=0.1kN F=0.2kN

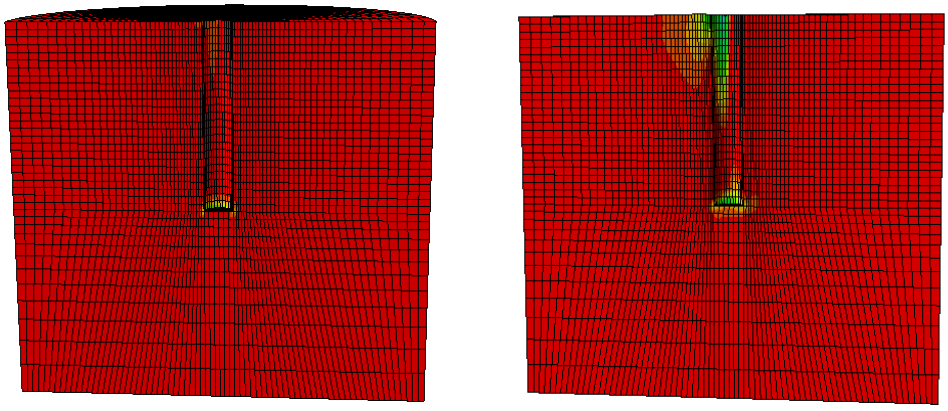

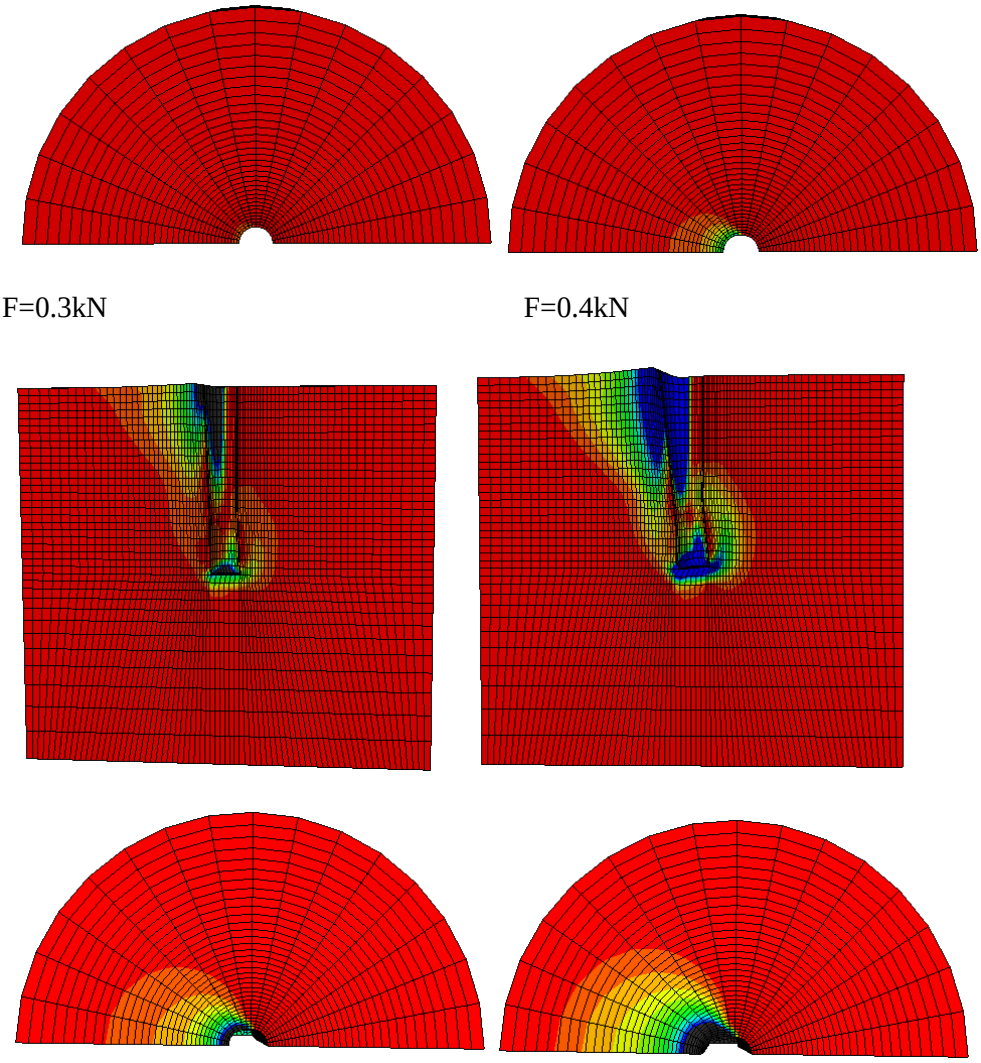

Figure 3.33: Plastic strain contours with increase force in unplugged pile

- P-y curves at different depths

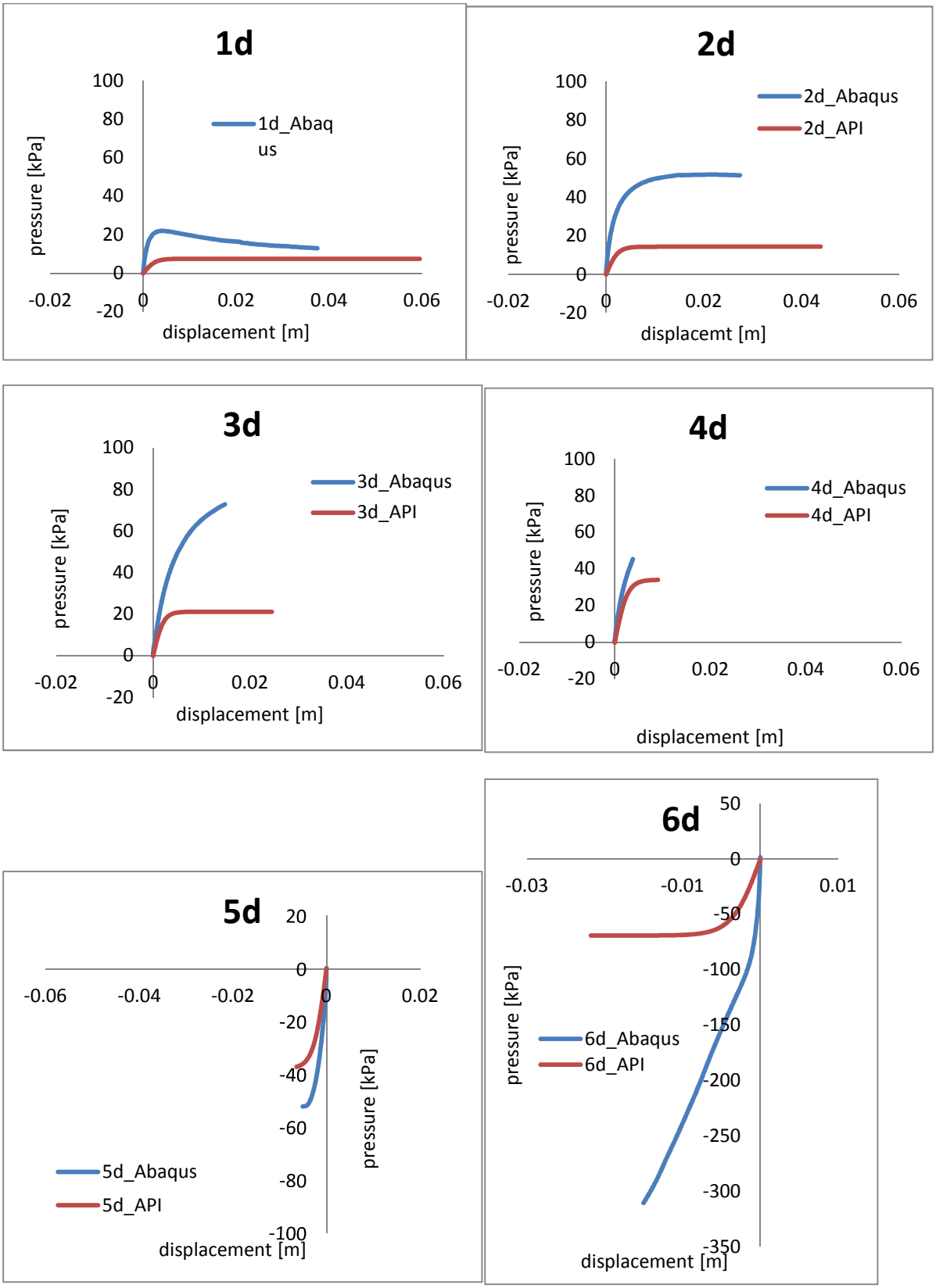

Figure 3.34: Comparison of p-y curves of rigid pile with API [6] provision

Increase of interface shear strength

- Lateral force-horizontal displacement curve and Moment- rotation curve at the top of the pile

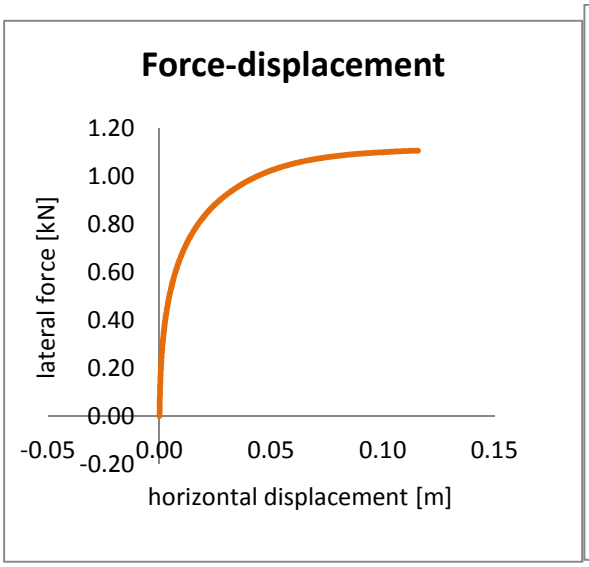

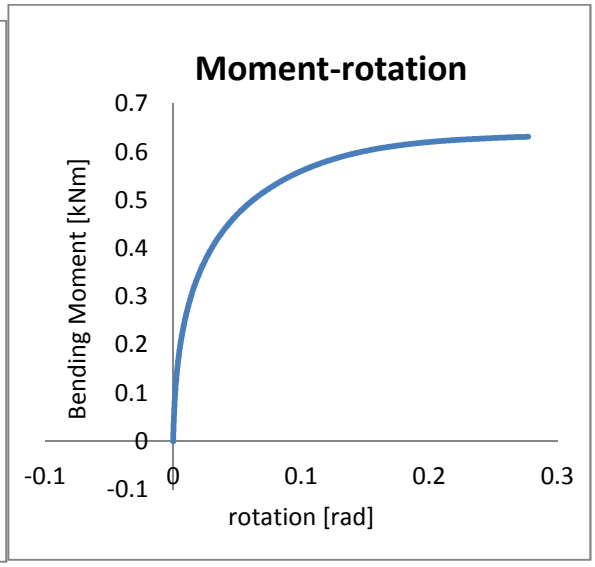

Figure 3.35: Force displacement curve in rigid pile **Figure 3.36:**Moment rotation curve in rigid pile

The ultimate force is1.1kN with a deflection of 0.12m and a ultimate moment of 0.62kNm with a rotation of 0.28 rad (15.8°).

- Moment distribution along the pile (sand level 0.24m)

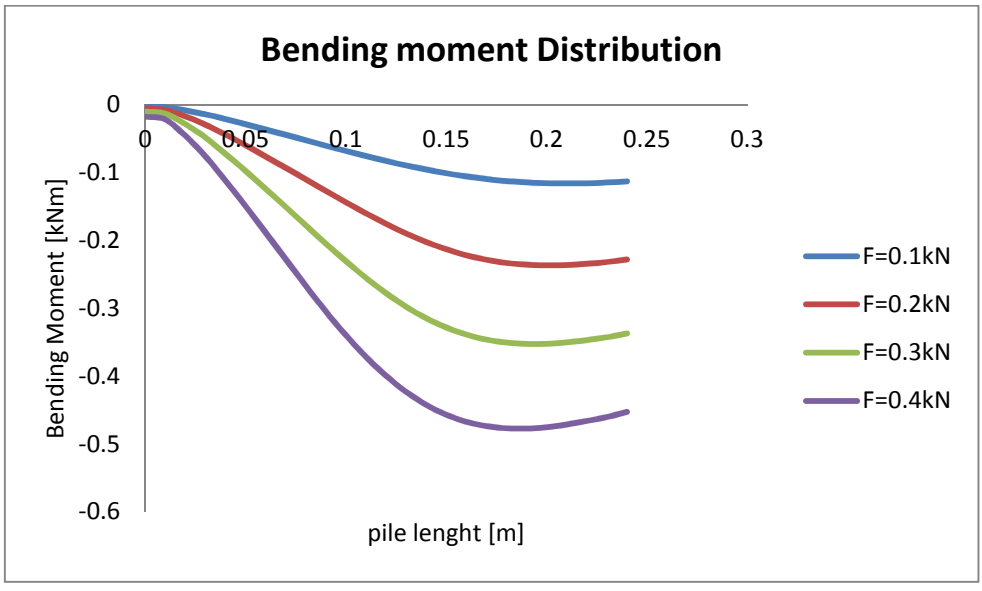

Figure 3.37: Bending moment distribution in unplugged pile

- P-y curves at different depths

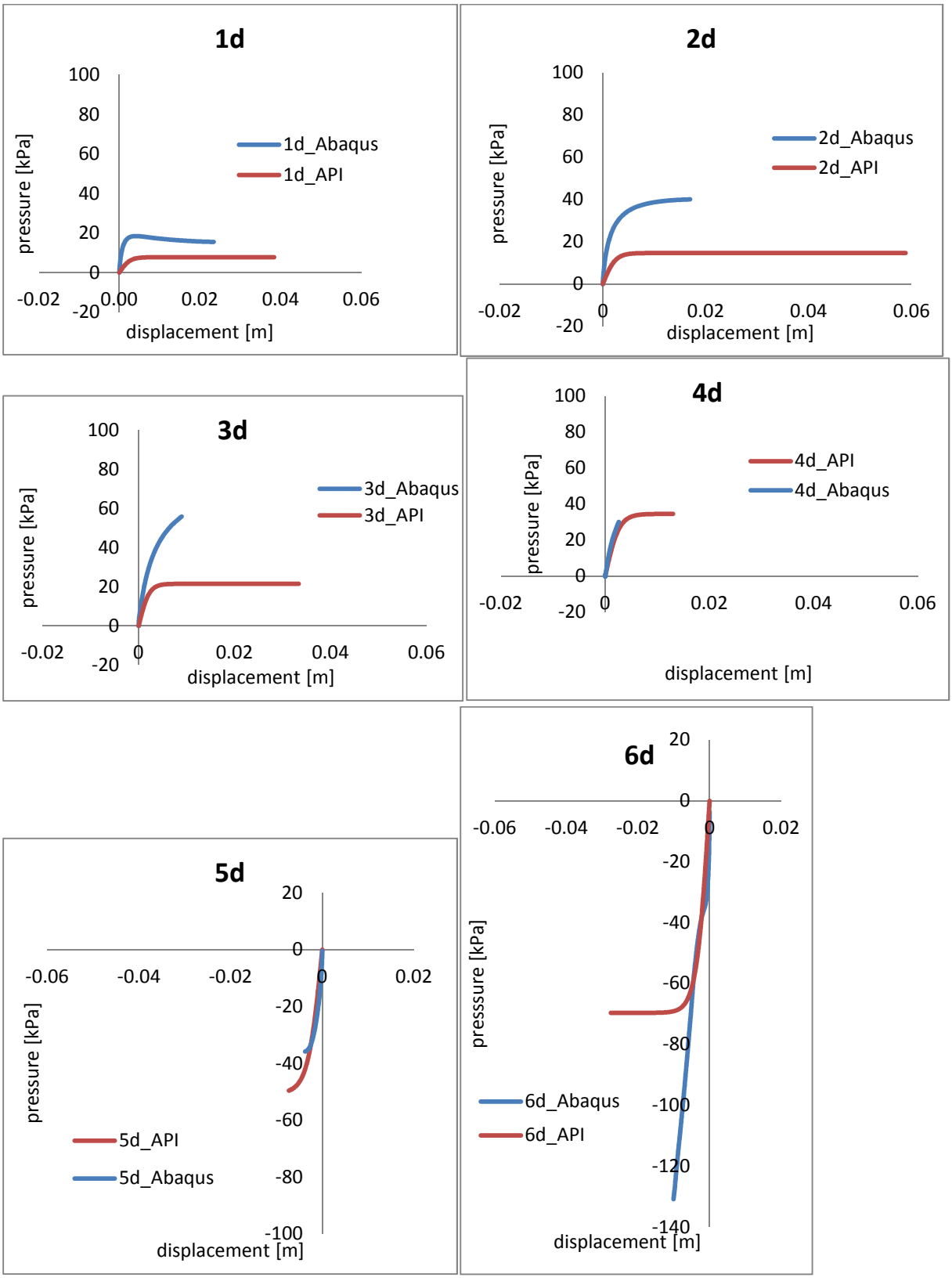

Figure 3.38: Comparison of p-y curves of rigid pile with API [6] provision

Increase of shear strength soil

- Lateral force-horizontal displacement curve and Moment- rotation curve at the top of the pile

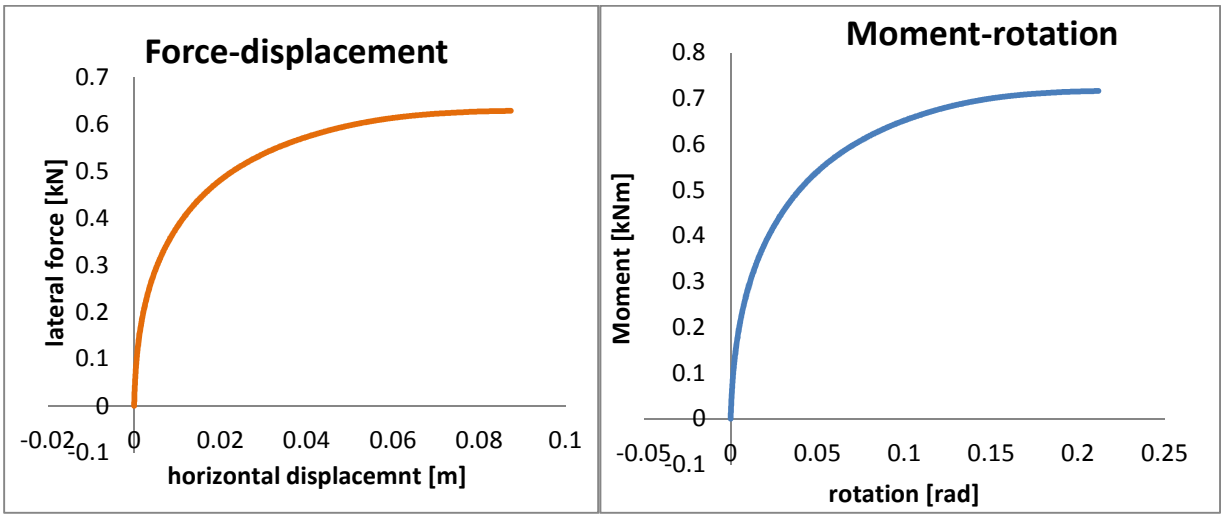

Figure 3.39: Force displacement curve in rigid pile **Figure 3.40:**Moment rotation curve in rigid pile

The ultimate force is 0.63kN with a deflection of 0.087m and the ultimate moment is 0.72kNm with a rotation of 0.21rad (12°).

- Moment distribution along the pile (sand level 0.24m)

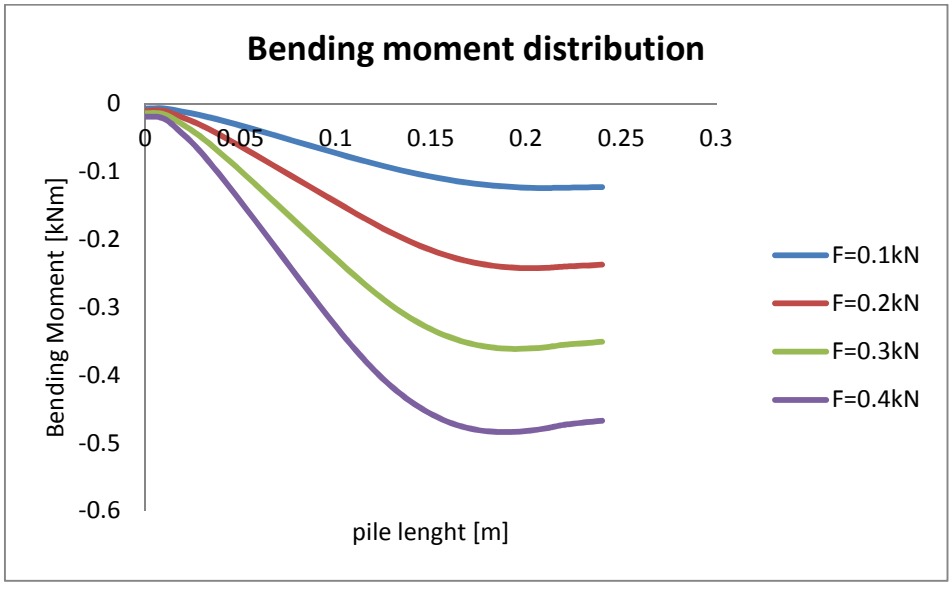

Figure 3.41: Bending moment distribution in rigid pile

- P-y curves at different depth

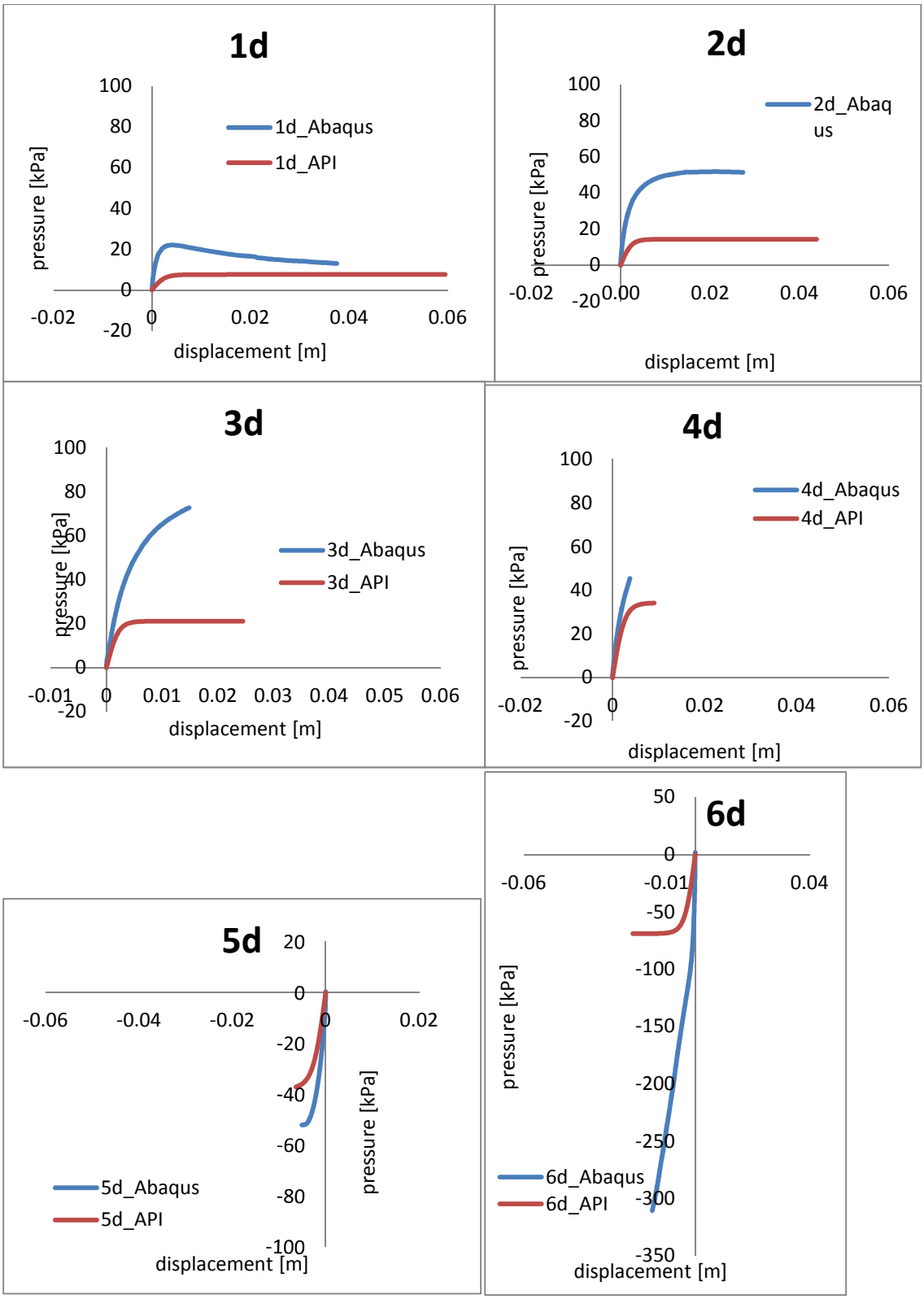

Figure 3.42: Comparison of p-y curves of rigid pile with API [6] provision

4. Discussion of the results

4.1 Effect of pile's stiffness

The following graphs regards the reference soil.

- Force displacement curve

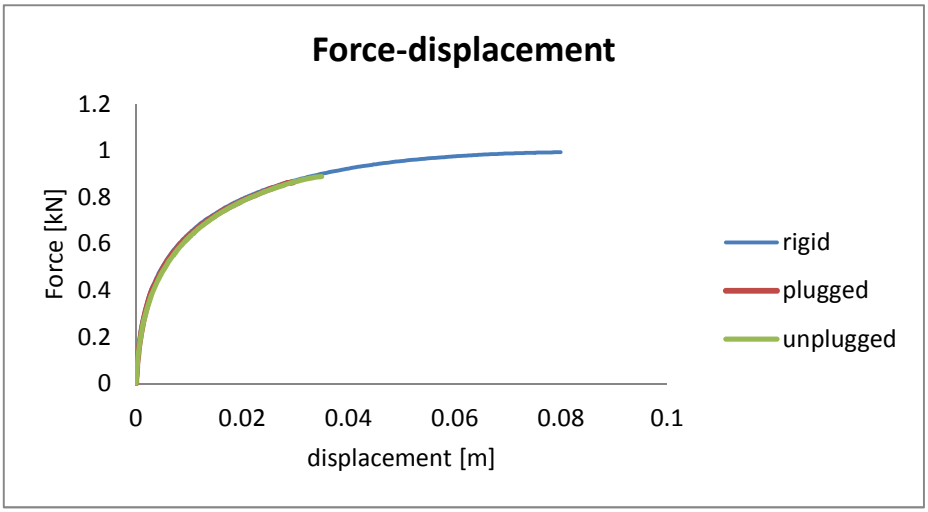

Figure 4.1: Comparison of force displacement curves in rigid and hollow piles

The lateral capacity of the pile out of the sand is the same with the three type of pile used. It means that the stiffness of the pile does not affect the ultimate load and the corresponding deflection at the top of the pile.

- Moment-rotation (moment calculated as it is shown in the appendix)

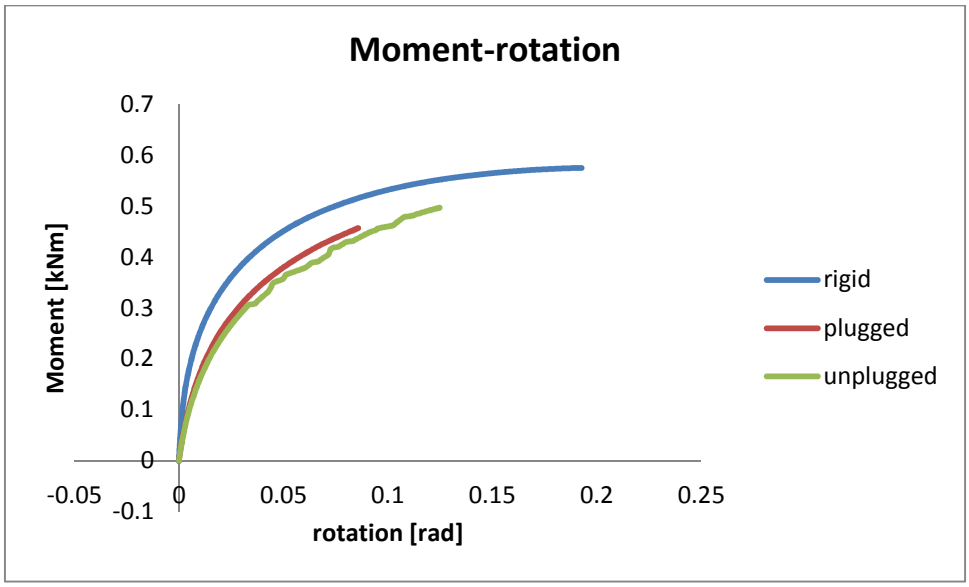

Figure 4.2: Comparison of moment – rotation curves in rigid and hollow piles

The stresses and the section forces in the pile used to calculate the moment are different in the rigid and in the flexible piles. A possible explanation is that the failure mechanism and the shape of the deformed configuration of the pile are different. In the rigid pile there is a rigid body rotation, hence for same value of moment the rotation is smaller.

- p-y curves

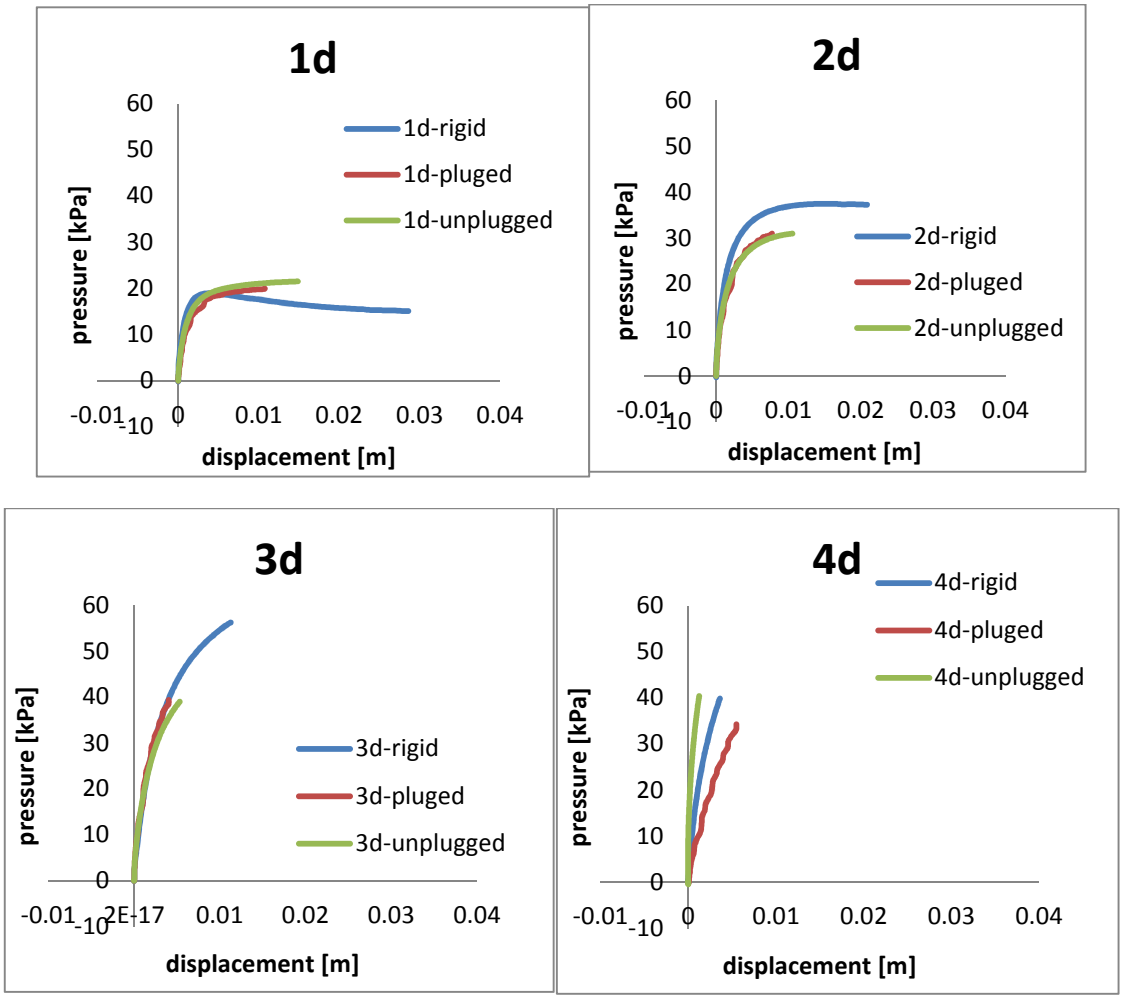

Figure 4.3: Comparison of p-y curves in curves in rigid and hollow piles

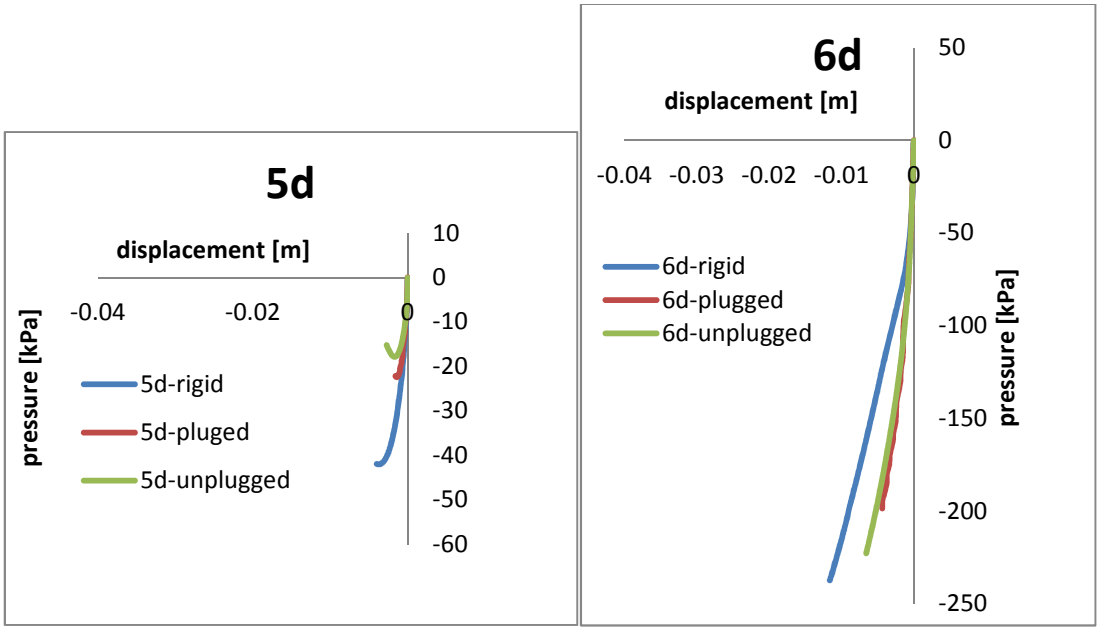

Figure 4.3: Comparison of p-y curves in curves in rigid and hollow piles

The variation of stiffness kx is evident just at 4d where probably is located the rotation point. The ultimate soil strength varying significantly after 4d, this change in the p-y curves is probably due to a different failure mechanism (rigid body rotation and flexible rotation)

Increase of interface shear strength

- Force displacement curve

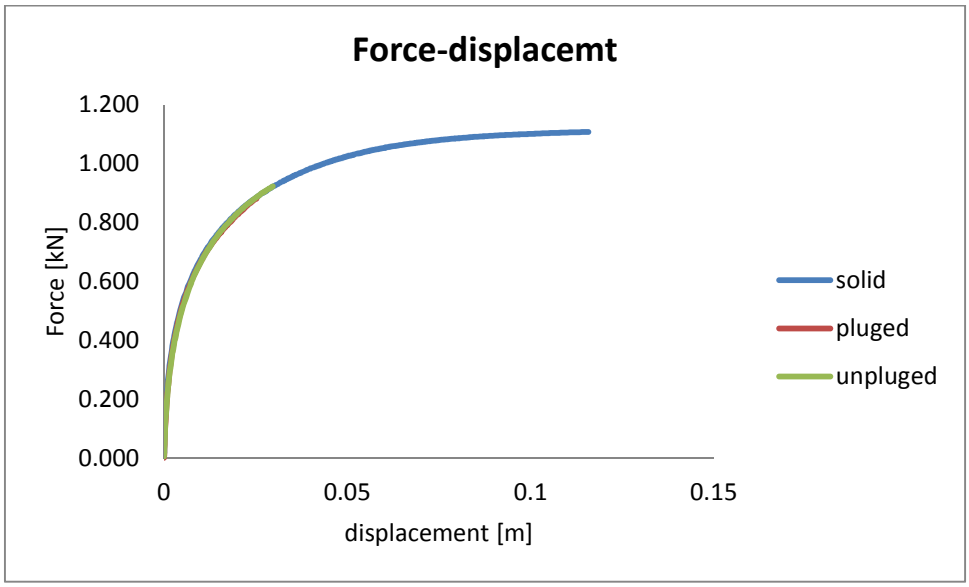

Figure 4.4: Comparison of force displacement curves in rigid and hollow piles

Also at higher interface shear strength, the stiffness of the pile does not affect the lateral capacity.

- Moment rotation(moment calculated as it shown in the appendix)

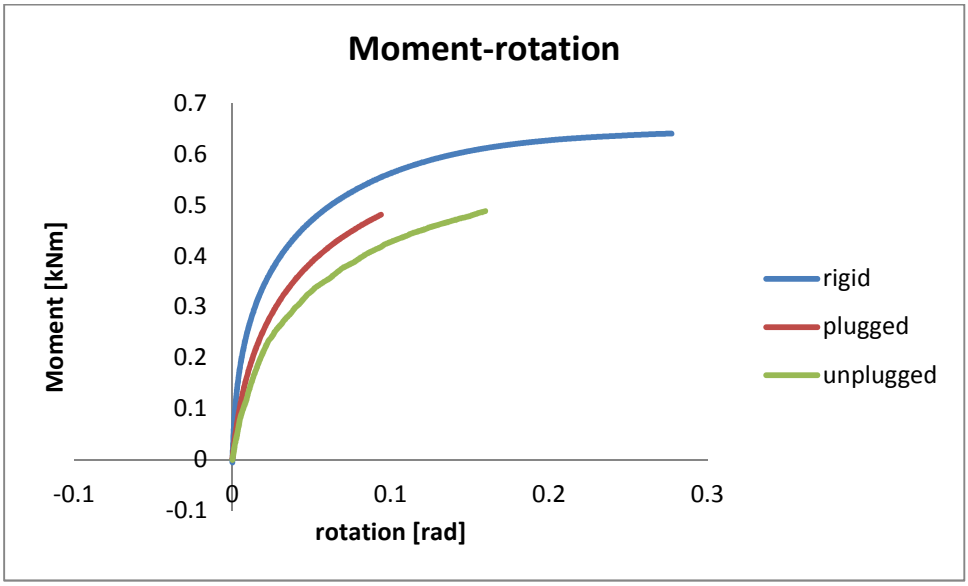

Figure 4.5: Comparison of moment – rotation curves in rigid and hollow piles

For higher interface friction the moment at the sand surface depends on the type of pile. This difference in the maximum moment that is not present in the lateral capacity can be explained considering different failure mechanisms, that are more evident for higher interface friction.

- P-y curves

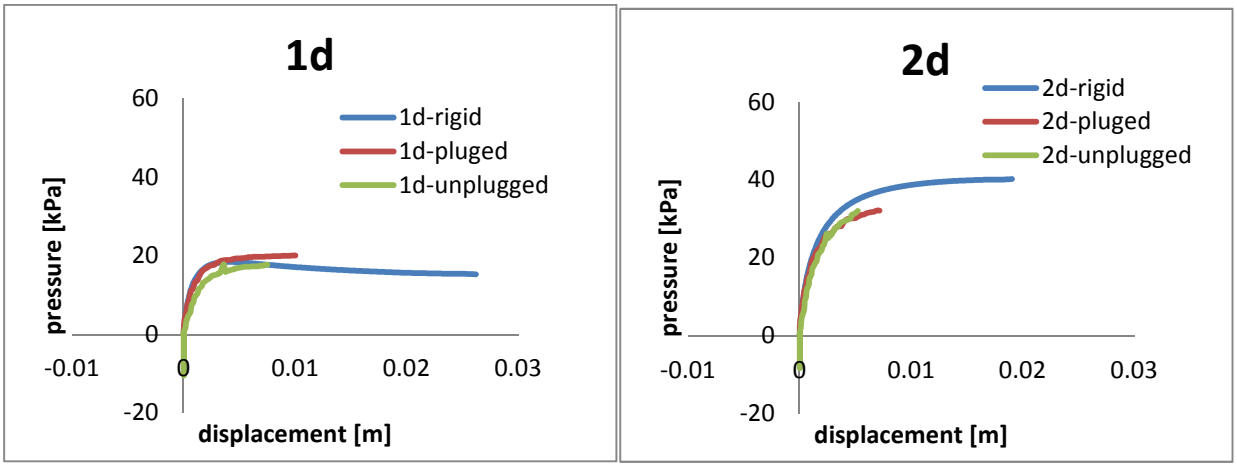

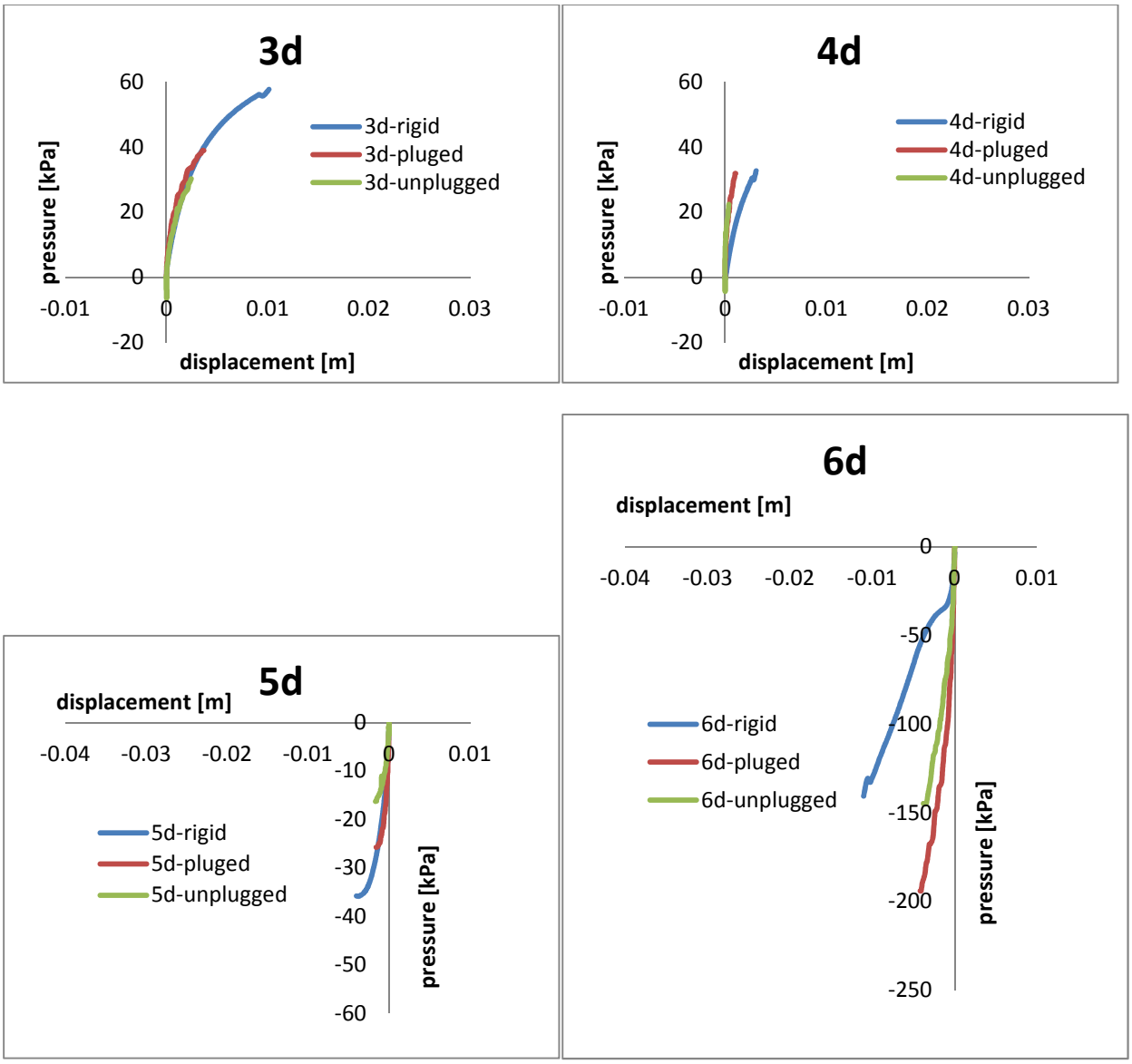

Figure 4.6: Comparison of p-y curves in curves in rigid and hollow piles

At higher interface shear strength the stiffness effect are the same. The lateral pile capacity of piles in cohesionless soil is independent of the type of pile and the stiffness. On the other hand in the p-y curves the stiffness effect can be observed at high depth especially in the ultimate value.

Increase of soil shear strength

- Force displacement curve

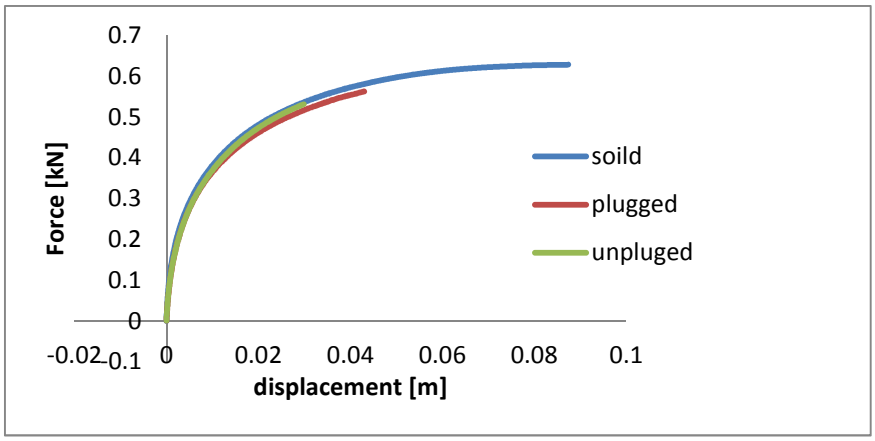

Figure 4.7: Comparison of force displacement curves in rigid and hollow piles

- Moment rotation(moment calculated as it shown in the appendix)

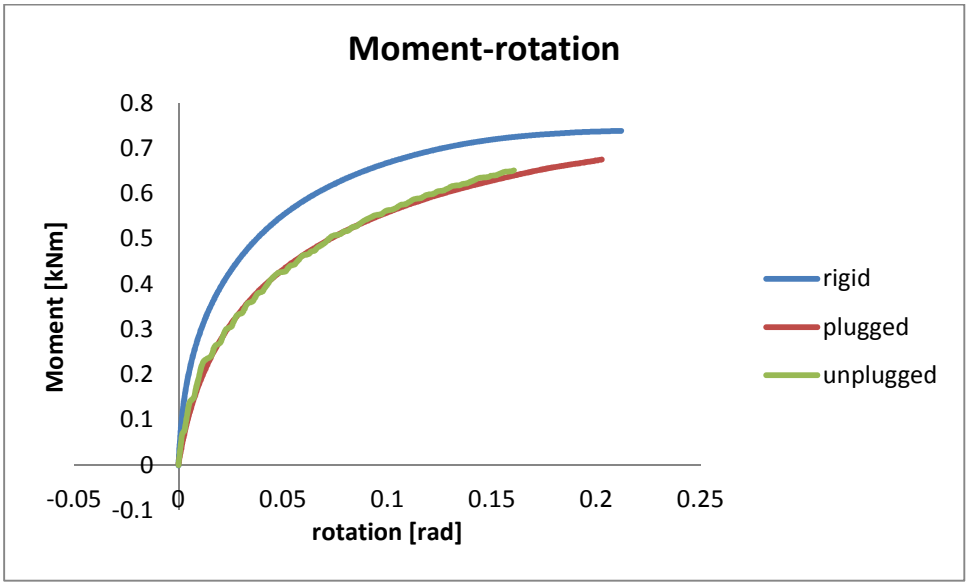

Figure 4.8: Comparison of moment- rotation curves in rigid and hollow piles

Increasing the soil friction in the moment rotation curve , the gap between flexible and rigid piles becomes more evident. The same bending moment produces a higher rotation in the flexible piles than in the rigid pile, the reason could be the different failure mechanism which is exposed by rigid and flexile pile expose.

- P-y curves

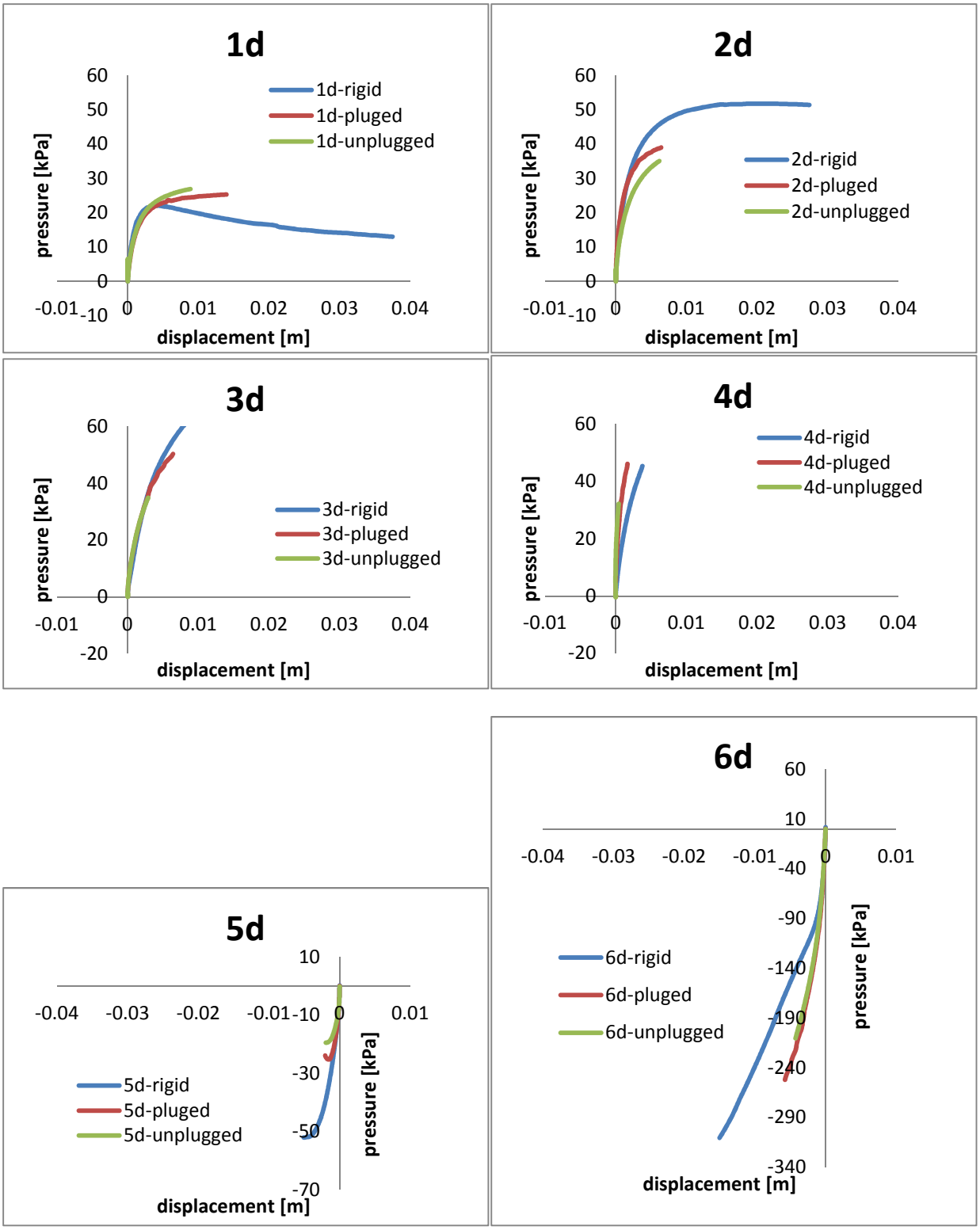

Figure 4.9: Comparison of p-y curves in curves in rigid and hollow piles

Moreover, for higher soil shear strength the stiffness effects are the same.

4.2 Effect of soil and interface properties

In this results discussion it is assumed:
Soil1: reference model with soil shear strength ϕ=33°; interface shear strength δ=2/3ϕ
Soil2: model with increase of interface shear strength δ=ϕ
Soil3: model with increase of soil shear strength ϕ=36°.

Unplugged flexible pile

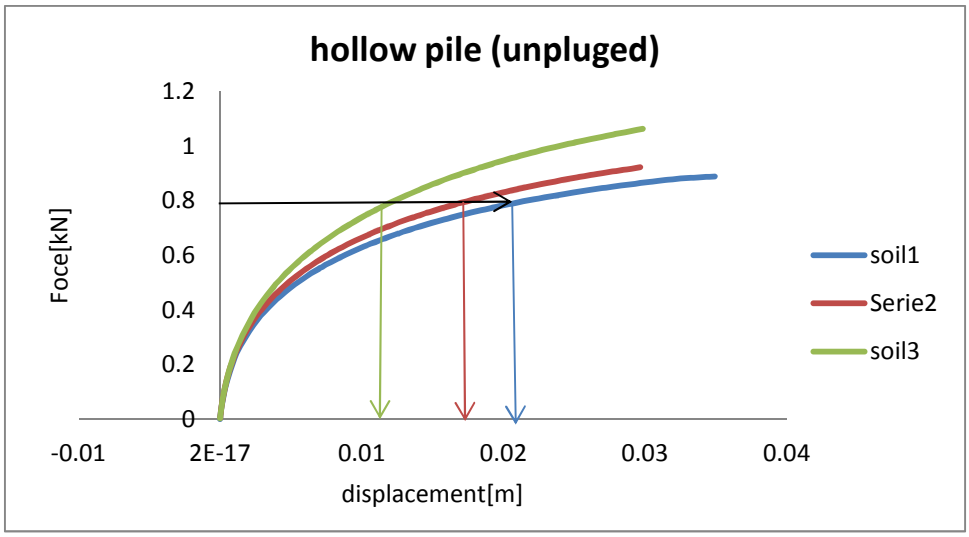

Figure 4.10: Comparison of force displacement curves in hollow unplugged piles

Increasing interface shear strength and soil shear strength the resistance to the lateral force improves.
The alteration of the soil shear strength induces a higher variation of the soil resistance. In particular for the same value of force the pile in the reference soil deflects more than the same pile in a “stiffer” soil (as it is shown by the arrows in figure 4.10)
Hence the lateral capacity of the flexible piles increases as the interface friction and the soil friction increase. This indicates that the increase of the shear stress along the soil-pile interface and in the soil provides additional resistance to the rotation of the pile.

- p-y cuves

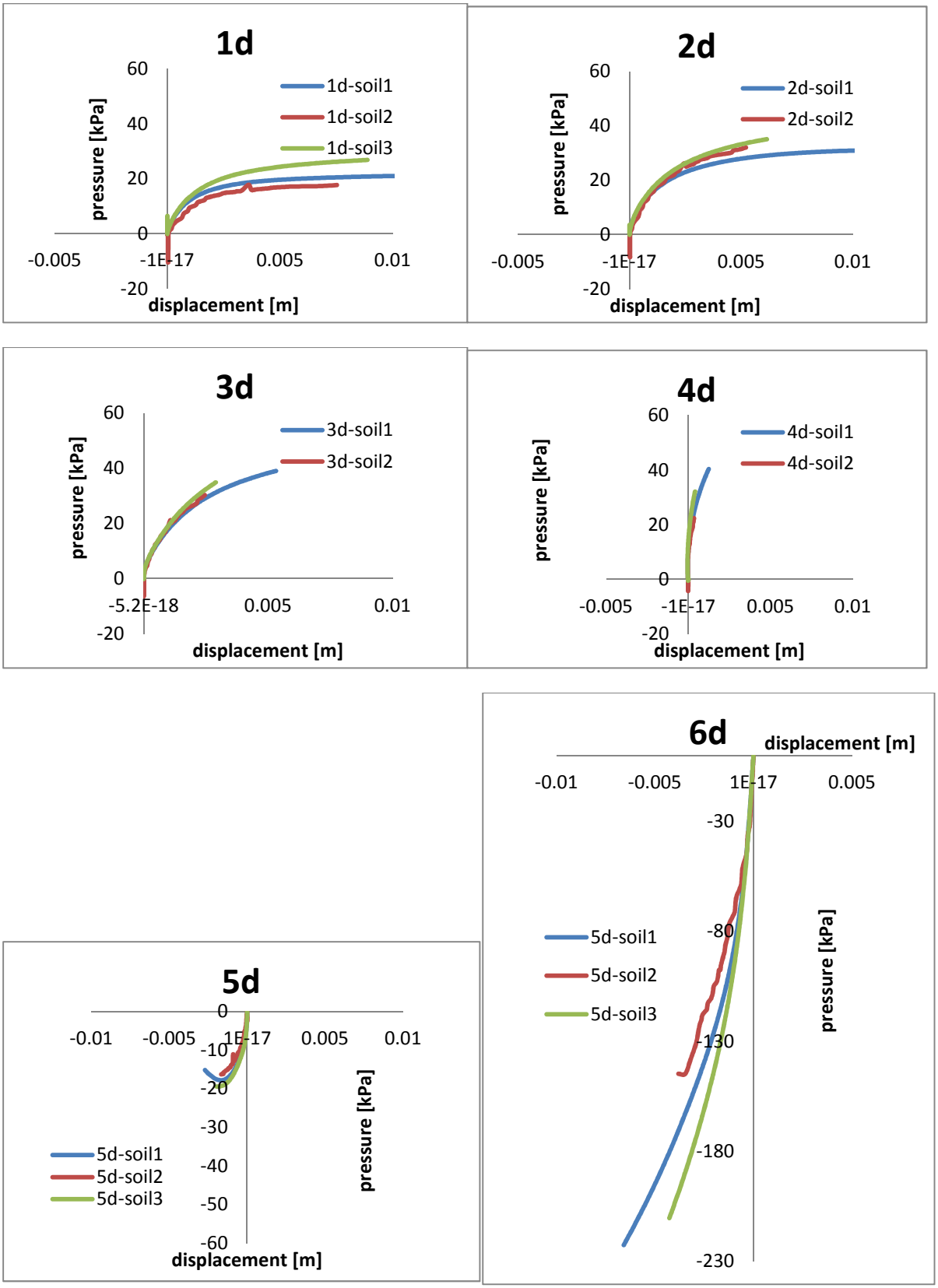

Figure 4.11: Comparison of p-y curves in hollow unplugged piles

The p-y curves of the 3 type of soil are not very different except for the bottom of the pile (6d) the increase of soil strength increase the stiffens of the p-y curve and probably also the ultimate soil resistance.

Plugged flexible pile

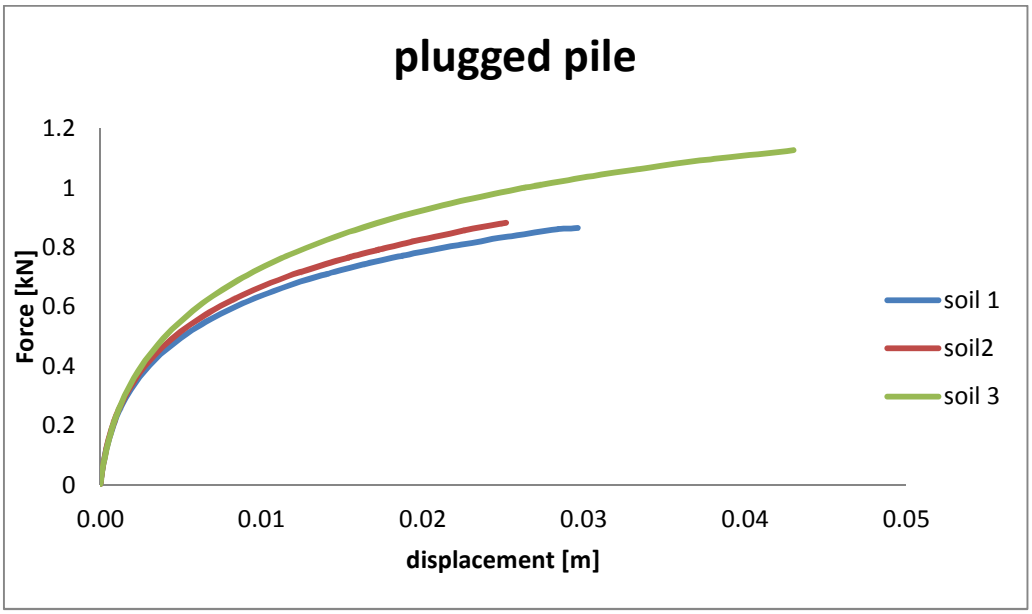

Figure 4.12: Comparison of force displacement curves in hollow plugged piles

- p-y cuves

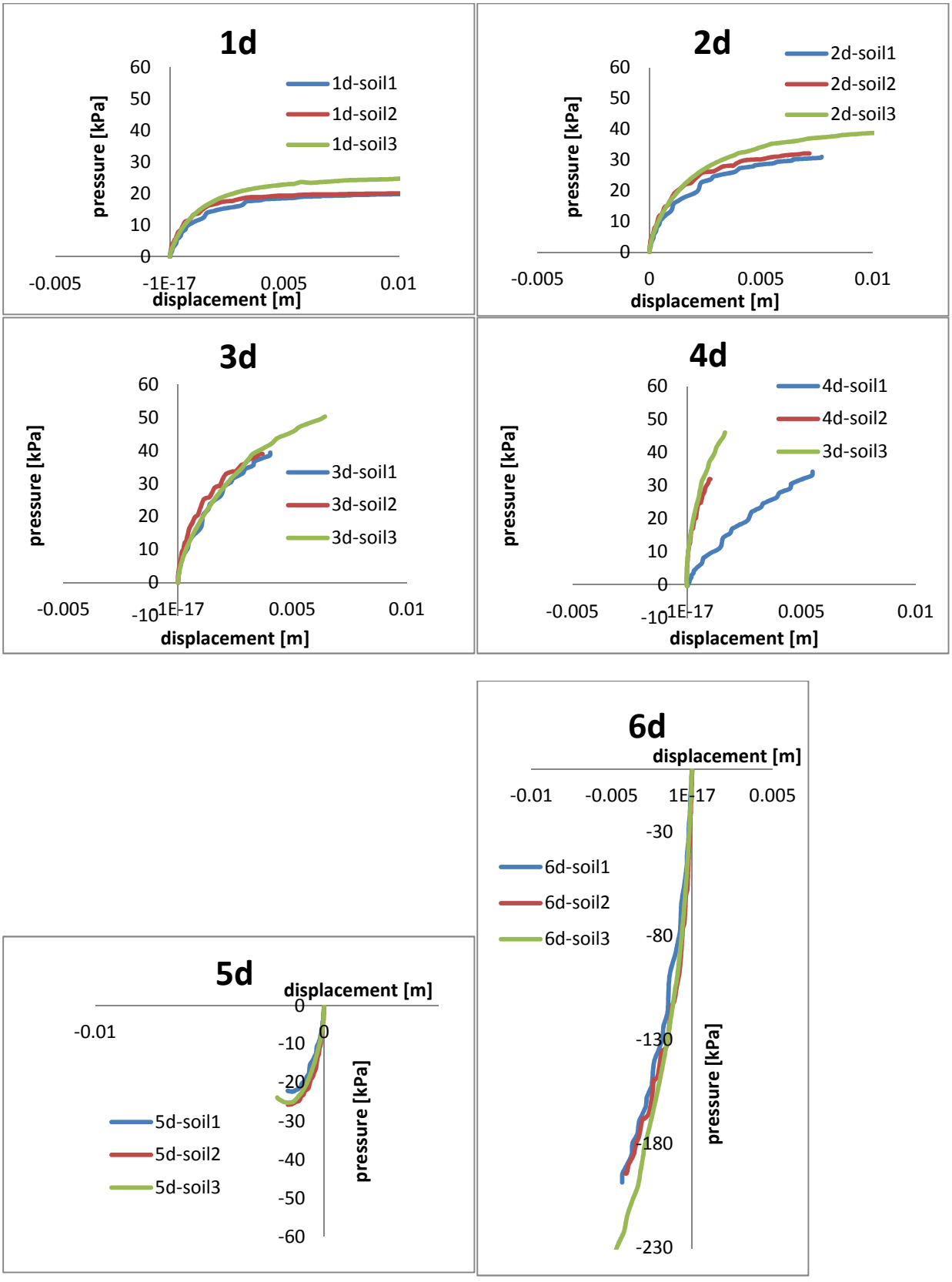

Figure 4.13: Comparison of p-y curves in hollow plugged piles

In the plugged flexible pile the interface friction and the soil friction influences both the load-displacement curve and the p-y curves. The lateral capacity increases in the same way as the hollow unplugged pile. The stiffness of the p-y curves and the ultimate resistance increases a bit as interface friction or soil friction increases. Also in the p-y curves the soil friction effects more the results respect to the interface friction.

Rigid pile

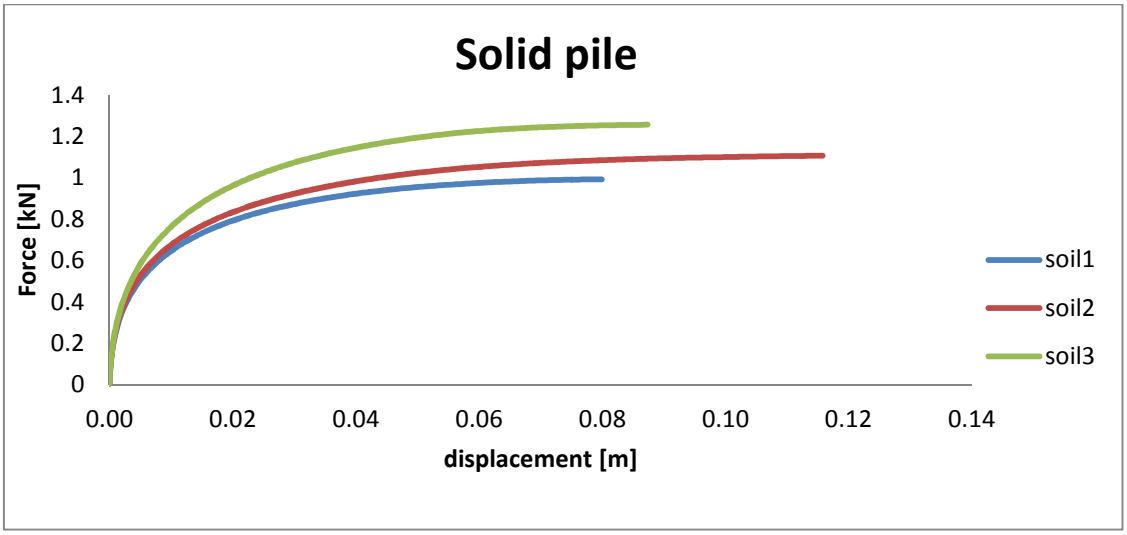

Figure 4.14: Comparison of force displacement curves in rigid piles

The variation of ultimate load with different type of soil can be estimated from the model of rigid pile because it is the only one that reaches the failure.

- p-y curves

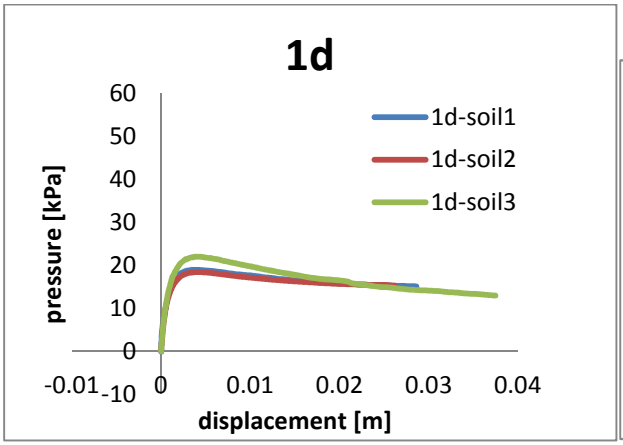

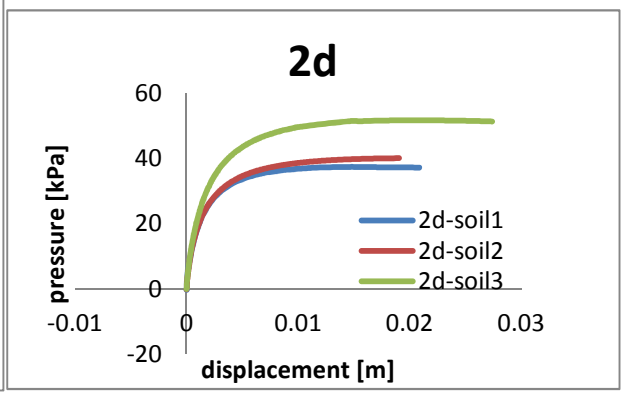

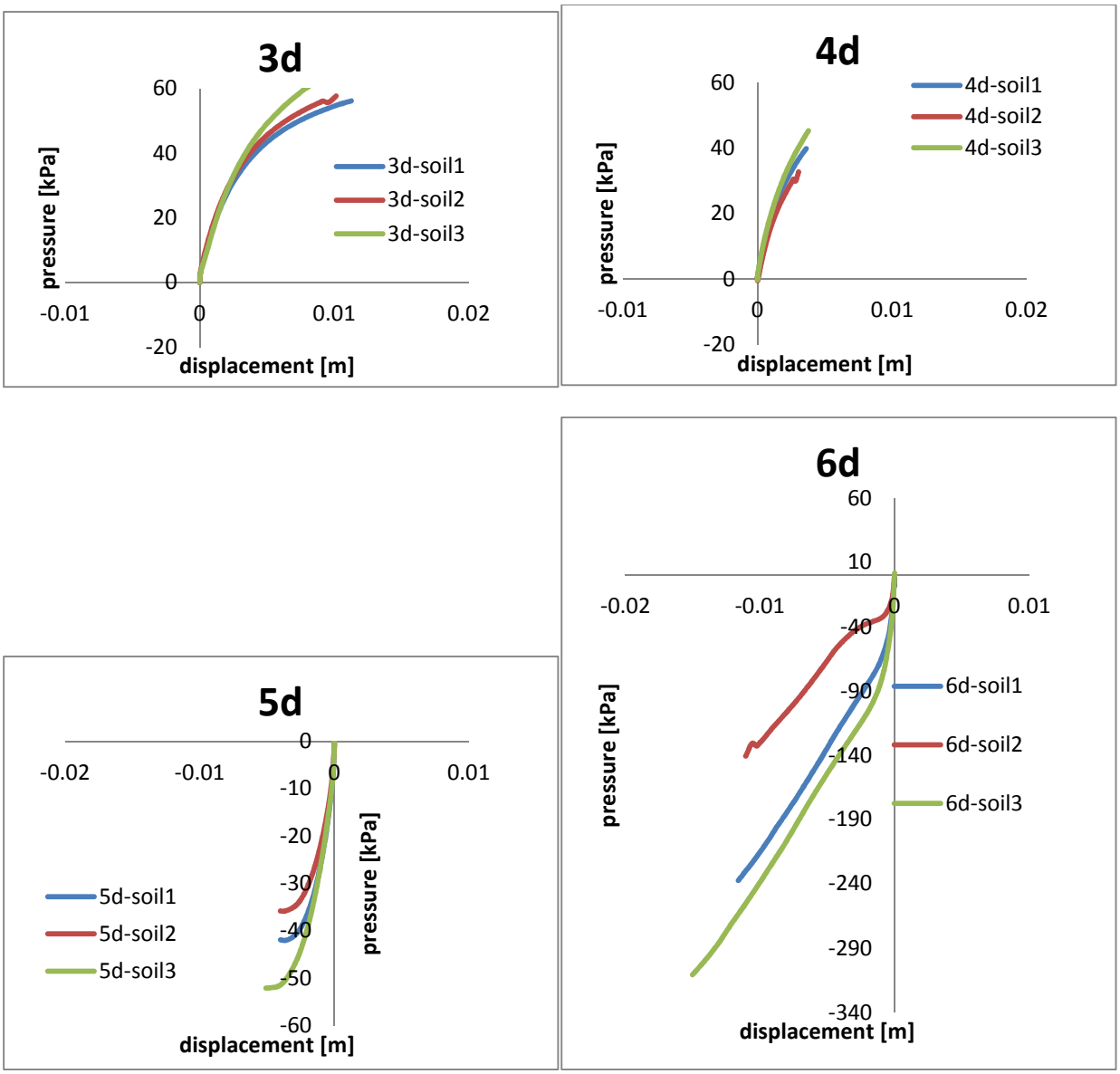

Figure 4.15: Comparison of p-y curves in rigid piles

The soil properties affect significantly both the lateral capacity and the p-y curves. The variation of soil shear strength impacts more than the variation of interface shear strength and this will be relevant in order to find the soil properties that fit more with the properties of the sand in the lab tests.

4.3 Comparison with design Method

4.3.1 Ultimate load (Broms)

In this chapter the ultimate load of the Broms theory is compared with the obtained results. The ultimate force of Broms theory is computed for the prototype pile using the following formula (explained in details in paragraph 1.1.2.1) is the pile is rigid:

$$H_u = \frac{0.5\gamma' D L^3 K_p}{e + L} = \begin{matrix} 276kN\ for\ \phi = 33° \\ 314kN\ for\ \phi = 36° \end{matrix}$$

where
D: pile diameter → 1m
e: eccentricity →15D=15m
L: pile length → 6m
γ': effective unit weight → 16.67kN/m^3
K_p: passive lateral earth pressure coefficient→ $K_p = \frac{1+sen\phi}{1-sen\phi} = \begin{matrix} 3.39\ for\phi = 33° \\ 3.85 for\phi = 36° \end{matrix}$

If the pile is flexible it means that the moment corresponding to the ultimate load calculated using the previous formula is higher than the yielding moment.

$$M_u > M_y = \frac{J\, f_y}{\frac{D}{2}}$$

where

J: inerzia moment → $J = \frac{\pi D^4}{64} = 0.039\ m^4 \quad for\ rigid$
$J = \frac{\pi(D_e{}^4 - D_i{}^4)}{64} = 0.0059\ m^4 \quad for\ flexible$

fy: steel strength → $f_y = 300\ MPa$

Since the models are in a reduced scale (N=25g), to compare the results with Broms' theory the forces are multiplied by the scale factor to the square and the displacements are multiplied by the scale factor N=25.

Hollow pile plugged and unplugged

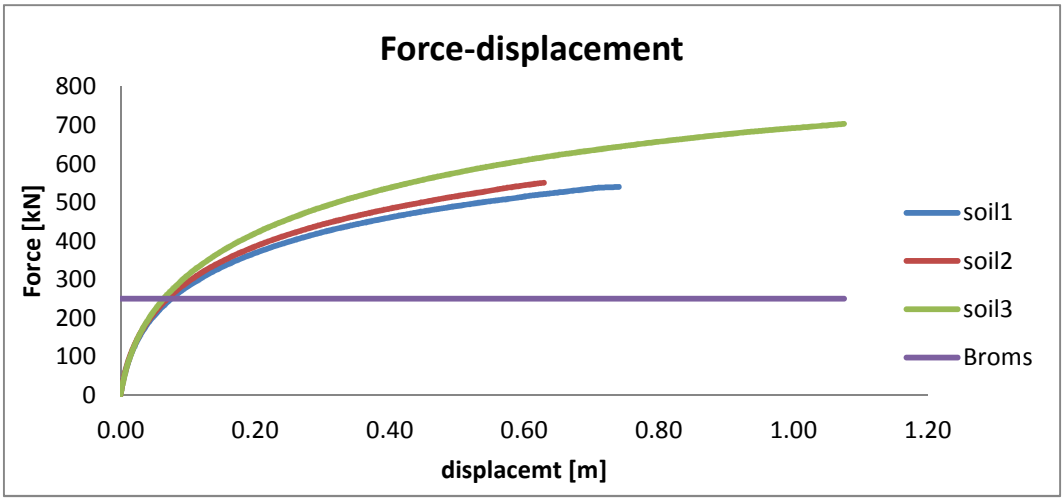

Figure 4.16: Comparison of force displacement curves in flexible piles with Broms theory

Rigid pile

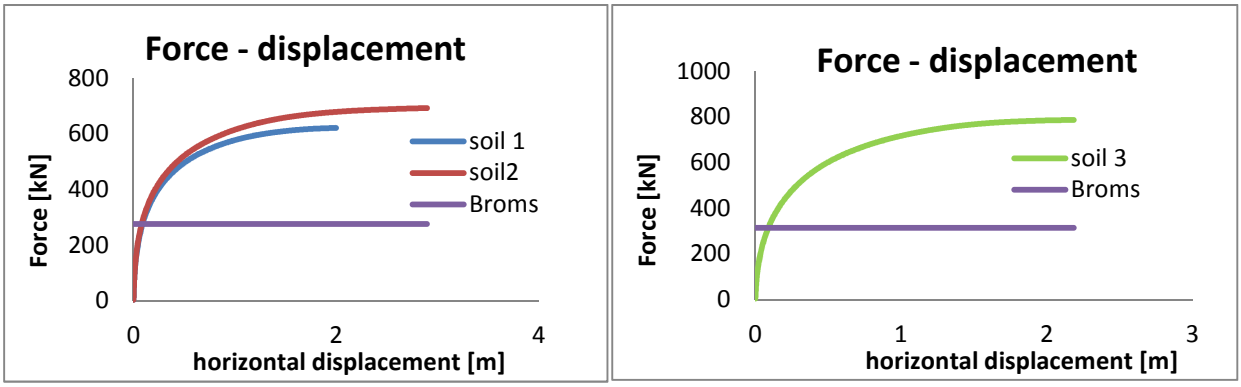

Figure 4.17: Comparison of force displacement curves in rigid piles with Broms theory

First of all it is important to mention that Broms' theory gives just the ultimate load that the soil can bear and not all failure criteria of the system. For this reason the relevant graphs in this paragraph are the ones of the rigid pile since they reach the ultimate force. The argument can be generalized for all the thee type of pile

Regarding the reference soil (soil1), the ultimate force calculated by Broms matches the ones obtained with the Abaqus simulation.

Broms' theory does not take into account the interface shear strength, hence it underestimates the ultimate force for higher interface strength than 2/3ϕ (soil2).

Increasing shear strength angle both the ultimate load from Broms' law and from the Finite element model increase, but the one from the FE Model is considerably higher. Broms' theory also in this case underestimate the force.

4.3.2 API p-y curves

In order to compare the p-y curves, 2 parameters are observed. The ultimate pressure(ultimate soil resistance) is the value by which the curve becomes horizontal, not at all the depth this value has been reached in the Finite Element Models. The initial stiffness kx of the p-y curve is the tangent of the curve at zero defection.
Looking at the p-y curves of chapter 3 (graph 3.14, 3.20, 3.24, 3.28, 3.34, 3.38, 3.42), it is evident that mostly the p-y curves calculated with the API formula (explained in pagaraph 1.1.2.2, chapter 1) underestimates the ultimate pressure and the initial stiffness kx respect to the curves obtained with the Finite Element Model. For shallow depth (1d and sot times 2d) there are some exceptions usually at depth 4Dimeters and 5Diametrs (0.16 and 0.20m under the ground level).
In the unplugged pile at 5D the initial stiffness computed with the two methods present the same values with all the type of soil; moreover in the soil with higher interface strength (soil 2) also the ultimate value is the same with API formulas and FEM results.
In the plugged pile at 5D the stiffness is very similar with the two methods for all the type of soil. In the reference soil (soil 1) also the ultimate pressure is the same at this depth and at 4D the stiffness is the same too.
In the rigid pile the stiffness of the p-y curves calculated with the finite element method coincide with the API provision at the depth of 4D for all the type of soil. For the soil with higher interface strength (soil 2) at 5D the stiffness is the same but the ultimate pressure calculated with the API formulas is higher than the one obtained with the FEM simulation.
The discrepancy between the code provision (API curves) and the curves predicted by the 3D FE analyses may be attributed to the negligence of the contribution of interface shear resistance of the API curves and to the inappropriate consideration of the variation of ultimate soil resistance with depth in the code provision[16].

4.4 Comparison with centrifuge modelling

In this paragraph the Finite Element Models are related with centrifuge test described in Thesis "Centrifuge testing for installation and stiffness effects on lateral load behaviour of monopiles"[1]. The lab test are two for each type of pile:

- Lab test 1: installation and loaded phases at 25g(increase of gravity). Since the installation phase in the numerical models has not been done, they should be compared with this lab tests 1.
- Lab test 2: installation phase at 1g (standard gravity) and loaded phase at 25g(increase of gravity). Since in these tests during the installation phase the gravity is less than the one used to have the stresses of the prototype, the soil properties could have been distorted. For this reason is usually used the other lab test for the comparison.

The curves analysed are the force- displacement curves because they give information on the lateral load capacity. At the moment the p-y curves cannot be compared because the calculation of the deflection from the lab test results is still under research.

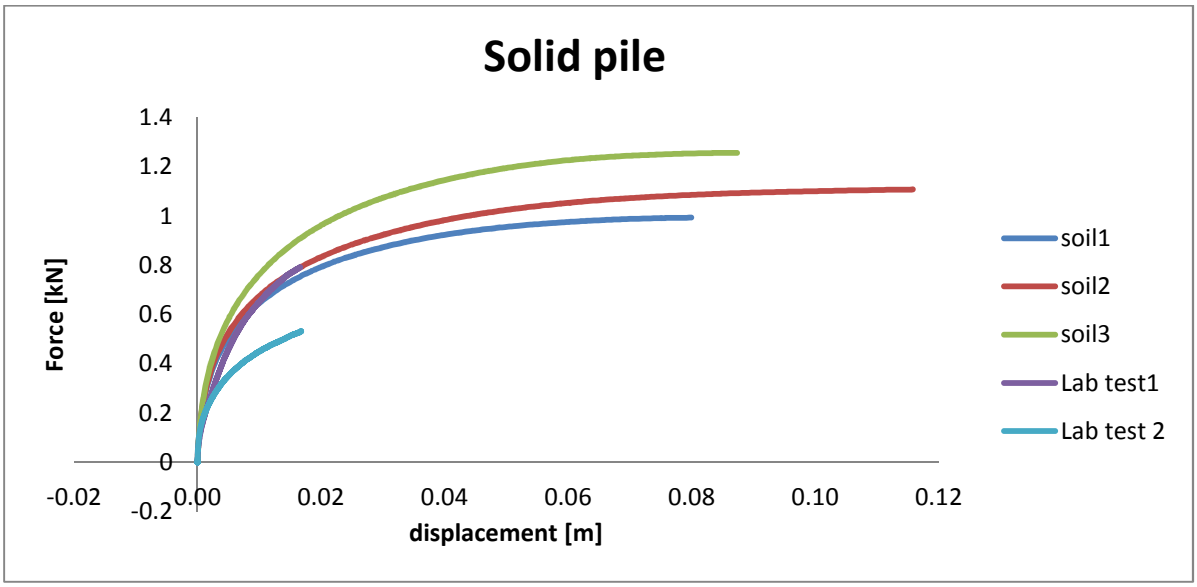

Figure 4.18: Comparison of force displacement curves in solid piles obtained with FE analysis with curves obtained with centrifuge tests

The results of the lab test 1 of the centrifuge (25g installation) regarding the force displacement curve fit better the FE analysis than the results of test 2 (1g installation) as it is expected because the installation phase is not modelled in the FE models.
For rigid pile the lab test 1 with the installation at 25g (test 1) fits perfectly with the FE model where the angle of interface shear strength is $\varphi=\phi=33°$ (soil 2).
The interface shear strength is generally different from the residual strength of the soil itself, and depends on the interface material and its roughness as well as on the properties of the soil, the grain size distribution and shape of the soil particles, the magnitude of the normal stress and the rate of shear displacement. It is usually assume equal to 2/3 of the soil strength but since it depend on several parameter it is very difficult to estimate. From this graph it seems that the shear strength of the sand in the Lab test 1 is equal to the soil strength.

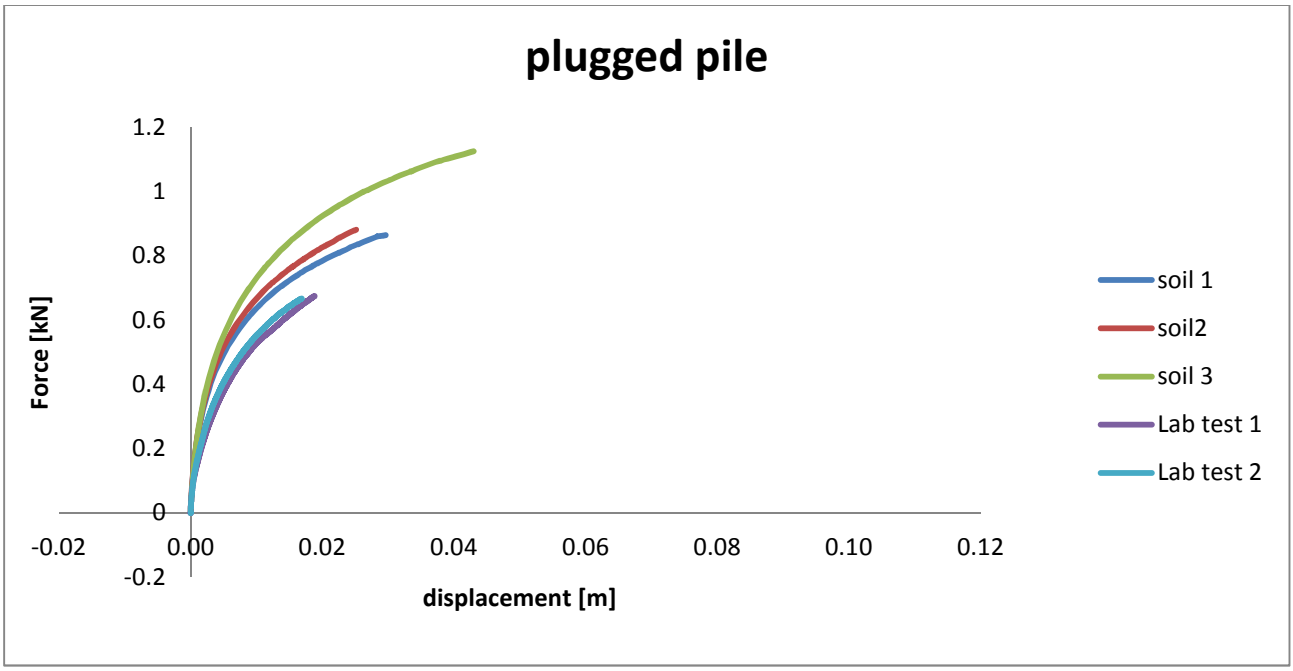

Figure 4.19: Comparison of force displacement curves in plugged piles obtained with FE analysis with curves obtained with centrifuge tests

In the plugged pile, the centrifuge results in the two tests are very similar. The piles do not reach the ultimate lateral force, because the tests were stopped before, in the FE analysis numerical problems due to the distortion of the finite elements and in the lab tests it was necessary to avoid the breaking of the pile. However the pattern suggests where the ultimate value is located; the lateral capacity of the piles in the centrifuge tests appears considerably smaller than the ones of the FE analysis.

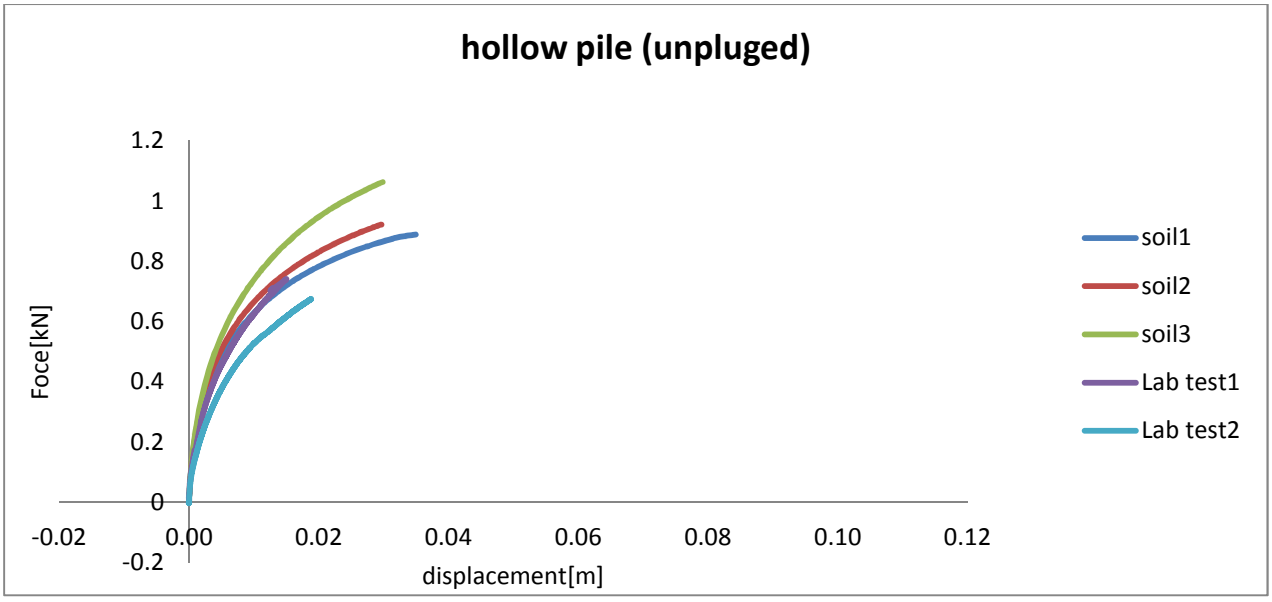

Figure 4.20: Comparison of force displacement curves in unplugged piles obtained with FE analysis with curves obtained with centrifuge tests

The results of the Lab test 1 (installation at 25g) merge the FE analysis better than the Lab test 2 as it is expected.
The trend of the force – displacement curve of the lab test 1 is between curve of the reference soil (soil 1) and the one of soil with interface shear strength equal to the soil shear strength $\varphi=\phi=33°$ (soil 2).
Also the unplugged pile does not reach the ultimate lateral force but the elastoplastic behaviour is evident also in this first part of the curves.

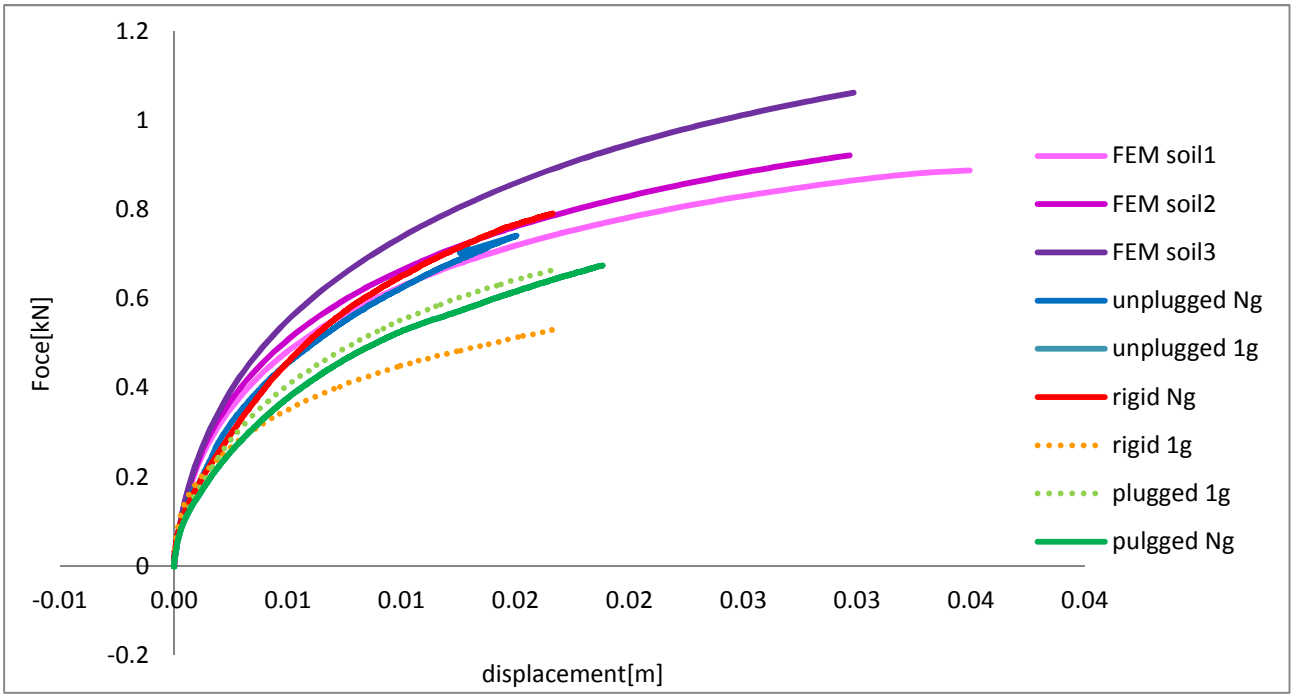

Figure 4.21: Comparison of force displacement curves in flexile and rigid piles piles obtained with FE analysis with curves obtained with centrifuge tests

The force-displacement curve in the FE analysis does not change varying the type of pile and consequently seems that the lateral load capacity does not depend on the pile stiffness. On the other hand from the centrifuge tests is evident that with the same installation procedure, the force-displacement curve varies as the type of pile is changed.
The reason of this phenomena could be that the installation effects occurs in the centrifuge also just changing the type of pile and not the installation procedure. The installation of plugged and unplugged piles produces different type of alteration of the soil, that gives a different soil response to the application of a lateral load. This phenomena does not occur in the FE analysis because the installation phase is not modelled.

5 Conclusions

In the current study the lateral response of rigid and flexible piles in cohoesionless soil was investigated. The effects of pile stiffness and soil properties were examined by analysing 3D FE models, which account for soil non linearity and geometric non linearity induced by sliding along the soil-pile interface and gap formation. The effect of pile stiffness and installation effects were examined by analysing the results of centrifuge tests in laboratory. The comparison of the two procedure helps in the interpretation of the results of the centrifuge test.

The results of the 3D FE models indicate that the induced failure mechanism is complex, including development of slip displacement along the soil-pile interface and plastic soil deformations.
The effect of the pile stiffness in the lateral capacity of the pile is found negligible even if the flexible and rigid piles present different deformed configuration. On the other hand, the stiffness and the type of pile (rigid or flexible) produces variations in the moment rotation curves and in the p-y curves. The failure mechanism (rigid body rotation or flexible deformation) might affect the moment rotation curves since the ones of flexible piles (plugged and unplugged piles) are generally more similar to the one of the rigid pile.
The effects of the increase of the interface shear strength and soil shear strength are shown to be significant affecting the pile lateral response. The lateral load capacity of the pile increases as the interface friction or the soil friction increases, the soil friction affect more this variation. The stiffness of the p-y curves and the ultimate soil resistance increase with shear strength of the interface or of the soil just at sallow soil depth; than the behaviour becomes more complex and depends also on the rotation point of the pile.

The comparison with the centrifuge tests highlightes the importance of the installation effects. The parameters and the assumptions used in the 3D models seem correct because the Lateral capacity obtained in the FE analysis fits well the results of the centrifuge tests at Ng installation for the rigid and the hollow unplugged pile. The interface soil friction of the experiments may be between $2/3\phi$ (reference soil) and ϕ (soil with increase of interface shear strength). The Lateral capacity in the centrifuge test varies also with different type of piles at the same installation condition while in the FE analysis the stiffness effects in the lateral capacity are found negligible. This may be attributed to installation effects that occurs during the installation of different type of pile which modifies the soil resistance in according to the shape of the pile.

Appendix: Cross section Bending Moment investigation

The objective of this benchmark is to prove the reliability of the results of the finite element analysis made by software Abaqus in terms of internal forces and deflection for the pile used in the model. Moreover the procedure used to find the bending moment distribution is used in the thesis.
The pile analysed is a hollow steel pile 6m long fixed at one side and loaded with a distributed force of 250kN/m, and figure 1 and table 1 shown.

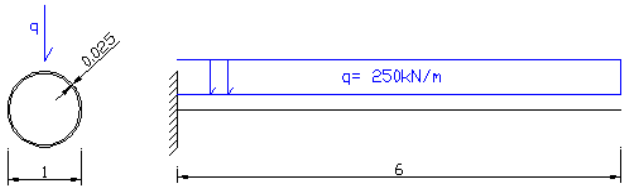

Figure A.1: pile´s static scheme

Hollow Pile properties		
material	steel	
Elastic modulus E	209 000	MPa
diameter D	1	m
thickness t	0.0375	m
length L	6	m
Moment of inertia I	0.0131508	mm^4
Load q	250	kN/m

Table A.1: pile properties

The analytical solution of a clamped beam is compared with the solution obtained from the Finite Element Analysis, where the pile is modelled both with solid element and shell element. The best procedure to obtain the bending moment from the output of the software is identify for the tow type of elements.

➢ Analytical solution

A clamped Eulero-Bernulli beam loaded with a distributed force is an isostatic problem since the DOFs are equal to the internal constrains. Therefore the equations for moment and shear distribution and deflection of the beam are easily founded.

Figure A.2: moment distribution

➢ Finite Element Solution

The Finite Element solution is based on the following approximate method. The structure is beaked into finite elements and it is assumed a deformed shape for each element. Than quantifying the shape by minimizing the distributed energy in the structure, the stresses and the displacement behaviour is predicted.

The problem is treated in two ways, the pile is modelled firstly with a shell element with the same properties of the given problem and then with a solid full pile with the same stiffness EI of the given problem in order to compare the results.

- **Shell element**

Shell structures are three dimensional structures, thin in one direction and long in the other two. The choice of this elements for the case studied is appropriate as long as the thickness of the pile is small respect to the diameter and the length of the pile.
Different type of mesh has been used in the model whose characteristics are listed in the table below.

Abaqus Input	
Part	
element	3D, Shell
Property	
Material	Elastic, Solid, Homogenous
Load	
Boundaryconditions	encastre
Load	shellload
Mesh	
Type	S8R, S4,S4R*
Size and shape	0.15quad
Elements along the cross section	20
Elements along the length	40

Table A.2: Shell element input

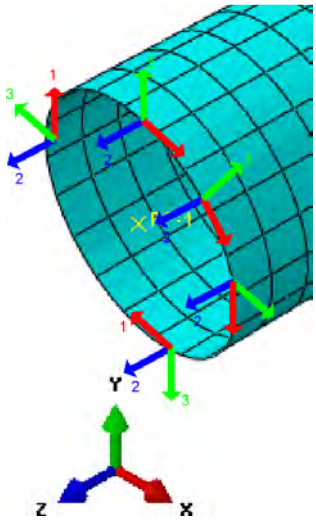

Figure A.3: local and global reference system

* S8R: quadratic elements with reduced integration
S4: linear elements without reduced integration
S4R: linear elements with reduced integration

The field output is set in order to obtain stresses (S)section forces (SF) section moments (SM) referred to the local reference system 1-2-3 of every element; and displacements(U1,U2.U3) and rotations (UR) referred to the global reference system xyz.

- <u>deflection</u>

The displacement U2 corresponds to the deflection of the pile and the values analysed are the one along the lateral edge of pile length where there are not fluctuations due to the load (figure 3).

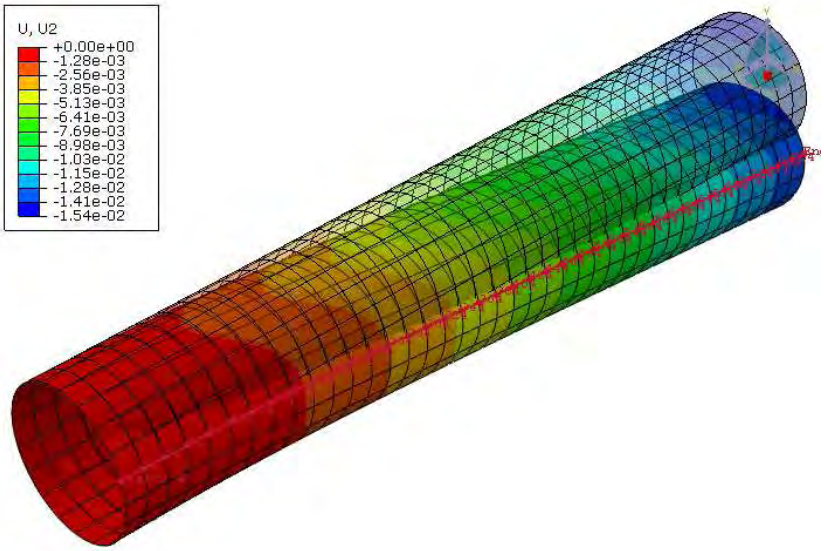

Figure A.4: Displacement U2 and path considered (red line)

In the graph it is compared the deflection founded using different mesh type with the deflection of the Bernoulli theory.

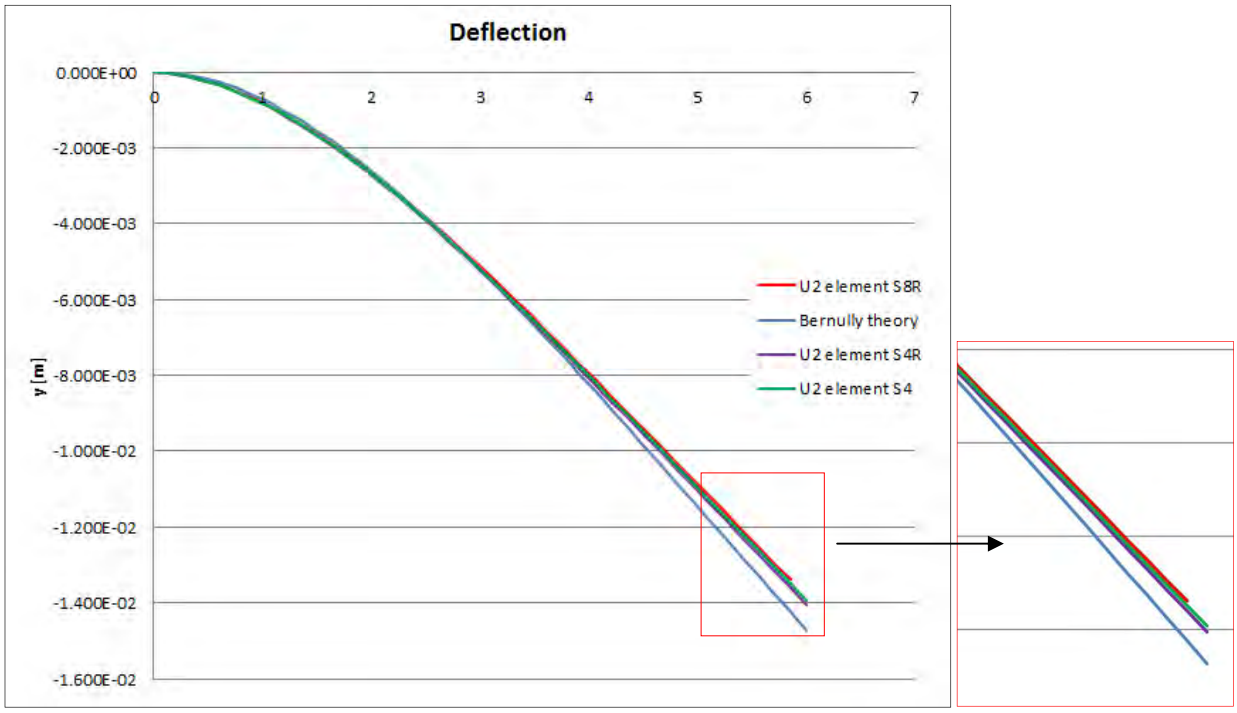

Figure A.5: deflection of the shell of the pile using different mesh type

Observing the graph is evident that there is not a big difference in the results according with the element type; although, the better elements to be used are the S4R (linear elements with reduced integration). They will be used later on in the benchmark and in the project.

- internal forces of cross sections

Internal forces of the section are not output of the program and they can be calculated using different methods. In this benchmark two procedures are compared: “integration” of forces in the section and calculation from horizontal stress.
The momet distribution is fistly calculate using the orizontal internal stresses σ (S22) at the top of the pile, in the Sant-Venant formula:

$$M = \frac{\sigma}{D/2} I_{solid}$$

The moments founded are compared with the theoretical solution in the graph 3.

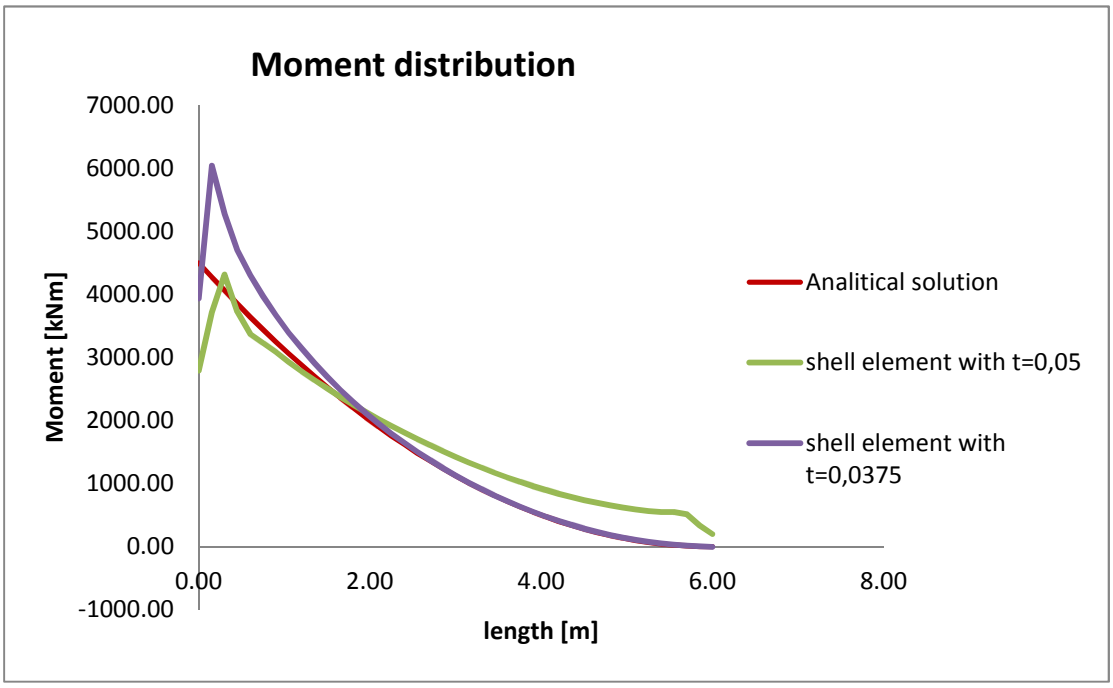

Figure A.6: Shell element moment distribution found with stresses method

The solution of the finite element method (green line) is quite different from the theoretical one ecspecially at the end of the pile, far from the constrain, because the cross section are defomed in this region and do not remain plane since the thikness of the pile is small (figure A.7). The finite element analysis calulate the stesses from the relative displacement therefore the stesses are ae afected by this problem.

In order to solve this preoblem and crate a more rigid cross section the thikness of the pile hase been increase until 0.05m (violet line). Is evdent that the problem of the deformation of the cross section is solved but now there is a big discrepance in the first tow metrs because the thikness of the pile is too

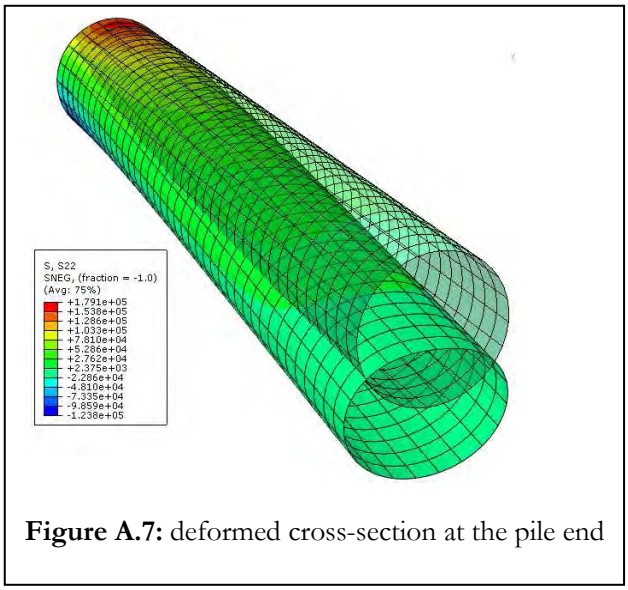

Figure A.7: deformed cross-section at the pile end

large to use shell elements.
The method of the stresses can not be use because it does not reliable solution, the second method is now analized.
In the “integration” of forces in the section, the moment in every cross section is calculated with an approximate integration of forces in the section.

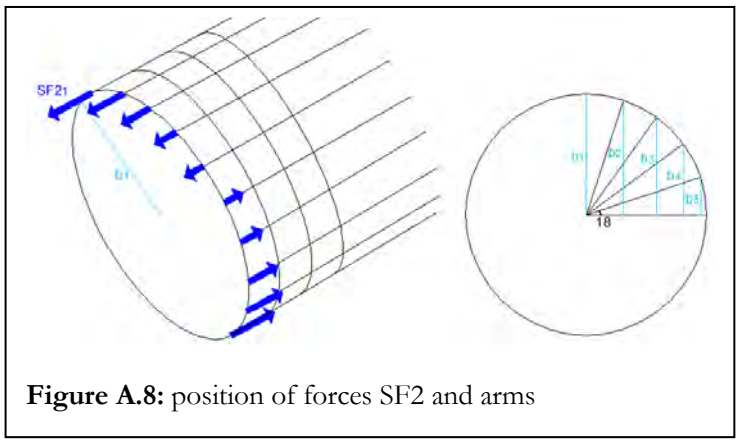

Figure A.8: position of forces SF2 and arms

where

$SF2_i$: Section forces in the i elements for every cross-section

b_i: arm of the force i respect to the canter of the pile→ $b_i = \frac{D}{2}\sin(18°i)$

The moments founded are compared with the theoretical solution in the graph 2.

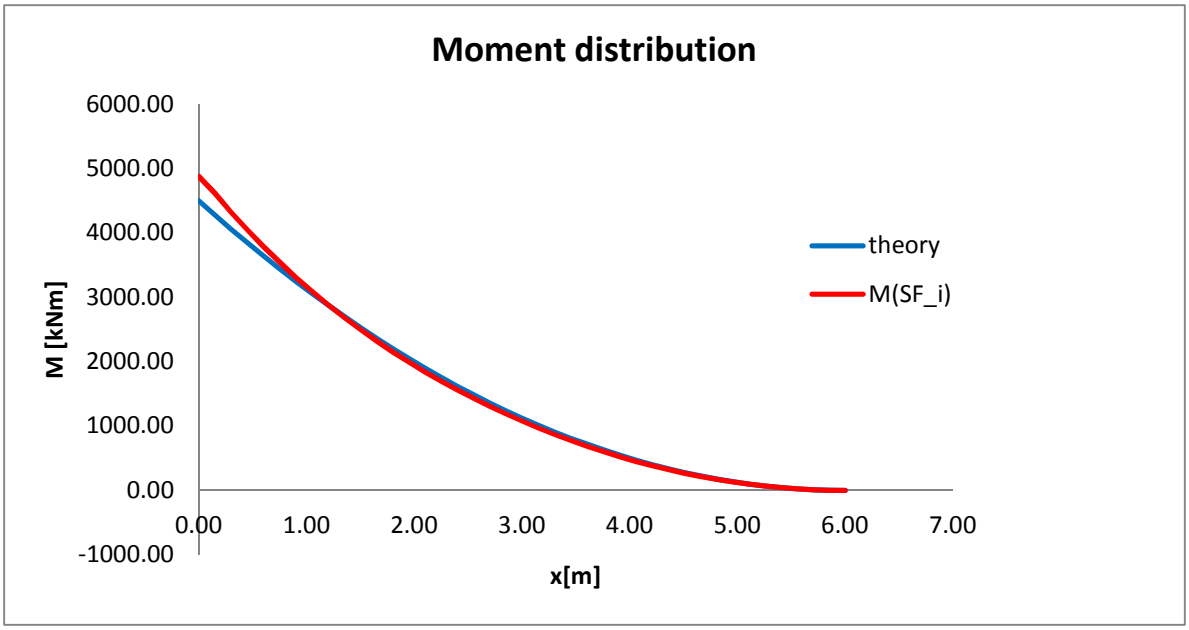

Figure A.9: moment distribution using “integration” of forces in the section

This method gives a solution very similar to the theoretical after 1meter length. The difference between the finite element solution and the theoretical one near the encstre is probably due to different behavior of the pile respect to the bernulli theory, indeed the ditribution of the forceses in this region is not linear alonge the cross section .
In coclusion this method to calculate the moment distibution of the pile is reliable and it will be use in the prject later on.

- **Solid elements**

Solid structures are three dimensional structures, with approximately the same dimensions in the three directions. For this reason the hollow pile is modelled as a full pile with the same stiffness EI of the datum one.
An equivalent elastic modulus is condidered in order to have the same stiffness and compare the results:

$$E^* = \frac{E\,I}{I_{solid}}$$

The load to a solid element must be pressure on a surface, so, in order to apply an equivalent load of the analysed problem, a pressure p an a thin surface at the top of the pile is applied.

$$p = \frac{q}{s} = \frac{250kN/m}{0.002m}$$

The properties of the solid pile considered and the characteristics of the model are summarized in tables.

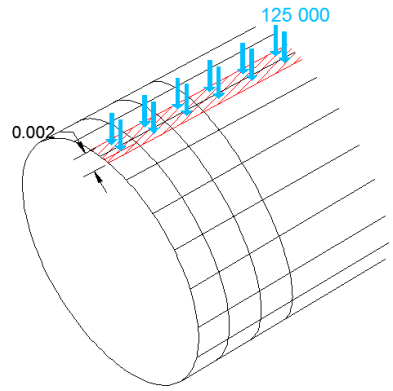

Figure A.10: pressure on the solid pile

Solid Pile properties		
material	steel	
Elastic modulus E*	55 992	MPa
diameter D	1	m
length L	6	m
Moment of inertia I	0.049087	mm^4
Load q	125000	kPa

Table A.3:equivalent solid pile properties

Abaqus Input	
Part	
element	3D, Solid
Property	
Material	Elastic, Solid, Homogenous
Load	
Boundaryconditions	encastre
Load	pressure
Mesh	
Type	C3D20, C3D20R*
Size and shape	0.15, hex
Elements along the lenght	40

Table A.4: **solid pile input**

* C3D20: quadraticbricks 20nodes
C3D20R: quadratic bricks 20nodes, reduced integration

The field output is set in order to obtain stresses (S), displacements(U) and rotations (UR) all referred to the global reference system xyz.

- internal forces of cross sections

The momet distribution is calculate using the orizontal internal stresses σ (S33) at the top of the pile, because there is not deformatin of the cross-section .The Sant-Venant formula is therefore used:

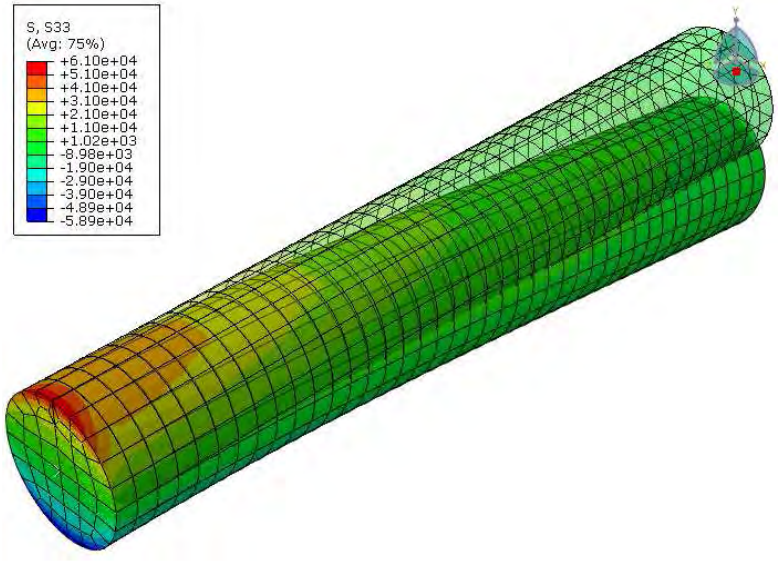

Figure A.11: orizontal internal stresses

In the following graph (Figure A.12) the finite different method is compared with the analytical solution using two different type of elements.

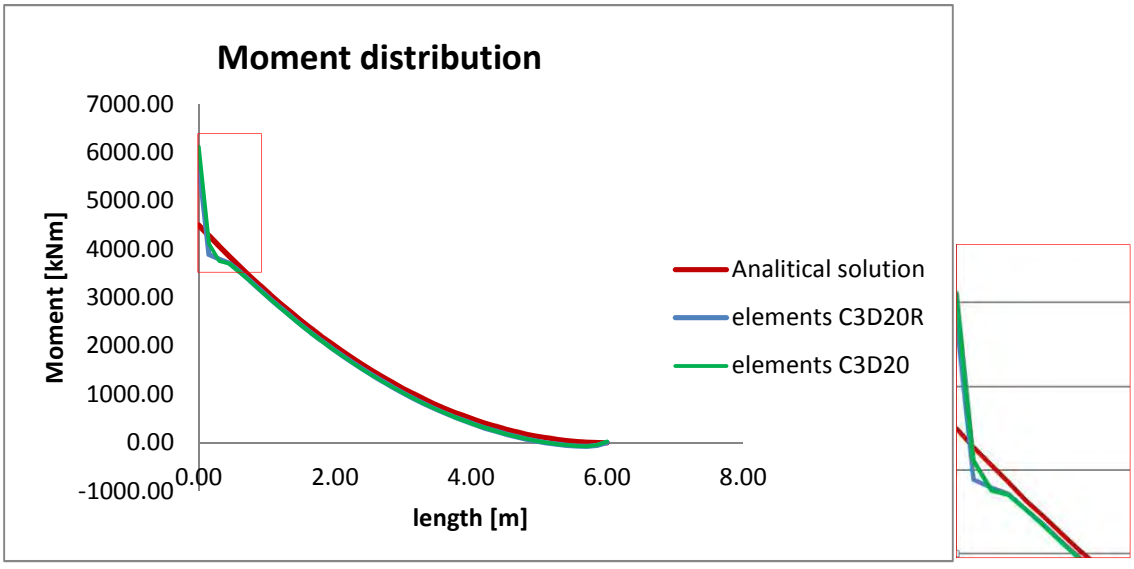

Figure A.12: Solid element moment distribution found with stresses method

The finite element solution is very similar to the theoretical one after 1m from the constrain because in that region the stresses are not linear and they do not follow the Bernoulli beam theory. The two element type chosen gives very similar results, anyway the elements C3D20 (quadratic bricks without reduced integration) are chosen because gives slightly better results.

Comparison and conclusions

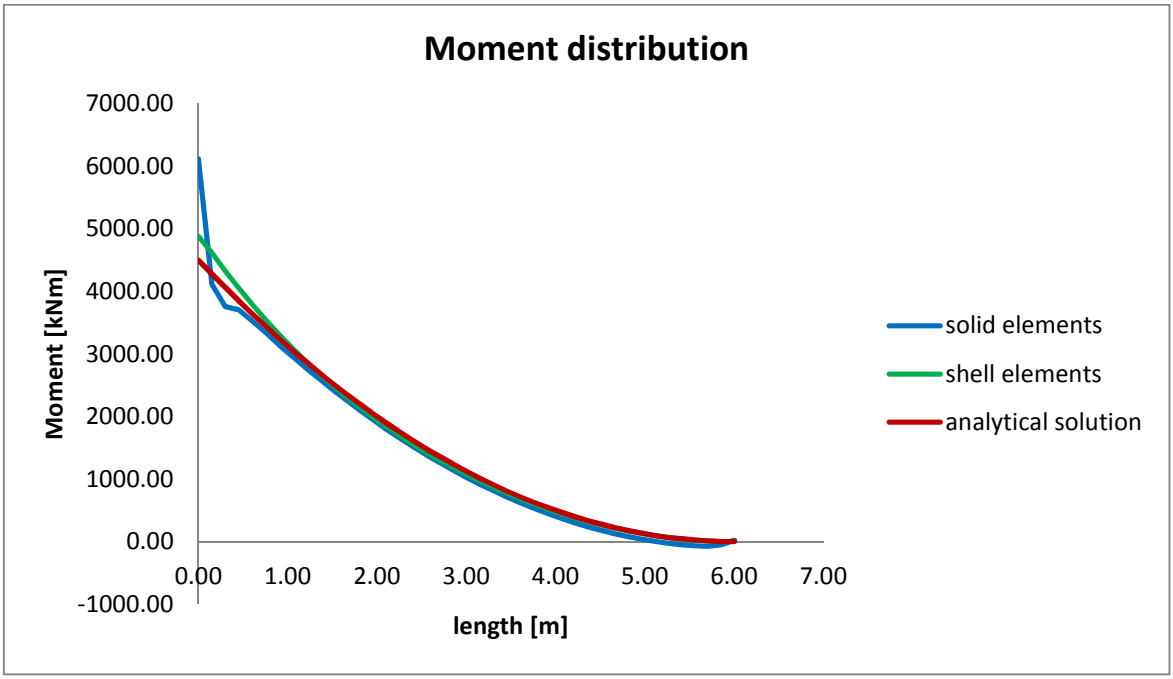

Graph 1: comparison between moment distribution of solid and shell elements

Comparing the moment distribution obtained from a finite element analysis using shell and solid elements to model a hollow pile, is evident that the best choice is the shell elements. Moreover using shell elements the deflection can also be considered and compared with Bernoulli theory.

References

1. C. Latini , " Centrifuge testing for installation and stiffness effects on lateral load behaviour of monopiles" Master thesis 2013
2. L. C. Reese; William M .Isenhower., Shin-Tower Wang , "Geotechnical design of driven piles under axial loads"(chapter 10) and "Fundamental concepts regarding deep foundation under lateral loading" (chapter 12) in "Analysis and Design of Shallow and Deep Foundations", John Wiley & Sons, 2006.
3. M.Gurnaratne, "Design of Laterally Loaded Piles"(chapter 8) in " The foundation engineering handbook", Taylor & Francis Group, 2006
4. B.B. Broms,M. ASCE "Design of laterally loaded piles", Journal of Soil Mechanics and foundation division, May 1965
5. I.F. Møller, T. Christiansen, "Laterally loaded monopole in dry and saturated sand-Static and cyclic loading" Master Project, June 2011
6. American Petroleum Institute, "Recommended Practice for Planning Designing and Constructing Fixed Offshore Platforms-Working Stress Design" API RP-2A-WSD, 2000
7. D-pile group manual
8. V. Adams, Abraham Askenazi, "Building Better Products with Finite Element Analysis"
9. K. J. Bathe ,E. L. Wilson, "Numerical Methods in Finite Element Analysis, Prentice-Hall", 1976.
10. L. C. Reese, William F. Van Impe, " Single Pile and pile groups under lateral loading" 2001 A.A. Balkema, 2011
11. D.A.Brown, C.-F .Shie,"Three dimensional finite element model of laterally loaded piles", Computers and Geotechnics,10(1),59-79,1990.
12. D.A.Brown, C.-F .Shie "Some numerical experiments with a three dimensional finite element model of laterally laded pile", Computers and Geotechnics,10(1),59-79,1990.
13. M.Laman, G.J.W. King, E.A. Dickin, "Three dimensional finite element studies of the moment-carrying capacity of short pier foundation in cohesionless soil" ", Computers and Geotechnics,25(3),141-55.1999.
14. C.-C.Fan, J.H. Long , "Assesment of existing methods for predicting soil responce of laterally loaded piles in sand" Computers and Geotechnics,32(4),274-289,2005.

15. Z.Yang, B. Jeremic, “Numerical analysis of pile behaviour under lateral loads in layered elastic-plasic soils”,International Journal for Numerical and Analytical Methods in Geomechanics,26,1385,1406,2002.
16. V. Zania, O. Hededal, “The Effects of Soil-Pile Interface Behaviour on laterally Loaded Piles”, 2011
17. M. Eskesen, J. Buhrkall, J. Henningsen, “Triaksialforsøg- Laboratoriepraktik”, Danmarks Tekniske Universitet, 2010
18. Abaqus manual

Table of contents

0.Introduction

0.1 Motivation

In this study, the lateral response of monopiles embedded in sand is investigated, since the actual methodology is not calibrated for design of large diameter stiff monopiles and does not account for stiffness and installation effects.

Nowadays new wind farms are being constructed in deeper and deeper waters and the type of foundations for such offshore wind turbines is the monopile. A monopile is a single large diameter tubular steel pile driven 5 to 6 times its diameter (4-6 meters) into the seabed. This structure is subject to the lateral loads from wind and waves, which determine a force with a significant eccentricity at the base of the pile[2].

In design method, the lateral load capacity is determined by considering two different failure mechanisms: (1) ultimate soil resistance and (2) acceptable lateral deflection of single piles. In rigid piles the failure is due to the shear failure of the soil against the pile (1° criterion); while in flexible piles the ultimate capacity can also be reached due to the excessive lateral deflection (2° criterion)[3]. The lateral load pile response can be evaluated assuming a linear elastic or non-linear elastic behaviour of the soil. In the first one the Winkler-soil-model(1867) is assumed, the soil along the pile is considered as a series of infinitely closely spaced independent and elastic springs with a constant stiffness at each depth. Assuming a nonlinear behaviour, the soil stiffness is not constant and there is a non-linear relationship between the soil resistance and its displacement (p-y curve). The large diameter stiff monopiles exhibits a nonlinear behaviour of the soil and consequently the ultimate soil resistance, the soil stiffness and the lateral load capacity depend on the p-y curves ,but the ones recommended by the American Petroleum Institute (API)do not consider the installation and stiffness effects.

0.2 Scope of the work

The scope of this work is to study installation and stiffness effect on the response of a lateral loaded monopiles in clean fine sand.
This thesis is focus on the stiffness effects investigated with numerical models and it is a comparison to the thesis entitled “Centrifuge testing for installation and stiffness effects on lateral load behaviour of monopiles”[1].
The lateral capacity and the soil stiffness at different depth of three-dimensional numerical models of rigid and flexible piles embedded in sandy soil are estimated. The the friction angle and interface friction properties of the pile are the parameters which vary in the F.E. Models.

1. Background - theory

The theory behind this study regards geotechnical knowledge and some overall information about Finite Element Modelling.
Geotechnical theory about the design of lateral loaded mopiles is cohesionless soil is presented in paragraph 1.1. Even if the numerical models do not consider the installation phase, it is presented a summary of the actual theory concerning both axial and lateral load needed to better compare FEM results to centrifuge test.

1.1 Design of piles

In this chapter two theoretical aspects regarding the pile behaviour are introduced: (1) the end bearing capacity which is to account during the installation phase and (2) the lateral response to compare with tests results. These are two different load carrying mechanisms and the corresponding resistance. This provides the resistance of the pile to axial and lateral loading respectively.

1.1.1 Axial Load Capacity

The ultimate load that can be applied to a given pile depends on the resistance that the pile can produce in terms of side friction (shaft resistance) and point bearing resistance.[2]

Therefore, the ultimate bearing capacity is computed by use of the following equation:

$$Q_t = Q_s + Q_b$$

Q_s: total skin-friction resistance

Q_b: total end bearing resistance

According to Meyerhof's theory (1951-1976), the end bearing capacity of the tip of the pile can be assumed to increase linearly to a critical depth and then remains constant. The end bearing capacity can be determined as follows:

$$Q_b = \sigma_v' N_q A_p$$

σ_v': the vertical effective stress at the pile tip

$$\sigma_v' = \gamma' z$$

N_q: bearing capacity factor, which depends on the friction angle φ of the soil as reported in Figure 1.1 or it can be calculated according to the Terzaghi's formula (1943):

$$N_q = e^{\pi tan\varphi} tan^2\left(45 + \frac{\varphi}{2}\right)$$

A_p : gross end area of the pile

The diagram reported in Figure 1.1 has been traced considering several loading tests taken from different sources. Meyerof (1953) used the length to diameter ratio L_c/d, whose value corresponds to the penetration depth for which the bearing capacity reaches the limit.

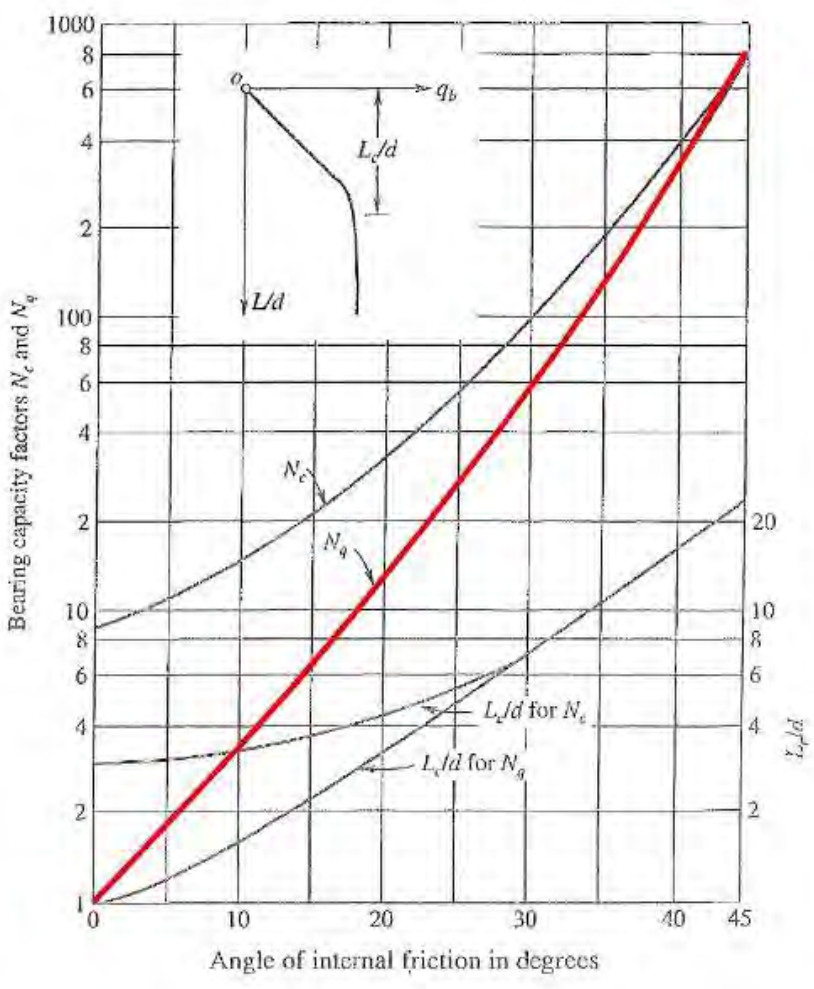

Figure 1.1: bearing capacity factor according to Meyerof's theory

And the shaft resistance can be obtained as:

$$Q_s = \int_L \tau_f A_s dz$$

where

τ_f: skin friction

A_s: side surface area of the pile

Since the origin of skin friction in granular soils is due to the frictional interaction between piles and granular material, the unit skin friction can be expressed as:

$$\tau_f = K\tan\delta\sigma'_{v0} \leq \tau_{f,max}$$

where

K: coefficient of lateral earth

$$K = \begin{cases} 0.8 \text{ for open} - \text{ended, unplugged piles} \\ 1 \text{ for closed} - \text{ended or plugged piles} \end{cases}$$

σ'_{v0}: effective overburden pressure at the point in question

δ: friction angle between the soil and the pile wall

1.1.2 Lateral Load Capacity

For proper functioning of structures subject to lateral load, two criteria must be satisfied: (1) a pile should be safe against ultimate failure (H_u); and (2) horizontal deflection (y) at working loads should be within the permissible limit. The ultimate lateral resistance and the working load deflection of single piles depend of the dimensions, the strengths, and the fixity conditions at the top on the deformation characteristics of the soil surrounding the loaded pile [3].The lateral response can be determined considering different assumptions of the soil and pile behavior.
Regarding the behavior of the pile, two failure mechanisms can be distinguished. For “rigid” piles the behavior is elastic and the yielding does not occur; while in “flexible” piles the plastic hinge formation has to account. In this study, the “rigid” pile behavior is only considered.

1.1.2.1 Lateral Load Capacity Based on Ultimate Load

From literature the common procedures to estimate the ultimate lateral resistance are the Brinch Hansen’s theory (1970) [2] and the Broms’ theory (1965)[4]. The latest is presented and discussed in this study. Broms assumed that the rigid pile developing negligible elastic deformation, whereas the considered failure mode is rigid body rotation. In addition, the active pressure at the back of the pile and friction soil-pile interaction are neglected. In cohesionless soils the assumed lateral earth pressure distribution at failure for a laterally loaded pile is shown in Figure 1.2.

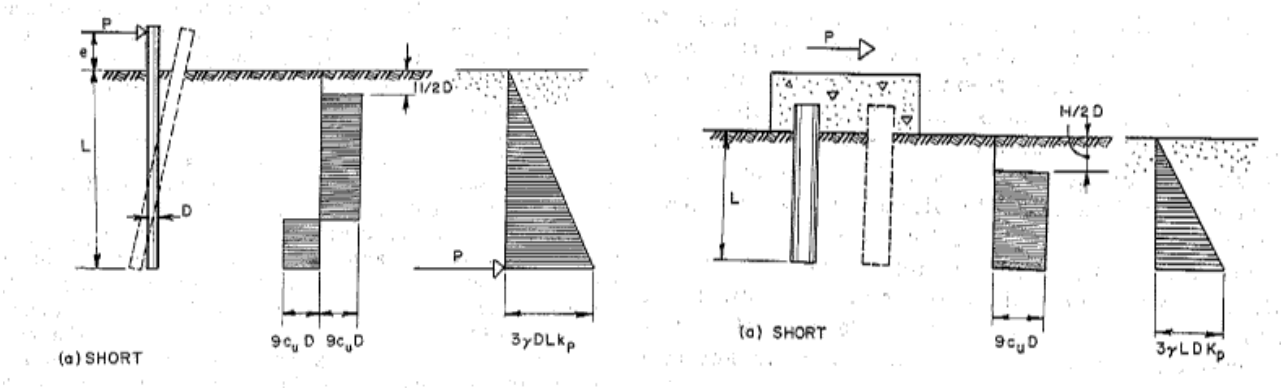

Figure 1.2: failure mode for short - free head pile (on the left) and short, restrained piles (on the left) [4].

The lateral earth pressure distributions shown in Figure 1.2, derive from the following considerations. At failure, it is possible to recognize that the soil disposed in front of the loaded pile moves upwards, whereas the soil in back of the pile moves into space created at the back of the laterally loaded pile. Around a depth of one pile diameter below the ground level the lateral earth pressure can be calculated by Terzarghi's theory, while below this depth it is observed the arching within the soil in proximity of the pile and this affects considerably the lateral earth pressures. For depths greater than one pile diameter, the passive lateral earth pressures, at failure, overcome the Rankine passive pressure, whereas the lateral earth pressure achieving on the back side significantly smaller than the active Rankine lateral earth pressure. Comparison with available test data have indicated that the lateral earth pressure at failure can be estimated as three times the passive Rankine earth pressure.

$$p_p = 3\sigma_v' K_p$$

where

σ_v': effective vertical overburden pressure

K_p: passive lateral earth pressure coefficient. which is a function of the friction angle φ $\rightarrow K_p = \frac{1+\sin\varphi}{1-\sin\varphi}$

As mentioned before, the maximum load calculated according to Broms' theory that can be applied on the pile depends on the type of failure mechanism ("rigid"/ "flexible" pile) and the fixity conditions at the top.

For this study the failure for rigid free head piles occurs when the pile rotates as a unit through the soil around a point located at the some depth below the ground surface [4]. The ultimate lateral resistance of the soil develops along the total length of the pile and it is given by the following formula:

$$H_u = \frac{0.5\gamma' D L^3 K_p}{e+L}$$

where

e: eccentricity

D: pile diameter

L: pile length

γ': effective unit weight

In addition, it is possible to estimate the maximum bending moment associated to H_u. The location of the maximum moment can be determined by the following equation:

$$f = 0.82\sqrt{\frac{H_u}{D\gamma' K_p}}$$

Thus, the maximum moment can be calculated as

$$M_{max} = H_u\left(e + \frac{2}{3}L\right)$$

When the maximum bending moment M_{max} value, due to the ultimate load H_u is larger than the yielding moment M_y for the pile material, then obviously the pile behaves as a "flexible" pile and the actual ultimate lateral load H_u can be computed by setting $M_{max} = M_y$.

1.1.2.2 Lateral Load Capacity Based on Deflection

The true stress-strain response of the soil can be described as elasto-plastic. Analytical theories account only for the elastic response of the soil, while numerical methods need to be employed in order to consider the full elasto-plastic (nonlinear) soil response. Two commonly adopted methods to determine the lateral deflection are discussed in the ensuing sections.

- ***Elastic soil response***

The theory of the beam in an elastic foundation is given by Hetenyi (1946) and the following assumptions are considered:

- linear soil response
- pile is straight with uniform cross section
- longitudinal plane of symmetry
- pile material is homogeneous and isotropic
- elastic pile response
- Young modulus is the same for loading and unloading
- deflections due to shearing are small
- transverse deflections are small

In order to derive the equation of deflection, the equilibrium of moments for an infinitely small unloaded element, bounded by two horizontals a distance dx apart (see Figure 1.3), is presented in the following formula.

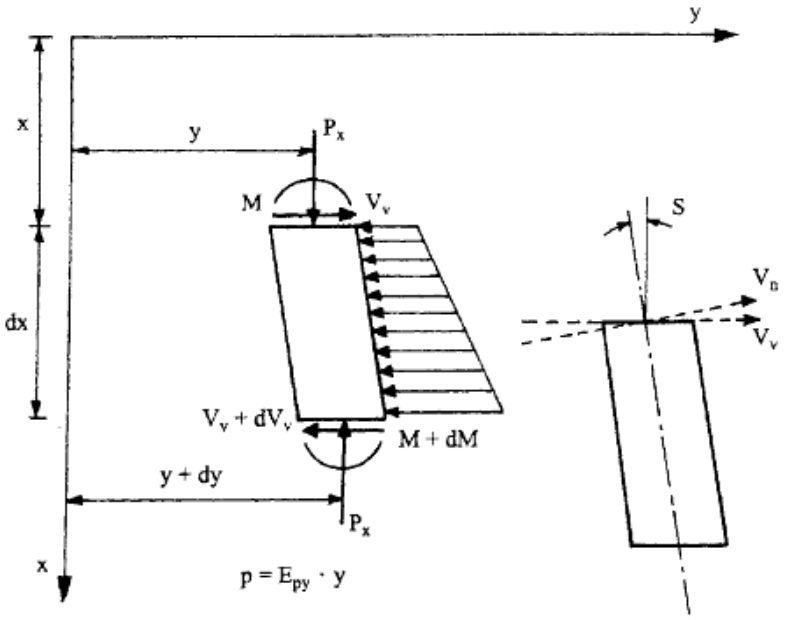

Figure 1.3: element from a beam column (after Hetenyi, 1946) [5]

$$(M + dM) - M + P_x dy - V_v dz = 0$$

Simplifying, the expression below is obtained:

$$\frac{dM}{dz} + P_x \frac{dy}{dz} - V_v = 0$$

Differentiating the previous expression with respect to x, the following equation is obtained:

$$\frac{d^2M}{dz^2} + P_x \frac{d^2y}{dz^2} - \frac{dV_v}{dz} = 0$$

The following identities are noted:

$$\frac{d^2M}{dz^2} = E_p I_p \frac{d^4y}{dz^4}; \quad \frac{dV_v}{dz} = p$$

where

E_p: elastic modulus of the pile

I_p: moment of inertia of the pile

p: the unit soil reaction

And at working loads the lateral deflection can be estimated by assuming that the unit soil reaction p increases linearly with increasing lateral deflection y as defined as:

$$p = k_h y$$

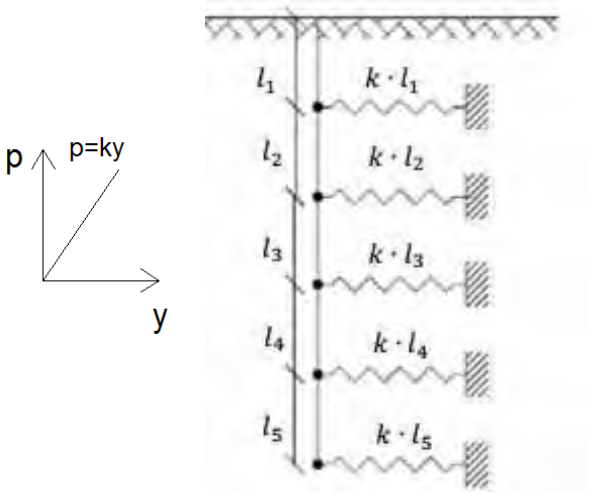

Figure 1.4: sketch of the model

The governing differential equation for the pile's deflection is the following:

$$E_p I_p \frac{d^4y}{d^4z} + P_x \frac{d^2y}{dz^2} - k_h y = 0$$

where

y: pile deflection

z: depth along the pile

k_h: is the coefficient of horizontal subgrade reaction, that depends of the deformation properties of the soil and on the dimension and stiffness of the pile.
In cohesionless soil, the lateral deflection of the pile can be computed considering that the coefficient of lateral subgrade reaction increasing linearly with depth and it is constant with the deflection:

$$k_h = \frac{n_h z}{D}$$

where

z: depth along the pile

n_h: coefficient which depends on the relative density of the soil

D: diameter of the loaded area

A simpler form of the differential equation if the assumptions are made that no axial load is applied, that the bending stiffness $E_p\ I_p$ is constant with depth. Thus, a reduced expression of the differential equation is:

$$E_p I_p \frac{d^4 y}{d^4 z} + 4\beta^4 y = 0$$

in which

$$\beta = 4\frac{k_h}{E_p I_p}$$

The solution may be directly written as

$$y = e^{\beta x}(C_1 \cos(\beta z) + C_2 \sin(\beta z)) + e^{-\beta x}(C_3 \cos(\beta z) - C_4 \sin(\beta z))$$

The coefficients of the integration are calculated according to the boundary conditions.

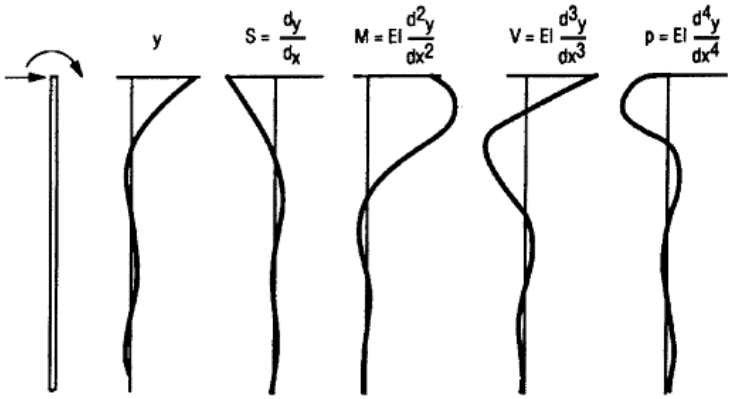

Figure 1.5: deflection, rotation, bending moment, shear and soil reaction obtained from a complete solution [4]

- ***Nonlinear soil response***

The key to determining the behavior of a pile under lateral loading is the ability to develop a family of curves (p-y curves) that give soil reaction as a function of the lateral deflection of a pile [3]. The nonlinear differential equation is the same of the one abovementioned, but the assumption of linear soil response is not account as expressed in the following formula:

$$E_p I_p \frac{d^4 y}{d^4 z} + P_x \frac{d^2 y}{dz^2} - k_h(y) y = 0$$

where

E_p: elastic modulus of the pile

I_p: moment of inertia of the pile

z: depth along the pile

y: deflection

$k_h(y)$: subgrade reaction, which varies nonlinearly with deflection y

The third member of the equation is the lateral earth pressure p and it can be calculated with $p - y$ curves approach. Once obtained the $p - y$ curves, the pile deflection, pile rotation, bending moment, shear and soil reaction for any load applied to the pile can be obtained solving the differential equations.

The p-y approach has been widely used to design piles subjected to lateral static or dynamic loading [4]. Based on the p-y approach the lateral soil-structure interaction can be modeled using empirically derived nonlinear uncoupled springs, so-called p-y curves, as boundary conditions in structural analysis.

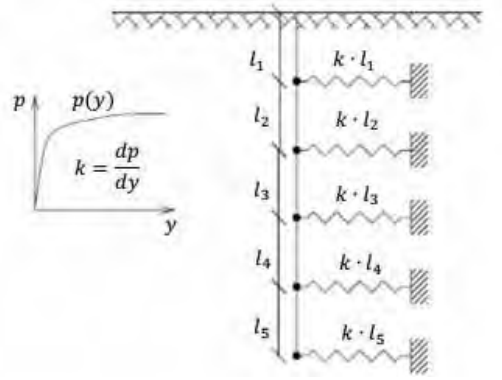

Figure 1.6: illustration of p-y method [5]

The stiffness of this springs, so the shape of the p-y curves depend on many variables as depth and soil properties. The American Petroleum Institute (API) developed a set of formulas to estimate the p-y curves for different type of soil. In the following paragraph it is shown the procedure for sandy soil.

p-y curves from code provisions API

The p-y curves adopted by the API are based on the method developed by O'Neil and Murchison (1983) [6] and it is referred to as the extended hyperbolic model. The expression for p-y curves in sand is given as following:

—

where

A: empirical adjustment factor

: initial modulus of subgrade reaction

z: depth along the pile

: ultimate bearing capacity

p: resistance of the soil

y: displacement of the pile in the considered level.

The empirical adjustment factor A depending on the depth z and the pile diameter D is determined from equation (1.22):

—

The initial modulus of subgrade reaction is usually determined from Figure 1.7

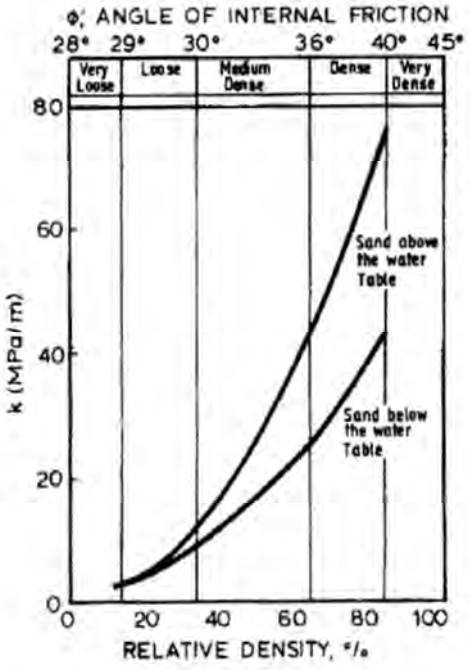

Figure 1.7: variation of k with φ' [8].

The method is based on the concept of ultimate soil resistance, p_u. The formulation of p_u given in the present API originates from the research report by O'Neill and Murchison who reviewed an article by Reese from 1962. In the formulation, two types of soil resistance are assumed to exist. Near the ground surface and in moderate depths a passive wedge develops to resist the lateral movement of the pile, and in greater depths the soil moves horizontally around the pile. The two formulas are referred to wedge failure mechanism and flow failure mechanism.

$$p_u = \min \begin{cases} (C_1 z + C_2 D)\gamma' z \\ C_3 D \gamma' z \end{cases}$$

where

C_1, C_2: coefficients determined from considerations on wedge failure

C_3: coefficient determined from considerations on flow failure

D: diameter of the pile

γ': effective weight of the soil

z: depth of the point considered

C_1, C_2, C_3 can be determined from Figure 1.8 to simplify the calculation of the p-y curves or from the analytical formulas according to the type of failure, reported in the next paragraphs.

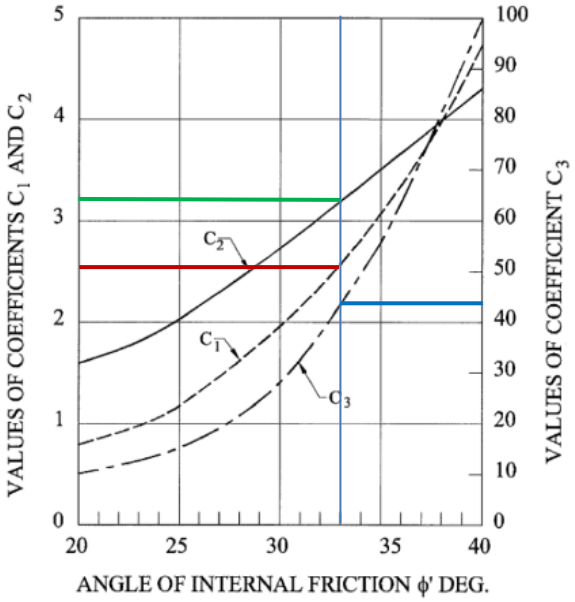

Figure 1.8: values of coefficients C1,C2,C3 according to φ'[1]

- **wedge failure**

For moderate depth and close to the ground surface a failure wedge is supposed to occur when the maximum capacity of the soil is achieved, and the ultimate resistance of the soil is then computed from this wedge. The assumed failure wedge is shown in Figure 1.9.

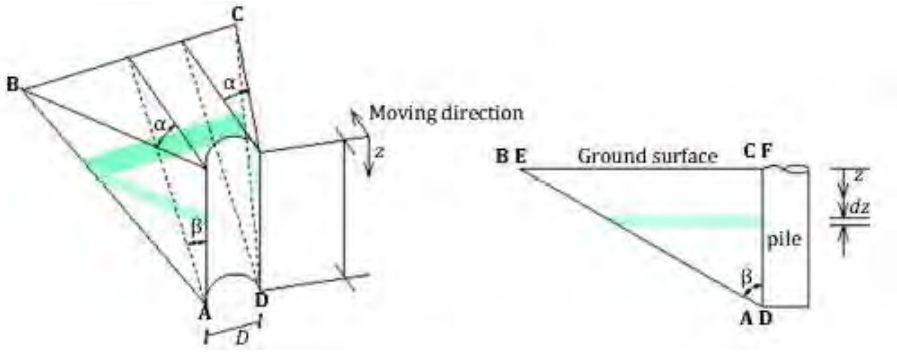

Figure 1.9: assumed failure wedge [5].The differential area is marked in green.

In wedge failure a mass of sand shaped as a wedge is pushed in front of the pile hence the planes ABC, DEF and ABED are failure planes and the Mohr-Coulomb failure criterion is used [5].

$$C_1 = \frac{K_0 \tan\varphi \sin\beta}{\tan(\beta-\varphi)\cos\alpha} + \frac{\tan^2\beta \tan\alpha}{\tan(\beta-\varphi)} + K_0 \tan\beta(\tan\varphi\sin\beta - \tan\alpha)$$

$$C_2 = \frac{\tan\beta}{\tan(\beta-\varphi)} - \tan^2(45° - \alpha)$$

- **flow failure**

For some depth below the surface, the soil moves horizontally around the pile instead of moving upwards following the wedge mechanism. This type of failure is referred to as flow failure, see Figure 1.10.

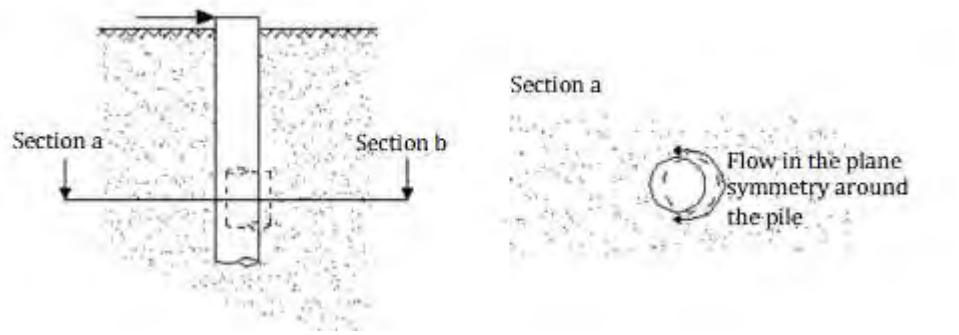

Figure 1.10: flow failure [5]

In this case C_3 is computed as

$$C_3 = 0.4 tan\varphi tan^4\beta + tan^2(45° - \alpha) tan^8\beta$$

The nonlinear method considered is the lateral force deflection (p-y) approach. It accounts that the soil stiffness parameter k_h (subgrade reaction) is not constant and there is a non-linear relationship between the soil resistance and its displacement (equal to the pile deflection). The nonlinear differential equations considering deformed configurations are given by the following formula:

$$E_p I_p \frac{\mathrm{d}^4\mathrm{y}}{\mathrm{d}^4\mathrm{z}} + \mathrm{pD} = 0$$

They are solved applying the finite difference numerical technique. For each set of applied boundary loads, an iterative solution is needed which satisfies the static equilibrium and achieves compatibility between force and deflection in every element. Since the analysis is based on an iterative procedure, it is necessary to use a computer program to achieve a sufficient number of iteration and have a reliable solution .

In this study **D-PILE GROUP** software has been used, setting from the beginning Cap method option which models a nonlinear behavior of the soil.

D-PILE GROUP

D-PILE GROUP (formerly known as MPile) enables the analysis of the three-dimensional behavior of single piles and pile groups. D-PILE GROUP describes the relation between pile and surrounding soil by the use of lateral and axial vertical soil springs along the piles. The program provides several calculation models, which mainly are *Poulus model*, where linear soil behavior is considered and *Cap model*, in which the nonlinear soil response is examined. In this case of study the model adopted is *Cap model*, for which D-PILE GROUP determines the nonlinear relation between the force and displacement on basis of a design rule which can be selected by the user (e.g. API or NEN Dutch standard) [7]. Cap model is based on p-y curve, but it does not account pile-soil-pile interaction.

This program uses the finite element method to study the pile behavior and the stiffness matrix analysis method for the soil behavior. First, the pile is discretized into a number of one-dimensional (beam) elements. From structural analysis, the stiffness relation can be written for a free pile element. The solution of the n equations corresponding to the pile discretization gives the deflection of the pile at each depth. If the pile is assumed to be a beam on an elastic foundation, then the modulus of lateral subgrade reaction k_h at any depth can be related to the lateral pile deflection at that depth. Hence the spring stiffness can be expressed as the modulus of lateral subgrade reaction k_h [3]. If the soil behavior is considered nonlinear then the computer code begins with an arbitrary set of values for k_h and solves for a set of deflections along the length of the pile. The p-y curves are employed and new values of k_h are obtained and a new set of y-values is computed. The new values of y are

compared with the previous set and the solution continues until convergence occurs where all values of y for the present computation are within a given tolerance of the values of y in the just previous solution. The tolerance is set at a very small value of deflection to ensure an accurate solution of the difference equations [2].

The program interface requires standard soil parameters for each layer, which are distinguished between soil type (sand and clay) and load type (drained, undrained and cyclic).

1.2 Finite Element Modelling

Numerical methods have been used form the 90's to solve complex problems and investigate phiscal phenomena. In this paragraph the basic of the Finite Element Method is explained and then a brief overview of the past numerical models regarding Lateral loaded piles is presented. [8]

1.2.1 Basics and history of the Finite Element Method

Finite element models are based on the Principle of Virtual Displacement and in this chapter is shown the derivation of the general formulation FEM from the PVD.

A three dimensional body that models the structure to analyse is defined in a global coordinated system XYZ. (See Figure 1.11)

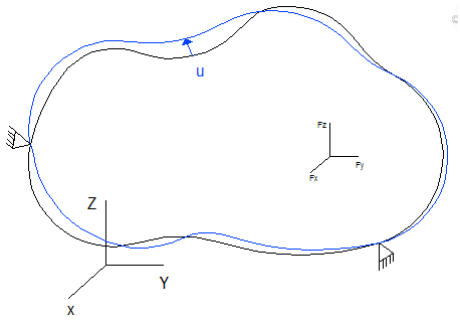

Figure1.11: sketch 3D body

It is subjected to a set of forces and is properly constrained with different type of supports. The set of forces is made by: body forces per unit volume f^B(including also dynamic forces) , distributed surface forces f^S(as water pressure) and concentrated surface forces F^I at point i ; all the forces have components in the three directions of the global coordinate system.

The unknown of the problem are global displacements U, strains ε and stresses σ of the structure, all function of a global reference system XYZ.

The principle of virtual displacements states that, given a virtual displacement that satisfied the Boundary conditions imposed by the constrains, the external work computed by the set of forces is equal to the internal work of the body.

$$\int_v \varepsilon^T \sigma dV = \int_V U^T f^B dV + \int_S U^{ST} f^s dS + \sum U^i F^i$$

In finite element analysis, the structure is idealized as an assemblage of element and the displacements of structure will be express in terms of the displacements of the elements in order to invoke the Principle of Virtual Displacement.

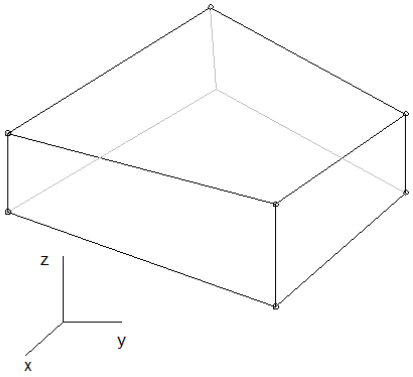

Figure1.12: example of Brick element

To be more general Brick element (8 nodes) are chosen in this explanation (Figure 1.12). If displacement of each Brick element is a function of the nodal point displacement expressed in terms of local coordinate system (xyz), then also the displacement of the structure is a function of the nodal point displacement.

Now to pass from the local coordinate system to the global one, the major assumption of the finite element discretization is considered. For every element m:

$$u^m = H^m \widehat{U}$$

The displacement of element m in the local coordinate system (u^m) is equal to the displacement interpolation matrix, function of the local system,(H^m) times all the nodal point displacements that occur in the finite element discretization ($\widehat{U}$).

From the finite element assumption the strain and the stresses in element m can be derived:

$$\varepsilon^m = B^m \widehat{U} \text{Compatibility condition}$$

$$\sigma^m = C^m \varepsilon^m + \sigma_o^m \text{Stress} - \text{strain low}$$

where: B^m: strain interpolation matrix (derived differentiating the rows of matrix H^m)

C^m: stress strain matrix (dependent on the material)

σ_o^m: initial stress

Beside the Compatibility condition and the stress-strain law, the last condition to be fulfilled in the Finite Element analysis is the equilibrium. The Equilibrium condition is embodied in principle of virtual work.
Since the Principle of Virtual Displacement is applied at the finite element discretization and the differential equations of the equilibrium are solved numerically , the equilibrium conditions at element level is satisfied in an approximate way. But if the finite element discretization is appropriate(means convergence is satisfied), encasing the number of elements, the approximate solution converges to the real one.
The first step is to rewrite the principle of virtual displacement as sum of integration over the elements and then the assumption of finite element discretization, the compatibility condition and the stain law are substituted. It means that the principle of virtual displacement is rewritten in terms of nodal point displacement and interpolation matrixes and it satisfied the boundary conditions.[9]
The solution of the problem is found solving the system of matrixes based on the principal for virtual displacements n times, every time reaching a more accurate solution. The iterative procedure and the dimension of the matrixes require the use of computer programs as Abaqus.

1.2.1Numerical modelling of laterally loaded piles

Three dimensional finite element modelling can be used to predict the lateral pile response. The more relevant studies dealing with this computational approach are analysed in this paragraph. First of all a finite element model should[10]:

- Replicate as precisely as possible the response of the upper soil, i.e. upward bulging in front of the pile and gap backward.
- Account non linear stress-strain soil behaviour.

The earliest studies, conducted by Dan A. Brown and Chine-FengShiein the 90's [11, 12], analyzed the response of a flexible pile, and demonstrating the impact of the before mentioned assumptions on a accurate 3D FE model.
The analysis conducted in the first study [11] includes gap formation and plastic deformation of the soil around the pile. A solid pile with modify stiffness is used to model an equivalent hollow pile. Von Mises and Drucker-Prager soil models are considered and frictional interface elements provide for slippage at the interface and gap formation. Results of this study indicate deformation patterns and development of areas of plastic deformation around the pile , moreover p-y curves are produced from the reduction of bending moment data.
In the second study [12] a similar model (Figure 1.13) was used to investigate several factors on p-y curves

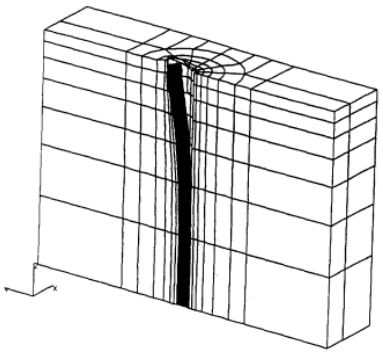

Figure 1.13: View of the 3D mesh with pile dipalced laterally [10]

derived from the model. The importance of appropriate simulation of contact between the pile and the soil was highlighted by examining the effect of different interface properties along the pile on computed p –y curves .
Few years after, King G. J. W. and Laman M. start to adopt FE modeling to calibrate and predict centrifuge tests [13]. In this study 3D finite element analysis are carried out using different linear and non linear programs and also using a linear axi-symetric program. Linear three dimensional programs seems fit more to the centrifuge tests.

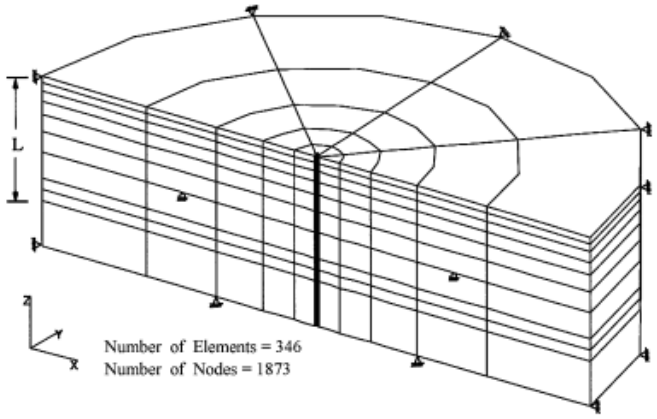

Figure 1.14:3D FE mesh used to analyse a pile subjected to lateral load [13]

The 3D FE Model developed by Chia-Cheng Fan and James H. Long [14], accounts for elastic-plastic sand behavior,slippage along the pile but not debonding, hence gap formulation was not modeled. The piles are modeled as linear elastic materials and the mesh used to analyze a pile subjected to lateral load is shown in Figure 1.14 . The computed load displacement curves fit well with the on site measured data, validating thus the accuracy of the modeling procedure. The effect of the pile stiffness on the p-y curves was not found significant, while the ultimate soil resistance was found to be strongly related to the coefficient of horizontal earthpressure and the soil dilatancy. The comparison between the ultimate soil resistance calculated numerically and the corresponding estimated applying of analytical procedures [2, 3,4], demonstrates that Hansen's method provides reasonable results.

The recent study of V. Zania and O. Hededal [16] the lateral capacity of three dimensional numerical models of 2m diameter rigid piles embedded in cohesionless soil is estimated using the software Abaqus. Both pile and soil are discretized with3D 20 nodes continuum elements, the dimension and the mesh of the Finite Element model are shown in Figure 1.15. The potential variability of the friction properties along the perimeter of the pile is considered changing the interface friction angle. This study shows that the interface properties affect the ultimate soil resistance and the stiffness of the soil pile response, while the effect of the pile stiffness (EI) in the lateral capacity of the pile and in the p-y curves results negligible for rigid piles.

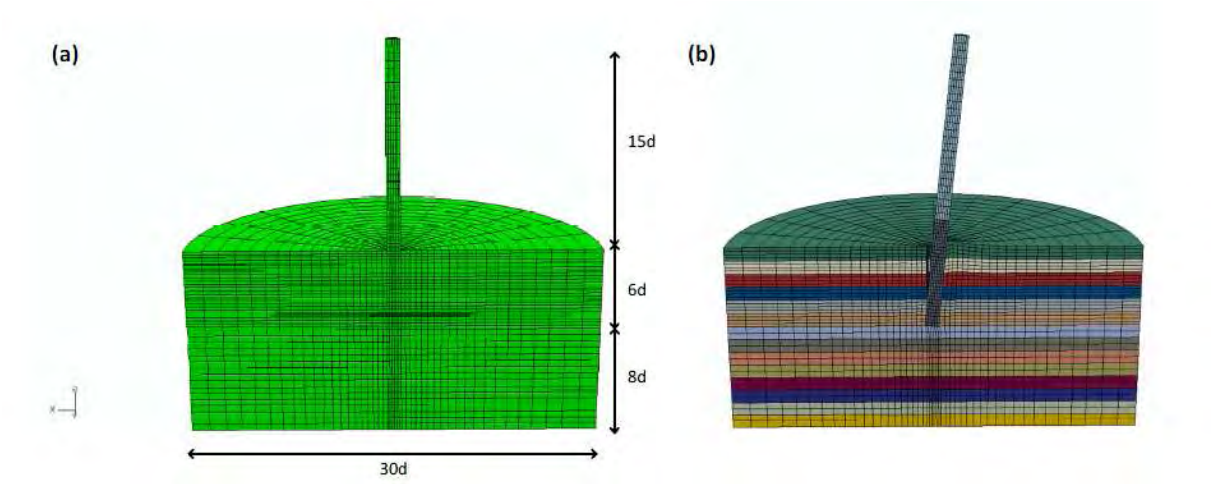

Figure 1.15: Finite element model developed and typical defomation pattern [16]

After the short review the following drawbacks regarding the lateral response of monopiles have been observed:

• ultimate soil resistance usually neglects the contribution of side shear resistance

• the p – y curves for cohesionless soils have been calibrated to the response of flexible piles modeled as rigid piles with equivalent stiffness, hence their validity for rigid and flexible piles is questionable

• 3D FE models of rigid piles have been studied reentry [16] and the procedure adopted is used in this thesis as guide line.

The current study aims at investigating the lateral response of rigid and flexible monopiles in cohesionless soil subject to load with high eccentricity. Hence advanced 3D FE models were developed and the soil nonlinearity, the pile type, and the geometric nonlinearity induced by sliding along the soil – pile interface and gap formation are taken into account. The effects of pile stiffness and soil properties are analyzed.

The generated failure mechanism resembles closely to the one reported in the literature. The lateral bearing capacity in the different type of piles is analyzed and compared with Broms' theory. The calculated pressure distribution, ultimate soil resistance and the generated p – y curves are matched to the corresponding proposed in the literature for rigid piles embedded in cohesionless soil (API curves).

1 Methodology

Since the objective of this thesis is to simulate the lab tests computed in the centrifuge using Finite Element Modelling, the first step is analysing the setup of the experiments to recreate it in the software Abaqus as close as possible.
In the experiments there are two phases: installation of the pile and application of lateral load. An effective procedure to model the installation phase in the numerical model for the flexible piles has been studied using a simplified problem; but the solution found was not applicable. Due to numerical problems the solution for the problem was giving not reliable solution in terms of contact pressure as it is shown in appendix 3. For this reason it have been chose to model just the second phase of the experiments.

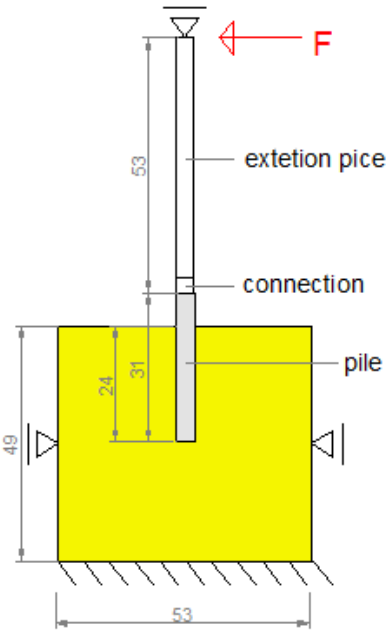

In order to investigate the lateral response of piles due to horizontal applied load with large eccentricity, 3D finite element models are developed. The selected pile diameter is 4 cm, the same of the lab tests which corresponds to a prototype diameter of 1m, reassembly the foundation of offshore platforms and wind turbines. The static schemeand the dimensionsof the soil-pile system that have been modelled in according to the lab conditions are represented in Figure 2.1.The embedment depth of the pile is 6 diameters (24cm) and the eccentricity of the lateral force is equal to 15 times the diameter. The dimension of the soil are the same of the barrel that contains the sand during the experiments

Figure1.1: Sketch 2D of the problem, measures in centimeters

1.2 Finite element modelling

Three 3D finite element models have been developed, one for each type of pile.
Hereafter all the features of the model for the rigid pile are explained in details; the models for the flexible piles are slightly different and the variations are reported below.

1.2.1 Laterally loaded rigid pile

In this paragraph the model of the rigid pile is described in terms of geometry, mesh discretization, material properties, load steps, boundary conditions, contact formulation.
The symmetry of the problem allows to take into account just half of the cylindrical pile and the corresponding surrounding soil.

Material Properties

In the model there are two materials the sand of the soil and the steel of the pile.
The properties of the steel are listed in Table 2.1; however two materials for the pile with different young modulus are created to simulate different cross-sections as it is explained in the next paragraph.
The soil material is medium-dense sand whose properties are in according to the lab test [1] and to the recent study on the effect of interface behaviour on laterally loaded rigid piles with FEM [16].
Since the unit weight of the sand sample in the 6 tests was respectively:16.37,17.03,16.32,15.93,16.7,16.39 kN/m^3[1], an average value of density has been chosen equal to 1.7 tn/m^3.
The strength of the soil is assumed to be constant along the pile depth and a Mohr-Culomb failure envelope characterized by angle of friction (φ) equal to 33° and a cohesion (c) equal to 6 kPa are selected in according to the results of the triaxial test performed on the lab sand [17].The graph in Figure 2.2 is used to estimate Young Modulus and the dilation angle, but note that it is referred to another cohesion coefficient, thus the values cannot be taken directly from the graph.

		Soil	Pile
Density	**ρ [tn/m^3]**	1.7	7.8
Elasticbehaviour			
Young Modulus	**E [kPa]**	60 000	209 000 000
Poisson ratio		0.3	0.3
MohrCulombPlasticity			
Friction Angle	**ϕ**	33°	
Dailation Angle	**ψ**	8°	
Cohesion	**c [kPa]**	6	

Table 2.1: Materials Properties

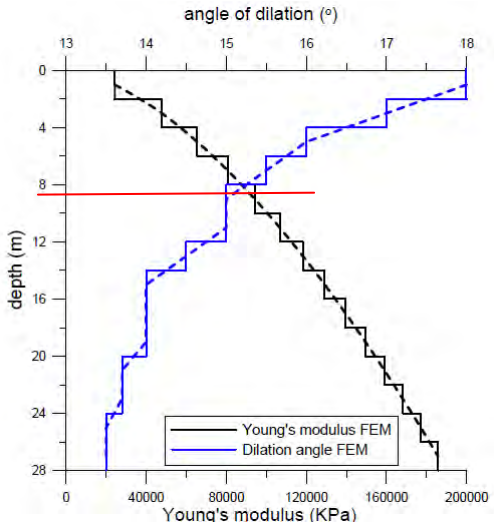

Figure 2.2: Variation of Young Modulus and dilation angle respect to depth [16] for φ= 33° and c = 3.5 kPa

Geometry

The model is made of 2 parts: pile and soil both created with solid elements in the rigid pile.

The part "pile" includes the rigid pile itself, the connection and extension piece. For the rigid pile the connection is identical to the extension piece. To simplify the calculation, just one part has been created for all these elements but a partition subdivides into section with different stiffness (see figure 2.2). The real geometry of the elements is shown in figures 2.3 and 2.4, in Abaqus it is used just the solid pile geometry and an equivalent Young Modulus is set for the extension piece in order to have the same stiffness of the real one.

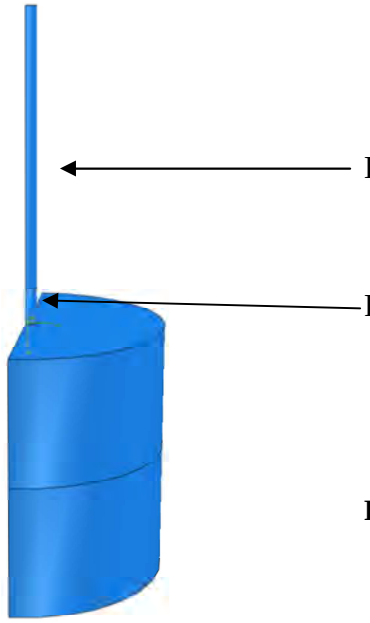

Figure 2.2: Geometry of the rigid pile model

Section 1: solidpile (0-31 cm)

- Moment of inertia $I = \frac{\pi D^4}{64} = 1.26 \cdot 10^{-7} m^4$
- Young Modulus E=209 000000kPa

Figure 2.3: real geometry of solid pile

Section 2: extension piece (0.31-0.84 cm)

- Moment of inertia $I = \frac{\pi D^4}{64} = 1.26 \cdot 10^{-7} m^4$ (calculated by Abaqus)
- Real moment of inertia $I_r = \frac{\pi (De^4 - Di^4)}{64} = 3.21 \cdot 10^{-8} m^4$
- Equivalent young Modulus $E_{eq} = \frac{E \cdot I_r}{I} = 53\ 48\ 200\ kPa$

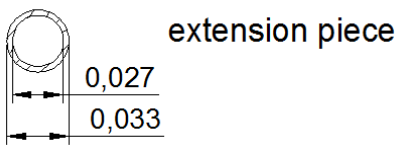

Figure 2.3: real geometry of extension piece

The equivalent Young Modulus in section 2 is adopted to obtain the real stiffness with an inaccurate geometry (of a full extension piece instead of a hollow smaller element).

Since the installation phase is not modelled, the shape of the soil is already adapted to the pile structure (Figure 2.4). To have this shape in Abaqus, half cylinder of soil has been created and then it have been cut by the pile with the command “cut geometry” in the module Assembly. Than the partitions show is figure 2.4 are done otherwise it is not possible to mesh the soil.

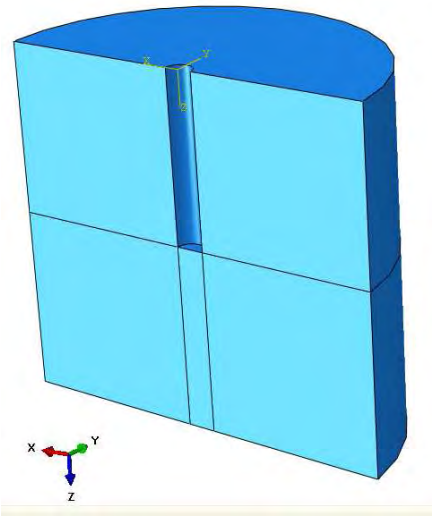

Figure 2.4:geometry of the part “soil”

Mesh discretization

Both pile and soil are discretized using 3D 20 nodes continuum elements (C3D20).It is set to have 12 elements along the pile circumference, this pair number helps in the calculation of the section moment along the depth of the pile (see appendix I). The element size of the soil close to the pile is approximately 0.003x0.003x0.009m (x,y,z) and it increase gradually to the borders (Figure 2.5). The element size of pile is the same in the 31 cm close to the soil (rigid pile part) and the height of the elements is double in the rest (connection and extension piece).

A more refine mesh adjacent to the interface soil-pile help to calculate precisely the contact algorithm and the solution of the mathematical equations that find the equilibrium of the problem; hence to calculate as accurately as possible the distribution of the normal and shear stresses along the perimeter. On the other hand the number of elements of the system pile-soil cannot be too high otherwise the time to solve the problem become too long, for this reason the element size is increased far from the interface pile-soil. [18]

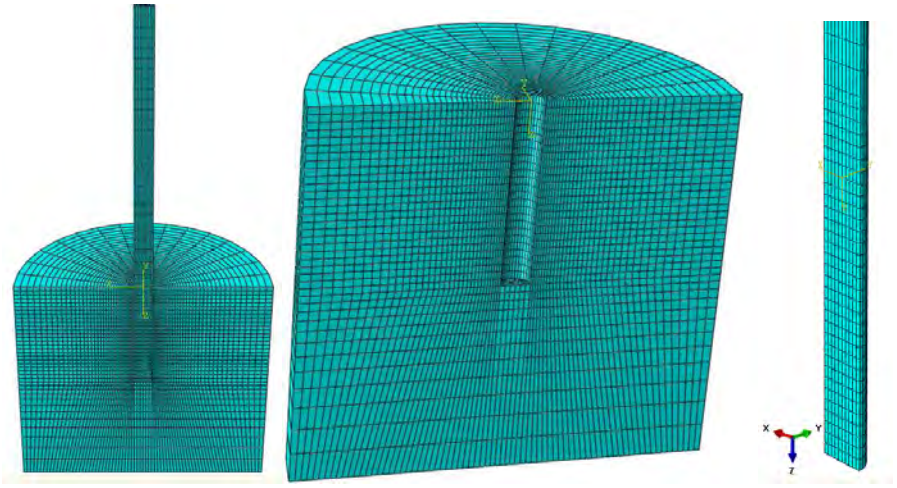

Figure 2.5: mesh discretization of the finite element model of the rigid pile

Load Step

It is chosen to adopt Abaqus Standard that applies Hiber-Hughes-Taylor operators in the computation instead of Abaqus Explicit because, even if is slower , it allows more functions and it better represent the contact formulation.[18]

The problem is divided into 6 steps in order to facilitate the solution of the mathematical equations.

- Step 0 (initial step): the geostatic stress, the boundary conditions and the contact formulation are created.
- Step 1(geostatic equilibrium): the gravity 1g is applied at the soil (load 1) and this step permit Abaqus to check for the equilibrium between the geostatic stress and applied loads plusboundary conditions
- Step 1b(intermediate step): before the incense for gravity to accelerate the computation
- Step 1c (increase of gravity): the gravity on the soil (load 1) is increased to 25g and another force of 25g is applied on the pile (load 2)
- Step 2: application of half lateral force at the top of the pile (load 3)
- Step3: increase of the lateral load to the required value

Boundary conditions

The boundaries are placed along the border of the element soil to block the movement and simulate the barrel of the lab test. Since solid elements do not have rotational degree of freedom, rotation is prevent blocking displacement in all the nodes of the surface that is required to be fix.[1]

Moreover a hinge is placed at the top of the extension piece since in the lab the load cell is attached to the frame but is free to rotate in the force direction.

1.Encastre at base of the soil element

2. hinge at the lateral face of the soil element

3. hinge at top of the pile, it must be applied on two pints in the line perpendicular to the lateral force (Figure 2.6) otherwise the pile gets stuck at the top.

4. symmetry of half cylindrical pile and soil

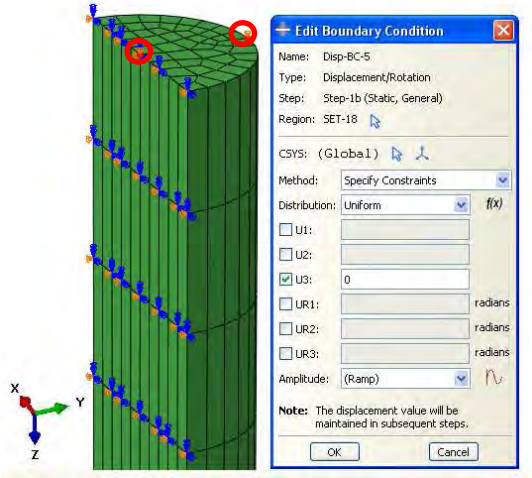

Figure 2.6: hinge at the top pile

Static Loads

The geostatic stress and three extra loads are applied in the system at different steps as it is explained later on.

The geostatic stress in the soil is an elevation-dependent initial stresses. When a geostatic stress state is prescribed for a particular element set, the stress in the vertical direction (assumed to be the *z*-direction in three-dimensional models) is assumed to vary piecewise linearly with this vertical coordinate and the displacement remains zero [18] (see Figure 2.7).

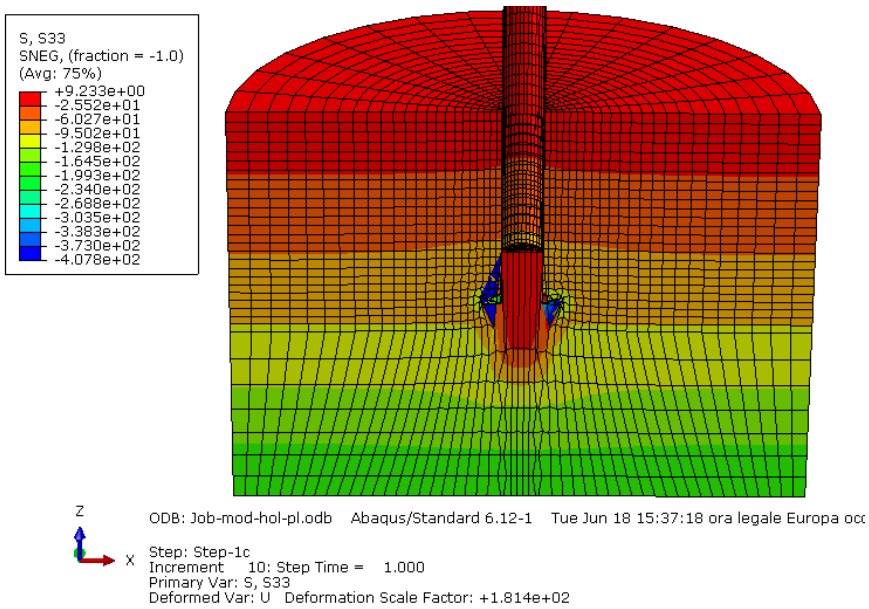

Figure 2.7: stress in the vertical direction S33 in the soil part

For the vertical stress component, two pairs of stress and elevation values are given to define the stress throughout the element set. For material points lying between the two elevations given, Abaqus will use linear interpolation to determine the initial stress; for points lying outside the two elevations given, Abaqus will use linear extrapolation. In addition, horizontal (lateral in x and y direction) stress components are given by entering one or two "coefficients of lateral stress," which define the lateral direct stress components as the vertical stress at the point multiplied by the value of the coefficient. The values of the stresses are calculated with the following formulas and the input of the program are shown in Table 2.2.

Predinedfield		
σ_v1	0	kPa
z1	0	m
σ_v2	-3.05	kPa
z2	0.49	m
Ko	0.428	

Table 2.2: parameters for the predifinied field

Vertical stress: $\sigma_v = \gamma \cdot z = \rho \cdot g \cdot z$

Horizontal stress: $\sigma_h = K_o \sigma_v$

where K_o: coefficient of vertical stress→ $K_o = \frac{\nu}{1-\nu} = \frac{0.3}{1-0.3} = 0.428$

The other loads in the FE Model are the gravity and the lateral force.

Load 1 is the gravity load applied on the soil. It is set in the first steps equal to g=9.81m/s^2 in order to equilibrate the geostatic stress and have zero deformations; than it increase to 25g=245.25m/s^2.

Load 2 is the gravity applied at the pile equal to 25g in the second steps of the calculation.

The gravity is set 25g during the lateral load application to simulate the lab test where the gravity is increased with a centrifuge to study the behavior of prototype pile of 1m diameter.

Load 3 is the lateral force at the top of the extension piece. It is a point load applied on the highest right node of the pile (extension piece). At first the intensity is 0.45kN and in the next step it increase to 0.9kN, this procedure is done in order to ensure the achievement of solution.

Contact Formulation

A contact formulation is assigned along the perimeter of the pile , in order to model the soil-pile interaction.
The contact algorithm to establish between soil and pile is very important because if it is not appropriate, it can create problems to the solution of the model.
Between the lateral face of the pile and the soil it is chosen a contact pair algorithm instead of a general contact. Both of them are based on surface definition, contact interaction, surface properties and mechanical properties. Even if the general contact has a simplified definition, the contact pair is selected because is more specific for this problem.

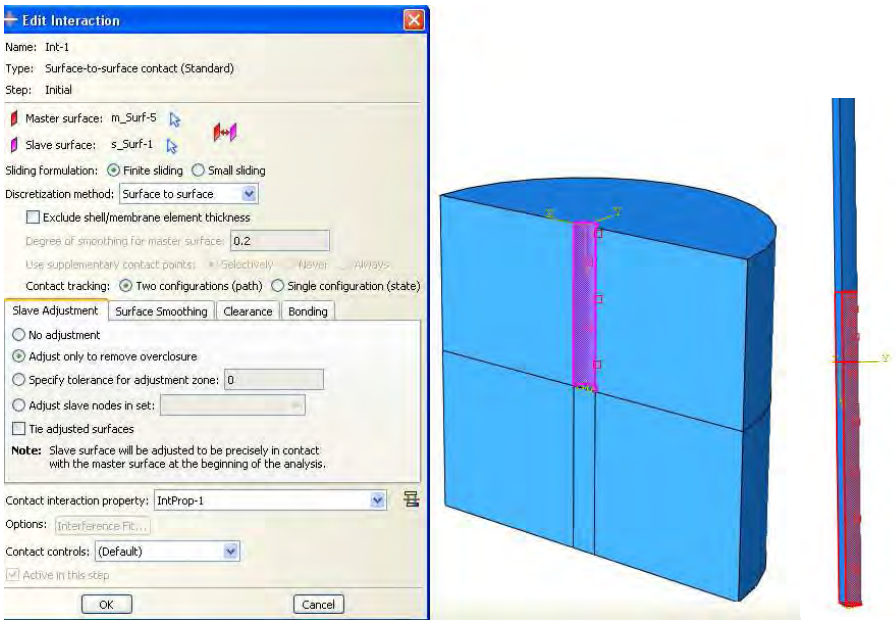

Figure 2.8: surface involved in the Contact formulation

The two surface for the interaction are highlighted in Figure 2.8, the master surface(red) is the pile one and the slave surface (purple) is the soil one. The type of interaction is surface-to surface with finite sliding formulation and the slave surface is adjusted to remove overclosure. The shear behaviour is assumed to follow the Coulomb friction law. Therefore in Abaqus, it sets, in the interaction property , a Tangential Behaviour with penalty friction formulation whose friction coefficient is equal to:

$$tg\delta = tg\left(\frac{2}{3}\varphi\right) = 0.4329$$

The normal behaviour is considered rigid-plastic permitting thus zero tensional stresses and zero elastic deformation normal to the surface. So it is included a Normal Behaviour with hard contact that allows separation after the contact of the nodes.
Between the base of the pile and the soil a tie constrain is established. The master surface is always the pile because is more rigid.

In order to study soil and interface properties, the simulation have been run three times.
The first one with properties listed before that are assumed as the reference one.
Then the interface soil friction coefficient have been increased from $tg\left(\frac{2}{3}\varphi\right)$ =0.44329 to $tg(\varphi)$ =0.649. The interface friction angle depends on the shape and the characteristic of the elements in contact, usually for concrete walls foundation in ground it is used $\frac{2}{3}\varphi$ and when the interface is between element of the same material it is used φ. It means that an interface soil friction coefficient equal to $tg(\varphi)$ is an extreme values that shows how this parameter effect the results.
The model has been run with an angle of fiction φ equal to 36° instead of 33°.

1.2.2 Laterally loaded flexible pile

The model for flexible piles is very similar to the one for the rigid pile. The main difference is that the piles are made of shell elements and the other differences regard the geometry and mesh discretization.
There are two different flexible piles: the hollow unplugged pile and the hollow plugged pile.

Geometry

The flexible piles are hollow piles with a thickness of 15mm (0.0015m) and the same length of the rigid pile.

They are made in Abaqus of three sections with different stiffness but same geometry. The real geometries are shown in Figures 2.9 and 2.10

Section 1: pile (0-31 cm)

- Moment of inertia $I = \frac{\pi\,(D_e{}^4 - D_i{}^4)}{64} = 1.78 \cdot 10^{-8} m^4$
- Young Modulus E=209 000 000 kPa

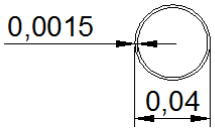

hollow pile

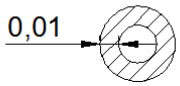

connection

Section 2: connection (31-34cm)

- Real moment of inertia $I_r = \frac{\pi\,(De^4 - Di^4)}{64} = 8.59 \cdot 10^{-8} m^4$
- Equivalent young Modulus $E_{eq} = \frac{E \cdot I_r}{I}$=220080000kPa

Figure 2.9: real geometry of pile and connection .

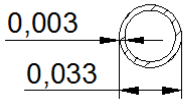

extension piece

Section 3: extension piece (0.34-0.84 cm)

- Real moment of inertia $I_r = \frac{\pi\,(De^4 - Di^4)}{64} = 3.37 \cdot 10^{-8} m^4$
- Equivalent young Modulus $E_{eq} = \frac{E \cdot I_r}{I}$ =131962000kPa

Figure 2.9: real geometry of extension piece

The unplugged pile has the soil also inside the pile because from the experiments it is known that the soil flows into the pile without the formation of soil plug.(Figure 2.10 a)
The plugged pile is a cylindrical shell element tied with a circular steel plate created using shell elements. In the plugged pile the soil cannot flow inside since there is a plug at the bottom. The connection between cylinder and plate is made by a tie constrain. (Figure 2.10b)

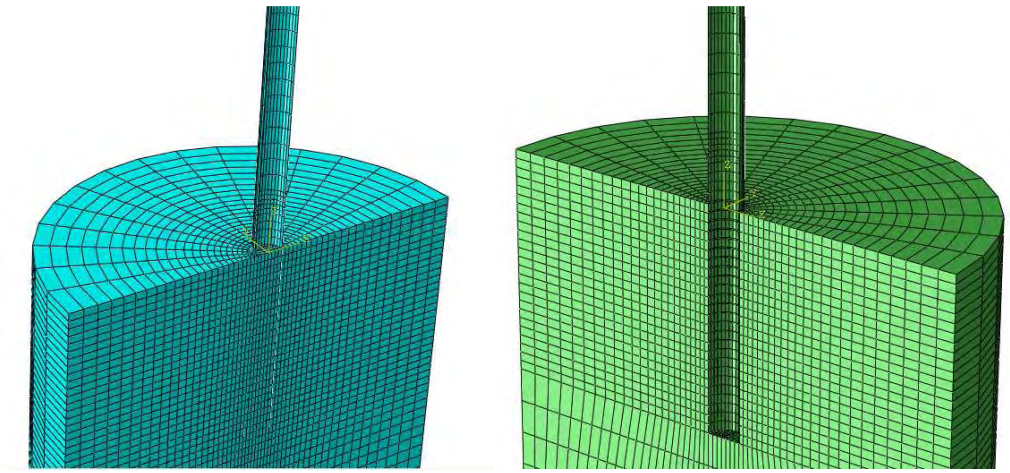

Figure 2.10: Finite Element Models of (a) unplugged and (b) plugged hollow piles

Since thin shell elements deform significantly in the surrounding of the load applied, the lateral force cannot be applied directly in one node of the pile. A Reference Point in the middle of the pile is created and it is connected with the pile trough a rigid body(Figure 2.11). This connection transmits equally the lateral force to the upper nodes of the pile and avoid a concentrated deformation of the pile in the application point of the force.

Figure 2.11: Application point of the lateral load

Mesh discretization

The flexible piles are discretised with 8 nodes shell elements with reduced integration (S8R). The mesh is made applying the same criteria of the rigid pile, starting from 12 elements for each circumference of the pile.
Also the models of the flexible piles are run adopting the reference soil properties and the increasing angle of friction and interface shear strength, in the same way it has been performed for the rigid pile.

2 Results of numerical investigation

In this chapter the results of the three numerical model are presented. Each model has been run applying the reference soil and then changing some soil parameters.
The parameters of the reference soil are shown in Table 2.1 of paragraph 2.1 and in particular the angle of friction is ϕ=33° and the interface shear strength δ=2/3ϕ. During the second run of each model the interface shear strength is increased to δ=ϕ while the angle of friction remains constant. In the last run the friction angle is increased to ϕ=36° while the interface shear strength remains δ=2/3ϕ. It has been chosen to change just one parameter per time in order to better understand the effects of this variation.

The graphs presented in this chapter are the following:

- Lateral Force – horizontal displacement at the top of the pile. The lateral force is applied at 15D= 57 cm from the sand surface and it increases with time until the maximum force is reached. The horizontal displacement is at 3 cm from the sand surface, this level has been defined because in the lab tests at the same position there is a displacement transducer. This type of graph shows when the ultimate Force is reach and how the young modulus changes increasing the force.
- Bending Moment –rotation at the top of the pile. The bending moment is obtained multiplying the Lateral Force by the eccentricity (0.57m). The rotation is obtained with the following formula:
- $r = \frac{y(3cm) - y(5cm)}{2cm}$ [rad]
- The point where the rotation is obtained is at 4 cm from the sand surface, a little bit below the top of the pile because at the same position is calculated the rotation from the lab tests.
- N.B. From the software Abaqus the output are in the nodes of the mesh (shown is chapter 2), hence the values of the deflection are not exactly at the required positions but in the closest node of the mesh. This approximation does not affect the reliability of the results.
- Moment distribution along the pile. The moment along the pile is obtained in according to the type of pile as it is explained in benchmark 1 and 2 . The moment distribution is plotted at different values of the lateral force.
- Plastic strain of the soil. It is an output of the softwer and it shows where the soil reach the yielding and how much it exceeds the deformation at the yielding. Figures of the soil are plotted at different values of the lateral force for the three type of pile in the reference soil.
- P-y curves.The deflection along the pile (y) is taken from nodes of the left side. The pressure is obtained by the second derivative of the moment distribution at each time instant. A polynomial interpolation of 6 degree has been fitted to each moment distribution corresponding a value of force. The 6th order equations of moments were

derived in 4 order equations and substituting the coordinate of pile depth, the pressure is established.

$$M(z) = c_1 z^6 + c_2 z^5 + c_3 z^4 + c_4 z^3 + c_5 z^2 + c_6 z + c_7$$

$$p(z) = \frac{\delta^2 M}{\delta z^2} = c_1 z^4 + c_2 z^3 + c_3 z^2 + c_4 z + c_5$$

From the p-y curves at different depth, the stiffenss kx and the ultimate soil strength are observed and compared with each other and with the API ones.

2.2 Laterally loaded flexible pile (unplugged)

The analytical methods explained in paragraph 1.1 establish a pressure distribution along the pile, by which all the other parameters depend. The assumption of the pressure distribution is based on the failure pattern within the soil. Hence, it is examined the failure mechanism after the analysis of the model for the unplugged pile under horizontal static load (see Figure 3.1). Figure 3.1 presents the minimum principal plastic strain that surrounds the pile within the soil when 0.45kN are applied at the top of the pile. Note that the force applied moves half of the system pile-soil, therefore to obtain the same effects to the whole system a double force is necessary.

The rainbow colours show the failure mechanism. A gap accrues at the back of the pile (left side), while at the left side the soil is sliding upwards along the soil-pile interface as the pile rotates and deflects. The deflection typical of flexible piles is more evident in Figure 3.1(b). The soil on back side of the pile in reality cannot form a vertical free standing edge because the sand should fill the gap at least until a certain depth. This approximation of the mathematical model is assumed to have a negligible impact on the results for monotonic load [15].

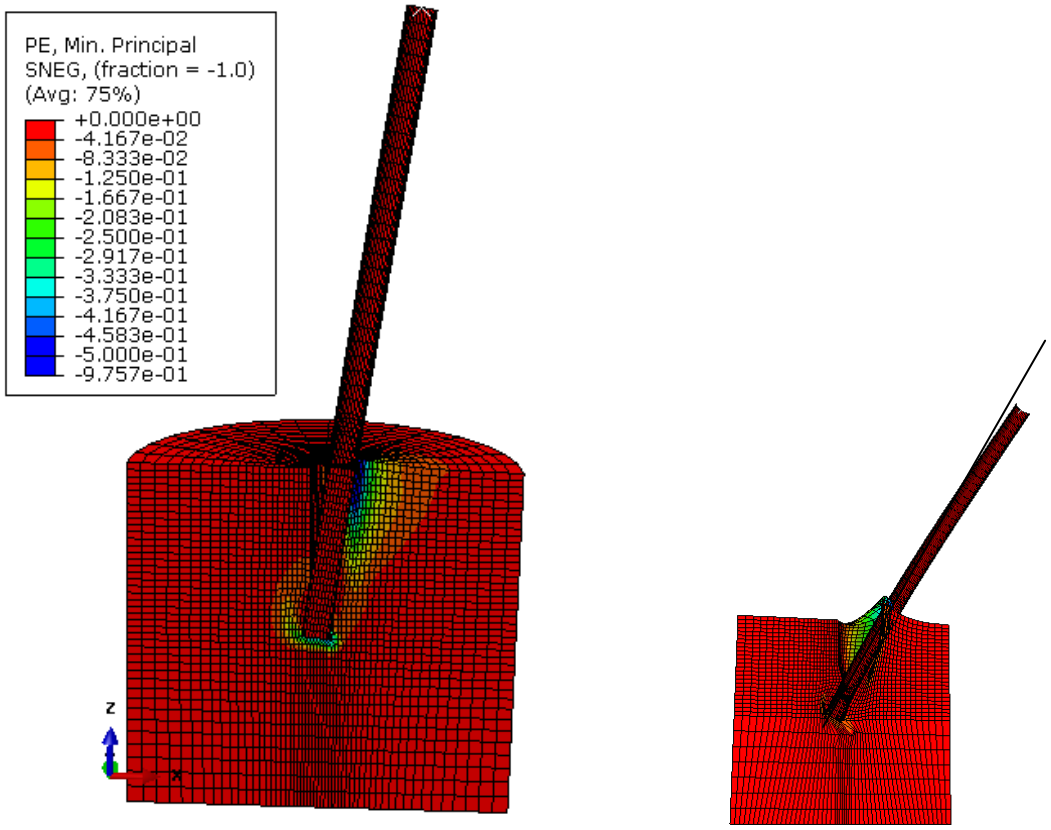

Figure 3.1: Plastic strain contours and failure pattern for hollow unplugged pile (a) real scale, (b) 1:4 scale

- Lateral force-horizontal displacement and Moment- rotation at the top of the pile

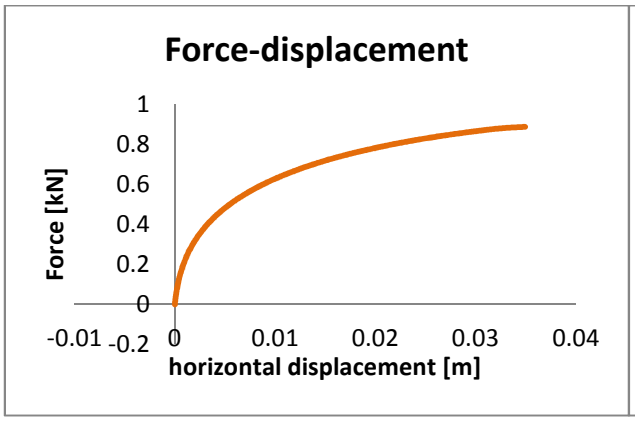

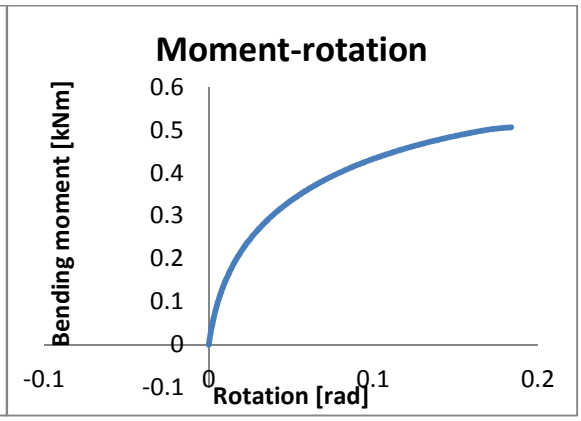

Figure 3.2: Force displacement curve in unplugged pile

Figure 3.3: Moment rotation curve in unplugged pile

The lateral force have an elastic behaviour just until 0.2kN, then the soil start to have plastic deformations. The maximum force is 0.89kN with a deflection 0.035 m. The ultimate force is not reached since the software killed the simulation when the soil is too distorted to compute the results, but it can be estimate not far from 0.9kN.

- Moment distribution along the pile (sand level 0.24m)

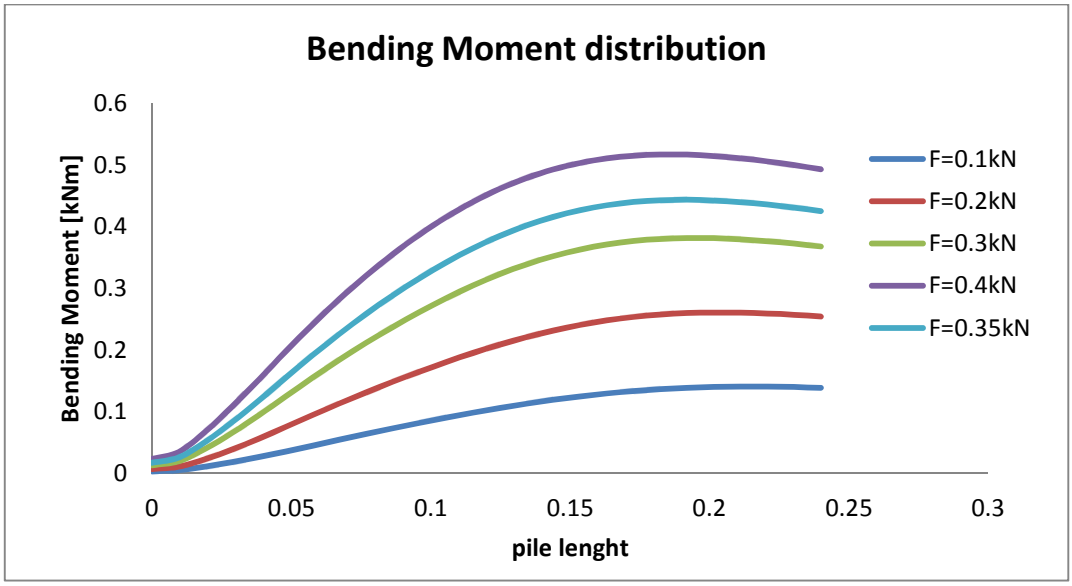

Figure 3.4: Bending moment distribution in unplugged pile

Bending moment is zero at the bottom of the pile (inside the sand) and it increase near the sand surface. For low forces the maximum value is at the sand surface, while after 0.3kN it moves gradually at ca. 6cm above the sand surface. It increase proportionally as the lateral force increase until approximately 0.5kNm, that is the same value obtained in the graph Moment rotation (Figure 3.3).For low values of forces (0.1kN,0.2kN) the soil does not reached the ultimate resistance since the force-displacement curve (figure3.2) is almost linear, and so the moment distribution follows the expected curve as if a linear elastic behaviour occurs [4].

- Plastic strain (PE min)

F=0.1kN

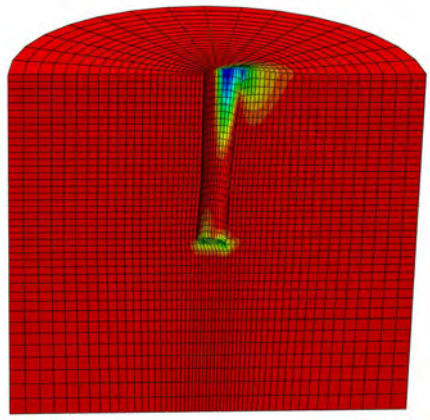

F=0.2kN

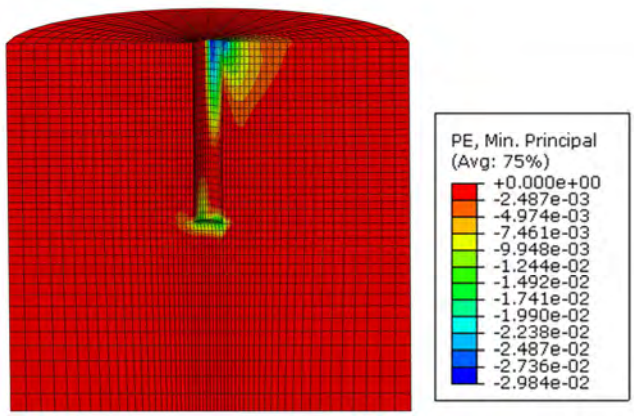

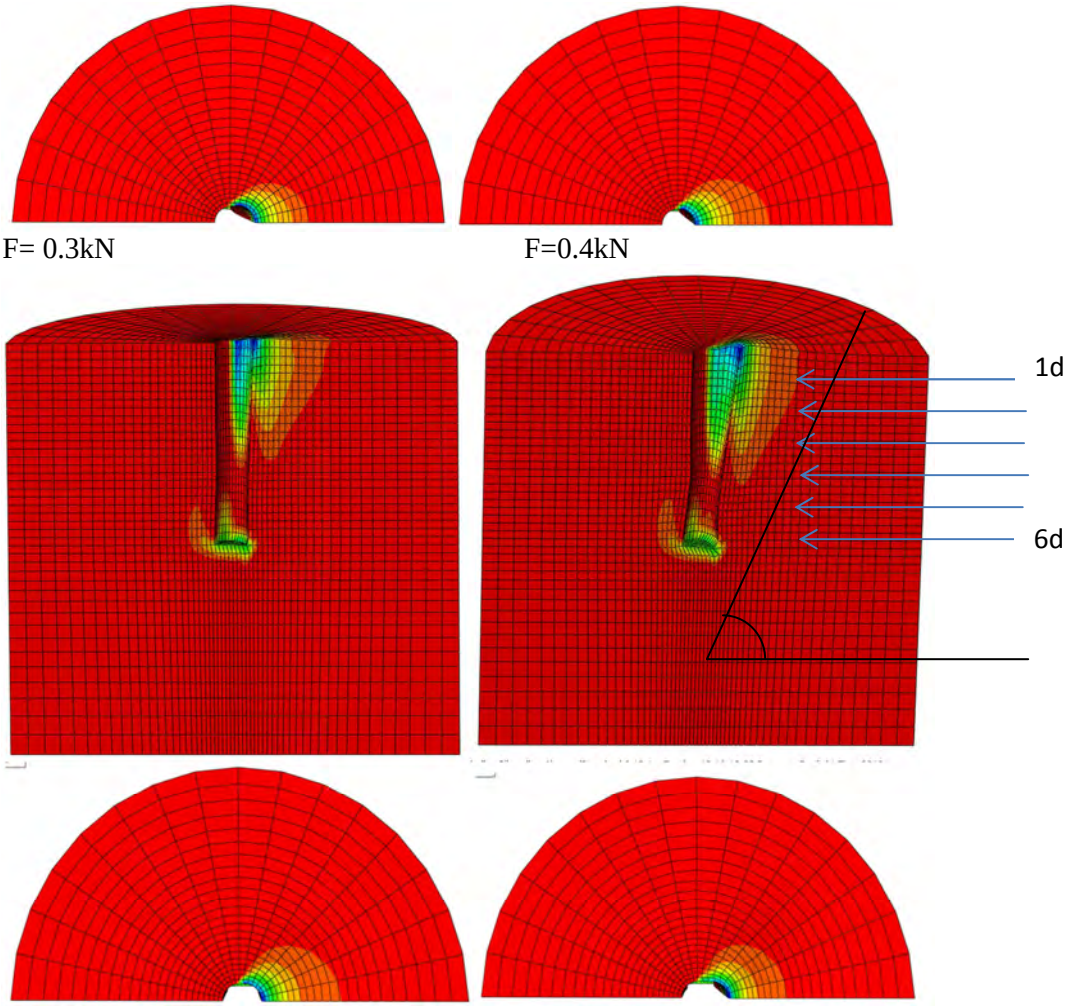

Figure 3.5: Plastic strain contours with increasing force in unplugged pile

The minimum principal plastic strain shows the failure pattern within the soil and the failure mechanisms. The wedge and flow failure for the soil are evident in this sketches and the p-y curves presented below are based on this mechanisms. Moreover from the figures it is evident at which soil level the failure is reached, that corresponds to the ultimate pressure in the p-y curves. For example at 0.4kN the failure is largely achieved at the depth of 1d and 2d while at 3d depth the pressure is near the ultimate value. Finally it is observed that the inclination of the failure wedge to the horizontal is approximately 60°, comparable with the theory 45°+φ/2.

- P-y curves at different depths

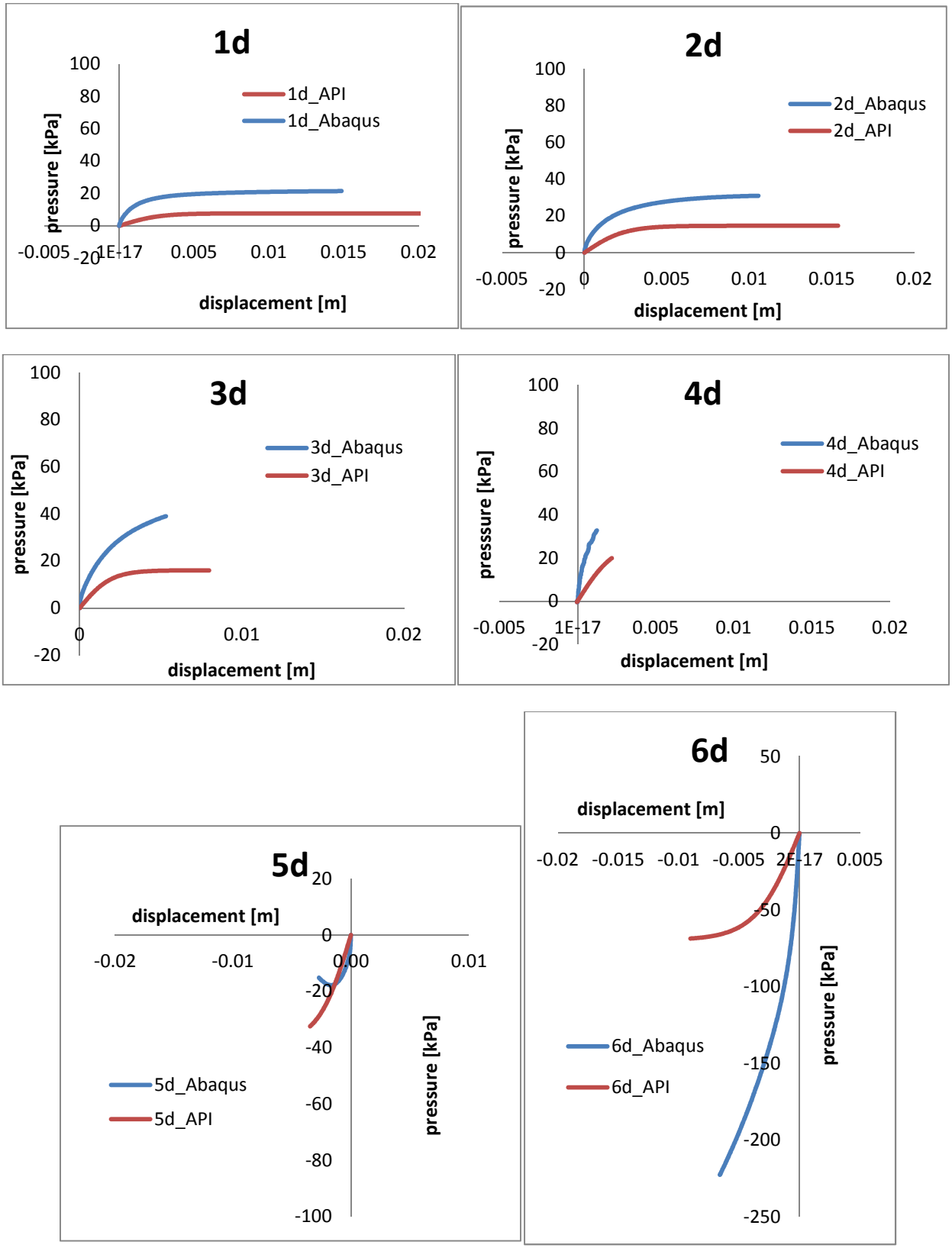

Figure 3.6: Comparison of p-y curves of unplugged pile with API [6] provision

The p-y curves obtained from the 3D numerical analysis (blue lines) exhibits a stiffness kx (initial inclination of the curve) that increases with depth of the pile. The ultimate soil resistance also rise up with the depth of the pile until 4d = 0.16m under the ground level and then it reaches negative values. Around 4d – 5d there should be the rotation point of the pile and it might cause the change of sign.

Increase of interface shear strength

The increment of interface shear strength does not change the failure mechanism of the system soil-pile but affects the lateral load capacity of the pile and the ultimate soil strength of the soil as figures 3.7 to 3.10 show.

- Lateral force-horizontal displacement curve and Moment- rotation curve at the top of the pile .

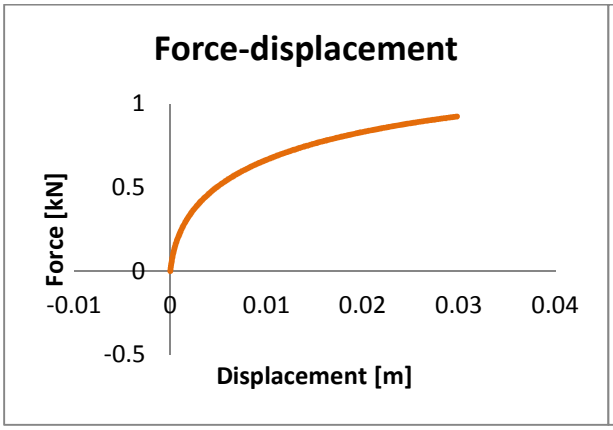

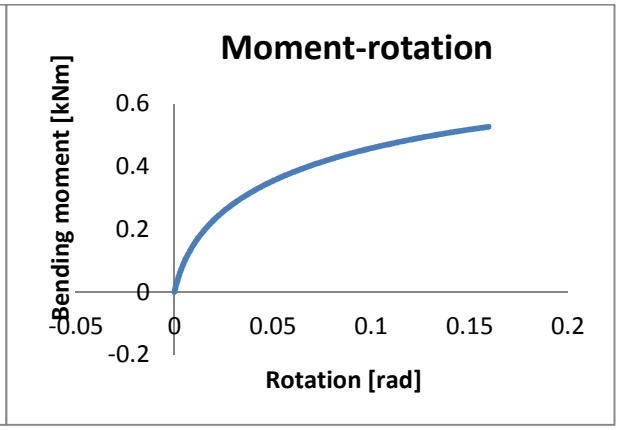

Figure 3.7: Force displacement curve in unplugged pile **Figure 3.8:**Moment rotation curve in unplugged pile

The ultimate force is not reached as in the reference soil but the same values of force produces a smaller displacement. The maximum force is 0.92kN corresponding to a deflection of 0.029m near the sand surface. The maximum moment 0.52kNm with a rotation of 0.16 rad (9.14°) is in the same position.

- Moment distribution along the pile (sand level 0.24m)

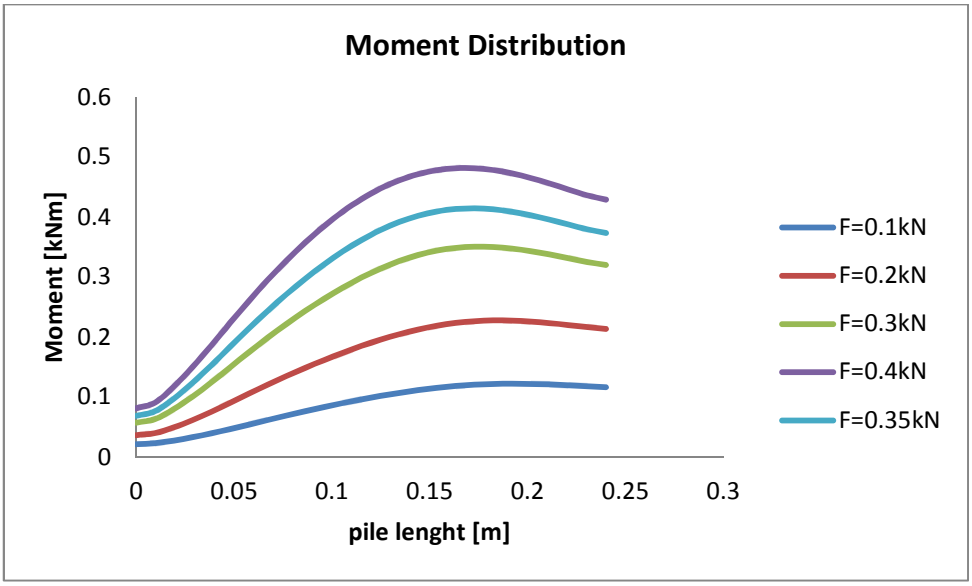

Figure 3.9: Bending moment distribution in unplugged pile

As in the reference soil, for low values of force the bending moment distribution is the one for elastic soil behaviour and the maximum moment is at the sand surface. Than for higher values of the lateral force the distribution varies and the maximum value moves gradually near the middle of the pile.

- P-y curves at different depth

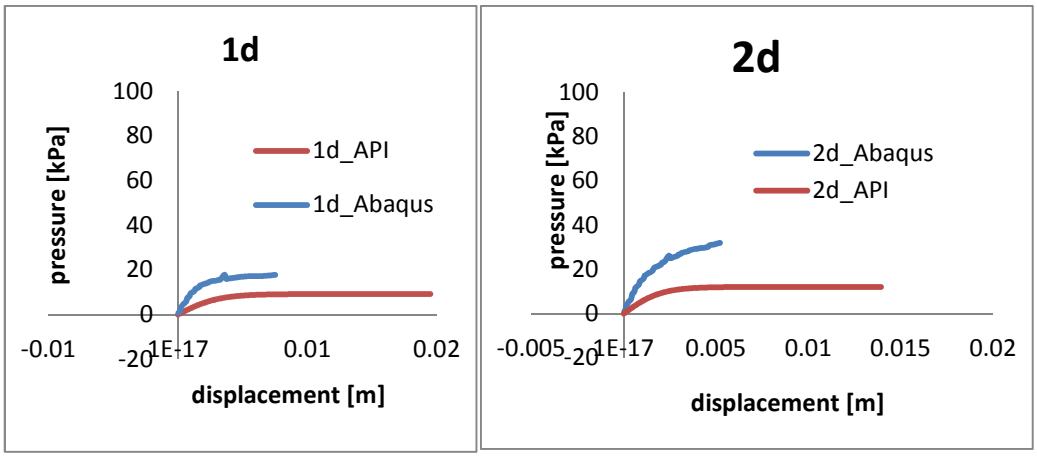

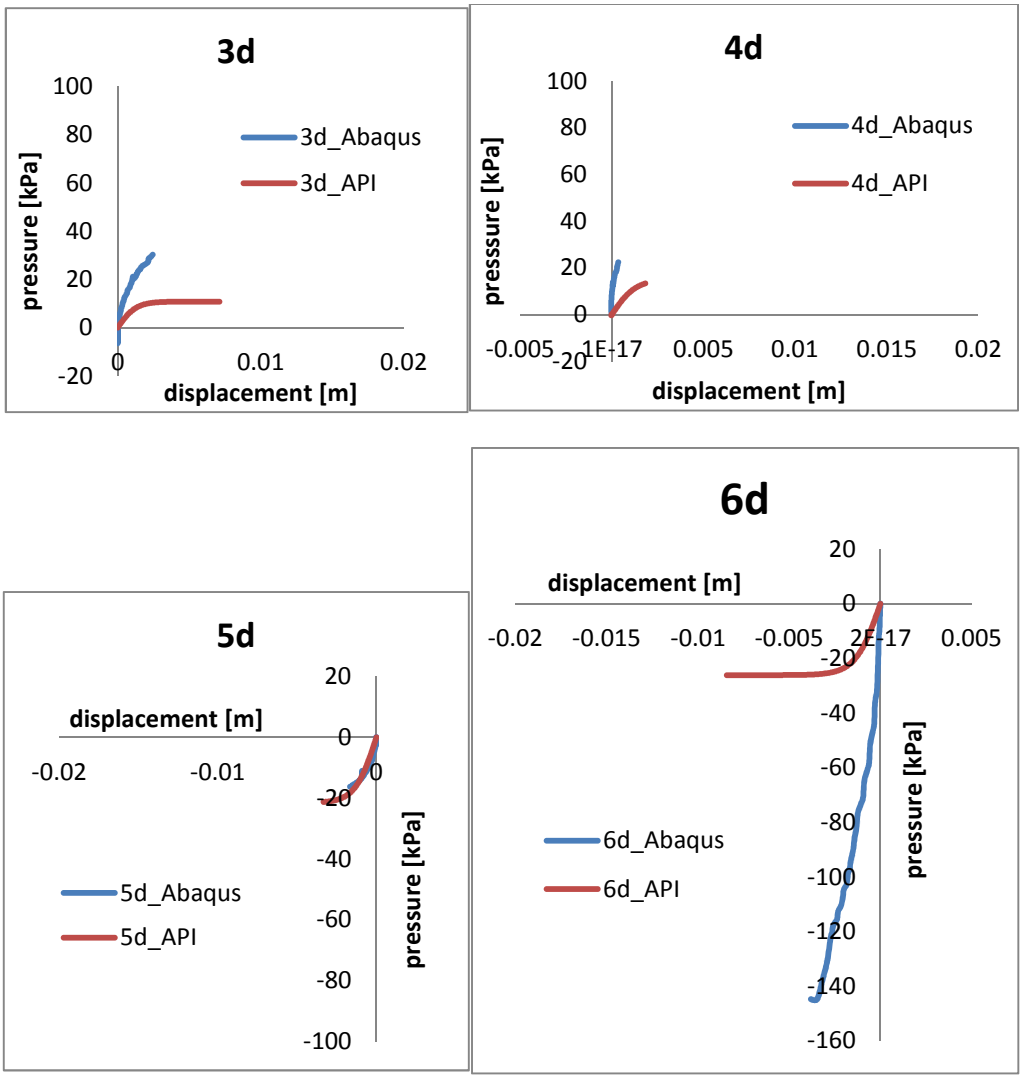

Figure 3.10: Comparison of p-y curves of unplugged pile with API [6] provision

The stiffness of the p-y curves obtained from the 3D numerical model (blue lines) increase as pile depth increase. The ultimate soil resistance is reached just at shallow depth (1d and 2d) but the pattern can be deduced from the graph; hence the value of ultimate soil resistance may increase with depth until 3d then it decreases and reach negative values.

Summarizing, the variation of interface shear strength does not change the pattern of the physical variables analysed, but the numerical values obtained are slightly different form the reference soil. In the next chapter a detailed comparison which underlines the variation of the lateral capacity and p-y curves is shown.

Increase of shear strength soil

The increment of shear strength of the soil does not change the failure mechanism of the system soil-pile but affect the values of lateral load capacity of the pile and the ultimate soil strength of the soil as figures 3.11 to 3.14 show.

- Lateral force-horizontal displacement curve and Moment- rotation curve at the top of the pile

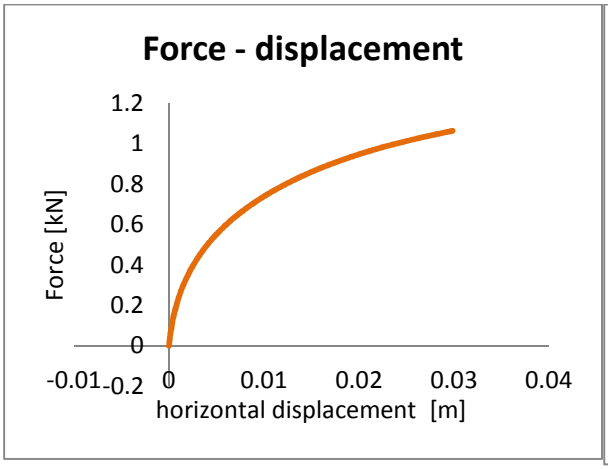

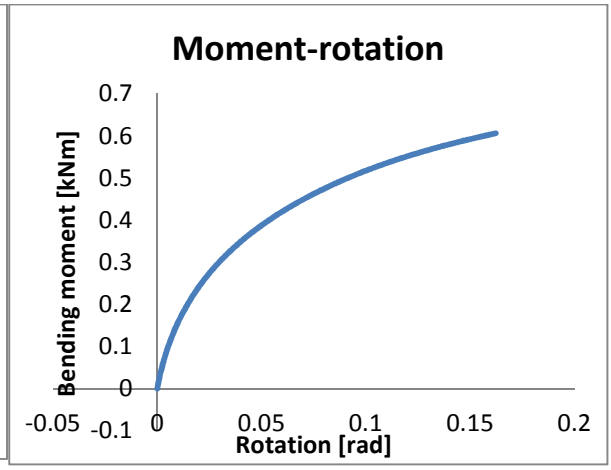

Figure 3.11: Force displacement curve in unplugged pile **Figure 3.12:**Moment rotation curvein unplugged pile

The lateral capacity is not reached but the value of the maximum force is 1.06kN with a deflection of 0.03m.The maximum moment is 0.60 kNm with a rotation of 0.16 rad (9.3°). The value of the maximum moment at 4 cm above the sand surface is comparable to the moment at the sand surface at 0.4 kN observed in figure 3.13.

- Bending Moment distribution along the pile (0.24m sand level)

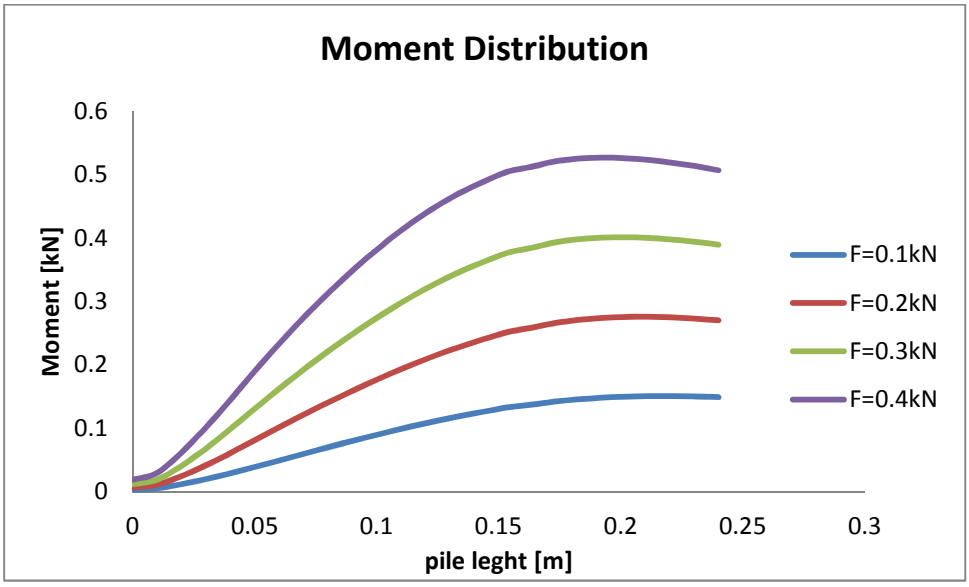

Figure 3.13: Bending moment distribution in unplugged pile

- P-y curves

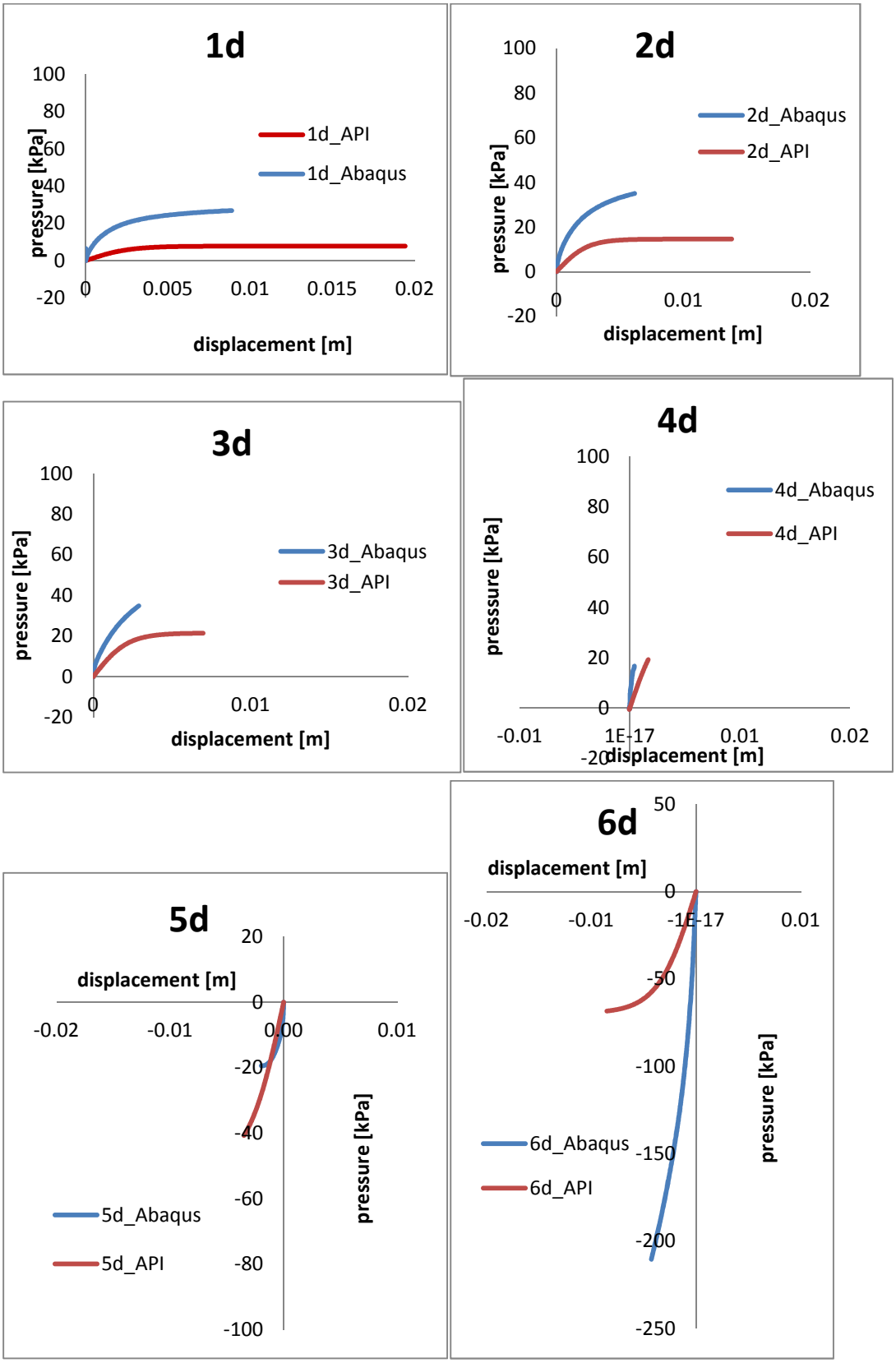

Figure 3.14: Comparison of p-y curves of unplugged pile with API [6] provision

Also the variation of soil shear strength does not change the pattern of the graphs analysed, but the numerical values obtained are slightly different from the reference soil. In the next chapter a detailed comparison which underlines the variation of the lateral capacity and p-y curves is shown.

2.3 Laterally loaded flexible pile (plugged)

It is expected a soil behaviour of the plugged flexible pile very similar to the rigid pile because the soil around the pile have the same shape and same properties. On the other hand the deformed configuration and the failure mechanism are expected to be very similar to the ones of the unplugged because both of the piles are flexible.

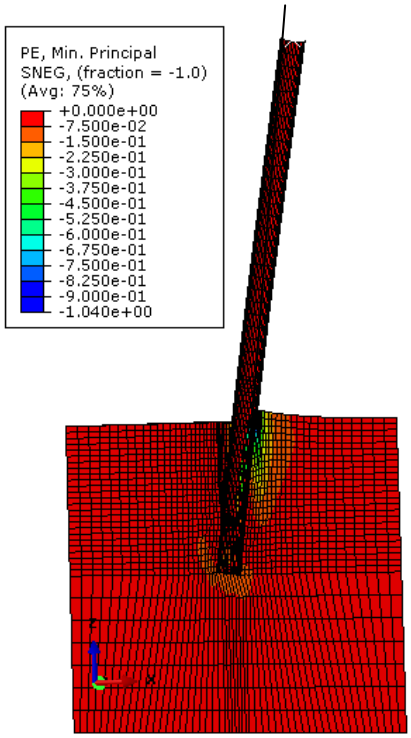

Figure 3.15: Plastic strain contours and failure pattern for hollow plugged pile

Figure 3.15 shows that there is not a rigid body failure since there is a small deformation of the pile very similar to the one of the hollow unplugged pile. The discrepancy from the rigid body failure is highlighted by the black line.

- Lateral force-horizontal displacement curve and Moment- rotation curve at the top of the pile

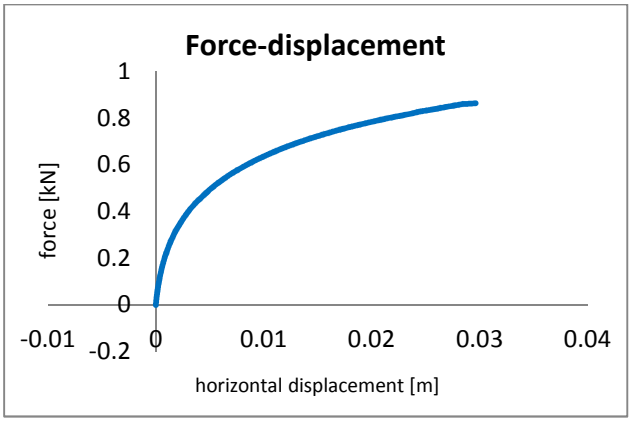

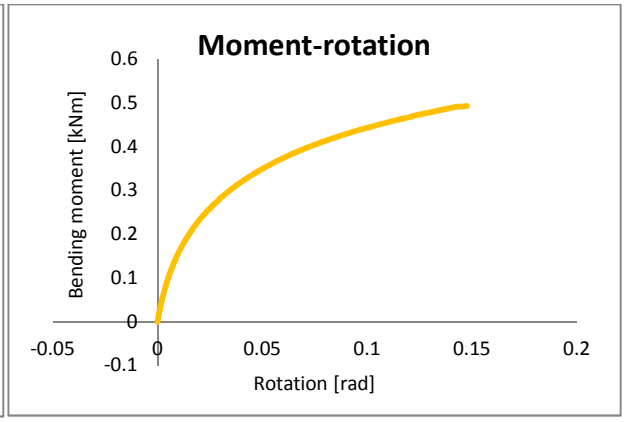

Figure 3.16: Force displacement curve in plugged pile **Figure 3.17:**Moment rotation curvein plugged pile

The maximum force is 0.86kN with a deflection of 0.029m and a maximum moment of 0.5kNm with a rotation of 0.15 radiant. The ultimate load is not reached in the hollow piles because of numerical problems of the shell elements in the software used .

- Bending Moment distribution along the pile (0.24m sand level)

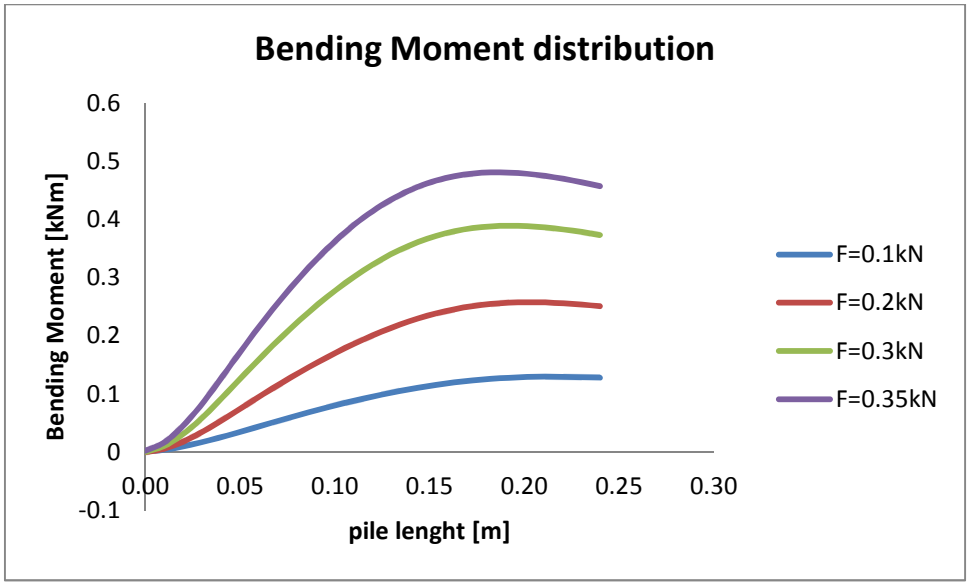

Figure 3.18: Bending moment distribution in plugged pile

The bending moment distribution at low value of forces is the one expected for linear elastic soil response. At higher values of lateral force the maximum value of the moment is located below the sand surface and the magnitude is comparable with the maximum bending moment in the moment-rotation curve(figure 3.17). The difference is due to the different positions and force magnitude analysed.

- Plastic strain

F = 0.1 kN

F=0.2 kN

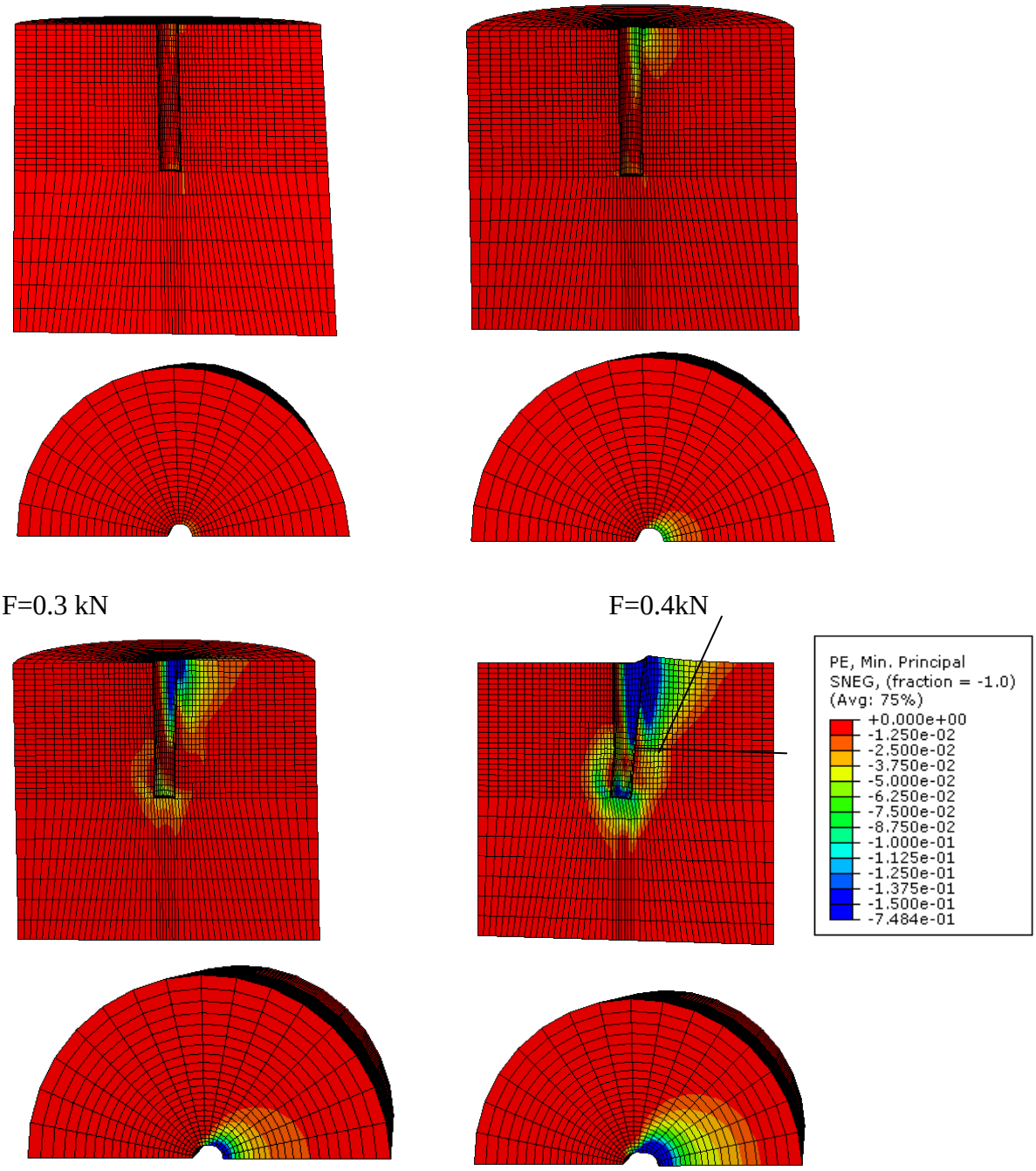

Figure 3.19: Plastic strain contours with increasing force in plugged pile

Also in the plugged pile the a failure wedge is developed until a depth of approximately 4d, and the inclination respect to the horizontal is almost 60°. The p-y curves presented below confirm the qualitative considerations noted from figure 3.19.

- P-y curves at different depth

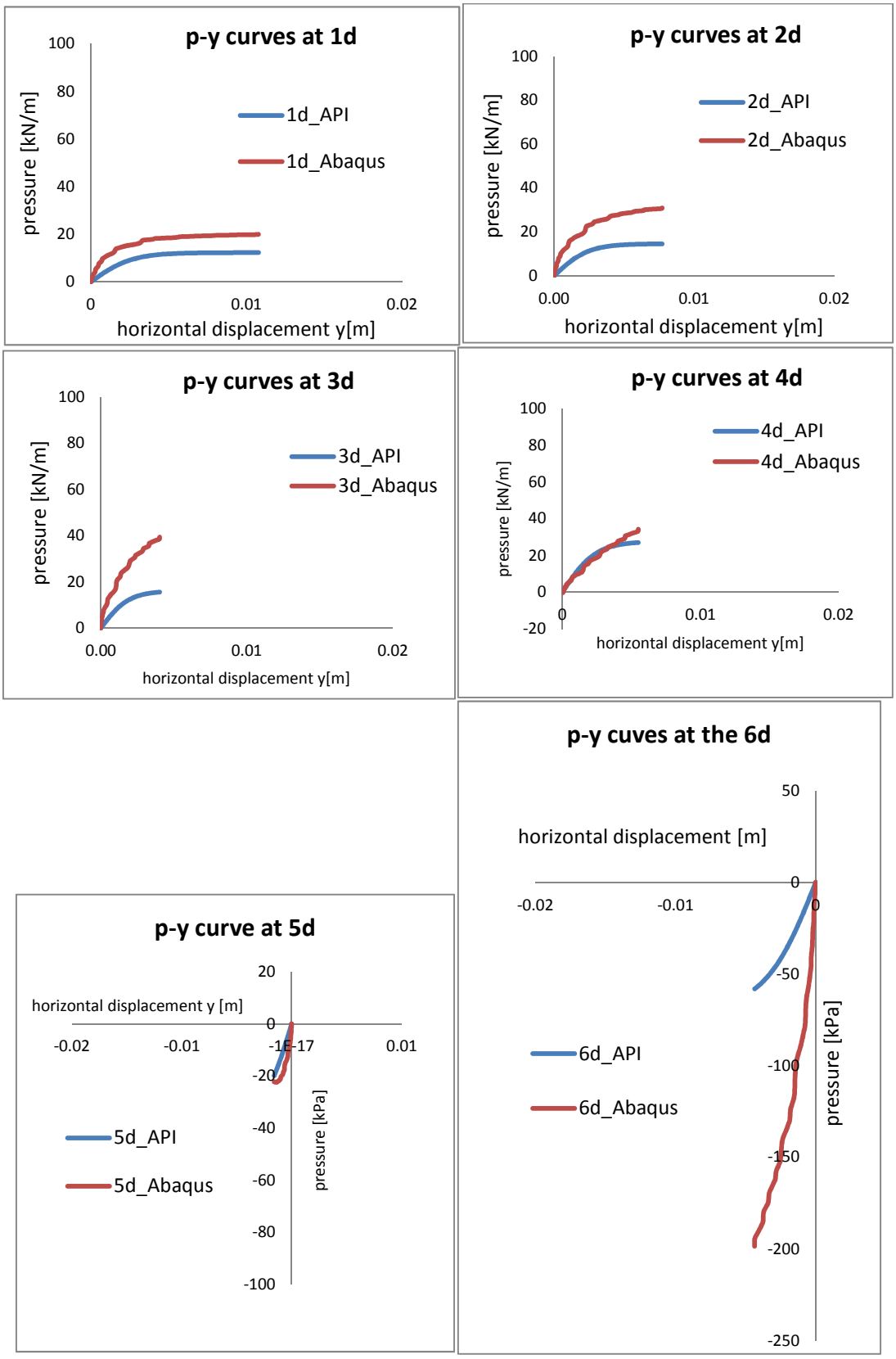

Figure 3.20: Comparison of p-y curves of plugged pile with API [6] provision

The p-y curves reached the ultimate shear strength just at the depth of 1d, 2d,3d, it means that the soil reach the plastic strain at this depth and so the height of the failure wedge corresponds approximately at 3d-4d.

Increase of interface shear strength

Since the plugged pile behaviour is very similar to the unplugged one, also in this case the increment of interface shear strength does not produce variation in the in the patterns of lateral forces, bending moments and pressure of the system pile-soil.

- Lateral force-horizontal displacement curve and Moment- rotation curve at the top of the pile

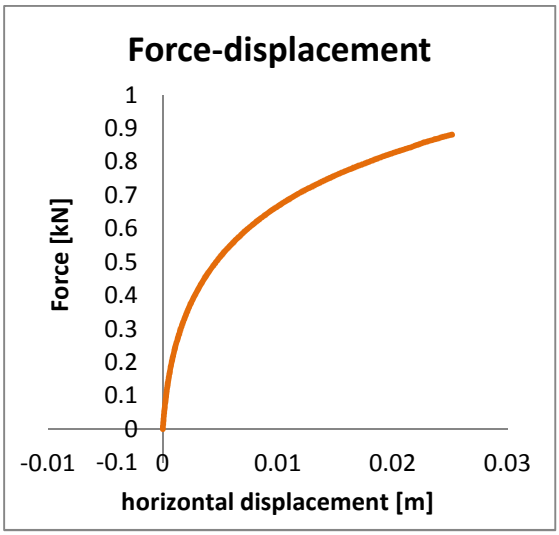

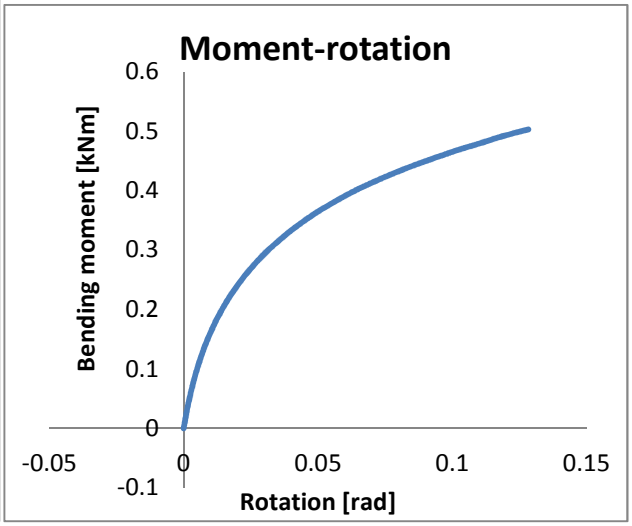

Figure 3.21: Force displacement curve in plugged pile **Figure 3.22:**Moment rotation curve in plugged pile

The lateral load capacity of the pile is not reached . The maximum force is 0.88 kN considering a deflection of 0.025m and the maximum moment is 0.53 kNm with a rotation of 0.148 radians

- Bending Moment distribution

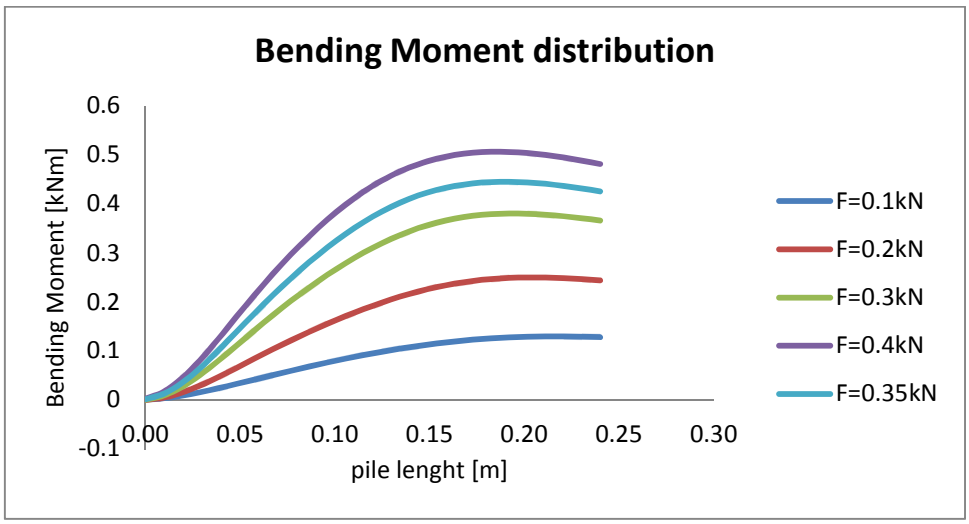

Figure 3.23: Bending moment distribution in plugged pile

- P-y curves

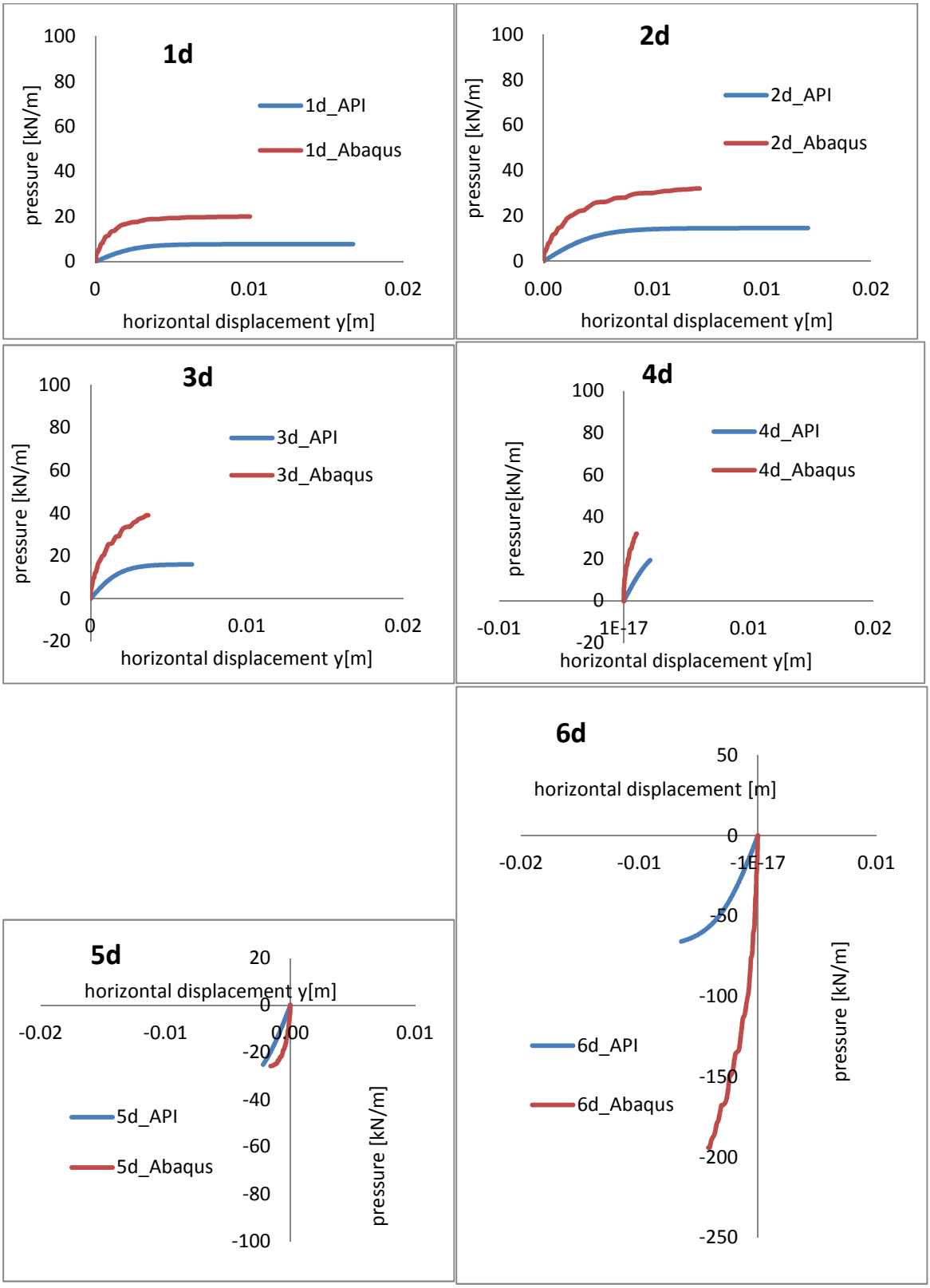

Figure 3.24: Comparison of p-y curves of plugged pile with API [6] provision

The pattern of the stiffness of the p-y curves and the ultimate soil resistance along the depth is always the same. The ultimate soil resistance is reached just for shallow depth.

The difference produced by the increased of interface shear strength can be seen in chapter 4 where the numerical values are compared.

Increase of shear strength soil

In figures 3.25 to 3.28 the effects of the increase of shear strength are presented.

- Lateral force-horizontal displacement curve and Moment- rotation curve at the top of the pile

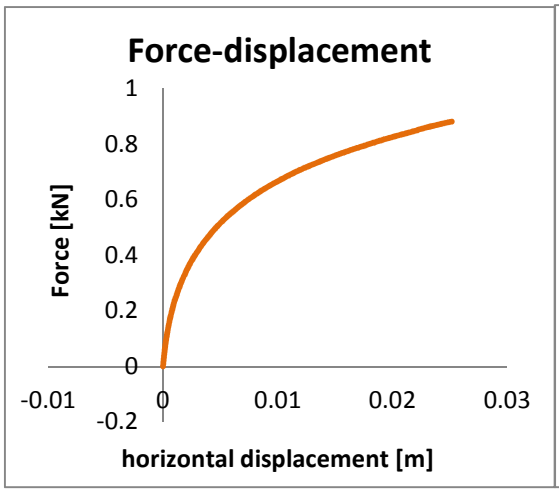

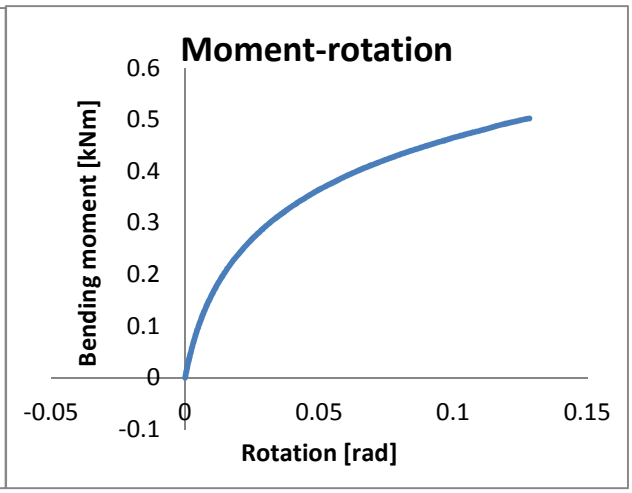

Figure 3.25: Force displacement curve in plugged pile **Figure 3.26:**Moment rotation curvein plugged pile

The maximum force is 0.88kN with a deflection 0.025m. The maximum moment is 0.503kNm at 0.123 radiants (7.3°).

- Moment distribution along the pile (sand level 0.24m)

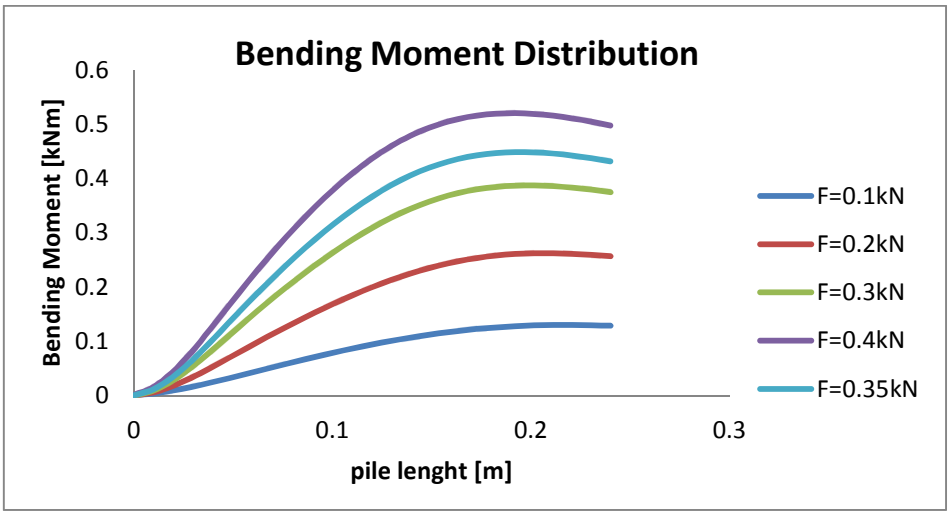

Figure 3.27: Bending moment distribution in plugged pile

- P-y curves at different depth

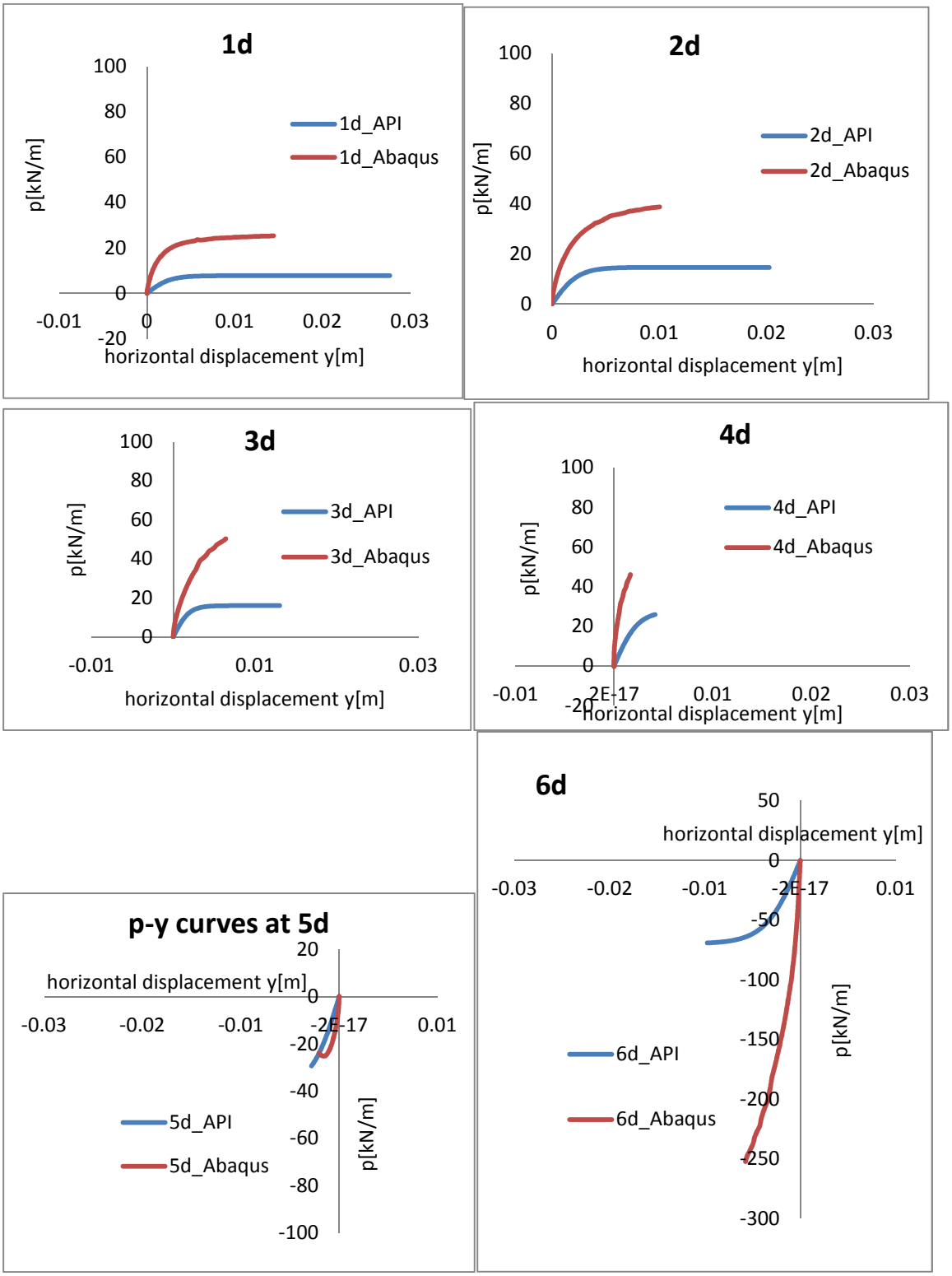

Figure 3.28: Comparison of p-y curves of plugged pile with API [6] provision

The characteristics of the graph are the same of the previous ones, hence in order to understand the differences graphs with comparison of the three soil types are shown in chapter 4.

2.4 Laterally loaded rigid pile

In the rigid pile mathematical problems during the solution of the model does not occur, so that the software can compute the results until the failure of the soil.

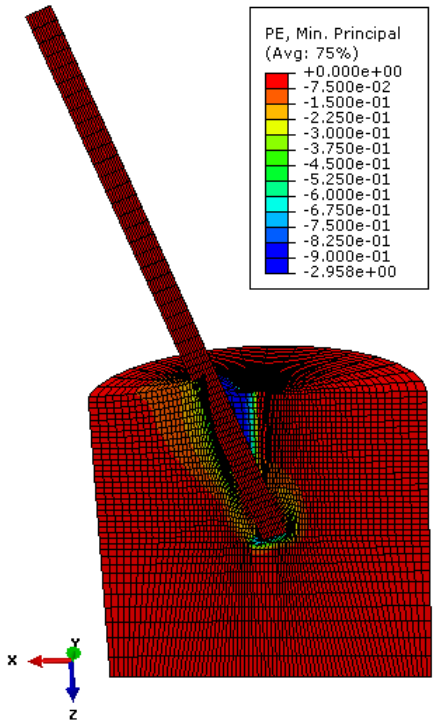

Figure 3.29: Plastic strain contours and failure pattern rigid pile

The displacement of the pile is bigger than the one of the flexible piles because in this case the pile reach the ultimate load.

The rigid body rotation, the bulging of soil at the side of the pile as well as the gap at the back side of the pile observed in Figure 3.29, are the main aspects of the failure mode of a rigid lateral loaded pile .

- Lateral force-horizontal displacement curve and Moment- rotation at the top of the pile curve

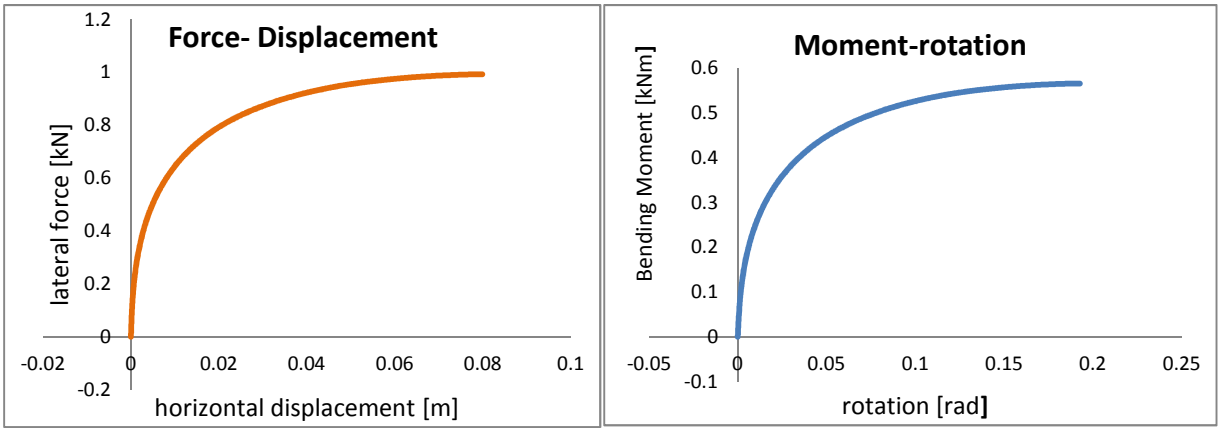

Figure 3.30: Force displacement curve in rigid pile **Figure 3.31:**Moment rotation curve in rigid pile

The maximum force correspond to the ultimate force and is equal to 0.99kN with a deflection of 7.8cm. The ultimate moment is 0.56kNm with a rotation of 0.19 rad (11°).
The pile reaches the lateral capacity , it can be seen in figure 3.30 because the force displacement curve became horizontal.

- Moment distribution along the pile (sand level 0.24m)

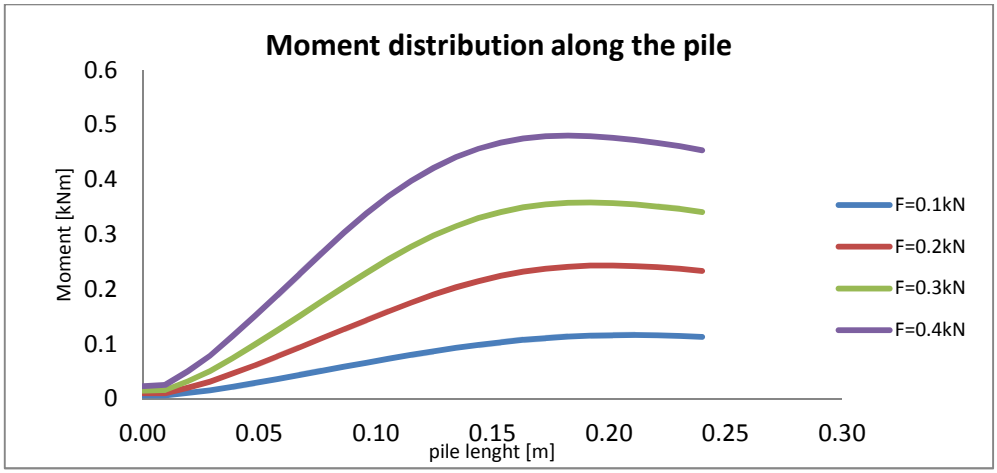

Figure 3.32: Bending moment distribution in rigid pile

Even if the failure mechanism of the rigid pile is different from the flexible ones, the pattern of moment distribution along the rigid pile is very similar to the one of the flexible piles. The bottom of the pile is not subject to bending moment. The position of the maximum moment is at the sand surface for low forces and it gradually moves as the force increases.

- Plastic strain

F=0.1kN F=0.2kN

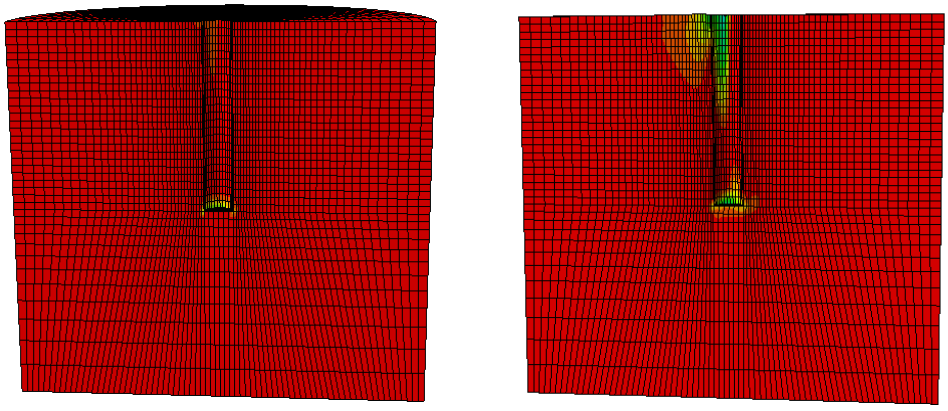

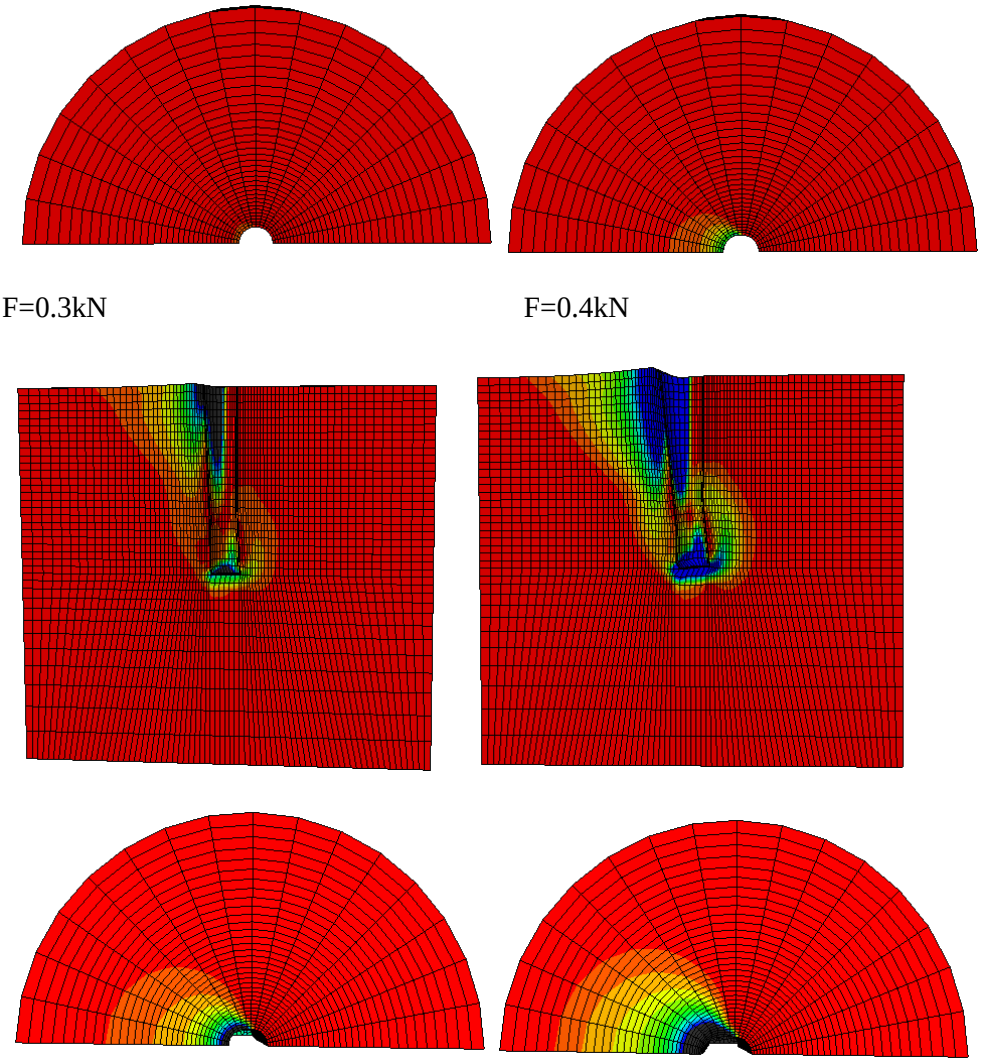

Figure 3.33: Plastic strain contours with increase force in unplugged pile

- P-y curves at different depths

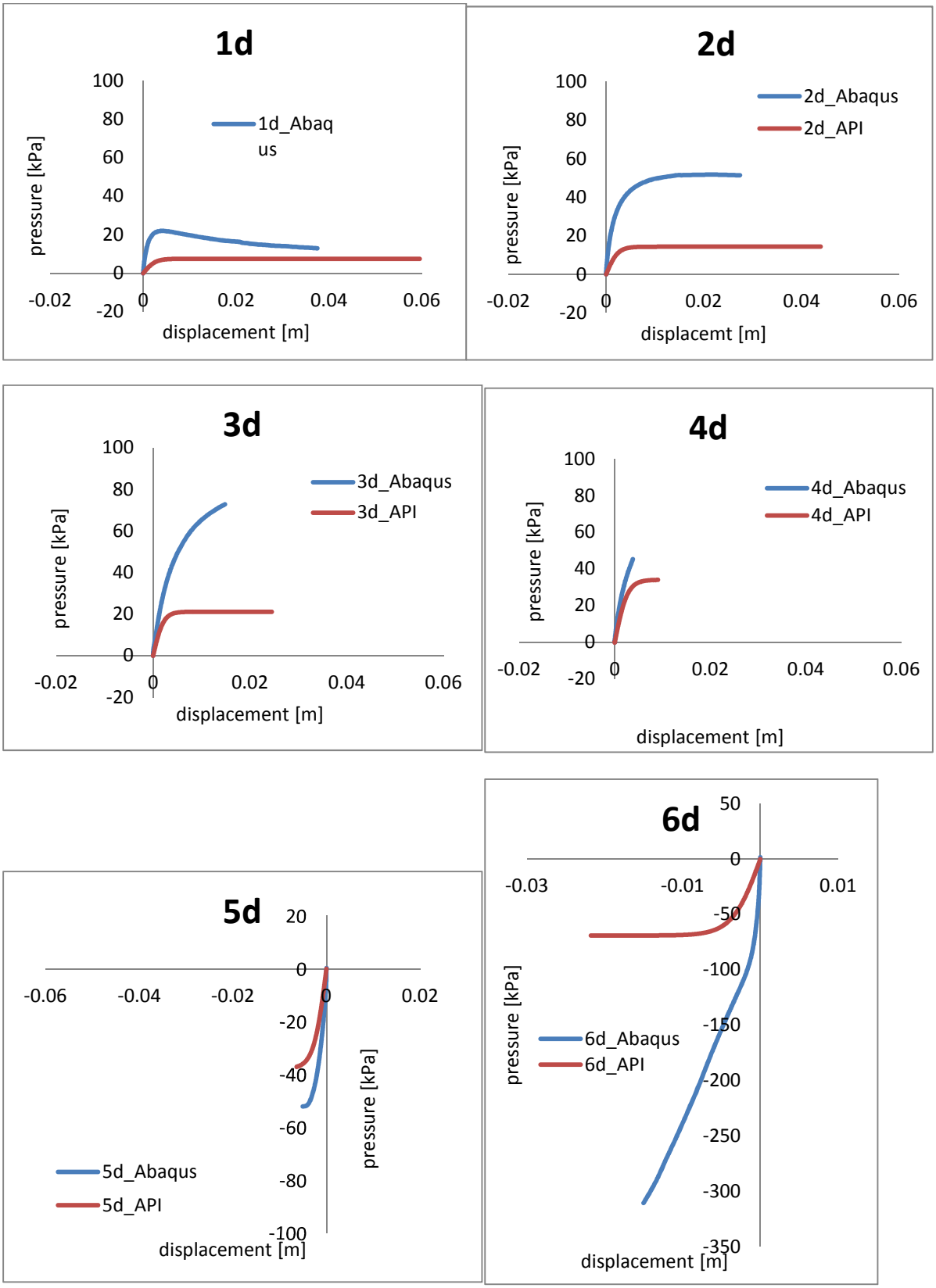

Figure 3.34: Comparison of p-y curves of rigid pile with API [6] provision

Increase of interface shear strength

- Lateral force-horizontal displacement curve and Moment- rotation curve at the top of the pile

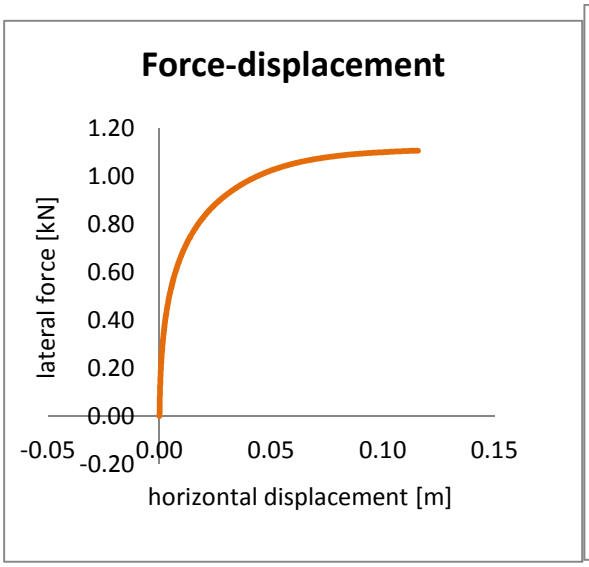

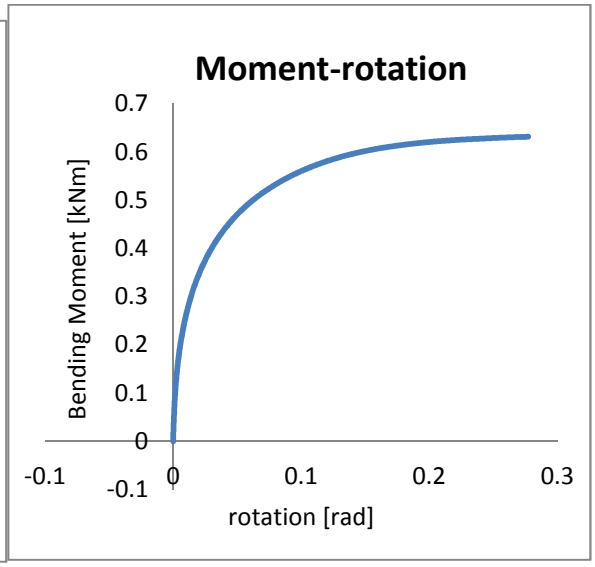

Figure 3.35: Force displacement curve in rigid pile **Figure 3.36:**Moment rotation curve in rigid pile

The ultimate force is1.1kN with a deflection of 0.12m and a ultimate moment of 0.62kNm with a rotation of 0.28 rad (15.8°).

- Moment distribution along the pile (sand level 0.24m)

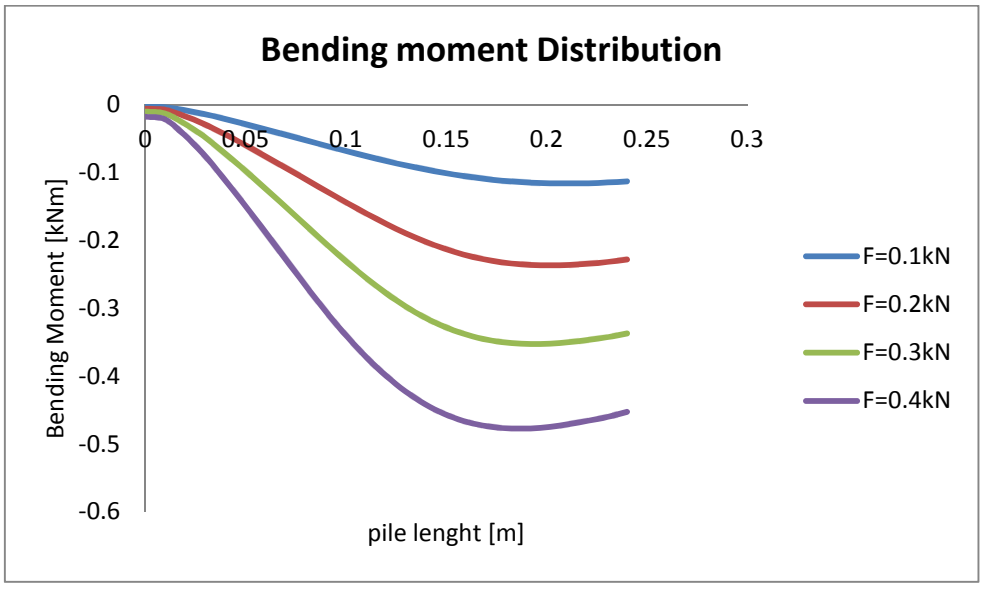

Figure 3.37: Bending moment distribution in unplugged pile

- P-y curves at different depths

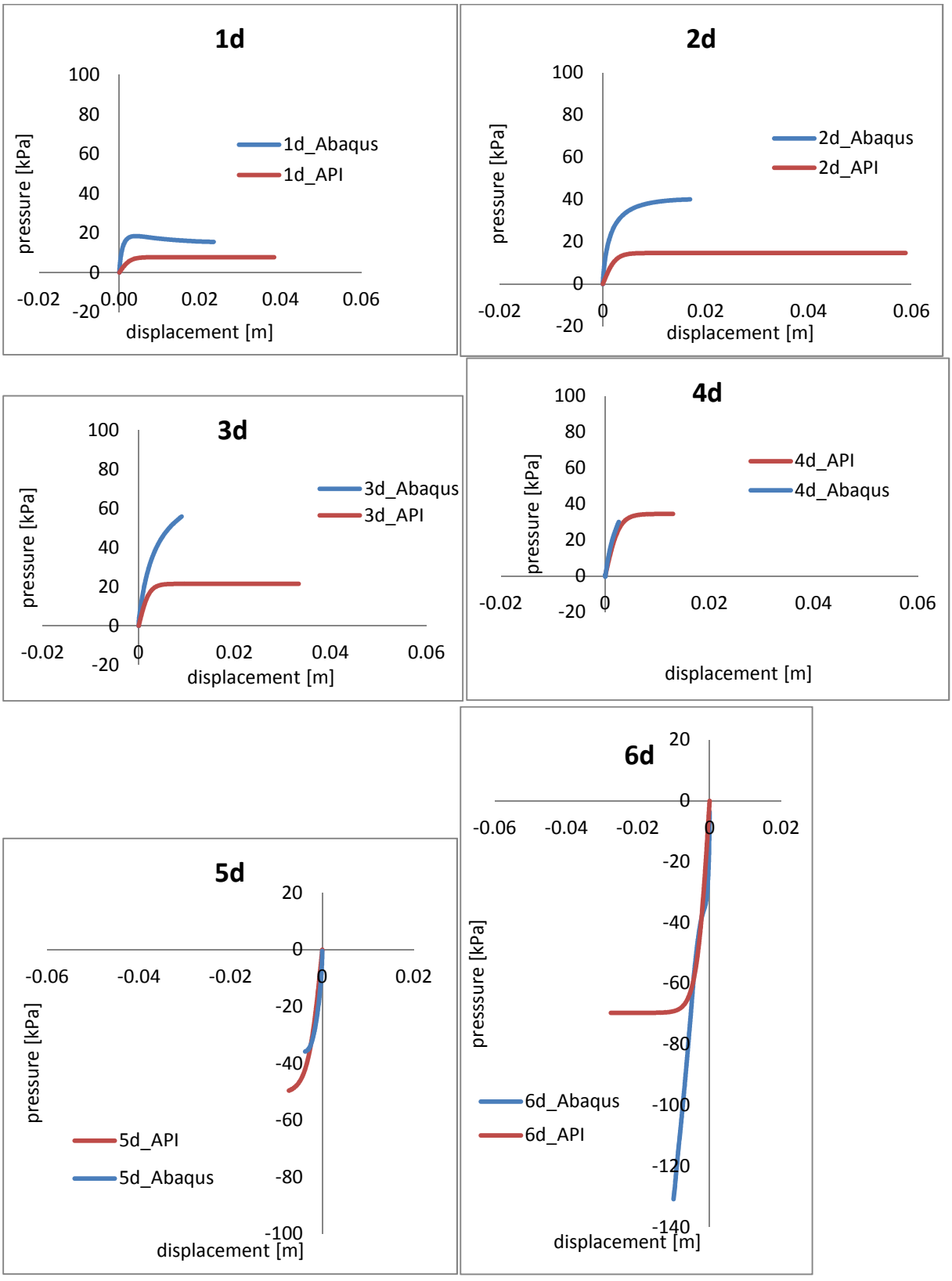

Figure 3.38: Comparison of p-y curves of rigid pile with API [6] provision

Increase of shear strength soil

- Lateral force-horizontal displacement curve and Moment- rotation curve at the top of the pile

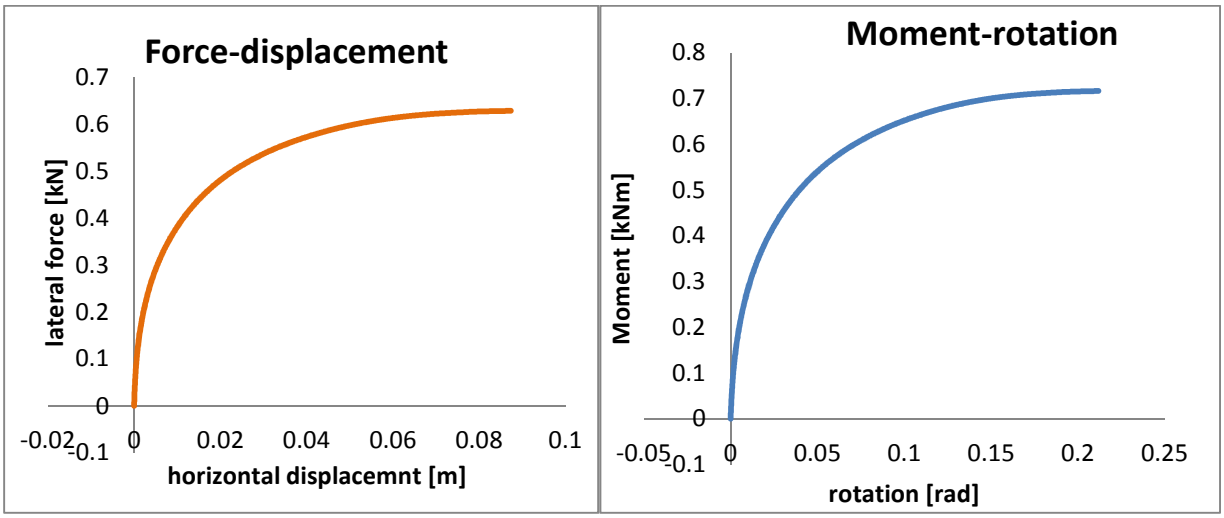

Figure 3.39: Force displacement curve in rigid pile **Figure 3.40:**Moment rotation curve in rigid pile

The ultimate force is 0.63kN with a deflection of 0.087m and the ultimate moment is 0.72kNm with a rotation of 0.21rad (12°).

- Moment distribution along the pile (sand level 0.24m)

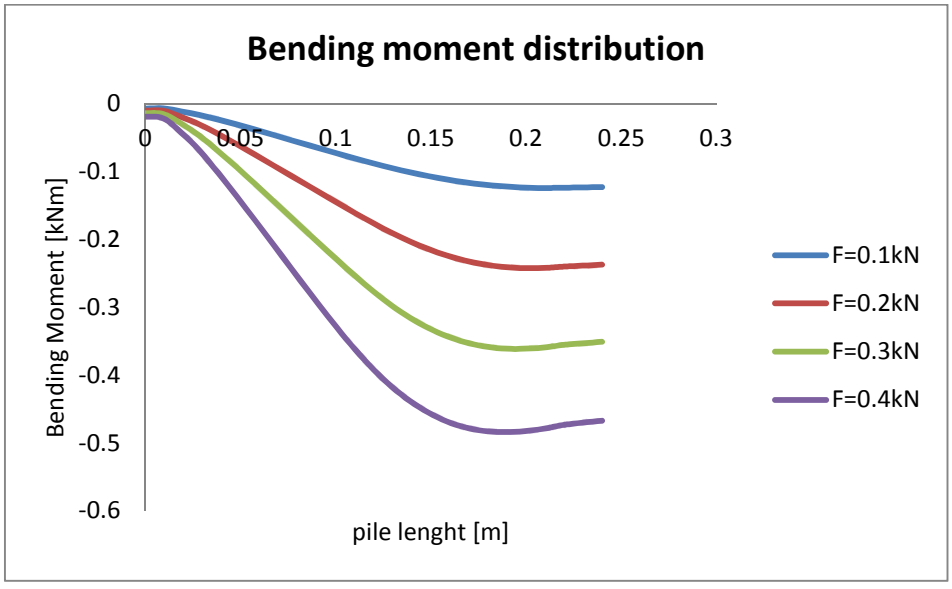

Figure 3.41: Bending moment distribution in rigid pile

- P-y curves at different depth

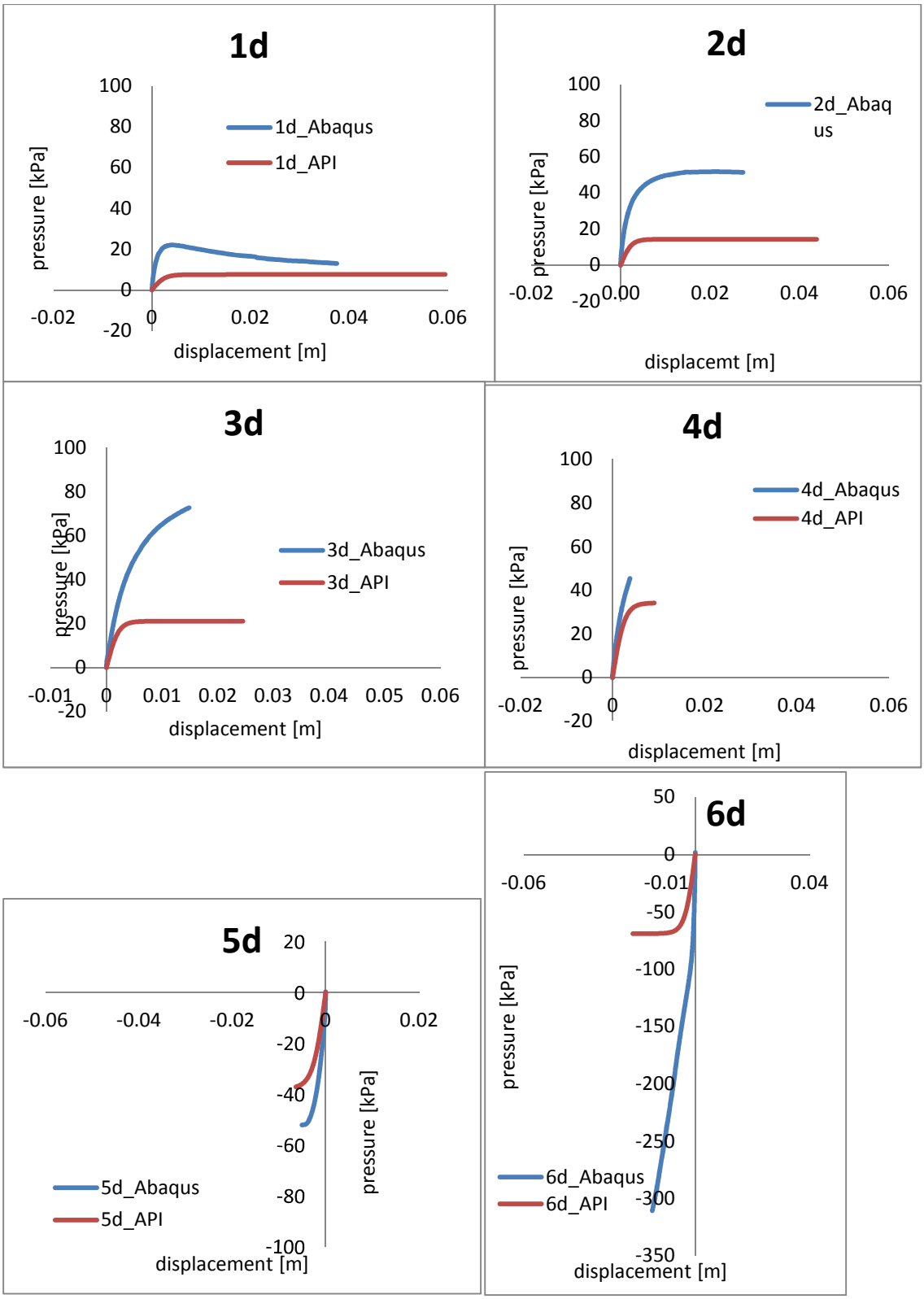

Figure 3.42: Comparison of p-y curves of rigid pile with API [6] provision

4. Discussion of the results

4.1 Effect of pile's stiffness

The following graphs regards the reference soil.

- Force displacement curve

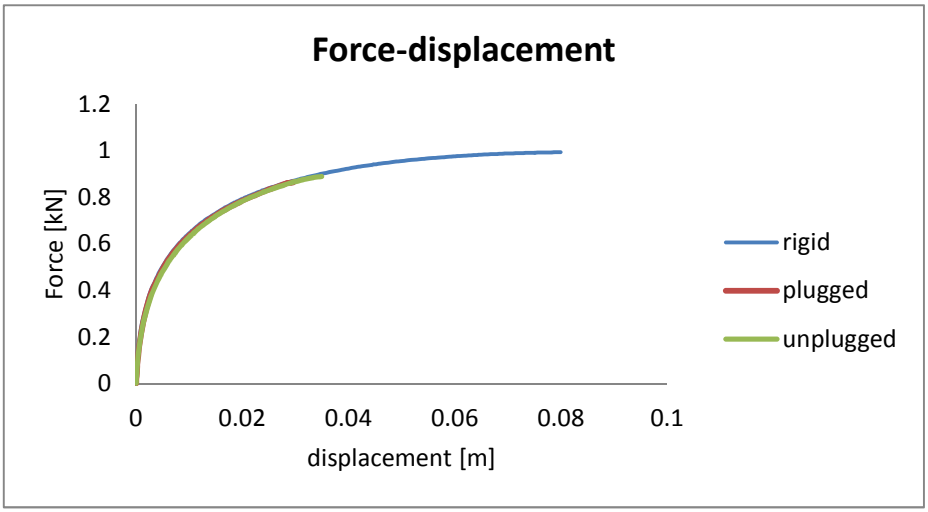

Figure 4.1: Comparison of force displacement curves in rigid and hollow piles

The lateral capacity of the pile out of the sand is the same with the three type of pile used. It means that the stiffness of the pile does not affect the ultimate load and the corresponding deflection at the top of the pile.

- Moment-rotation (moment calculated as it is shown in the appendix)

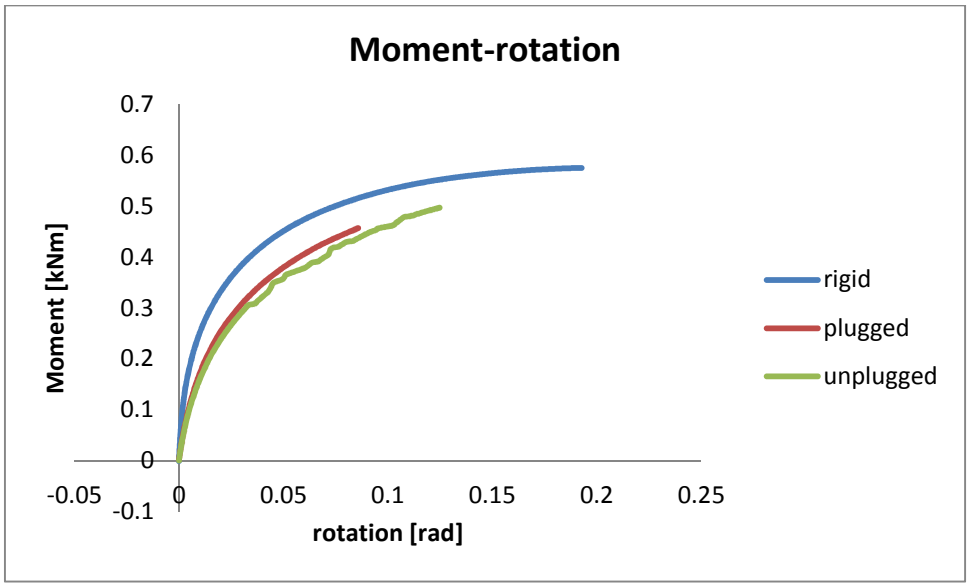

Figure 4.2: Comparison of moment – rotation curves in rigid and hollow piles

The stresses and the section forces in the pile used to calculate the moment are different in the rigid and in the flexible piles. A possible explanation is that the failure mechanism and the shape of the deformed configuration of the pile are different. In the rigid pile there is a rigid body rotation, hence for same value of moment the rotation is smaller.

- p-y curves

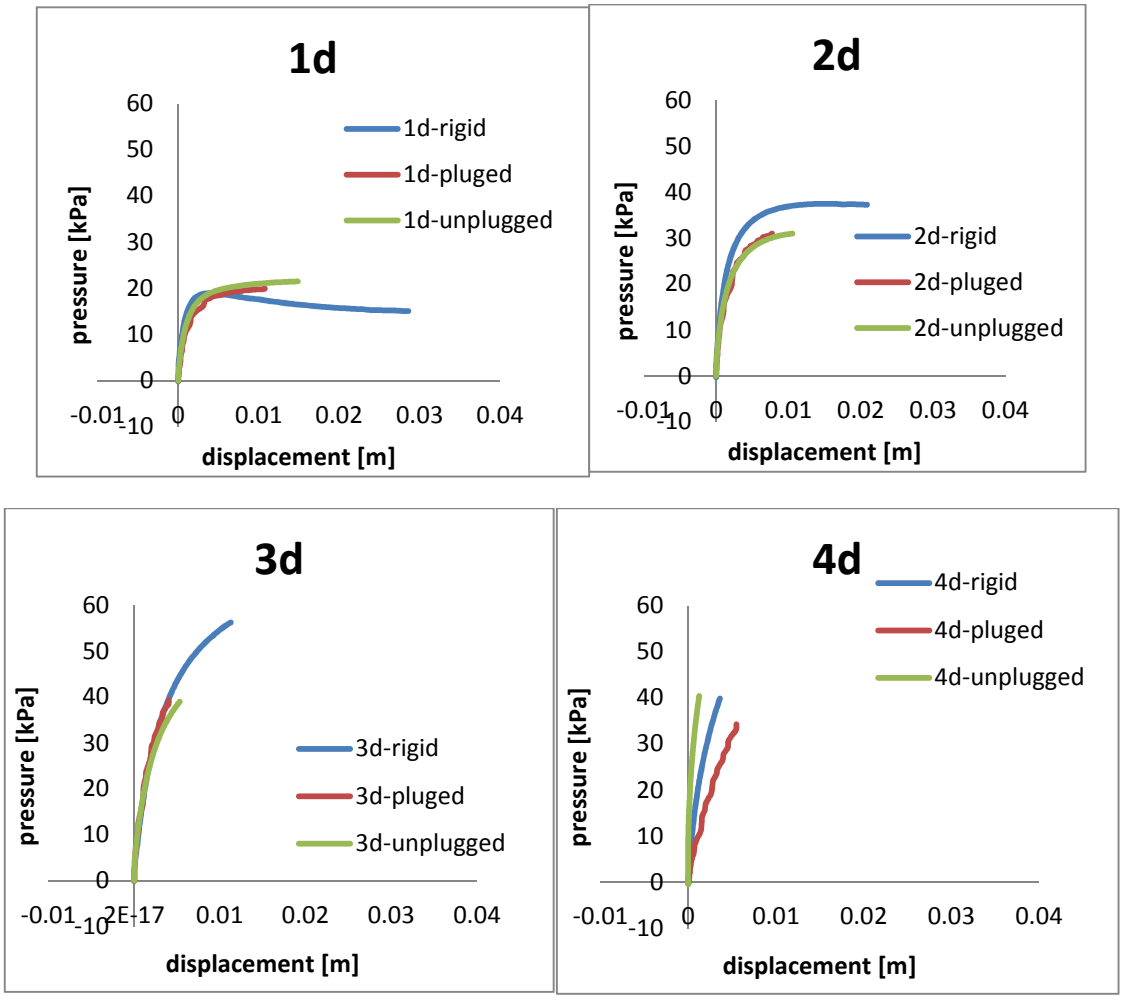

Figure 4.3: Comparison of p-y curves in curves in rigid and hollow piles

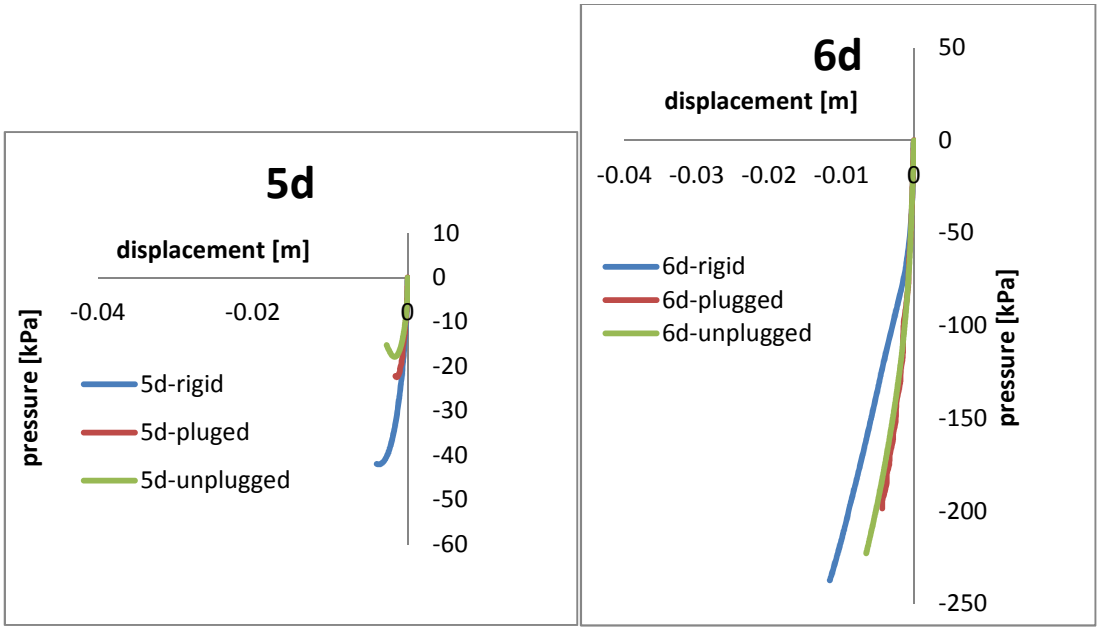

Figure 4.3: Comparison of p-y curves in curves in rigid and hollow piles

The variation of stiffness kx is evident just at 4d where probably is located the rotation point. The ultimate soil strength varying significantly after 4d, this change in the p-y curves is probably due to a different failure mechanism (rigid body rotation and flexible rotation)

Increase of interface shear strength

- Force displacement curve

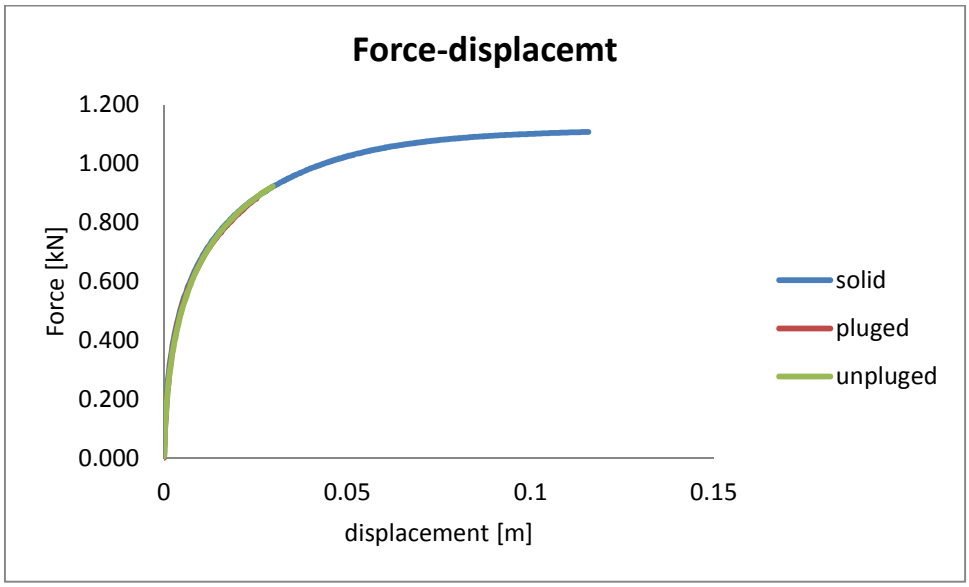

Figure 4.4: Comparison of force displacement curves in rigid and hollow piles

Also at higher interface shear strength, the stiffness of the pile does not affect the lateral capacity.

- Moment rotation(moment calculated as it shown in the appendix)

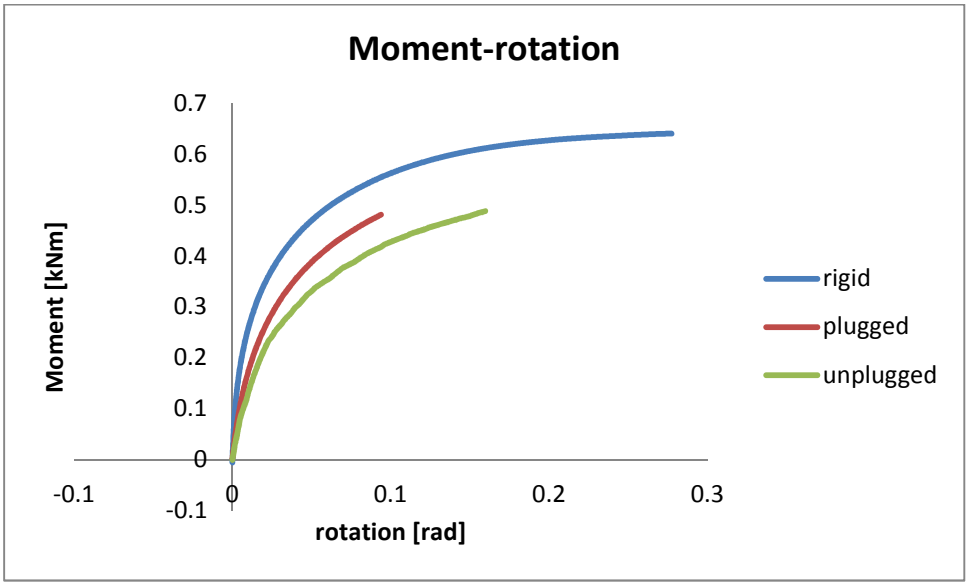

Figure 4.5: Comparison of moment – rotation curves in rigid and hollow piles

For higher interface friction the moment at the sand surface depends on the type of pile. This difference in the maximum moment that is not present in the lateral capacity can be explained considering different failure mechanisms, that are more evident for higher interface friction.

- P-y curves

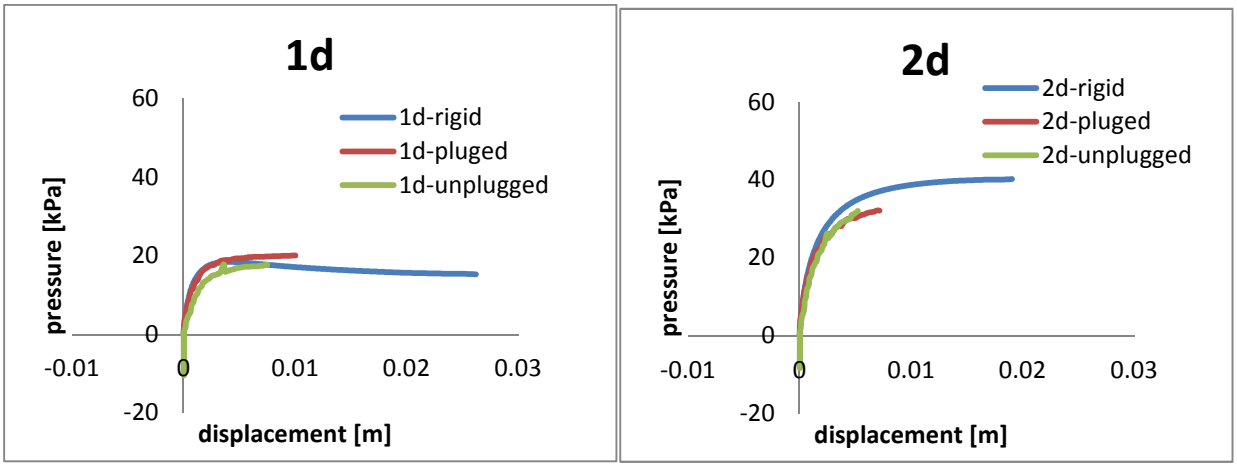

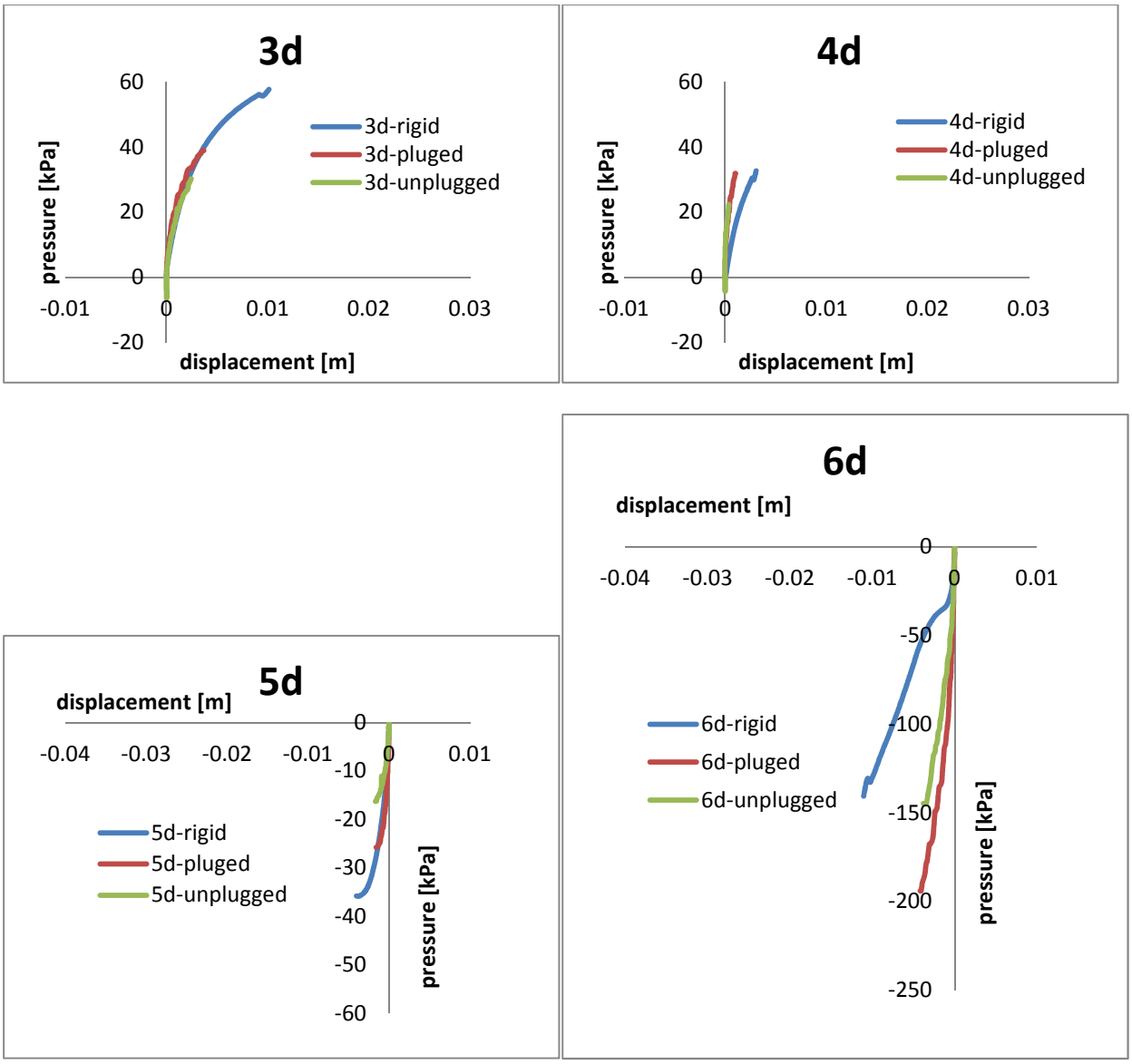

Figure 4.6: Comparison of p-y curves in curves in rigid and hollow piles

At higher interface shear strength the stiffness effect are the same. The lateral pile capacity of piles in cohesionless soil is independent of the type of pile and the stiffness. On the other hand in the p-y curves the stiffness effect can be observed at high depth especially in the ultimate value.

Increase of soil shear strength

- Force displacement curve

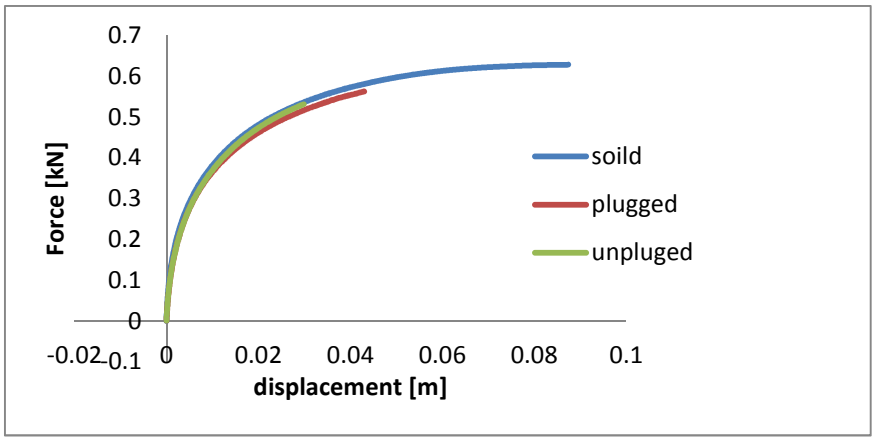

Figure 4.7: Comparison of force displacement curves in rigid and hollow piles

- Moment rotation(moment calculated as it shown in the appendix)

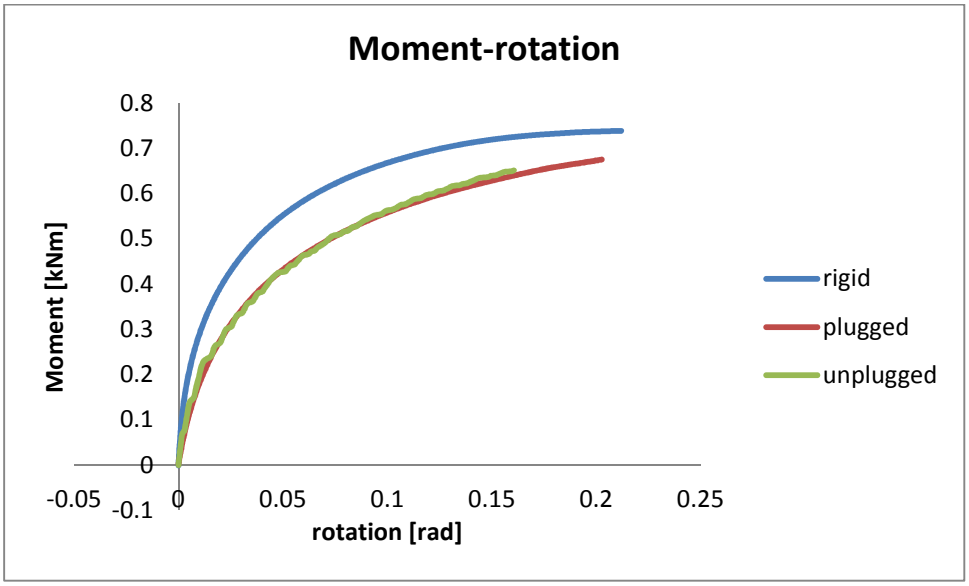

Figure 4.8: Comparison of moment- rotation curves in rigid and hollow piles

Increasing the soil friction in the moment rotation curve , the gap between flexible and rigid piles becomes more evident. The same bending moment produces a higher rotation in the flexible piles than in the rigid pile, the reason could be the different failure mechanism which is exposed by rigid and flexile pile expose.

- P-y curves

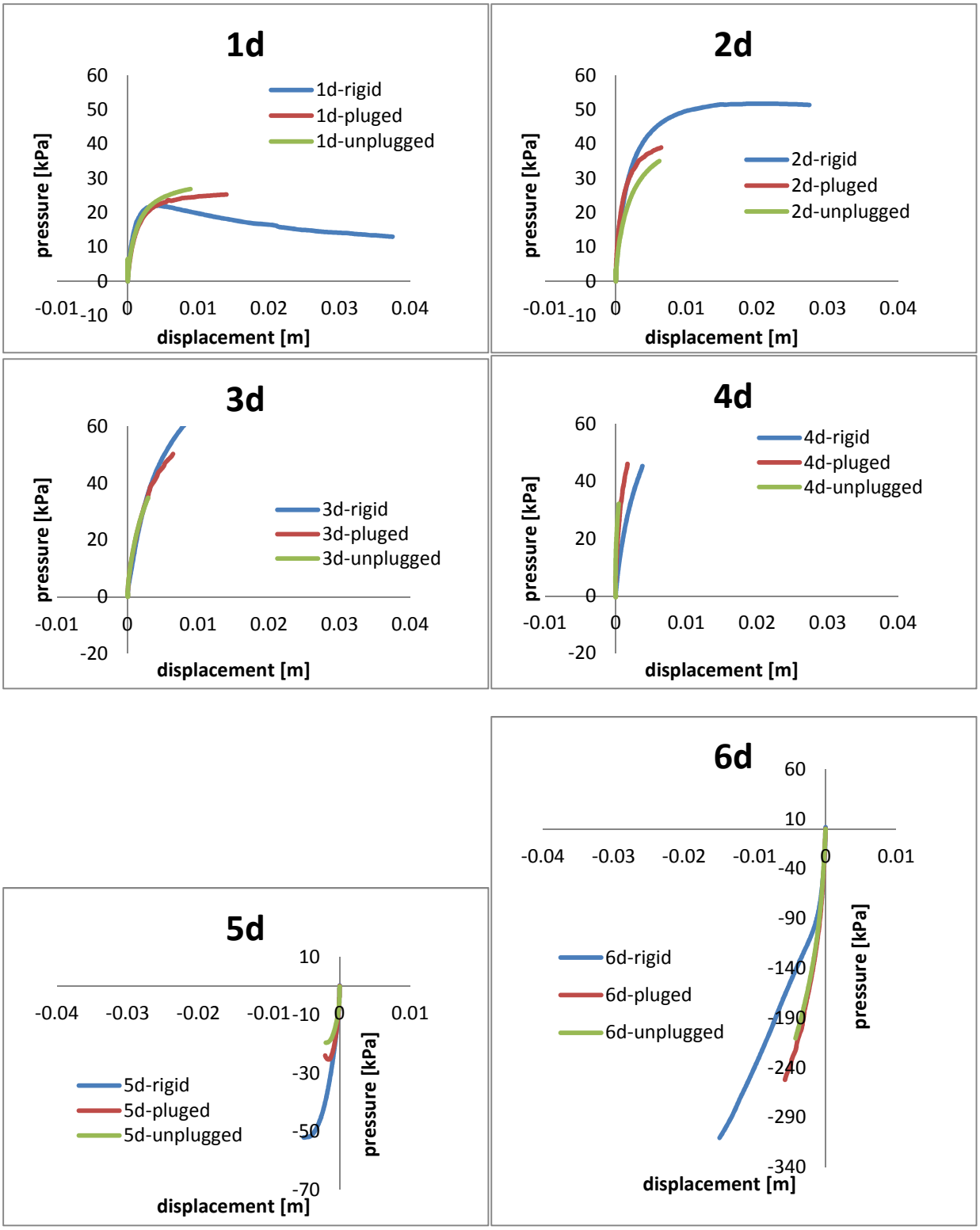

Figure 4.9: Comparison of p-y curves in curves in rigid and hollow piles

Moreover, for higher soil shear strength the stiffness effects are the same.

4.2 Effect of soil and interface properties

In this results discussion it is assumed:
Soil1: reference model with soil shear strength ϕ=33°; interface shear strength δ=2/3ϕ
Soil2: model with increase of interface shear strength δ=ϕ
Soil3: model with increase of soil shear strength ϕ=36°.

Unplugged flexible pile

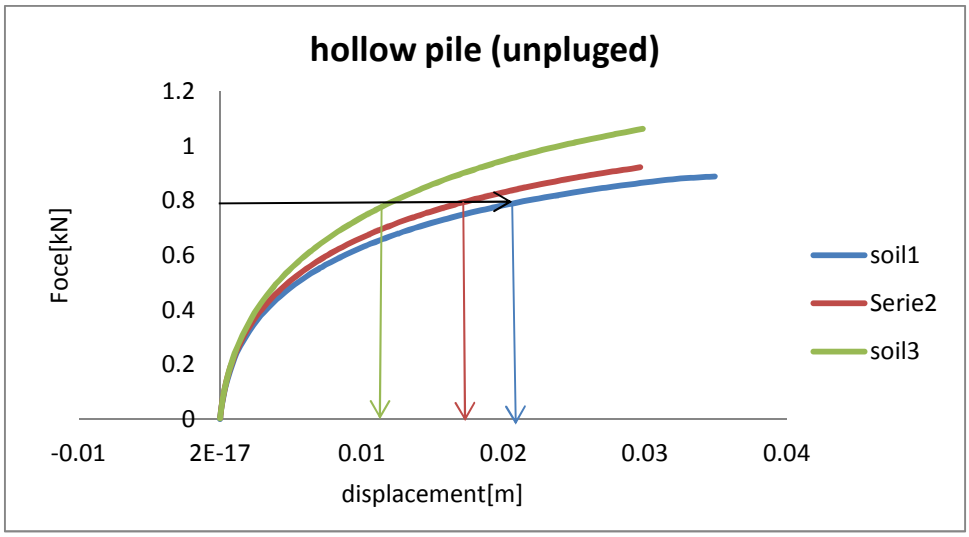

Figure 4.10: Comparison of force displacement curves in hollow unplugged piles

Increasing interface shear strength and soil shear strength the resistance to the lateral force improves.
The alteration of the soil shear strength induces a higher variation of the soil resistance. In particular for the same value of force the pile in the reference soil deflects more than the same pile in a “stiffer” soil (as it is shown by the arrows in figure 4.10)
Hence the lateral capacity of the flexible piles increases as the interface friction and the soil friction increase. This indicates that the increase of the shear stress along the soil-pile interface and in the soil provides additional resistance to the rotation of the pile.

- p-y cuves

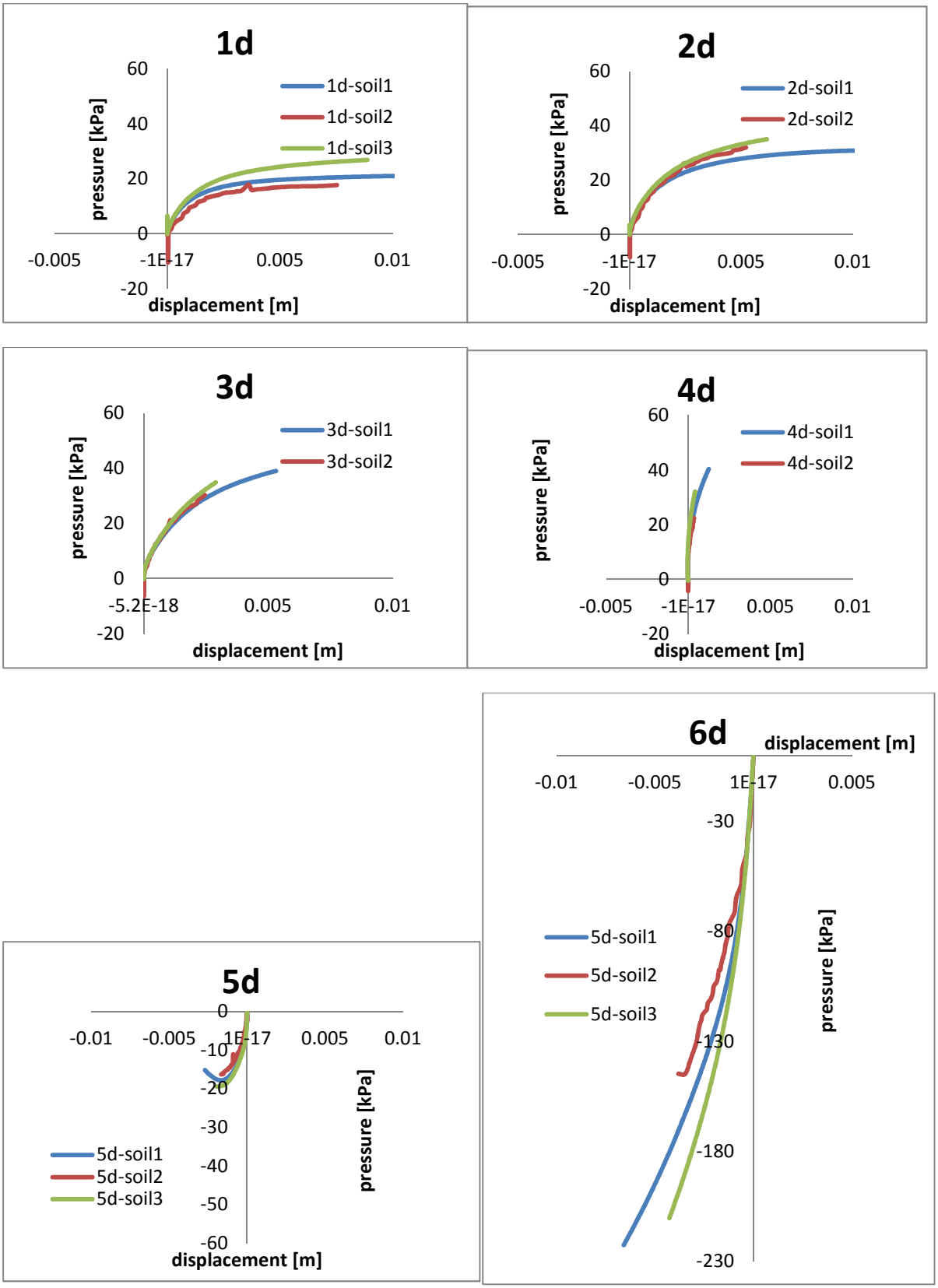

Figure 4.11: Comparison of p-y curves in hollow unplugged piles

The p-y curves of the 3 type of soil are not very different except for the bottom of the pile (6d) the increase of soil strength increase the stiffens of the p-y curve and probably also the ultimate soil resistance.

Plugged flexible pile

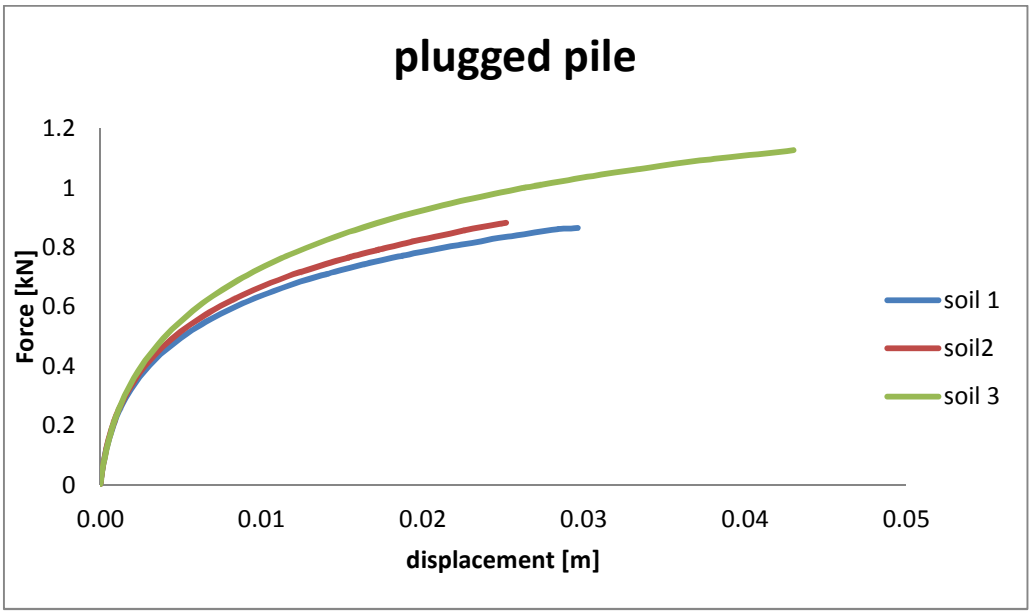

Figure 4.12: Comparison of force displacement curves in hollow plugged piles

- p-y cuves

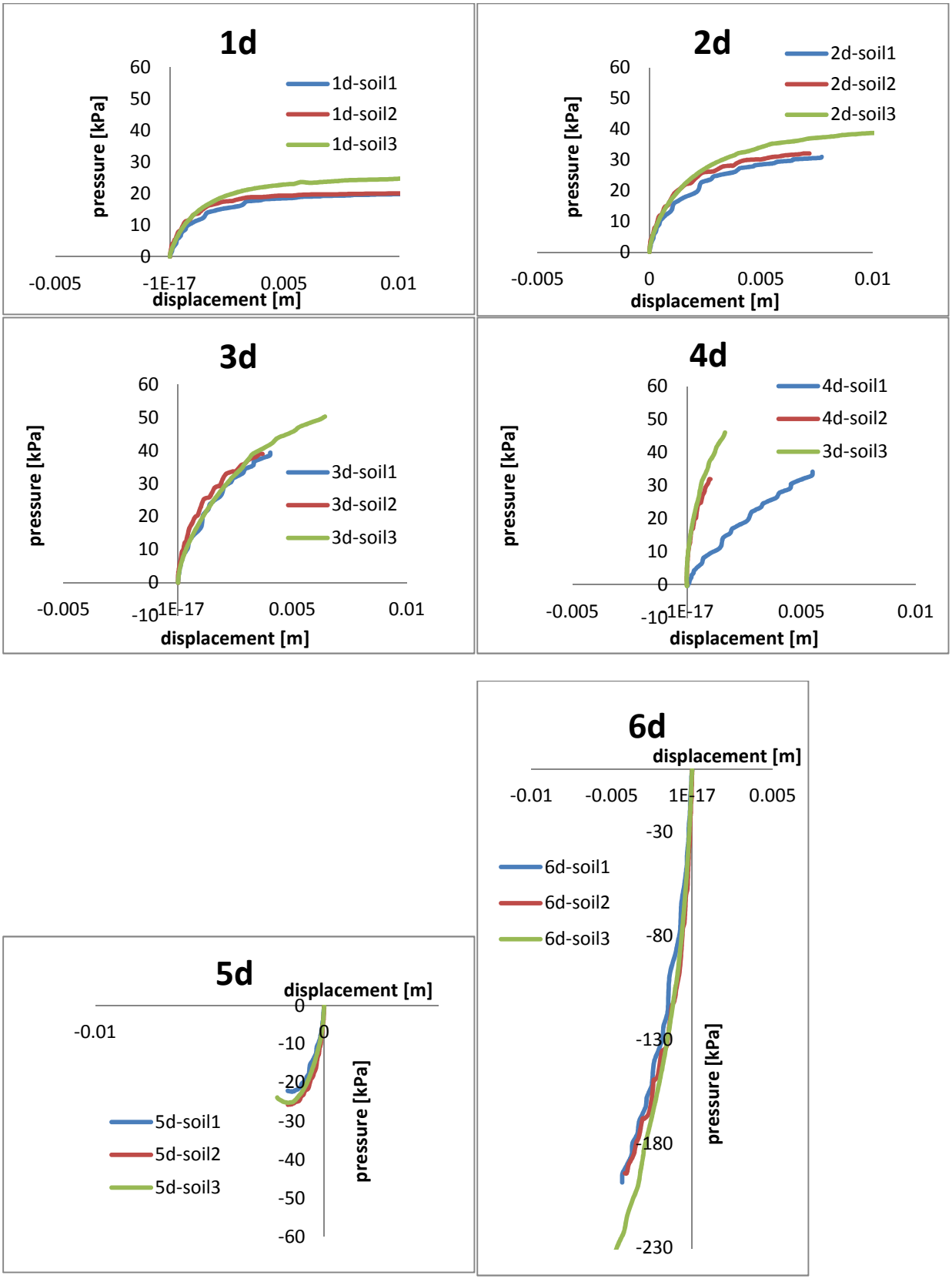

Figure 4.13: Comparison of p-y curves in hollow plugged piles

In the plugged flexible pile the interface friction and the soil friction influences both the load-displacement curve and the p-y curves. The lateral capacity increases in the same way as the hollow unplugged pile. The stiffness of the p-y curves and the ultimate resistance increases a bit as interface friction or soil friction increases. Also in the p-y curves the soil friction effects more the results respect to the interface friction.

Rigid pile

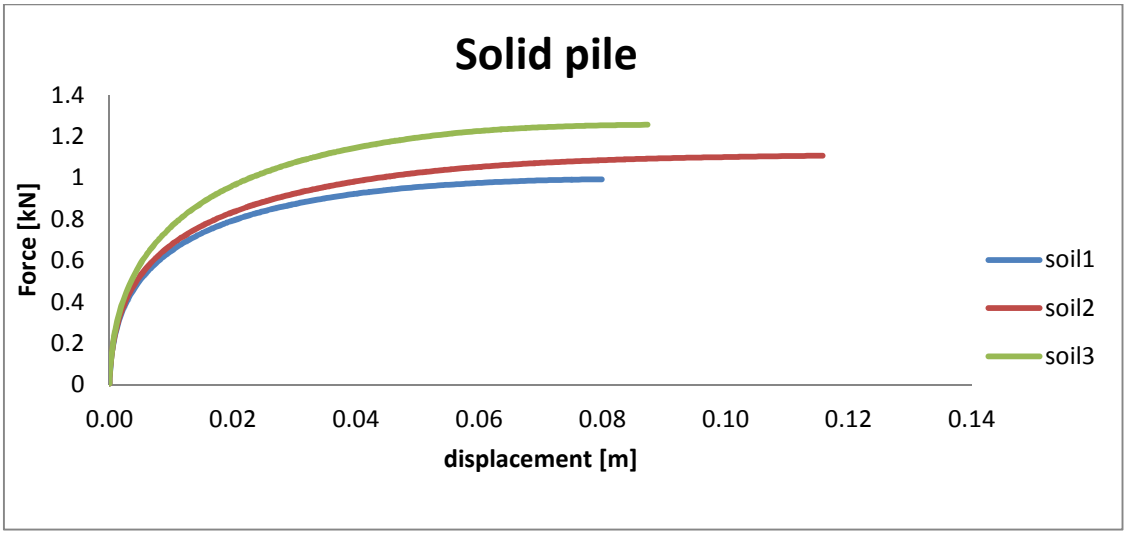

Figure 4.14: Comparison of force displacement curves in rigid piles

The variation of ultimate load with different type of soil can be estimated from the model of rigid pile because it is the only one that reaches the failure.

- p-y curves

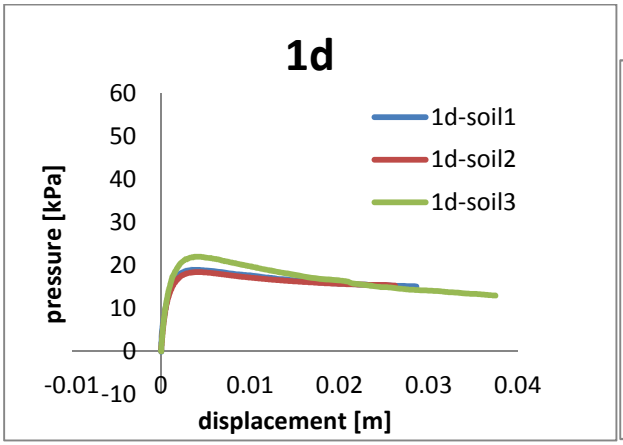

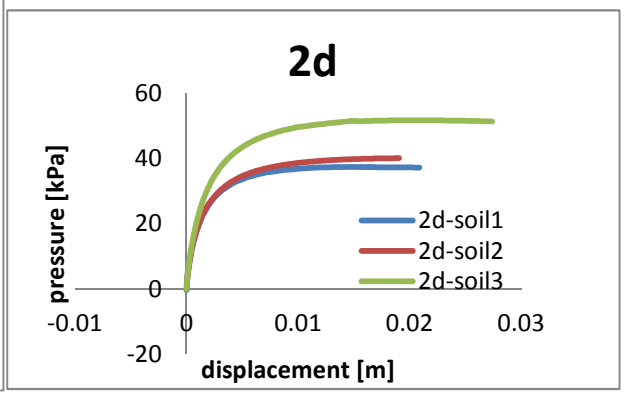

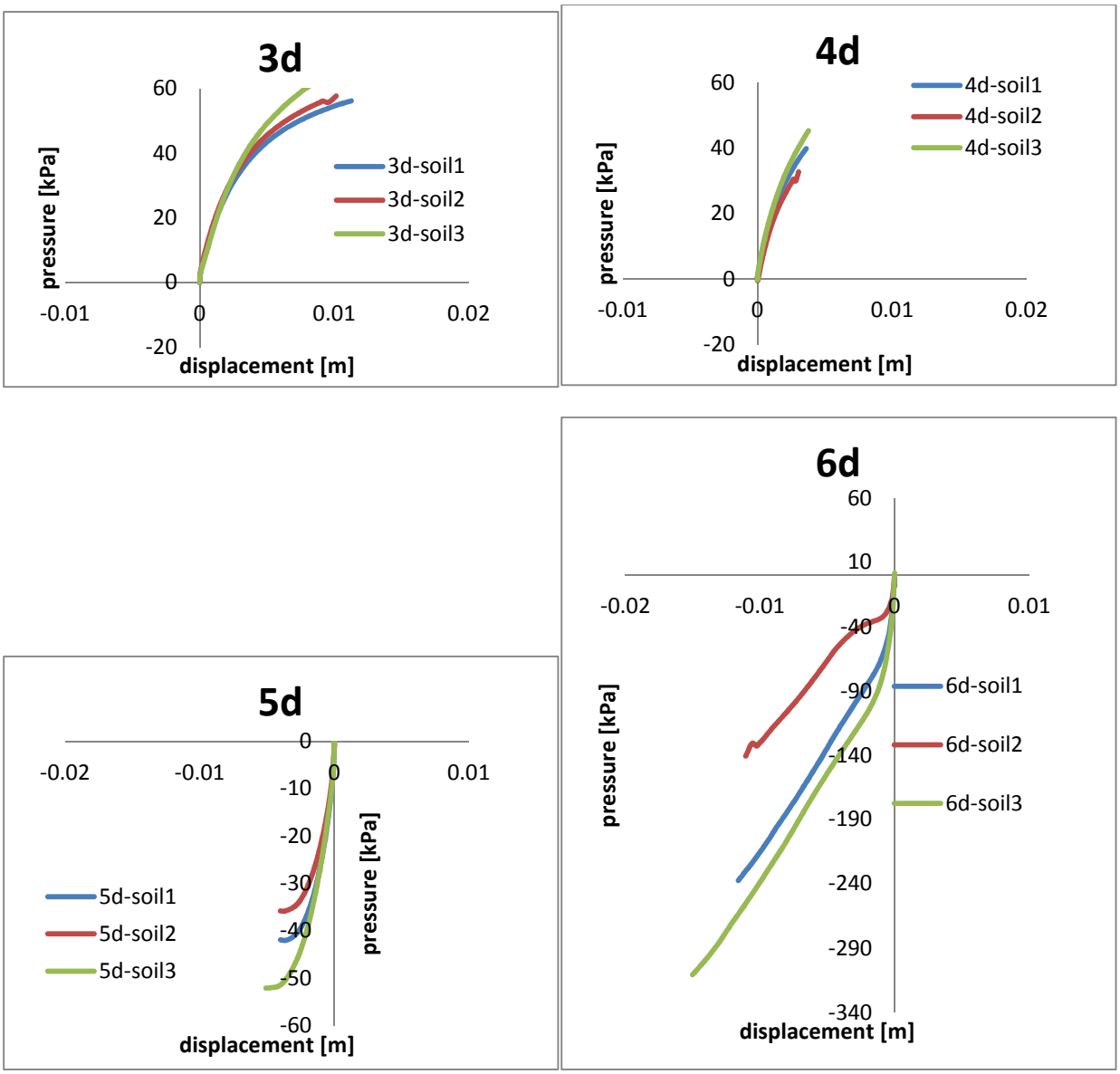

Figure 4.15: Comparison of p-y curves in rigid piles

The soil properties affect significantly both the lateral capacity and the p-y curves. The variation of soil shear strength impacts more than the variation of interface shear strength and this will be relevant in order to find the soil properties that fit more with the properties of the sand in the lab tests.

4.3 Comparison with design Method

4.3.1 Ultimate load (Broms)

In this chapter the ultimate load of the Broms theory is compared with the obtained results. The ultimate force of Broms theory is computed for the prototype pile using the following formula (explained in details in paragraph 1.1.2.1) is the pile is rigid:

$$H_u = \frac{0.5\gamma' D L^3 K_p}{e + L} = \begin{matrix} 276kN\ for\ \phi = 33° \\ 314kN\ for\ \phi = 36° \end{matrix}$$

where
D: pile diameter → 1m
e: eccentricity →15D=15m
L: pile length → 6m
γ': effective unit weight → 16.67kN/m^3
K_p: passive lateral earth pressure coefficient→ $K_p = \frac{1+sen\phi}{1-sen\phi} = \begin{matrix} 3.39\ for\phi = 33° \\ 3.85 for\phi = 36° \end{matrix}$

If the pile is flexible it means that the moment corresponding to the ultimate load calculated using the previous formula is higher than the yielding moment.

$$M_u > M_y = \frac{J\, f_y}{\frac{D}{2}}$$

where

J: inerzia moment → $J = \frac{\pi D^4}{64} = 0.039\ m^4 \quad for\ rigid$
$J = \frac{\pi(D_e{}^4 - D_i{}^4)}{64} = 0.0059\ m^4 \quad for\ flexible$

fy: steel strength → $f_y = 300\ MPa$

Since the models are in a reduced scale (N=25g), to compare the results with Broms' theory the forces are multiplied by the scale factor to the square and the displacements are multiplied by the scale factor N=25.

Hollow pile plugged and unplugged

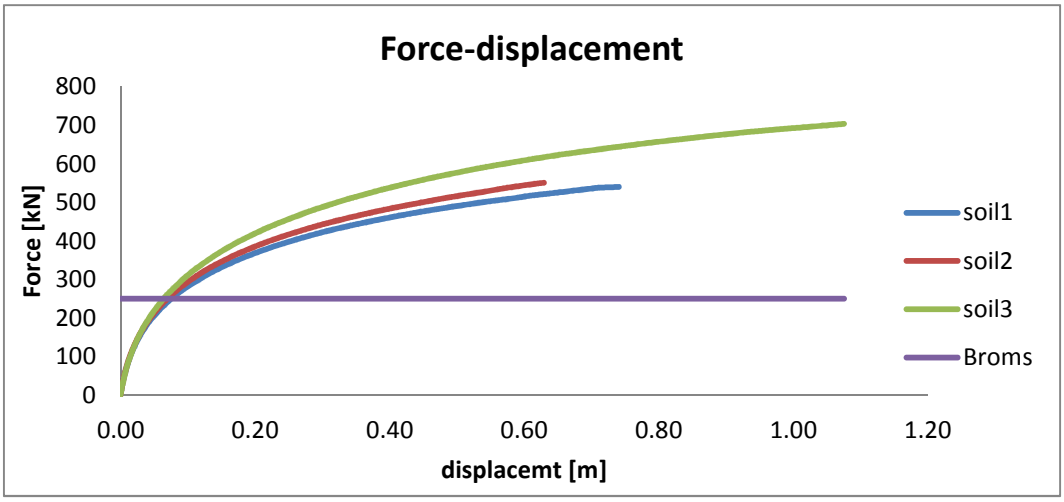

Figure 4.16: Comparison of force displacement curves in flexible piles with Broms theory

Rigid pile

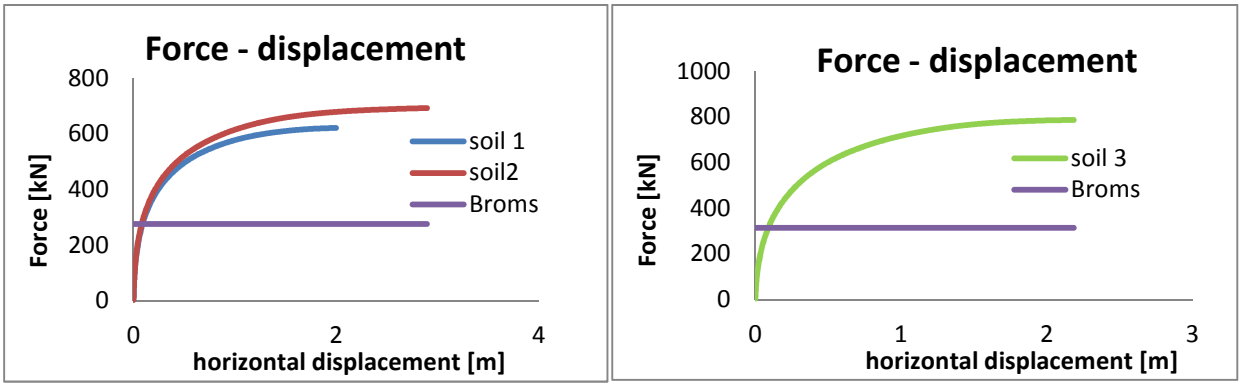

Figure 4.17: Comparison of force displacement curves in rigid piles with Broms theory

First of all it is important to mention that Broms' theory gives just the ultimate load that the soil can bear and not all failure criteria of the system. For this reason the relevant graphs in this paragraph are the ones of the rigid pile since they reach the ultimate force. The argument can be generalized for all the thee type of pile

Regarding the reference soil (soil1), the ultimate force calculated by Broms matches the ones obtained with the Abaqus simulation.

Broms' theory does not take into account the interface shear strength, hence it underestimates the ultimate force for higher interface strength than 2/3ϕ (soil2).

Increasing shear strength angle both the ultimate load from Broms' law and from the Finite element model increase, but the one from the FE Model is considerably higher. Broms' theory also in this case underestimate the force.

4.3.2 API p-y curves

In order to compare the p-y curves, 2 parameters are observed. The ultimate pressure(ultimate soil resistance) is the value by which the curve becomes horizontal, not at all the depth this value has been reached in the Finite Element Models. The initial stiffness kx of the p-y curve is the tangent of the curve at zero defection.
Looking at the p-y curves of chapter 3 (graph 3.14, 3.20, 3.24, 3.28, 3.34, 3.38, 3.42), it is evident that mostly the p-y curves calculated with the API formula (explained in pagaraph 1.1.2.2, chapter 1) underestimates the ultimate pressure and the initial stiffness kx respect to the curves obtained with the Finite Element Model. For shallow depth (1d and sot times 2d) there are some exceptions usually at depth 4Dimeters and 5Diametrs (0.16 and 0.20m under the ground level).
In the unplugged pile at 5D the initial stiffness computed with the two methods present the same values with all the type of soil; moreover in the soil with higher interface strength (soil 2) also the ultimate value is the same with API formulas and FEM results.
In the plugged pile at 5D the stiffness is very similar with the two methods for all the type of soil. In the reference soil (soil 1) also the ultimate pressure is the same at this depth and at 4D the stiffness is the same too.
In the rigid pile the stiffness of the p-y curves calculated with the finite element method coincide with the API provision at the depth of 4D for all the type of soil. For the soil with higher interface strength (soil 2) at 5D the stiffness is the same but the ultimate pressure calculated with the API formulas is higher than the one obtained with the FEM simulation.
The discrepancy between the code provision (API curves) and the curves predicted by the 3D FE analyses may be attributed to the negligence of the contribution of interface shear resistance of the API curves and to the inappropriate consideration of the variation of ultimate soil resistance with depth in the code provision[16].

4.4 Comparison with centrifuge modelling

In this paragraph the Finite Element Models are related with centrifuge test described in Thesis "Centrifuge testing for installation and stiffness effects on lateral load behaviour of monopiles"[1]. The lab test are two for each type of pile:

- Lab test 1: installation and loaded phases at 25g(increase of gravity). Since the installation phase in the numerical models has not been done, they should be compared with this lab tests 1.
- Lab test 2: installation phase at 1g (standard gravity) and loaded phase at 25g(increase of gravity). Since in these tests during the installation phase the gravity is less than the one used to have the stresses of the prototype, the soil properties could have been distorted. For this reason is usually used the other lab test for the comparison.

The curves analysed are the force- displacement curves because they give information on the lateral load capacity. At the moment the p-y curves cannot be compared because the calculation of the deflection from the lab test results is still under research.

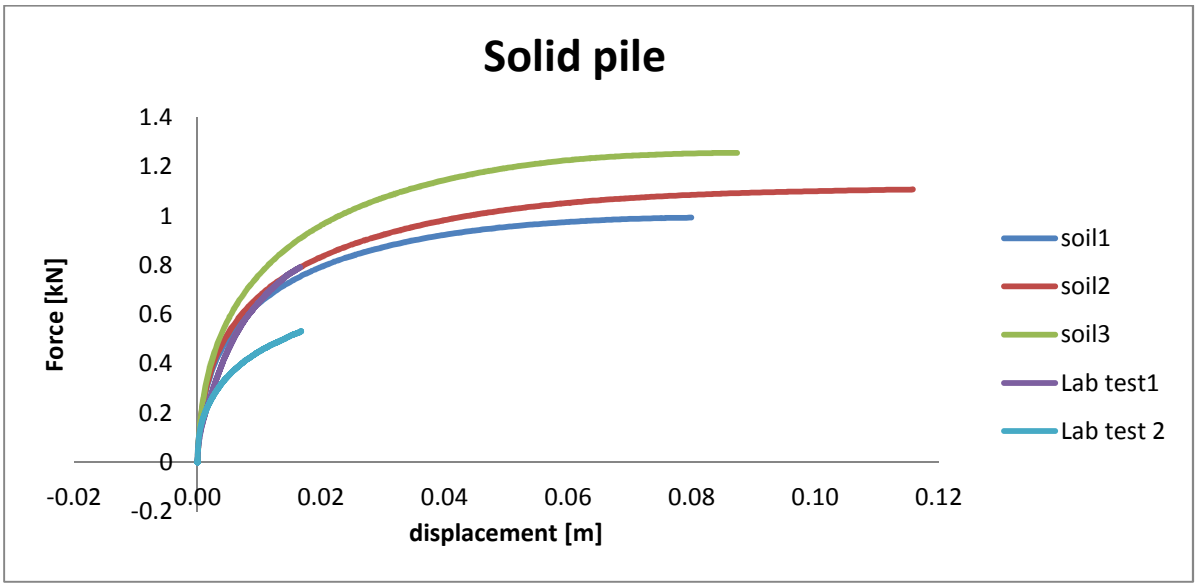

Figure 4.18: Comparison of force displacement curves in solid piles obtained with FE analysis with curves obtained with centrifuge tests

The results of the lab test 1 of the centrifuge (25g installation) regarding the force displacement curve fit better the FE analysis than the results of test 2 (1g installation) as it is expected because the installation phase is not modelled in the FE models.
For rigid pile the lab test 1 with the installation at 25g (test 1) fits perfectly with the FE model where the angle of interface shear strength is $\varphi=\phi=33°$ (soil 2).
The interface shear strength is generally different from the residual strength of the soil itself, and depends on the interface material and its roughness as well as on the properties of the soil, the grain size distribution and shape of the soil particles, the magnitude of the normal stress and the rate of shear displacement. It is usually assume equal to 2/3 of the soil strength but since it depend on several parameter it is very difficult to estimate. From this graph it seems that the shear strength of the sand in the Lab test 1 is equal to the soil strength.

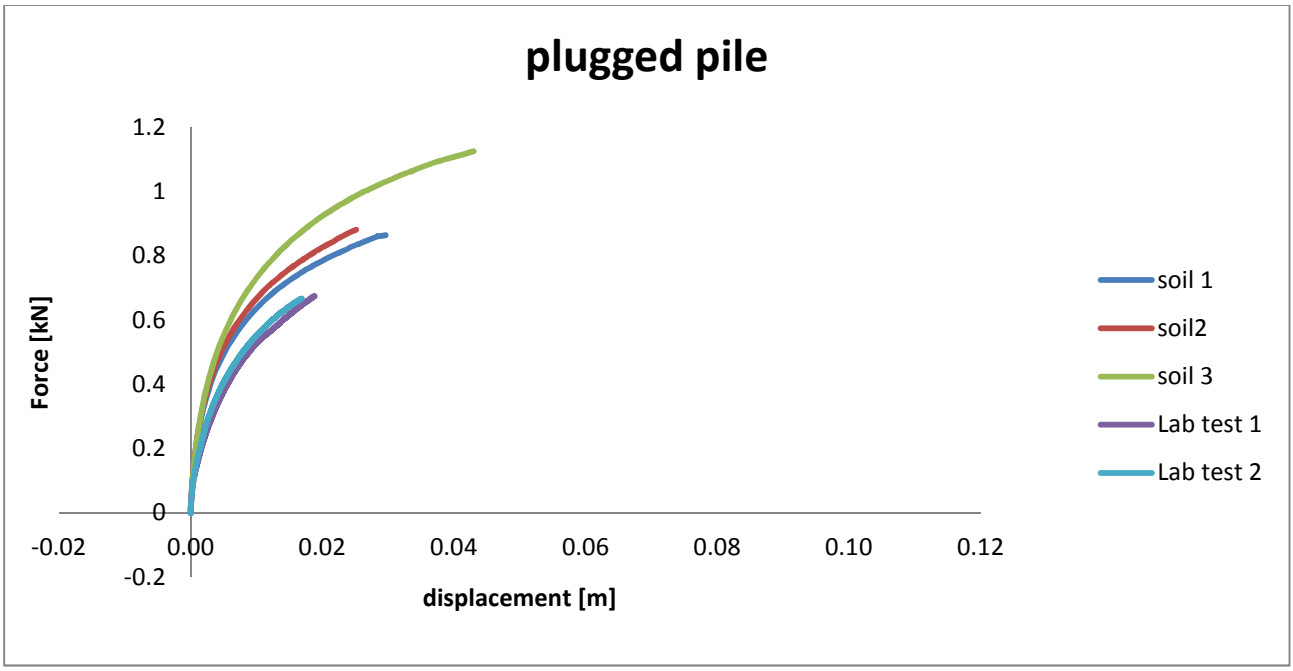

Figure 4.19: Comparison of force displacement curves in plugged piles obtained with FE analysis with curves obtained with centrifuge tests

In the plugged pile, the centrifuge results in the two tests are very similar. The piles do not reach the ultimate lateral force, because the tests were stopped before, in the FE analysis numerical problems due to the distortion of the finite elements and in the lab tests it was necessary to avoid the breaking of the pile. However the pattern suggests where the ultimate value is located; the lateral capacity of the piles in the centrifuge tests appears considerably smaller than the ones of the FE analysis.

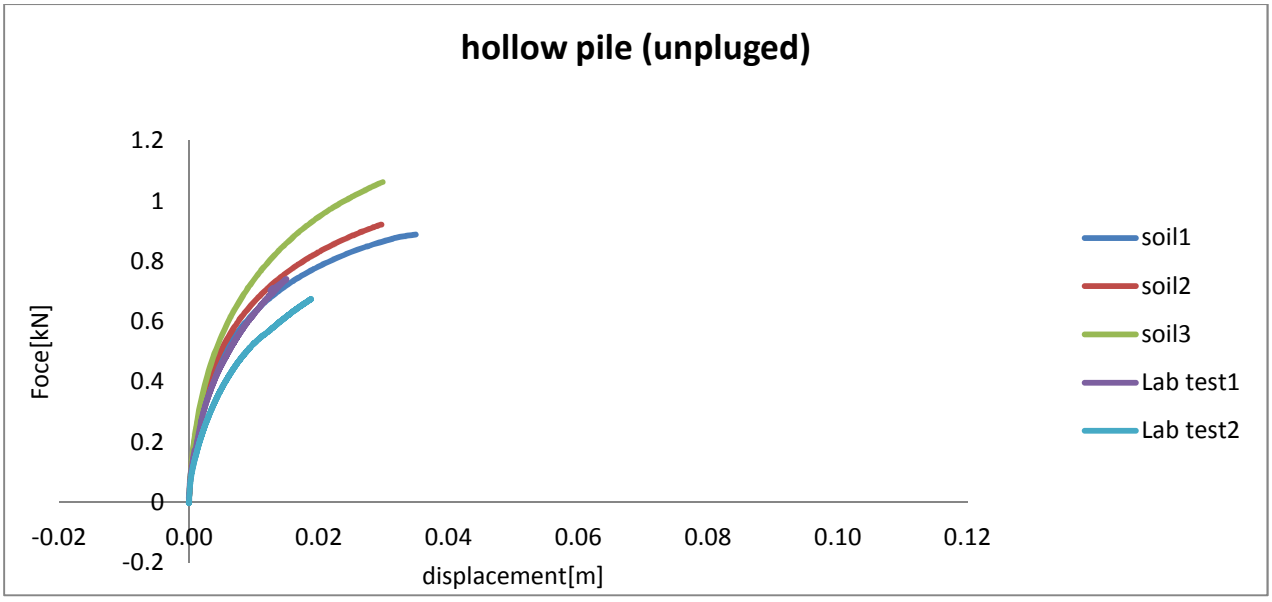

Figure 4.20: Comparison of force displacement curves in unplugged piles obtained with FE analysis with curves obtained with centrifuge tests

The results of the Lab test 1 (installation at 25g) merge the FE analysis better than the Lab test 2 as it is expected.
The trend of the force – displacement curve of the lab test 1 is between curve of the reference soil (soil 1) and the one of soil with interface shear strength equal to the soil shear strength $\varphi=\phi=33°$ (soil 2).
Also the unplugged pile does not reach the ultimate lateral force but the elastoplastic behaviour is evident also in this first part of the curves.

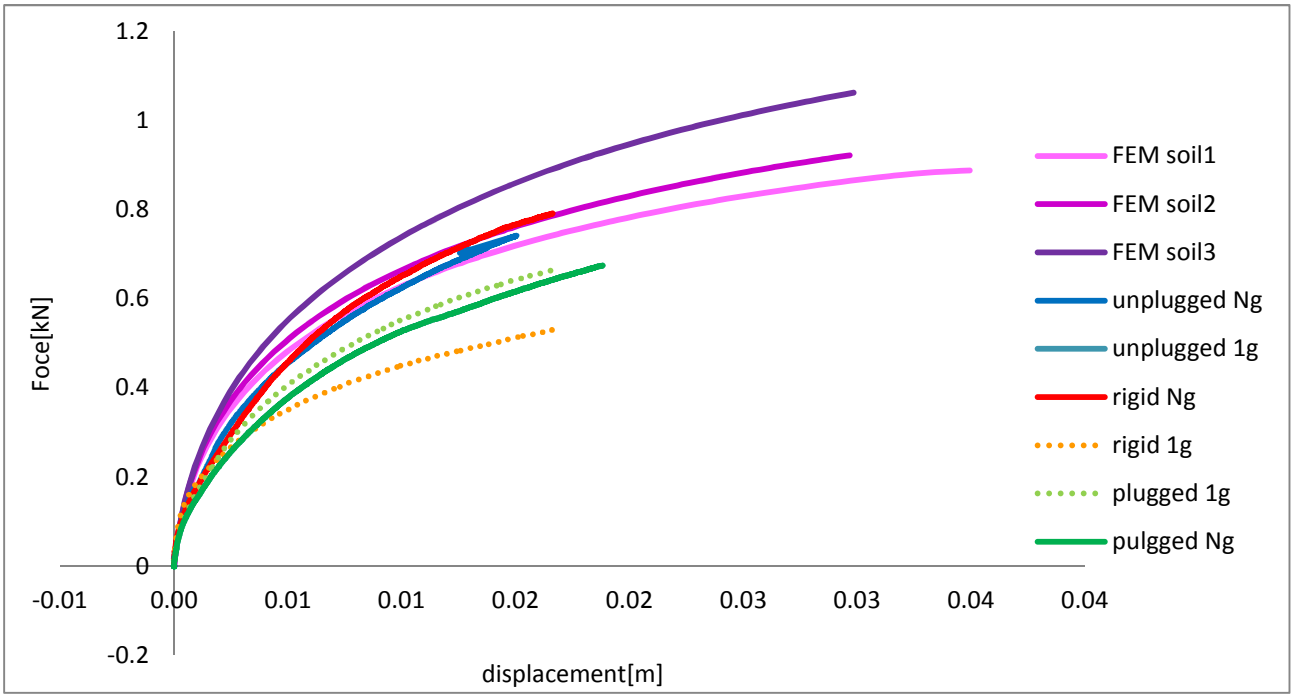

Figure 4.21: Comparison of force displacement curves in flexile and rigid piles piles obtained with FE analysis with curves obtained with centrifuge tests

The force-displacement curve in the FE analysis does not change varying the type of pile and consequently seems that the lateral load capacity does not depend on the pile stiffness. On the other hand from the centrifuge tests is evident that with the same installation procedure, the force-displacement curve varies as the type of pile is changed.
The reason of this phenomena could be that the installation effects occurs in the centrifuge also just changing the type of pile and not the installation procedure. The installation of plugged and unplugged piles produces different type of alteration of the soil, that gives a different soil response to the application of a lateral load. This phenomena does not occur in the FE analysis because the installation phase is not modelled.

5 Conclusions

In the current study the lateral response of rigid and flexible piles in cohoesionless soil was investigated. The effects of pile stiffness and soil properties were examined by analysing 3D FE models, which account for soil non linearity and geometric non linearity induced by sliding along the soil-pile interface and gap formation. The effect of pile stiffness and installation effects were examined by analysing the results of centrifuge tests in laboratory. The comparison of the two procedure helps in the interpretation of the results of the centrifuge test.

The results of the 3D FE models indicate that the induced failure mechanism is complex, including development of slip displacement along the soil-pile interface and plastic soil deformations.
The effect of the pile stiffness in the lateral capacity of the pile is found negligible even if the flexible and rigid piles present different deformed configuration. On the other hand, the stiffness and the type of pile (rigid or flexible) produces variations in the moment rotation curves and in the p-y curves. The failure mechanism (rigid body rotation or flexible deformation) might affect the moment rotation curves since the ones of flexible piles (plugged and unplugged piles) are generally more similar to the one of the rigid pile.
The effects of the increase of the interface shear strength and soil shear strength are shown to be significant affecting the pile lateral response. The lateral load capacity of the pile increases as the interface friction or the soil friction increases, the soil friction affect more this variation. The stiffness of the p-y curves and the ultimate soil resistance increase with shear strength of the interface or of the soil just at sallow soil depth; than the behaviour becomes more complex and depends also on the rotation point of the pile.

The comparison with the centrifuge tests highlightes the importance of the installation effects. The parameters and the assumptions used in the 3D models seem correct because the Lateral capacity obtained in the FE analysis fits well the results of the centrifuge tests at Ng installation for the rigid and the hollow unplugged pile. The interface soil friction of the experiments may be between $2/3\phi$ (reference soil) and ϕ (soil with increase of interface shear strength). The Lateral capacity in the centrifuge test varies also with different type of piles at the same installation condition while in the FE analysis the stiffness effects in the lateral capacity are found negligible. This may be attributed to installation effects that occurs during the installation of different type of pile which modifies the soil resistance in according to the shape of the pile.

Appendix: Cross section Bending Moment investigation

The objective of this benchmark is to prove the reliability of the results of the finite element analysis made by software Abaqus in terms of internal forces and deflection for the pile used in the model. Moreover the procedure used to find the bending moment distribution is used in the thesis.
The pile analysed is a hollow steel pile 6m long fixed at one side and loaded with a distributed force of 250kN/m, and figure 1 and table 1 shown.

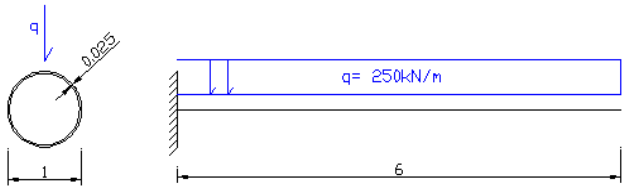

Figure A.1: pile´s static scheme

Hollow Pile properties		
material	steel	
Elastic modulus E	209 000	MPa
diameter D	1	m
thickness t	0.0375	m
length L	6	m
Moment of inertia I	0.0131508	mm^4
Load q	250	kN/m

Table A.1: pile properties

The analytical solution of a clamped beam is compared with the solution obtained from the Finite Element Analysis, where the pile is modelled both with solid element and shell element. The best procedure to obtain the bending moment from the output of the software is identify for the tow type of elements.

➢ Analytical solution

A clamped Eulero-Bernulli beam loaded with a distributed force is an isostatic problem since the DOFs are equal to the internal constrains. Therefore the equations for moment and shear distribution and deflection of the beam are easily founded.

Figure A.2: moment distribution

➢ Finite Element Solution

The Finite Element solution is based on the following approximate method. The structure is beaked into finite elements and it is assumed a deformed shape for each element. Than quantifying the shape by minimizing the distributed energy in the structure, the stresses and the displacement behaviour is predicted.

The problem is treated in two ways, the pile is modelled firstly with a shell element with the same properties of the given problem and then with a solid full pile with the same stiffness EI of the given problem in order to compare the results.

- **Shell element**

Shell structures are three dimensional structures, thin in one direction and long in the other two. The choice of this elements for the case studied is appropriate as long as the thickness of the pile is small respect to the diameter and the length of the pile.
Different type of mesh has been used in the model whose characteristics are listed in the table below.

Abaqus Input	
Part	
element	3D, Shell
Property	
Material	Elastic, Solid, Homogenous
Load	
Boundaryconditions	encastre
Load	shellload
Mesh	
Type	S8R, S4,S4R*
Size and shape	0.15quad
Elements along the cross section	20
Elements along the length	40

Table A.2: Shell element input

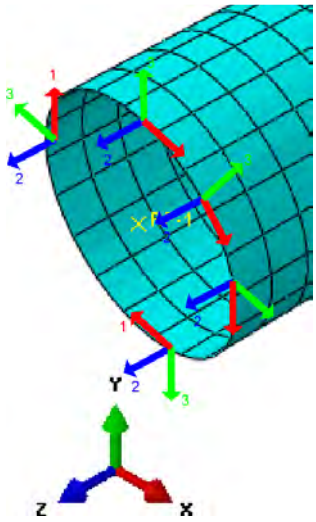

Figure A.3: local and global reference system

* S8R: quadratic elements with reduced integration
S4: linear elements without reduced integration
S4R: linear elements with reduced integration

The field output is set in order to obtain stresses (S)section forces (SF) section moments (SM) referred to the local reference system 1-2-3 of every element; and displacements(U1,U2.U3) and rotations (UR) referred to the global reference system xyz.

- <u>deflection</u>

The displacement U2 corresponds to the deflection of the pile and the values analysed are the one along the lateral edge of pile length where there are not fluctuations due to the load (figure 3).

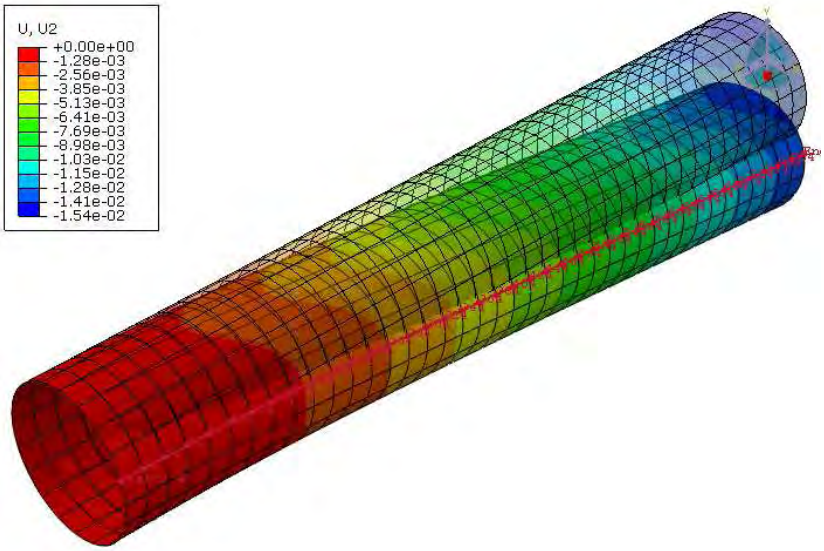

Figure A.4: Displacement U2 and path considered (red line)

In the graph it is compared the deflection founded using different mesh type with the deflection of the Bernoulli theory.

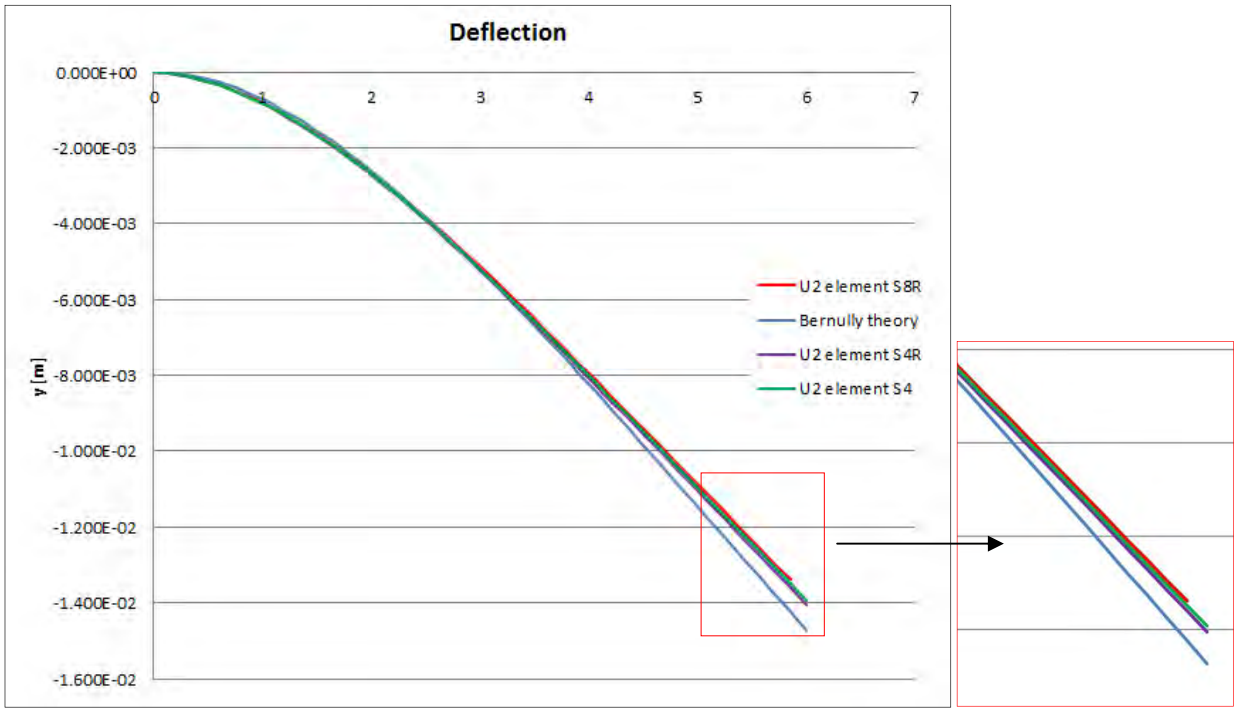

Figure A.5: deflection of the shell of the pile using different mesh type

Observing the graph is evident that there is not a big difference in the results according with the element type; although, the better elements to be used are the S4R (linear elements with reduced integration). They will be used later on in the benchmark and in the project.

- internal forces of cross sections

Internal forces of the section are not output of the program and they can be calculated using different methods. In this benchmark two procedures are compared: “integration” of forces in the section and calculation from horizontal stress.
The momet distribution is fistly calculate using the orizontal internal stresses σ (S22) at the top of the pile, in the Sant-Venant formula:

$$M = \frac{\sigma}{D/2} I_{solid}$$

The moments founded are compared with the theoretical solution in the graph 3.

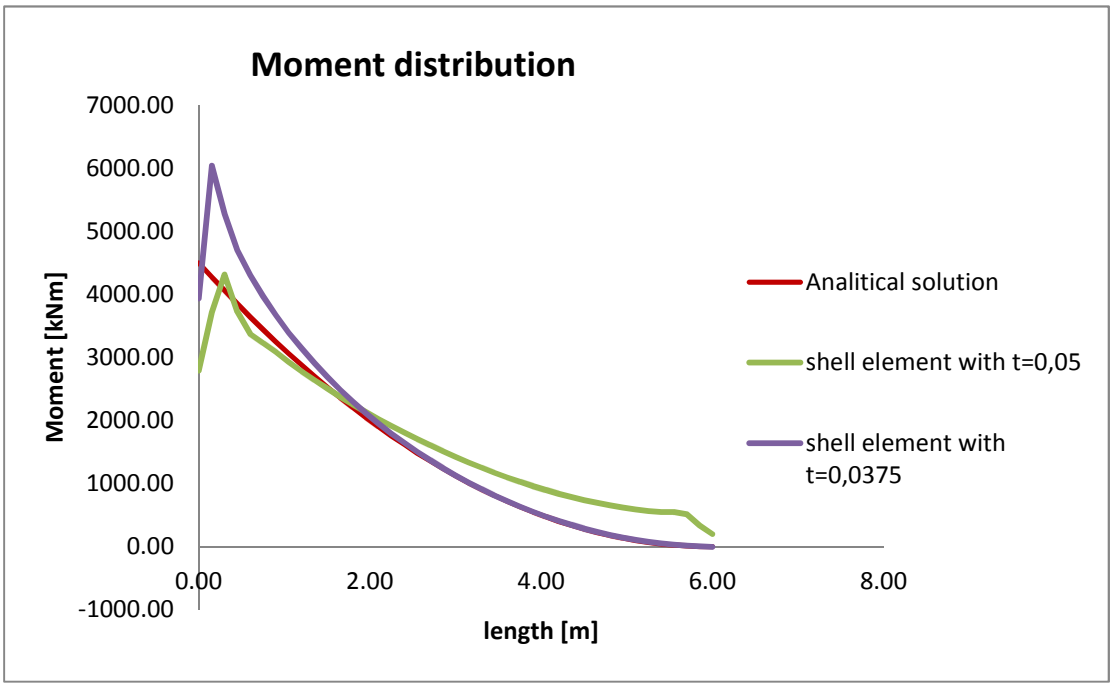

Figure A.6: Shell element moment distribution found with stresses method

The solution of the finite element method (green line) is quite different from the theoretical one ecspecially at the end of the pile, far from the constrain, because the cross section are defomed in this region and do not remain plane since the thikness of the pile is small (figure A.7). The finite element analysis calulate the stesses from the relative displacement therefore the stesses are ae afected by this problem.

In order to solve this preoblem and crate a more rigid cross section the thikness of the pile hase been increase until 0.05m (violet line). Is evdent that the problem of the deformation of the cross section is solved but now there is a big discrepance in the first tow metrs because the thikness of the pile is too

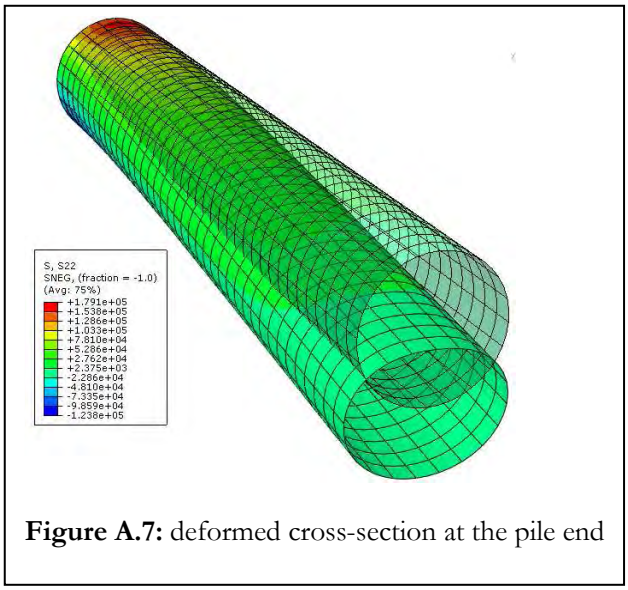

Figure A.7: deformed cross-section at the pile end

large to use shell elements.
The method of the stresses can not be use because it does not reliable solution, the second method is now analized.
In the “integration” of forces in the section, the moment in every cross section is calculated with an approximate integration of forces in the section.

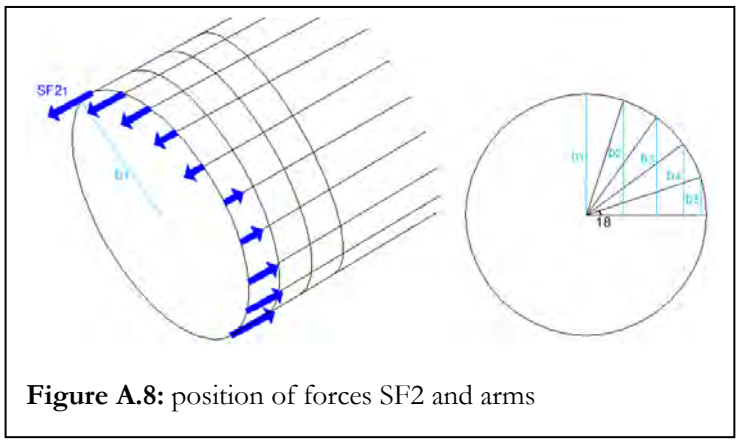

Figure A.8: position of forces SF2 and arms

where

$SF2_i$: Section forces in the i elements for every cross-section

b_i: arm of the force i respect to the canter of the pile→ $b_i = \frac{D}{2}\sin(18°i)$

The moments founded are compared with the theoretical solution in the graph 2.

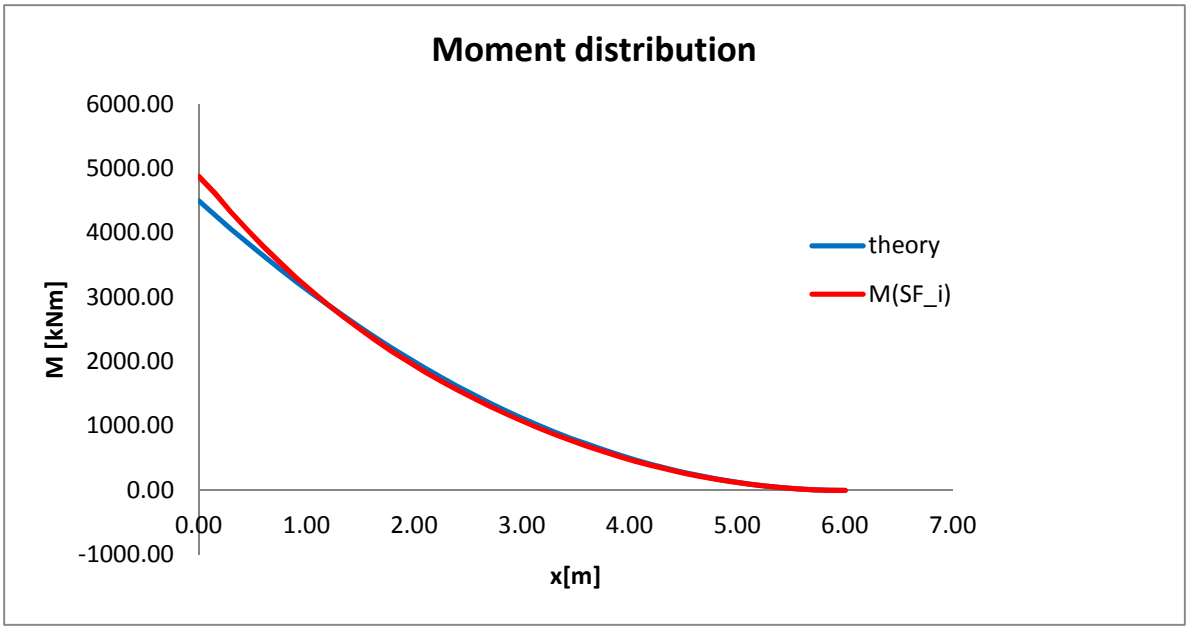

Figure A.9: moment distribution using “integration” of forces in the section

This method gives a solution very similar to the theoretical after 1meter length. The difference between the finite element solution and the theoretical one near the encstre is probably due to different behavior of the pile respect to the bernulli theory, indeed the ditribution of the forceses in this region is not linear alonge the cross section .
In coclusion this method to calculate the moment distibution of the pile is reliable and it will be use in the prject later on.

- **Solid elements**

Solid structures are three dimensional structures, with approximately the same dimensions in the three directions. For this reason the hollow pile is modelled as a full pile with the same stiffness EI of the datum one.
An equivalent elastic modulus is condidered in order to have the same stiffness and compare the results:

$$E^* = \frac{E\,I}{I_{solid}}$$

The load to a solid element must be pressure on a surface, so, in order to apply an equivalent load of the analysed problem, a pressure p an a thin surface at the top of the pile is applied.

$$p = \frac{q}{s} = \frac{250kN/m}{0.002m}$$

The properties of the solid pile considered and the characteristics of the model are summarized in tables.

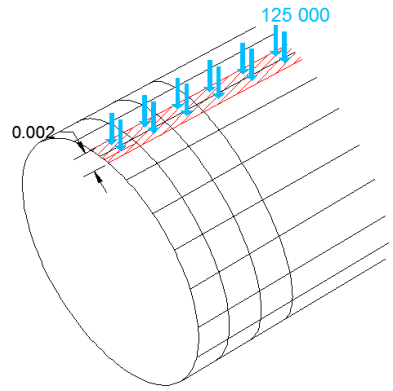

Figure A.10: pressure on the solid pile

Solid Pile properties		
material	steel	
Elastic modulus E*	55 992	MPa
diameter D	1	m
length L	6	m
Moment of inertia I	0.049087	mm^4
Load q	125000	kPa

Table A.3:equivalent solid pile properties

Abaqus Input	
Part	
element	3D, Solid
Property	
Material	Elastic, Solid, Homogenous
Load	
Boundaryconditions	encastre
Load	pressure
Mesh	
Type	C3D20, C3D20R*
Size and shape	0.15, hex
Elements along the lenght	40

Table A.4: **solid pile input**

* C3D20: quadraticbricks 20nodes
C3D20R: quadratic bricks 20nodes, reduced integration

The field output is set in order to obtain stresses (S), displacements(U) and rotations (UR) all referred to the global reference system xyz.

- internal forces of cross sections

The momet distribution is calculate using the orizontal internal stresses σ (S33) at the top of the pile, because there is not deformatin of the cross-section .The Sant-Venant formula is therefore used:

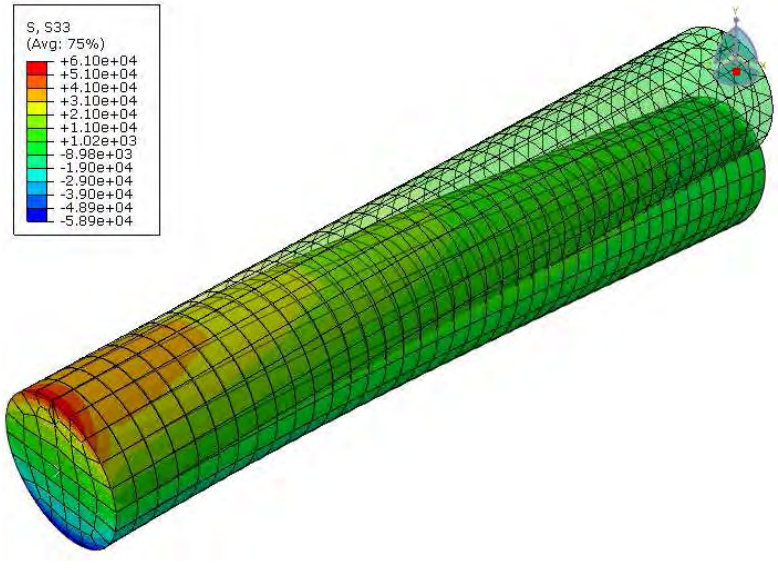

Figure A.11: orizontal internal stresses

In the following graph (Figure A.12) the finite different method is compared with the analytical solution using two different type of elements.

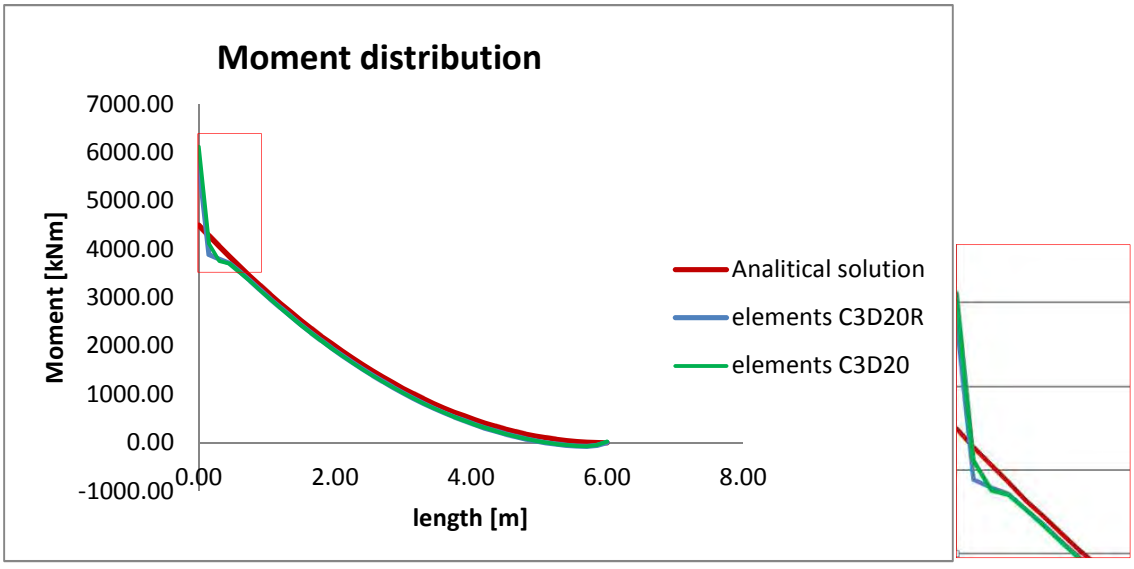

Figure A.12: Solid element moment distribution found with stresses method

The finite element solution is very similar to the theoretical one after 1m from the constrain because in that region the stresses are not linear and they do not follow the Bernoulli beam theory. The two element type chosen gives very similar results, anyway the elements C3D20 (quadratic bricks without reduced integration) are chosen because gives slightly better results.

Comparison and conclusions

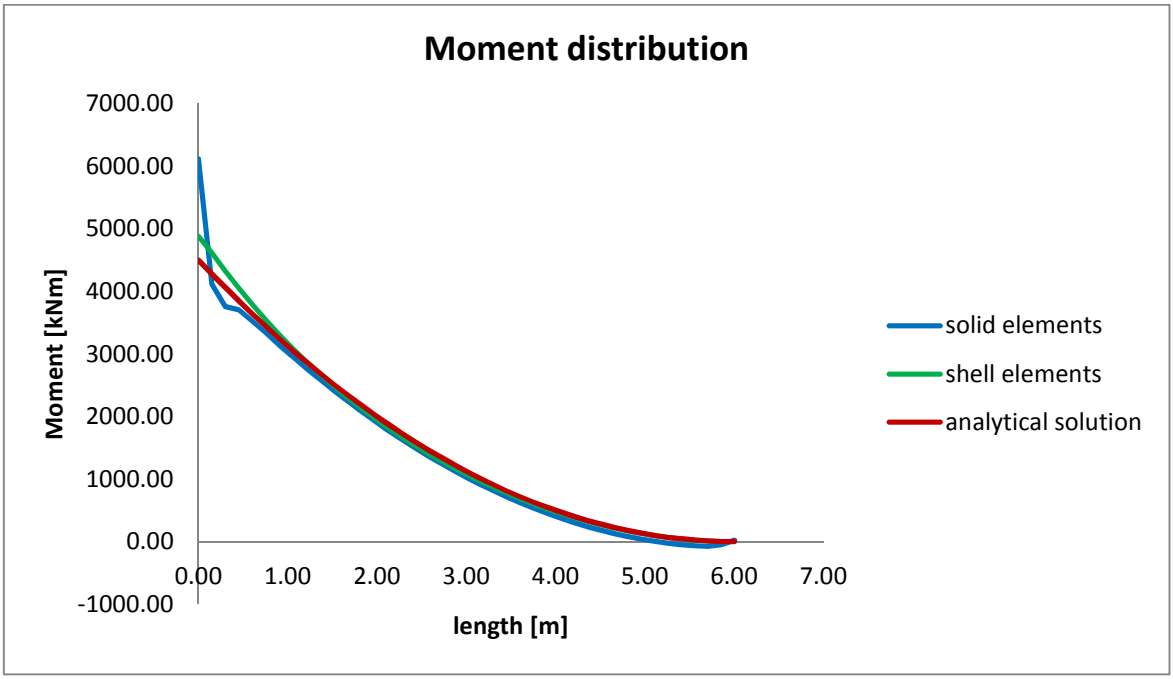

Graph 1: comparison between moment distribution of solid and shell elements

Comparing the moment distribution obtained from a finite element analysis using shell and solid elements to model a hollow pile, is evident that the best choice is the shell elements. Moreover using shell elements the deflection can also be considered and compared with Bernoulli theory.

References

1. C. Latini , " Centrifuge testing for installation and stiffness effects on lateral load behaviour of monopiles" Master thesis 2013
2. L. C. Reese; William M .Isenhower., Shin-Tower Wang , "Geotechnical design of driven piles under axial loads"(chapter 10) and "Fundamental concepts regarding deep foundation under lateral loading" (chapter 12) in "Analysis and Design of Shallow and Deep Foundations", John Wiley & Sons, 2006.
3. M.Gurnaratne, "Design of Laterally Loaded Piles"(chapter 8) in " The foundation engineering handbook", Taylor & Francis Group, 2006
4. B.B. Broms,M. ASCE "Design of laterally loaded piles", Journal of Soil Mechanics and foundation division, May 1965
5. I.F. Møller, T. Christiansen, "Laterally loaded monopole in dry and saturated sand-Static and cyclic loading" Master Project, June 2011
6. American Petroleum Institute, "Recommended Practice for Planning Designing and Constructing Fixed Offshore Platforms-Working Stress Design" API RP-2A-WSD, 2000
7. D-pile group manual
8. V. Adams, Abraham Askenazi, "Building Better Products with Finite Element Analysis"
9. K. J. Bathe ,E. L. Wilson, "Numerical Methods in Finite Element Analysis, Prentice-Hall", 1976.
10. L. C. Reese, William F. Van Impe, " Single Pile and pile groups under lateral loading" 2001 A.A. Balkema, 2011
11. D.A.Brown, C.-F .Shie,"Three dimensional finite element model of laterally loaded piles", Computers and Geotechnics,10(1),59-79,1990.
12. D.A.Brown, C.-F .Shie "Some numerical experiments with a three dimensional finite element model of laterally laded pile", Computers and Geotechnics,10(1),59-79,1990.
13. M.Laman, G.J.W. King, E.A. Dickin, "Three dimensional finite element studies of the moment-carrying capacity of short pier foundation in cohesionless soil" ", Computers and Geotechnics,25(3),141-55.1999.
14. C.-C.Fan, J.H. Long , "Assesment of existing methods for predicting soil responce of laterally loaded piles in sand" Computers and Geotechnics,32(4),274-289,2005.

15. Z.Yang, B. Jeremic, “Numerical analysis of pile behaviour under lateral loads in layered elastic-plasic soils”,International Journal for Numerical and Analytical Methods in Geomechanics,26,1385,1406,2002.
16. V. Zania, O. Hededal, “The Effects of Soil-Pile Interface Behaviour on laterally Loaded Piles”, 2011
17. M. Eskesen, J. Buhrkall, J. Henningsen, “Triaksialforsøg- Laboratoriepraktik”, Danmarks Tekniske Universitet, 2010
18. Abaqus manual